Universidad de Valladolid

FACULTAD DE CIENCIAS

DEPARTAMENTO DE QUÍMICA ANALÍTICA

TESIS DOCTORAL:

BIOFUNCTIONAL HYDROGELS BASED ON ELASTIN-LIKE RECOMBINAMERS AS EXTRACELLULAR MATRIX ANALOGUES

Presentada por
Israel González de Torre
para optar al grado de

Doctor por la Universidad de Valladolid

Dirigida por:
Dra. Matilde Alonso Rodrigo
Dr. José Carlos Rodríguez Cabello

BIOFUNCTIONAL HYDROGELS BASED ON ELASTIN-LIKE RECOMBINAMERS AS EXTRACELLULAR MATRIX ANALOGUES

"La ventura va guiando nuestras cosas mejor de lo que acertáramos a desear; porque ves allí, amigo Sancho Panza, donde se descubren treinta o poco más desaforados gigantes con quien pienso hacer batalla, y quitarles a todos las vidas, con cuyos despojos comenzaremos a enriquecer: que esta es buena guerra, y es gran servicio de Dios quitar tan mala simiente de sobre la faz de la tierra".

Miguel de Cervantes Saavedra (El Quijote)

A todos los que me ayudan a luchar contra mis gigantes

Agradecimientos

Escribir esta tesis me ha hecho recordar todo lo que han sido los últimos cuatro años de mi vida y por tanto recordar a las personas que los han compartido conmigo. Todas de algún modo u otro han dejado una pequeña parte de ellas en este trabajo y por tanto en mí.

En primer lugar quiero expresar mi mas sincero agradecimiento a mis dos directores de tesis, Matilde y Carlos, por toda su ayuda y paciencia, pero sobre todo por creer y confiar en mi, y por su apoyo en todos los proyectos que en estos años hemos emprendido. Gracias también por ese intercambio de ideas que me ha proporcionado un punto de vista diferente, nuevo y estimulante de los proyectos en los que he participado y que es lo que ha hecho posible los resultados que aquí se presentan.

No quisiera dejar de mencionar a Javier y Alessandra, que han tenido una paciencia infinita para enseñarme parte de los secretos de la biología molecular y de todo lo relaccionado con células que haya podido aprender en estos años.

Quiero agradecer también a mis "dos orgánicas" Merche y Ana. Gracias por esos siempre apreciados consejos en química y en muchas otras cosas me han dado perspectiva tanto en el trabajo como en cuestiones más mundanas.

Muchas gracias Luis por haber compartido codo con codo los últimos años batallando con poroviscoelasticidades, microreologías, nanocapas y demás monstruos que desconocíamos.

Muchas gracias a todos mis compañeros que han compartido "trincheras" conmigo aunque no siempre haya sido fácil, nunca

perdieron su paciencia conmigo y probablemente tuvieron más de una ocasión para hacerlo, pero siempre siguieron ahí. Con ellos he pasado momentos de risas y bromas que han hecho de estos cuatro años un periodo de mi vida que no cambiaría. Gracias Menchu, María, Ali, Guille, Mohamed, Chus, Arturo, Ito, Sergio, Lucia, Jorge Dori y Tati (las dos chicas de oro) y a todos los que han pasado por el laboratorio.

Laura, muchas gracias por enseñarme a que las botellas de cocacola no se iban a colocar solas en las estanterías. Desde ese día siempre me has ayudado, ojalá que eso siga así muchos años.

¿Como llamar a la pieza mas pequeña e imprescindible de un engranaje para que toda la maquinaria pueda funcionar? Rocío. Gracias de todo corazón, aunque más de una vez casi paro el tuyo de un susto.

Vanesa e Irene, que grandes conversaciones arreglando el mundo o riéndonos de niñas unicornios… sin esos momentos, es posible que parte de mi escasa cordura se hubiese perdido.

De todos vosotros me llevo amigos, no solo compañeros.

Quiero agradecer a todos los que han trabajado conmingo en Alemania, especialmente a Petra, Luis, Miriam, Fredi y Ricardo, que tanto me han enseñado de válvulas y stents.

Gracias a mis amigos y famila por haber estado ahí estos años, aguantando mi cháchara sobre Elastin-likes, células y válvulas, menos mal que tenían cervezas para aguantarlo.

Por supuesto y por encima de todo, muchas gracias a mis Padres, ellos nunca me fallan, siempre están, siempre apoyan aunque no entiedan por qué me tienen que apoyar y sobre todo han

puesto mucha mas cordura en mi de lo que soy capaz de admitir. Por su amor incondicional, Gracias.

Para el final te dejo a ti, Cris, el amor que siempre me acompaña, que brilla donde quiera que vaya, que hace que sepa cual es mi rumbo y objetivo incluso en mis momentos mas oscuros, esos que solo tu conoces y haces que se vayan para que pueda volver a ver el sol. Gracias Pequeña.

TABLA DE CONTENIDO

RESUMEN

1. OBJETIVOS

1. Uno de los objetivos principales de esta tesis consiste en la formación de hidrogeles mediante un proceso citocompatible que permita encapsular células dentro de dichos geles en el momento de su formación y que simulen las propiedades de las matrices extracelulares naturales para su utilización en ingeniería de tejidos. Dichos hidrogeles se obtendrán utilizando Polímeros Recombinantes tipo Elastina (ELRs) por presentar unas excelentes propiedades de partida como son su elevada biocompatibilidad o la posibilidad de incorporar diferentes bioactividades entre otras.

1.1. En primer lugar se pretende obtener geles híbridos formados por ELRs y fibrina. Una vez obtenidos se esclarecerán sus propiedades físicas y mecánicas, así como su citocompatibilidad y las posibilidades que ofrecen en el campo de la ingeniería de tejidos.

1.2. Se van a obtener también geles formados exclusivamente por ELRs y utilizando la tecnología "click chemistry" como método de entrecruzamiento. Para ello se modificará químicamente la estructura de distintos ELRs para que porten los grupos funcionales reactivos necesarios para la formación de dichas matrices extracelulares artificiales en condiciones citocompatibles, y si es posible sin ningún tipo de sustancia ajena que pueda afectar a la citocompatibilidad de los hidrogeles.

1.3. Una vez obtenidos estos hidrogeles se quiere proceder a la caracterización de sus propiedades físicas y

mecánicas para, de esta forma, comprender mejor tanto las propiedades macroscópicas como microscópicas y poder establecer el modelo que rige dichas propiedades.

1.4. Se evaluará la adhesión y proliferación de varias líneas celulares en hidrogeles formados por ELRs que portan distintas secuencias bioactivas, con el fin de constatar y estimar su bioactividad.

2. Se quiere desarrollar un sistema fractal de formación de nanogeles mediante tecnología click sin cobre, y comprobar la influencia de la temperatura en dicha fractalidad durante el proceso de formación de estos geles. Se pretende evaluar y caracterizar, mediante el estudio de las dimensiones así como de las propiedades microreológicas y eléctricas, las estructuras formadas para tener un mejor conocimiento de su validez como sistemas de dosificación de fármacos.

3. Por otro lado, se investigará la capacidad de estos hidrogeles para ser utilizados como recubrimiento de distintos materiales como poliestireno, vidrio y titanio mediante la tecnología "capa a capa" (layer by layer); siendo el titanio de especial interés debido a su creciente utilización como implante en procesos quirúrgicos. Se pretende obtener un sistema de formación de capas rápido, reproducible y escalable. Además dicho recubrimiento debe ser totalmente citocompatible y que nos permita incluir diferentes agentes terapéuticos que puedan ser de interés en futuras aplicaciones tanto en ingeniería de tejidos como en dosificación de fármacos.

4. Por último, otro objetivo fundamental de la tesis consistió en demostrar la eficacia de los hidrogeles formados por ELRs y obtenidos mediante tecnología click sin cobre, como "scaffolds" en

ingeniería de tejidos y más concretamente en el tratamiento de enfermedades cardiovasculares. Las características, tanto mecánicas como biológicas, de estos hidrogeles podrían convertirlos en biomateriales especialmente útiles en el tratamiento de ciertas afecciones del sistema circulatorio. Debemos tener presente que dichas afecciones son una de las principales causas de muerte hoy en día y los biomateriales empleados hasta ahora están todavía lejos de satisfacer las necesidades requeridas. Se pretende por tanto, obtener y caracterizar *in vitro* distintos dispositivos o implantes médicos para en una etapa posterior a esta tesis poder testarlos *in vivo*.

4.1. Dentro de este campo de aplicación, los hidrogeles se van a emplear en la obtención de "bioestents" para el tratamiento de problemas de estenosis de los vasos sanguíneos. Se quiere recubrir estents metálicos con los hidrogeles desarrollados y aprovechando su bioactividad, sus buenas propiedades mecánicas y su alta biocompatibilidad. Este recubrimiento, además de aumentar la biocompatibilidad del implante y soportar los esfuerzos mecánicos a los que va a ser sometido, debe ser capaz de inducir la endotelizacion del dispositivo antes de su implantación en el organismo, y por tanto, conseguir que presente una baja trombogeneicidad y en consecuencia disminuya el riesgo de restenosis.

4.2. Como último objetivo y también dentro del área de la ingeniería de tejidos y aplicaciones cardiovasculares, se pretende testar este tipo de geles como sustitutos artificiales de válvulas aórticas dañadas o poco operativas. Se moldearán válvulas aórticas artificiales y se evaluará el comportamiento mecánico de dichas válvulas en bioreactores especialmente

diseñados para imitar las condiciones del entorno aórtico. También se analizará el tejido formado después de la realización de cultivos dinámicos con estimulación.

2. INTRODUCCIÓN

Enfermedades, heridas, malformaciones y envejecimiento han acompañado a la humanidad durante toda su historia. Desde tiempos remotos en los que las antiguas civilizaciones se basaban en magia y mitos para explicar las vidas de dioses y semidioses que poseían increíbles poderes de regeneración, uno de los sueños que ha perseguido el hombre es conseguir imitar esas maravillosas propiedades de aquellos seres todopoderosos pudiendo así reparar o incluso regenerar órganos y miembros dañados, y así poder alargar la vida de los seres que les son queridos.

Para ello, ya desde la antigüedad, se han utilizado diversos materiales con el objeto de fabricar y reponer partes del cuerpo perdidas o dañadas. Entre esos materiales podemos encontrar desde madera y vidrio hasta aleaciones de diversos metales[1,2] . En la actualidad los materiales que se usan son más sofisticados, y entre ellos encontramos complejos composites, biomateriales e incluso tejidos vivos[3-5] que son trasplantados de un donante a un paciente. Todos ellos pueden ser englobados dentro de la categoría de ingeniería de tejidos o bioingeniería, concebida esta como una especialidad que aplica los principios de la ingeniería y las ciencias de la vida a la fabricación de sustitutos que mantengan, mejoren o restauren la función de tejidos y órganos en el cuerpo humano.

Actualmente, uno de los objetivos de los investigadores en el área de la ingeniería de tejidos consiste en la obtención de biomateriales reabsorbibles o biomateriales que no sean reconocidos por nuestro organismo como algo exógeno y asi evitar una reacción de rechazo; y que induzcan una completa

regeneración de la zona dañada. Esos materiales deben actuar como andamios y tienen que cumplir principalmente tres requisitos: el primero es facilitar la distribución y colocación de células en el sitio preciso donde son requeridas, el segundo es que deben constituir un espacio tridimensional, con la estructura y propiedades mecánicas apropiadas para la formación del nuevo tejido de sustitución; y el tercer y último requisito, pero no por ello menos importante, es que esos materiales deben servir de guía para el desarrollo del tejido a regenerar para que éste pueda cumplir con su función, sin que el resto de los tejidos se vean afectados y por tanto la vida del paciente[6].

En los últimos años una gran variedad de materiales están siendo diseñados y aplicados en el campo de la ingeniería de tejidos. Dependiendo del área concreta donde se vayan a implantar o las funciones específicas que vayan a tener estos materiales poseerán unas propiedades u otras. Entre los materiales más usados podemos encontrar materiales plásticos como el polietilenglicol, derivados del ácido hialurónico[7], del ácido poliláctico[8,9] y otros polímeros como derivados del poliacrilato [10-15]. También se han utilizado polímeros basados en sustancias naturales como celulosa, colágeno, seda, fibrina, gelatina entre otros y mezclas de ambos tipos de materiales[15,16]. Todos estos materiales presentan ciertas limitaciones, ya sean de tipo mecánico, de citocompatibilidad de los productos de degradación, problemas de falta de reabsorción o reabsorción muy rápida o incluso generar una respuesta excesiva del sistema inmune del paciente. Por todo ello es claro que no se ha conseguido todavía un material que satisfaga todos los requerimientos para poder obtener un sistema óptimo para la regeneración de tejidos.

Como es evidente a simple vista, este es un objetivo muy ambicioso, pues lo que se pretende es imitar a la matriz extracelular (ECM de sus siglas en inglés –extracellular matrix-), que tan eficazmente ha sido diseñada por la naturaleza a lo largo de miles de años de evolución.

2.1 La matriz extracelular.

La matriz extracelular (ECM) está formada por una serie de moléculas secretadas por las células y se encuentra presente en todos los tejidos y órganos. La ECM no solo constituye el micro-ambiente que rodea a la célula, también sirve de soporte físico y proporciona la mayoría de las propiedades mecánicas a los tejidos actuando como un andamio donde las células pueden crecer y desarrollarse modificando incluso la estructura física y química de la propia matriz extracelular. Además tiene un papel crucial en los procesos de señalización bioquímica y biomecánica requerida para la diferenciación celular, morfogénesis de tejidos y procesos de homeostasis. La matriz extracelular está básicamente compuesta por agua, polisacáridos y proteínas. Aun así, cada tejido tiene una matriz extracelular con una composición específica y con una topografía característica, generada durante el proceso de maduración del tejido a través de una comunicación dinámica y recíproca entre las células y el microambiente proteínico y celular donde se encuentran[17].

Principalmente, podemos encontrar dos tipos de macromoléculas conformando la matriz extracelular: proteoglicanos (PGs) y proteínas fibrosas[18].

La proteína más abundante en la matriz extracelular, y en todo el organismo humano, es el colágeno[19]. El colágeno es una gran

familia de proteínas con más de treinta miembros, y aunque no todos ellos están presentes en la matriz extracelular sí que comparten un diseño helicoidal común en todos ellos. Este diseño helicoidal está formado por fibrillas que se ensamblan en tres pares de subunidades. La principal función del colágeno es estructural y es el responsable de la resistencia mecánica a la tracción de los tejidos.

Junto con el colágeno, la elastina es el otro componente proteico mayoritario en la matriz extracelular. La elastina está formada por subunidades de tropo-elastina entrecruzadas entre sí para dar como resultado las cadenas de elastina ya maduras. La elastina es la proteína responsable de la flexibilidad de los tejidos[20].

Fibronectinas y lamininas son otro importante grupo de proteínas que se encuentran presentes en la matriz extracelular. La fibronectina tiene una importancia especial en los procesos de movimiento, diferenciación celular y adhesión celular al sustrato[21]. Distribuidas a lo largo de la estructura de la fibronectina se pueden encontrar diferentes secuencias de aminoácidos que promueven la adhesión celular. Algunas de esas secuencias son RGD (Arg-Gly-Asp), RDGS (Arg-Gly-Asp-Ser), LDV (Leu-Asp-Val) y REDV (Arg-Glu-Asp-Val). Dicha adhesión a la matriz extracelular se produce por complejos mecanismos en los que intervienen receptores como las integrinas (una de las más grandes familias de receptores para la adhesión celular[22,23]) dominios de discoidinas proteoglicanos y sidecanos. Todos ellos son capaces de reconocer esas secuencias de aminoácidos y promover la adhesión celular. Por último la laminina se encuentra principalmente en las membranas que sirven como suestento y junto con el colágeno proporcionan a los tejidos resistencia mecánica a la tracción. Está formada por tres

subunidades (α, β y γ) las cuales juntas forman un modelo en forma de cruz que es capaz de unirse a otras proteínas de la matriz extracelular[24].

2.2 Recombinámeros tipo elastina (ELRs).

Como se ha comentado, la elastina es uno de los componentes mayoritarios de la matriz extracelular y tiene un papel crítico en la elasticidad y resistencia de muchos tejidos de los animales vertebrados, como por ejemplo la piel, pulmones, arterias, ligamentos y cartílagos. La elastina posee, además, diversas secuencias que pueden interactuar con diversos receptores en la superficie celular[25]. Por todos estos motivos es importante conseguir matrices extracelulares artificiales que contengan elastina. Por otro lado, como la elastogénesis no es un proceso sencillo ni que se produzca in vitro con facilidad[26], la síntesis artificial de polímeros que imiten la estructura y propiedades de la elastina natural es un avance importante para poder dotar a las matrices extracelulares artificiales de las propiedades tanto mecánicas como biológicas necesarias para poder ser aplicadas en diversas técnicas biomédicas.

El uso de técnicas recombinantes nos permite obtener materiales basados en proteínas naturales, y que combinen o presenten algunas de las propiedades de dichas proteínas naturales además de otras que pueden tener interés tecnológico. Mediante dichas técnicas se han sintetizado los denominados Recombinámeros tipo elastina (ELRs de sus siglas en inglés elastin-like recombinamers), Este tipo de polímeros están basados en la repetición de ciertas secuencias de la elastina natural y han acaparado la atención de muchos investigadores debido a la

capacidad de estas moléculas para formar una amplia variedad de estructuras tales como nano partículas, nano fibras, películas o hidrogeles[27-29]

Su versatilidad junto con su biocompatibilidad, bioactividad y comportamiento termosensible convierte a los ELRs en unos excelentes candidatos para ser utilizados en aplicaciones biomédicas, incluyendo implantes y sistemas de dosificación de fármacos [30].

Además, los ELRs son biopolímeros que presentan respuesta a estímulos, y están basados en la repetición del pentapéptido Val-Pro-Gly-Xaa-Gly. En donde Xaa puede ser cualquier aminoácido excepto prolina aunque el polímero más estudiado es el poli(VPGVG).

Todos los ELRs funcionales presentan un cambio de fase reversible como respuesta a las variaciones de temperatura[31]. En disolución acuosa y por debajo de cierta temperatura denominada temperatura de transición inversa (ITT de sus siglas en inglés inverse transition temperature) o dicho de otra forma por debajo de una temperatura crítica de solubilidad (LCST de sus siglas en inglés lower critical solubility temperature), las cadenas de polímero permanecen desordenadas y relativamente extendidas con una ordenación tipo *random coil,* y totalmente hidratadas[32].Esta hidratación hidrofóbica está generada por la presencia de una serie de clatratos de agua que se disponen rodeando cadenas laterales apolares de los biopolímeros y dicha estructura es similar a la descrita para los hidratos cristalinos de los gases aunque más heterogénea y de estabilidad variable[33,34].

Al superar dicha temperatura se produce un reordenamiento de la estructura del ELR de tal forma que la cadena polimérica adopta

una disposición plegada mantenida mediante interacciones hidrofóbicas. El agua que rodeaba a la proteína formando los clatratos es desplazada y se produce una segregación de tal forma que el ELR precipita formando agregados.

EL orden y la secuencia de aminoácidos tienen una gran importancia en el proceso de ITT[35]. De hecho, variaciones en el aminoácido de la cuarta posición (Xaa) del pentámero producen modificaciones en los valores de le T_t, dependiendo de la polaridad del aminoácido introducido. Así aminoácidos polares producen una disminución de la hidratación hidrofóbica, lo que produce un incremento de la T_t y una disminución del incremento de la entalpía (ΔH_t) asociada a este proceso de hidratación hidrofóbica. De esta forma el proceso de solubilización de la proteína estará más favorecido siendo más fácil su disolución. La temperatura de transición se puede ver también afectada por otras variables como el pH, concentración de sales y la presencia de ciertas moléculas e iones[36]

Como ya se ha mencionado, los ELRs están basados en la fórmula general (VPGXG); donde X puede ser cualquier aminoácido excepto prolina. Así, todos los ELRs con esta fórmula general son funcionales y presentan el comportamiento termosensible. No obstante, conseguir ELRs funcionales mediante la sustitución de cualquiera de los otros cuatro aminoácidos no es sencillo. La prolina no puede ser reemplazada y la primera glicina no puede ser sustituida por otro aminoácido que no sea la l-alanina. Esto es debido a que cada giro de la hélice β tipo II requiere la presencia de glicina y prolina para estabilizar el estado plegado de la proteína. La presencia de restos voluminosos en aminoácidos con quiralidad L impide la formación de la hélice β, y el polímero resultante deja

de ser funcional. Por lo tanto, solo la alanina puede ser sustituida sin que afecte a la funcionalidad del polímero y en estos casos el polímero resultante suele presentar propiedades mecánicas y térmicas muy diferentes al original[37].

2.3 Hidrogeles.

Los hidrogeles, como es bien sabido, son redes tridimensionales de polímeros entrecruzados, que en presencia de agua aumentan de tamaño hasta alcanzar el equilibrio, generalmente son insolubles en agua, son blandos y elásticos.

Durante los últimos cuarenta años, los hidrogeles se han utilizado en aplicaciones farmacéuticas y biomédicas, principalmente debido a su alto contenido acuoso, a su semejanza con ciertos tejidos naturales y a la biocompatibilidad y respuesta a estímulos que poseen alguno de ellos[38,39]. De hecho fueron unos de los primeros biomateriales diseñados para ser aplicados en el cuerpo humano[40,41].

Los hidrogeles pueden ser clasificados en dos grandes grupos atendiendo a la manera en que se forma la red tridimensional que los constituyen: pueden ser físicos y reversibles o químicos y permanentes. En un hidrogel físico, la red tridimensional se mantiene por asociaciones moleculares, fuerzas de Coulomb, puentes de hidrógeno o uniones hidrofóbicas[42,43]. Normalmente los geles físicos no son homogéneos presentando áreas donde las asociaciones moleculares de dominios iónicos o hidrofóbicos son más fuertes. Los geles químicos o permanentes están formados por redes tridimensionales estabilizadas por enlaces covalentes de tal forma que esas uniones entre cadenas de polímero no pueden ser fácilmente eliminadas.

3. MATERIALES Y MÉTODOS

3.1.Materiales

3.1.1. Reactivos

Los reactivos empleados en el presente trabajo se enumeran en la siguiente tabla (Tabla 1).

Tabla 1. *Reactivos empleados*

Reactivo	Proveedor
(1R,8S,9S)-bicyclo[6.1.0]non-4-in-9-ilmetil succinimidil carbonato	Synaffix
1-etil-3-(3-dimetilaminopropil)carbodiimida (EDAC)	Sigma Aldric h
Acetona	Sigma Aldrich
Ácido clorhídrico	Sigma Aldrich
Ácido pentinoico	Sigma Aldrich
Alamar blue	Invitrogen
Anhídrido tríflico	Sigma Aldrich
Anticuerpo monoclonal anti αSMA	Sigma
Anticuerpo monoclonal de conejo anti colágeno I	Acris Antibodies GmbH
Anticuerpo monoclonal de conejo anti colágeno III	Acris Antibodies GmbH
Ascorbato sódico	Sigma Aldrich
Azida de sodio (NaN_3)	Sigma Aldrich
Carbonato sódico (Na_2CO_3)	Sigma Aldrich

Reactivo	Proveedor
Cloruro de metileno (CH_2Cl_2)	Sigma Aldrich
Colagenasa	Sigma, Seelze
DAPI	Invitrogen
Dietileter (Et_2O)	Sigma Aldrich
Dimetilformamida (DMF)	Sigma Aldrich
Dimetilsulfóxido deuterado (DMSO-d_6)	Sigma Aldrich
Estents de nitinol	Institut für Textiltech
Estreptomicina	Invitrogen
Etanol (EtOH)	Merck
Faloidina-Alexa-Fluor 488	Invitrogen
Fibrinógeno humano	Calbioochem
Glutaraldehído	Sigma Aldrich
Goat serum	Dako

Reactivo	Proveedor
Cloruro de Calcio ($CaCl_2$)	Sigma Aldrich
Heparina	Lonza
HEPES	Invitrogen
LIVE/DEAD® Kit	Invitrogen
Medios de cultivo (DMEN, EGM, EBM)	Lonza
Metanol (MeOH)	Merck
N,N'-diciclohexilcarbodiimida (DCC)	Sigma Aldrich
Normal Human Adipose-Derived Mesenchymal Stem Cells (hMSCs)	Invitrogen
Human Foreskin Fibroblast (HFF-1)	Invitrogen
Human Umbilical Vein Smooth Muscle Cells (HUVSMCs)	UKA Aachen
Human Umbilical Vein Endothelial Cells (HUVECs)	Invitrogen/ UKA Aachen
Paraformaldehído	Sigma
Penicilina	Invitrogen
Placas de cultivo	Nunnc/Greiner

Reactivo	Proveedor
Rodamina-alexafluor 594	Invitrogen
Goma de silicona	Elastosil R&G Faserverbundwerkstoffe
Solución antibiótica y antimicótica	Gibco
Suero fetal bovino (FBS)	Invitrogen
Sulfato de cobre ($CuSO_4$)	Sigma Aldrich
Tampón fosfato salino (PBS)	Gibco
Trazadores de melanina (1020 nm)	Microparticles GmbH
Trazadores de poliestireno (1101 nm)	Thermo Scientific
Trifluoroetanol (TFE)	Sigma Aldrich
Tripsina-EDTA	Invitrogen
Triton X-100	Sigma Aldrich
Trombina	Sigma
Trypan Blue	Invitrogen

Todas las disoluciones empleadas se preparan utilizando agua tipo I (Millipore) y el pH se ajusta añadiendo pequeñas cantidades de HCl o NaOH 1M.

Las disoluciones acuosas que se emplearán en técnicas que impliquen dispersión de luz serán filtradas a través de membranas de *polifluoruro de vinilideno* (PVDF, Whatman©), de tamaño de

poro de 0,45 μm, para asegurar la eliminación de residuos de polvo que pudieran interferir en la medida de las muestras. Así mismo, la limpieza del material de vidrio o plástico utilizado para esas técnicas se lavan rigurosamente para evitar cualquier presencia de polvo o grasa que pudieran afectar a los valores obtenidos en medidas basadas en la dispersión de la luz. El procedimiento de limpieza conlleva una primera etapa de enjuagado con abundante agua corriente para eliminar posibles restos de polvo, después se lava con agua-jabón (Hellmanex® II) en un baño de ultrasonido durante 15 minutos. Para finalizar, se enjuaga con agua tipo I y el material de vidrio se seca en estufa a 60°C durante 4 horas. El de plástico se seca a 40°C durante 6 horas.

Los estent utilizados fueron producidos en el Institut für Textiltechnik de la universidad RWTH (Aachen, Germany) a partir de un hilo de nitinol de un diámetro de 76 μm (NiTi Nr.1SE; FortWayneMetals, Indiana, USA) con una maquina (Karl Mayer, Obertshausen, Germany), obteniendo una densidad de 12 vueltas por pulgada. Las dimensiones de estos estents son 2,5 cm de alto y 0,6 cm de diámetro.

El resto del material de laboratorio (puntas de pipetas, frascos para liofilizar, placas de cultivo, tubos y diferentes moldes, etc.) se adquieren estériles o bien se esterilizan en autoclave (Autester E-75) a 121°C y 1 atmósfera de sobrepresión durante 20 minutos.

3.1.2. Recombinámeros tipo elastina (ELRs) empleados.

Todos los recombinámeros tipo elastina (ELRs) utilizados en esta tesis han sido diseñados mediante tecnología de ADN recombinante. Este es un proceso multietapa que comienza con el diseño y construcción del gen que codificará la proteína. Sigue con

un proceso de clonación dentro de un vector de clonación específico. Para ello se pueden seguir diferentes estrategia como puede ser la unión de dos oligonucleótidos complementarios sintetizados químicamente[44,45]; mediante la extensión de dos iniciadores complementarios en el extremo 3' terminal[46]; y por último mediante reacción en cadena de la polimerasa (PCR, Polymerase Chain Reaction)[47]. Una vez que el gen monomérico ha sido clonado en el vector de clonación tiene que ser oligomerizado. Esta oligomerización se produce con orientación "cabeza-cola" y se puede realizar siguiendo el método de concatenación o el método iterativo recursivo[48,49]. Cuando la construcción génica final es obtenida se lleva a cabo su clonación dentro de un vector de expresión y este es transfectado dentro las cepas de bacterias *Escherichia coli* adecuadas que llevarán a cabo la bioproducción de los ELRs. Los ELRs así obtenidos son purificados mediante sucesivos ciclos de segregación reversible termo-dependientes. Finalmente y tras un proceso de diálisis en a agua tipo I a 4°C son filtrados para garantizar su esterilidad, liofilizados y conservados a -20°C hasta su ulterior utilización[29,35,50,51].

Los distintos ELRs empleados en esta tesis, junto con su abreviatura y peso molecular (PM) se pueden encontrar en la siguiente tabla (Tabla 2)

Tabla 2. *Abreviatura, estructura y PM de los ELRs empleados*

Abreviatura	Composición de aminoácidos	PM (kDa)
VKVx24	MESLLP VG VPGVG [VPG**K**G(VPGVG)$_5$]$_{23}$ VPG**K**G VPGVG VPGVG VPGVG VPGV	60,5
HRGD6	MGSSHHHHHHSSGLVPRGSHMESLLP [(VPGIG)$_2$(VPG**K**G)(VPGIG)$_2$]$_2$AVTG**RGD**SPASS[(VPGIG)$_2$(VPG**K**G)(VPGIG)$_2$]$_2$	60,6
REDVx10	MESLLP[(VPGIG)$_2$(VPG**K**G)(VPGIG)$_2$EEIQIGHIP**REDV**DY HLYP(VPGIG)$_2$(VPG**K**G)(VPGIG)$_2$(VGVAPG)$_3$]$_{10}$V	83.1

Los tres recombinámeros son polímeros ricos en el aminoácido lisina lo que les confiere un pH básico en disolución acuosa.

En el caso del VKVx24, este es un polímero estructural que no posee ningún tipo de secuencia bioactiva y está basado en la repetición del pentámero VPGVG siendo sustituida la valina situada entre las valinas por una lisina una de cada 5 veces. Este polímero tiene un peso molecular total de 60,5 kDa. Los ELRs HRGD6 y REDVx10 son polímeros basados en la repetición del monómero VPGIG y ambos comparten la característica de que poseen secuencias bioactivas que promueven la adhesión celular. En el caso del HRGD6 esta es una secuencia de adhesión general formada por los aminoácidos arginina, glicina y ácido aspártico (RGD). El HRGD6 tiene un peso molecular de 60,6 kDa. En el caso del REDVx10 la secuencia bioactiva es una secuencia de adhesión celular específica para células endoteliales formada por los aminoácidos arginina, ácido glutámico, ácido aspártico y valina (REDV). Este ELR tiene además una segunda secuencia bioactiva repetida tres veces a lo largo de la cadena polimérica, formada por el hexapéptido valina, glicina, valina, alanina, prolina y glicina (VGVAPG), que es reconocida por enzimas elastasas, esta secuencia una vez liberada por la acción proteolítica presenta propiedades bioactivas adicionales, como control y modulación de la proliferación y migración celular entre otras. El REDVx10 es un polímero más grande que tiene un peso de 83,1 kDa.

3.1.3. Modificación química de ELRs

Los ELRs anteriormente descritos se modificaron químicamente. El grupo amina de las lisinas se utilizó para incorporar grupos azida o alquino en la estructura de los ELRs

3.1.3.1. Modificación con azidas

La modificación de los ELRs para la obtención de los derivados que contienen grupos azida se lleva a cabo mediante una reacción de diazotransferencia usando azida tríflica como reactivo y una sal de cobre (II) como catalizador, esta reacción se realiza en diclorometano como disolvente. De esta forma se consiguen grados de conversión de entorno al 70-90%.

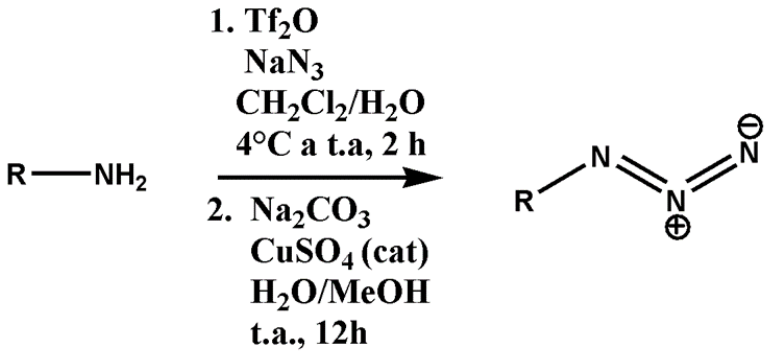

Figura 1. Esquema de la reacción de funcionalización con azidas

Para esta reacción la azida tríflica se tiene que preparar justo antes de ser usada, para ello se disuelve Azida sódica (100 equivalentes) en 14 mL de agua ulta-pura y 17 mL de cloruro de metileno. La mezcla de reacción se agitó a 4°C y se añadió gota a gota una disolución de anhídrido tríflico (20 equivalentes). Se mantuvo a baja temperatura durante una hora y posteriormente se agitó a temperatura ambiente (t.a.) durante otra hora más. El crudo de reacción se decantó y las fases orgánicas se lavaron con agua

ulta-pura (2x10 mL) y con una disolución saturada de carbonato sódico (2x10 mL). La disolución de azida tríflica resultante se utilizó sin más purificaciones. Esta disolución se añadió gota a gota a una disolución de ELR (1 eq), carbonato sódico (1,5 eq.) y sulfato sódico (0,01 eq.) en agua ultra-pura (24 mL) y metanol (4 mL). El crudo de reacción se agitó a temperatura ambiente durante toda la noche. Los disolventes orgánicos se eliminaron a baja presión. Los ELRs así modificados se purificaron por diálisis a 4°C, posteriormente se filtraron y liofilizaron para obtener el ELR ya modificado (ELR-azida) con rendimientos superiores al 85%. Los ELRs ya modificados se caracterizaron mediante FTIR, MALDI-TOF y DSC[52].

3.1.3.2. Modificación con alquinos

La modificación de los ELRs para la obtención de los derivados que contienen grupos alquinilo se lleva a cabo mediante una reacción de amidación mediante la utilización de un anhídrido.

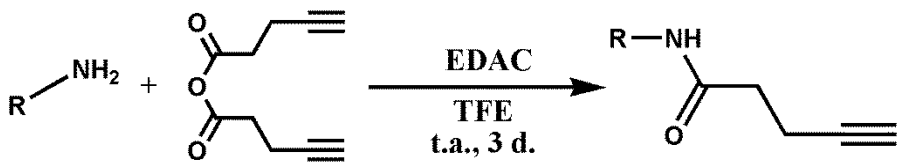

Figura 2. Esquema de la reacción de funcionalización con alquinos

A una disolución de ELR (1 eq.) en TFE (10 mL) se le añadió anhídrido pentinoico (10 eq.) y EDAC (5 eq.) y se agitó a t.a. durante tres días. Los disolventes orgánicos se eliminaron a baja presión. Los ELRs así modificados se purificaron por diálisis a 4°C, posteriormente se filtraron y liofilizaron para obtener los ELR modificados con los grupos alquino (ELR-alquino), en rendimientos superiores al 89%. Los ELRs ya modificados se caracterizaron mediante FTIR, MALDI-TOF y DSC[52].

3.1.3.3. Modificación con ciclooctinos

La modificación de los ELRs para la obtención de los derivados que contienen grupos ciclooctino se lleva a cabo mediante una reacción de amidación en DMF, pudiendo controlar estequiométricamente el grado de sustitución obtenido.

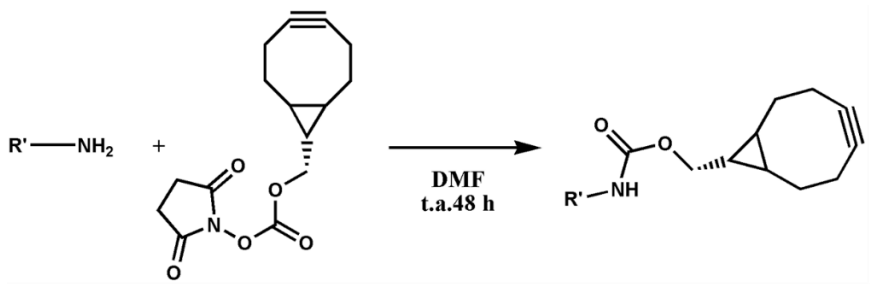

Figura 3. Esquema de la reacción de funcionalización con ciclooctinos

Una disolución de carbonato de (1R,8S,9S)-biciclo[6.1.0]non-4-in-9-ilmetil succinimidilo (0,6 eq.) en DMF (1 mL) se añadió gota a gota y a t.a, a una disolución de ELR (1 eq.) en DMF (5 mL). La mezcla se agitó a t.a. durante 48 horas. Transcurrido ese tiempo se añaden 15 mL de EtO_2 y se obtiene un precipitado que es centrifugado a 10000 r.p.m. El sobrenadante se descarta y el precipitado se lava con acetona (3x15 mL) y se seca a presión reducida. El sólido obtenido se disuelve en agua ulta-pura (20 mL) a baja temperatura (4°C) y se dializa en agua ulta-pura (3x25 L), se filtra y liofiliza para obtener finalmente el ELR modificado (ELR-ciclo) y estéril. El rendimiento de esta reacción fue superior al 92% en todos los casos. Los ELRs ya modificados se caracterizaron mediante FTIR, MALDI-TOF y DSC[52].

3.1.4. Incorporación de sondas fluorescentes a los ELRs.

La incorporación de sondas fluorescentes se realizó mediante una reacción click, en este caso una cicloadición de Huisgen[53] (ver

figura 4), aprovechando la funcionalización con grupos azida o ciclooctinos introducidos en los ELRs como se ha descrito en los subapartados anteriores.

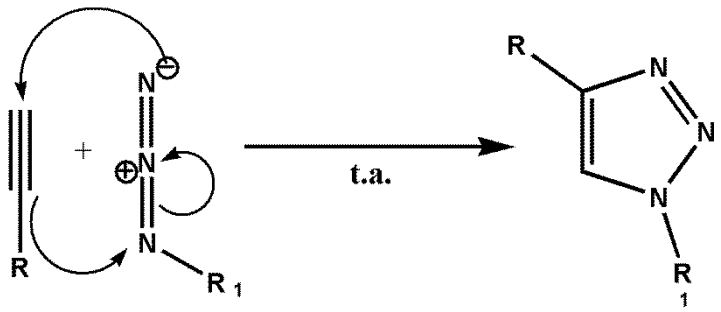

Figura 4. Esquema general de la cicloadicion de Huisgen (reacción click).

3.1.4.1. Incorporación de una sonda fluorescente a un ELR-azida

Sobre una disolución de HRGD6-azida (1 eq.) en DMF (4 mL) se añade una disolución de Acetylene Fluor 488 (0,083 eq.) en DMF (0,5 mL) a t.a., adoptando la mezcla un color verde amarillento. Sobre la mezcla se añade una nueva disolución de $CuSO_4$ (0,011 eq.) y L ascorbato sódico (0,029 eq.) en agua ultra-pura (200 μL). Al añadir esta disolución la mezcla adquiere un intenso color rosa. El crudo de reacción se agitó durante dos días. Sobre la mezcla se añadió EtO_2 (17,5 mL) apareciendo un precipitado rosa que se decantó tras centrifugarlo a 10000 r.p.m. El sólido se lavó con acetona (3x10 mL). A continuación, se secó mediante evaporación a baja presión y se purifico mediante diálisis en agua ultra-pura (3x25 L), posteriormente se liofilizó para obtener un sólido de color rosa, HRGD6-acet-fluor, con un rendimiento superior al 80%.

3.1.4.2. Incorporación de una sonda fluorescente a un ELR-Ciclooctino

Sobre una disolución de VKVx24-ciclo (1 eq.) en DMF (5 mL) se añadió una disolución de EterneonTM-Azide (480/635) (0,083 eq.) en DMF (0,5 mL) a t.a. bajo atmósfera de nitrógeno (globo). La disolución naranja que se obtiene se agita a t.a. durante tres horas, transcurrido ese tiempo se añadió EtO_2 (17,5 mL) apareciendo un precipitado naranja que se decantó tras centrifugarlo a 10000 r.p.m., El sólido se lavó con acetona (3x10 mL), a continuación, se secó mediante evaporación a baja presión y se purifico mediante diálisis en agua ultra-pura (3x25 L). Posteriormente se liofilizó para obtener un sólido de color naranja, VKVx24-eterneon, con un rendimiento superior al 89%.

3.2.Métodos

3.2.1. Preparación de geles de fibrina

Es bien sabido que la reacción entre el grupo γ-carboxiamina de la glutamina (Q) y el grupo ε-amino de la lisina (K) se ve favorecido por la presencia de la enzima transglutaminasa (factor XIII), el cual es dependiente de la presencia de cationes Ca^{2+} (Figura 5). Para obtener este tipo de geles se disuelve fibrinógeno en concentraciones variables, desde 2,5 hasta 15 mg/mL en TBS. Se prepara una segunda disolución que contiene un 30% de trombina y un 30% de $CaCl_2$ en TBS.

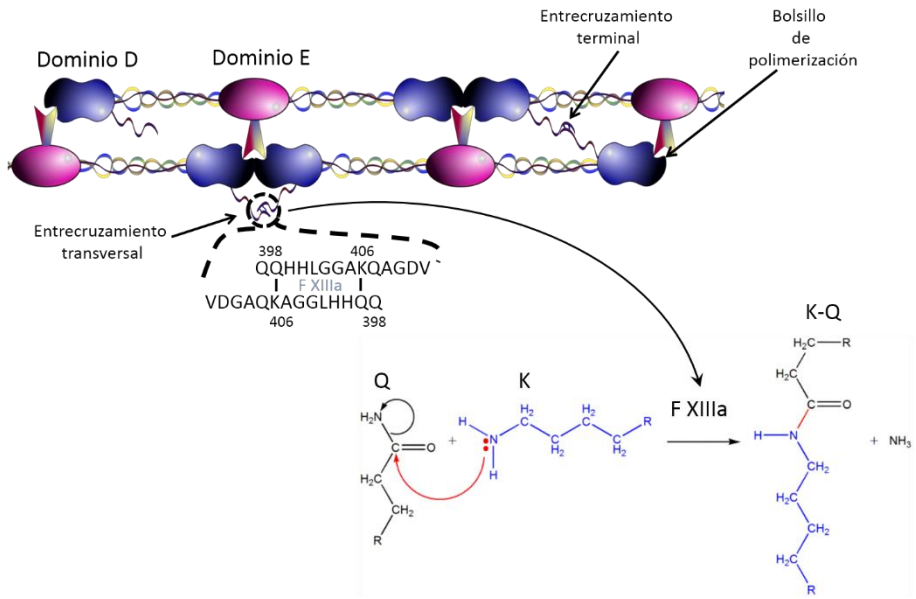

Figura 5. Esquema general de la formación de los geles de fibrina

Las dos soluciones se mezclaron homogéneamente en el molde apropiado a t.a. y se mantienen en el molde durante al menos 15 minutos. Después de este periodo, el gel ya formado y puede sacarse fácilmente del molde. Con este procedimiento y distintos moldes se han obtenido geles de fibrina de distintas concentraciones.

3.2.2. Preparación de geles híbridos de ELR y fibrina

Para obtener geles híbridos, se prepararon dos disoluciones, una de fibrinógeno y ELR en una proporción 1:1 y en concentraciones, de cada componente, variables desde 2,5 hasta 15 mg/mL en TBS. La segunda disolución contiene un 30% de trombina y un 30% de $CaCl_2$ en TBS. El proceso enzimático en el que está basado este entrecruzamiento se ilustra en la figura 6

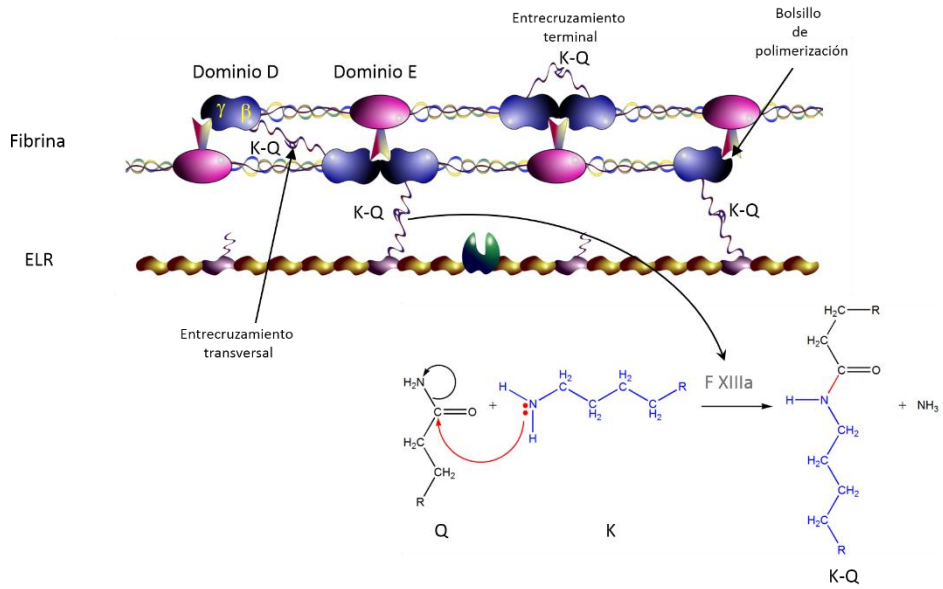

Figura 6. Esquema general de la formación de los geles híbridos ELR-fibrina

Las dos soluciones se mezclaron homogéneamente en el molde apropiado a t.a. y se mantuvieron en dicho molde durante al menos 15 minutos. Después de este periodo, el gel ya se ha formado y puede sacarse fácilmente. De esta forma se han obtenido geles híbridos de distintas geometrías y formas (cuya preparación se detallará más adelante) dependiendo del molde utilizado.

3.2.3. Preparación de geles de ELRs mediante tecnología "click" con catalizador

Para la preparación de geles de ELRs mediante la química click con catalizador se prepararon por separado disoluciones a 4°C, en agua ultra-pura de los biopolímeros anteriormente descritos ELR-azida y ELR-alquino; en concentraciones variables de entre 25 y 125 mg/mL con una proporción molar entre grupos alquino y azida 1:1. Las disoluciones equivalentes de ambos ELRs se mezclaron para obtener una disolución homogénea de ambos componentes.

Se preparó una segunda disolución, en agua ultra-pura, conteniendo ascorbato sódico y sulfato de cobre ($CuSO_4$). Ambas disoluciones se mezclaron a baja temperatura y en una relación molar azida: $CuSO_4$:ascorbato fue de 12:1:3 (dicha relación molar se obtuvo tras un proceso de optimización y con el fin de minimizar la cantidad de catalizador utilizado y así no comprometer la viabilidad celular en la aplicación final). La reacción que tiene lugar está repesentada en la figura 7.

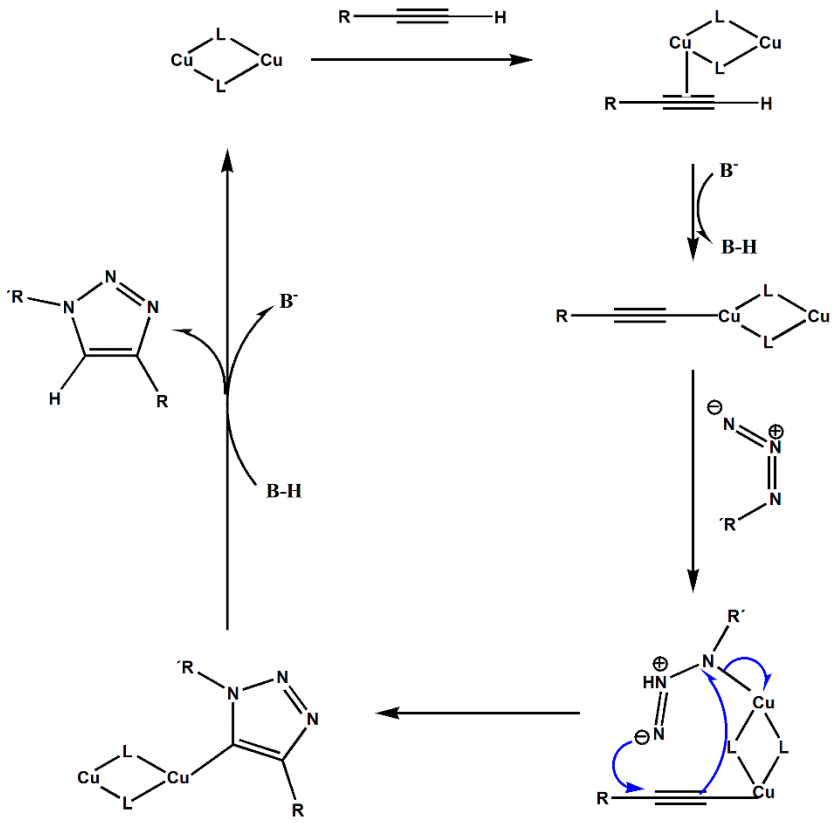

Figura 7. Esquema general de la formación de los geles de ELRs mediante metodología click con catalizador

La mezcla se depositó en un molde cilíndrico de 13,5 mm de diámetro y 2 mm de alto a 4°C. Se mantuvo a baja temperatura durante 5 minutos y posteriormente 1 hora más a temperatura ambiente para finalizar el proceso de gelificación. Para embeber

células dentro del gel se añadirá una suspensión de las mismas a la disolución que contiene los ELRs, y las disoluciones se llevarán a cabo en el medio de cultivo adecuado para cada tipo de célula, en vez de en agua ultra-pura.

3.2.4. Preparación de geles de ELRs mediante tecnología "click" sin catalizador

Con el fin de preparar geles de ELRs mediante la tecnología click sin catalizador se prepararon dos disoluciones, una de cada uno de los polímeros anteriormente descritos (ELR-azida y ELR-ciclo) a la concentración deseada (de 25 a 150 mg/mL) en agua ultra-pura y a baja temperatura (4°C).

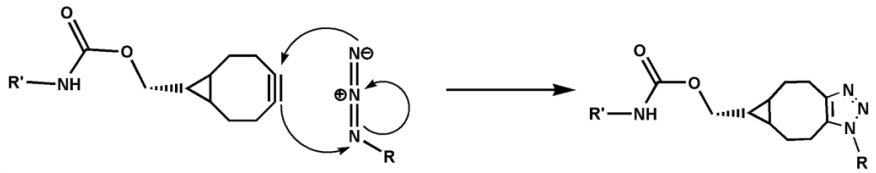

Figura 8. Esquema general de la formación de los geles de ELRs mediante metodología click sin catalizador

Ambas disoluciones mantuvieron a esa temperatura durante una noche para conseguir la total disolución de los ELRs modificados, se mezclaron en frio y depositaron en el molde adecuado para obtener los geles con la forma deseada. Transcurridos 20 minutos y a baja temperatura los geles están completamente formados y pueden ser extraídos del molde. En la figura 8 se puede observar la reacción que tiene lugar entre el grupo azida y el triple enlace del ciclooctino para formar un ciclo de cinco eslabones.

Alternativamente, si se quieren incluir células dentro de estos hidrogeles, se pueden suspender las células en la disolución de ELR-

ciclo. En este caso las disoluciones han de ser preparadas en PBS o en el medio de cultivo apropiado para el tipo de célula.

3.2.5. Preparación de hidrogeles para medidas reológicas.

Independientemente del tipo de gel que se vaya a preparar, híbrido, click catalizado por cobre o sin catalizador, el molde usado para su caracterización física y mecánica fue el mismo. Este es un molde de teflón con base móvil de PDMS, con unas dimensiones de 13,5 mm de diámetro y 2 mm de altura. Todos los geles, independientemente del tipo que sean, se prepararán de 600 μL volumen, si hubiese alguna variación en este método se especificará en el capítulo correspondiente de esta tesis. Las disoluciones de los distintos polímeros se mezclan en el molde a la temperatura anteriormente mencionada para cada tipo de gel y en las condiciones ya dichas.

3.2.6. Obtención de nanogeles mediante tecnología click sin catalizador.

Para la obtención de nanogeles mediante tecnología click sin catalizador se prepararon disoluciones de ELR-azida y ELR-ciclo en agua ultra-pura, en concentraciones lo suficientemente bajas (0,1; 0,5 y 1 mg/mL) como para que no se produjera el proceso sol-gel. De esta forma, todas las muestras eran homogéneas y la presunción ergódica permanece siendo válida. Dichas disoluciones se filtraron a través de un filtro de jeringuilla de PVDF con un tamaño de poro de 0,45 μm) y se mantuvieron a 4°C durante toda la noche. Posteriormente las disoluciones de ambos componentes, con las mismas concentraciones, se mezclaron a 4 y a 37°C para obtener los nanogeles. Las disoluciones mezcla se mantuvieron a 4 o 37°C respectivamente durante 24 horas.

3.2.7. Recubrimiento de superficies por multicapas de ELR mediante tecnología click sin catalizador

En el recubrimiento de superficies mediante la sucesión de capas reactivas de ELRs cada capa está formada por dos subcapas y cada una de ellas se obtiene con una disolución de ELR modificado con azida o cilcooctino respectivamente marcados con una sonda fluorescente. Las distintas superficies fueron previamente activadas mediante tratamiento previo con plasma de argón y oxígeno de manera que quedan cargadas negativamente al dejar grupos O^- expuestos en la superficie. La primera subcapa fue de VKVx24-eterneon (derivado del VKVx24-ciclo), el cual tiene lisinas cargadas positivamente que interactúan electrostáticamente con la superficie del sustrato cargado negativamente. La segunda subcapa aplicada será de HRGD6-acet-fluor (derivado del HRGD6-azida) que reaccionará químicamente con la primera subcapa para formar la primera capa completa, esta segunda subcapa reacciona de nuevo con la siguiente capa de VKVx24-eterneon y así sucesivamente. Este proceso se puede realizar de dos formas diferentes. La primera consiste en inmersiones de 15 segundos alternativas y sucesivas en cada disolución de recombinámero, con un periodo de secado de dos minutos entre cada inmersión; y la segunda requiere de una etapa de lavado en agua ultra-pura de cinco minutos previa al paso de secado de cada capa.

3.2.8. Preparación de ELR-Bioestents.

La preparación destents recubiertos con hidrogeles ELRs para su posterior endotelización se llevó a cabo mezclando las disoluciones de ELR-azida y ELR-ciclooctino, obtenidas como anteriormente se ha descrito en los apartados 4.1.3.1 y 4.1.3.3, en un molde que

consta de las siguientes partes: bases, cilindro interior, estent metálico y cilindro hueco exterior. El molde se monta de tal forma que el estent quede concéntrico con los dos cilindros, interior y exterior y sin tocarlos. El cilindro interior tiene un diámetro de 5,5 mm y el exterior de 8 mm. (Figura 9)

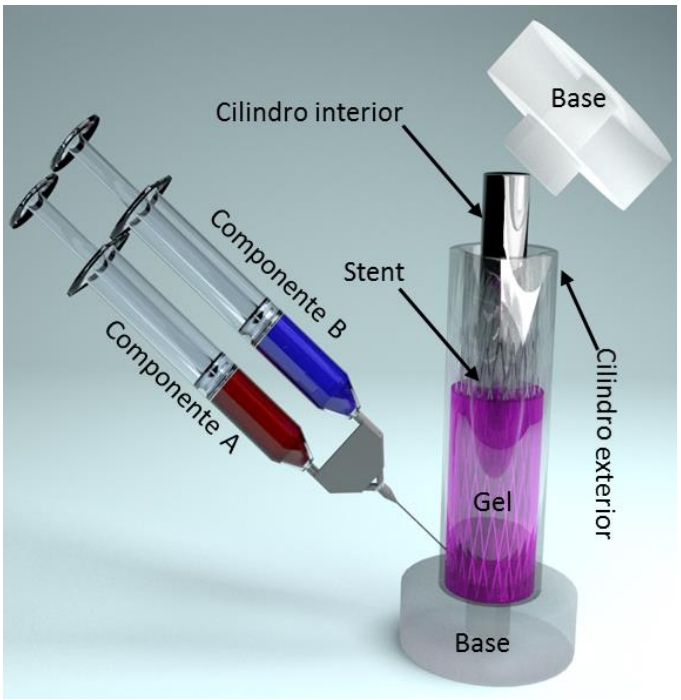

Figura 9. Esquema del proceso de recubrimiento con gel del estent metálico.

Se probaron distintas concentraciones de las disoluciones de partida para obtener el mejor recubrimiento optimizando la cantidad de material necesitado. Finalmente se eligió una concentración de 75 mg/mL. De esta forma se prepararon ELRs-Bioestents con distinta biofuncionalización según el biopolímero utilizado.

3.2.9. Preparación válvulas aórticas

La preparación de válvulas aorticas se llevó a cabo usando un molde para tal efecto. El molde utilizado tiene un diámetro de 15 mm y como se puede observar en la figura 10, consta de las siguientes partes: cilindro de silicona con red cosida para mejorar la sujeción de la válvula (Imagen A), cubiertas laterales (Imágenes B y E), parte superior del molde con dos orificios para la inyección de las disoluciones que formarán los geles (Imagen C), base del molde (Imagen D). Todas estas partes se ensamblan como se ve en las imágenes F y G de la misma figura 10. Las disoluciones de los polímeros se inyectan a través de los agujeros de la parte superior del molde, como también se muestra en la imagen G de la figura 10. Después de un tiempo no inferior a 45 minutos y no superior a 60 minutos se abre el molde y se extrae cuidadosamente la válvula formada. Esta válvula tiene las valvas unidas como se puede apreciar en la imagen H de manera que la apertura de las valvas se realiza mediante un corte cuidadoso y preciso, mediante bisturí. Este proceso se puede realizar con células embebidas dentro del gel, para ello primero se habrán esterilizado todas las partes e instrumentos necesarios para montar y desmontar las piezas del molde de la válvula y este proceso se realizará en campana de flujo laminar en condiciones estériles. Cualquier modificación de este método se especificará en el capítulo correspondiente de esta tesis.

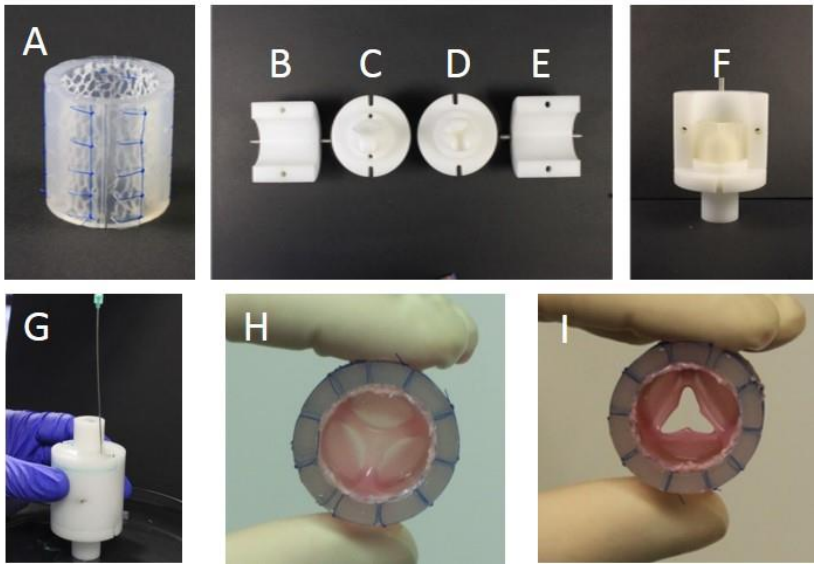

Figura 10. Partes del molde utilizado para preparar válvulas aórticas (A-F), proceso de inyección de los componentes (G) y válvula con las valvas cerradas (H) y abiertas (I).

3.3.Técnicas experimentales de caracterización y análisis

3.3.1. Calorimetría diferencial de barrido

El estudio de una de las características fundamentales, la temperatura de transición de los ELRs, y por extensión de todos los geles y estructuras formadas con ellos; se llevó a cabo mediante la calorimetría diferencial de barrido (Differential scanning calorimetry, DSC). Estos análisis se realizaron en un DSC Mettler Toledo 822e equipado con un controlador de temperatura, refrigerado con nitrógeno líquido y calibrado con muestras patrón de indio, zinc y *n*-octano. Para el análisis de los ELRs, se depositaron 20 μL de una disolución de concentración 50 mg/mL en agua ultra-pura en un crisol de aluminio de 40 μL sellado herméticamente. Como referencia se utilizó el mismo volumen de agua ultra-pura. Para el análisis de hidrogeles, se colocaron en el crisol 20 mg del gel hidratado como muestra. Para conocer

exactamente la cantidad de material que se usó en cada análisis, la muestra se liofilizó y pesó después de cada análisis. Los experimentos consistieron en una primera etapa isotérmica a 0°C durante 5 minutos, seguidos de una rampa de calentamiento a velocidad constante de 5°C/min desde 0 hasta al menos 50°C. Cualquier variación de este método será detallada en el capítulo en donde se produzca esa modificación.

3.3.2. Análisis de porosidad e hinchamiento

La medida de la porosidad de los distintos tipos de hidrogeles se llevó a cabo en base a la siguiente ecuación:

$$porosity\ (\%) = \left(\frac{W_1 - W_2}{d_{water}}\right) \times \frac{100}{V}$$

donde W_1 y W_2 se corresponden con el peso del hidrogel hidratado y liofilizado respectivamente, d_{water} es la densidad del agua pura y V es el volumen real del hidrogel en estado hidratado.

El porcentaje de hinchamiento ($Q_w(\%)$)se estimó según la ecuación:

$$Q_w(\%) = \frac{W_1 - W_2}{W_2} \times 100$$

Todas las mediciones se llevaron a cabo después de al menos una noche con el gel sumergido en agua a 4 o 37°C, según el caso. El exceso de agua superficial fue eliminado con un papel de filtro antes de cada medida.

3.3.3. Medidas reológicas

Las medidas de las propiedades mecánicas de los hidrogeles fueron evaluadas mediante ensayos reológicos, en un reómetro de

esfuerzo controlado (AR200ex, TA Instruments) equipado con una placa Peltier para controlar la temperatura en los ensayos de medidas del módulo de cizalla dinámico (medida de la rigidez dinámica de la matriz).

Las medidas se realizaron a dos temperaturas distintas, 4 y 37°C (por debajo y por encima de la temperatura de transición de los ELRs utilizados). Se utilizó una geometría de platos paralelos de 12 mm de diámetro, se aplicó una fuerza normal mínima y suficiente para evitar el deslizamiento de la muestra, y en consecuencia falsos resultados en las medidas. En primer lugar se realizó un barrido de amplitud para confirmar que las muestras se encontraban dentro de la región de viscoelasticidad lineal. Las medidas del módulo complejo (G^*), módulo de almacenamiento (G'), módulo de pérdidas o viscoso (G'') y tangente del ángulo ($\tan \delta$) se llevaron a cabo en función de la frecuencia (entre 0,1 y 10 Hz) con una deformación constante de un 1%.

3.3.4. Microscopía óptica y electrónica de barrido

El análisis morfológico de la microestructura de los geles y sistemas desarrollados en esta tesis se realizó, entre otras técnicas, por microscopía óptica con un microscopio Nikon ECLIPSE 80i mediante contraste interdiferencial (DIC).

También se ha evaluado la morfología superficial de las muestras (con células en algunos casos) mediante el uso de microscopía electrónica de barrido (SEM), con un equipo JEOL, JSM-820. Los procedimientos empleados para fijación y tratamiento de muestras previos al análisis microscópico fueron variados según del tipo de muestra a analizar y será detallado en el capítulo correspondiente de esta tesis.

3.3.5. Crio-Microscopía de transmisión electrónica

La visualización de los nano-geles se realizó mediante crio-microscopía electrónica de transmisión (Cryo-TEM). Estas medidas se llevaron a cabo en un microscópico JEOL JEM-FS2200 operado a un voltaje de 200 kV. Las muestras se colocaron en unas rejillas de cobre recubiertas de carbono y pre-tratadas por plasma. Se congelaron por medio de un criostato de la marca Gatan Cryopungle CP3. Se utilizó el modo "zeroloss" para mejorar el contraste de las imágenes.

3.3.6. Medidas de micro-reología, tamaño y potencial Z

Las medidas de dispersión dinámica de luz (DLS), de potencial Z y de micro-reología se llevaron a cabo usando un aparato Zetasizer Nano ZSP (Malvern Instruments) equipado con un láser de Helio-Neón a una longitud de onda de 633 nm.

Detalles más precisos sobre el tratamiento de cada muestra para cada una de las técnicas anteriores se podrán encontrar en el capítulo correspondiente de esta tesis.

3.3.7. Análisis de aminoácidos.

Para las muestras que lo requerían se realizaron análisis de aminoácidos en el Servicio Científico Técnico de la Universidad de Barcelona (España). Los aminoácidos se derivatizaron mediante hidrólisis con HCl y se analizaron por HPLC (Waters 600 HPLC) con un detector ultravioleta (Waters 2487). Cada muestra se analizó por triplicado.

3.3.8. Determinación del peso molecular

Los análisis para determinar el peso molecular de los polímeros, se han llevado a cabo en la Unidad de Proteómica (CRG/UPF) de la Universidad de Barcelona (España) mediante el sistema MALDI-TOF MS en un espectofotómetro de masas modelo Applied Biosystems Voyager STR.

3.3.9. Análisis por Espectroscopia de Fotoelectrones emitidos por Rayos X (XPS)

Las modificaciones producidas en las capas exteriores (1-10 nm) de las superficies fueron seguidas por XPS. Se utilizó un espectómetro Physical Electronics (PHI) 5500 equipado con una fuente monocromática de rayos X (banda Al-Ka con una energía de 1486,6 eV y 300 W de potencia), la presión en la cámara de análisis se fijó en 10^{-7} Pa. Todas las medidas se realizaron con un ángulo de 45° entre en analizador y la fuente de rayos X. Los escáneres se tomaron en el rango de 0 a 1100 eV y se obtuvieron escáneres de alta resolución para los picos de C_{15}, N_{15} y O_{15}. La composición elemental de la superficie se determinó en base al área bajo los picos de fotoemisión de los diferentes átomos modificados por sus correspondientes factores de sensibilidad.

3.3.10. Medidas de microscopía de fuerza atómica (AFM)

La topografía de las distintas superficies y sus propiedades mecánicas fueron obtenidas mediante el modo Peak Force Scan Asyst (QNM). Con una sonda AFM probe: TAP150, TAP525 y SNL-10 (dependiendo de la elasticidad de la muestra). Los experimentos se llevaron a cabo en atmosfera abierta (aire) utilizando el sistema:

Multimode 8, Nanoscope V electronics. Estos análisis se realizaron en la universidad de Barcelona (CCiTUB) (España)

3.3.11. Análisis estadístico

Los resultados se expresan como media ± desviación estándar (SD). Se ha realizado tratamiento estadístico sobre ellos utilizando un método de análisis de varianza (ANOVA) de una vía usando el método de Holm-Sidak. Se ha utilizado un nivel de significación de 0.05. Cualquier modificación sobre este criterio será especificado en la sección correspondiente en cada capítulo.

4. RESULTADOS Y DISCUSIÓN

En esta sección se presentará un resumen de los resultados más significativos de los capítulos 2 a 8 de esta tesis. Resultados y discusiones más detalladas se pueden encontrar en el capítulo correspondiente.

4.1. Geles híbridos de fibrina y recombinámeros tipo elastina (ELRs-FGs): caracterización física y evaluación *in vitro* de su potencial uso en ingeniería de tejidos y aplicaciones cardiovasculares.

En una primera etapa de la tesis se investigó la posibilidad de mejorar las propiedades mecánicas y biológicas de los geles de fibrina ampliamente empleados en el campo de ingeniería de tejidos.

Para ello nos basamos en la reacción que se produce entre el grupo γ-carboxi-amino de las glutaminas del fibrinógeno y el grupo ε-amino de las lisinas de los ELRs[54]. Esta reacción se ve favorecida por la presencia del factor XIII de la enzima transglutaminasa, enzima dependiente del catión Ca^{2+} (ver figura 5 apartado de materiales y métodos)[17] y que se encuentra de forma natural en el plasma de los mamíferos. De esta forma se han generado geles híbridos de fibrina y HRGD6 (ELR-FGs) en concentraciones variables de entre 2.5 a 15 mg/mL, y por otro lado respecto de los geles de fibrina se ha añadido biofuncionalización eles debido a la secuencia bioactiva de adhesión celular (RGD) que porta el ELR.

Primeramente se evaluó la proporción óptima entre ambos polímeros, y debido a que la composición del fibrinógeno comercial

puede ser variable debido a que es aislado de suero humano y la proporción entre los distintos tipos de fibrinógeno varía de un individuo a otro, se determinó que la mejor proporción sería aquella en la que el módulo complejo (|G*|) se maximizase. Obteniéndose un porcentaje de entorno al 50% de ambos materiales (ver resultados en capítulo 2). Una vez determinada la proporción de ambos polímeros se pasó a evaluar sus propiedades físicas y mecánicas. En la figura 1 podemos ver la evolución de los módulos elásticos y de perdidas (G' y G'' respectivamente) y del ángulo (δ) en función de la concentración. Vemos como G' y G'' crecen con la concentración para ambos tipos de geles (híbridos y de fibrina, que sería el control), pero este crecimiento es mayor para el caso de los geles híbridos, siendo esta diferencia significativa a partir de concentraciones iguales o mayores a 10 mg/mL. En el caso de δ este aumento también parece producirse con la concentración, pero siempre obteniendo valores inferiores a 10°. Estos bajos valores de δ nos indican que, en todos los casos, estamos ante geles altamente elásticos. De acuerdo con estos resultados, se puede concluir que la presencia del ELR aumenta las propiedades mecánicas de los geles de fibrina, siendo esta mejora más evidente cuanto mayor es la concentración del gel, posiblemente debido a la mayor cantidad, que no proporción, del ELR.

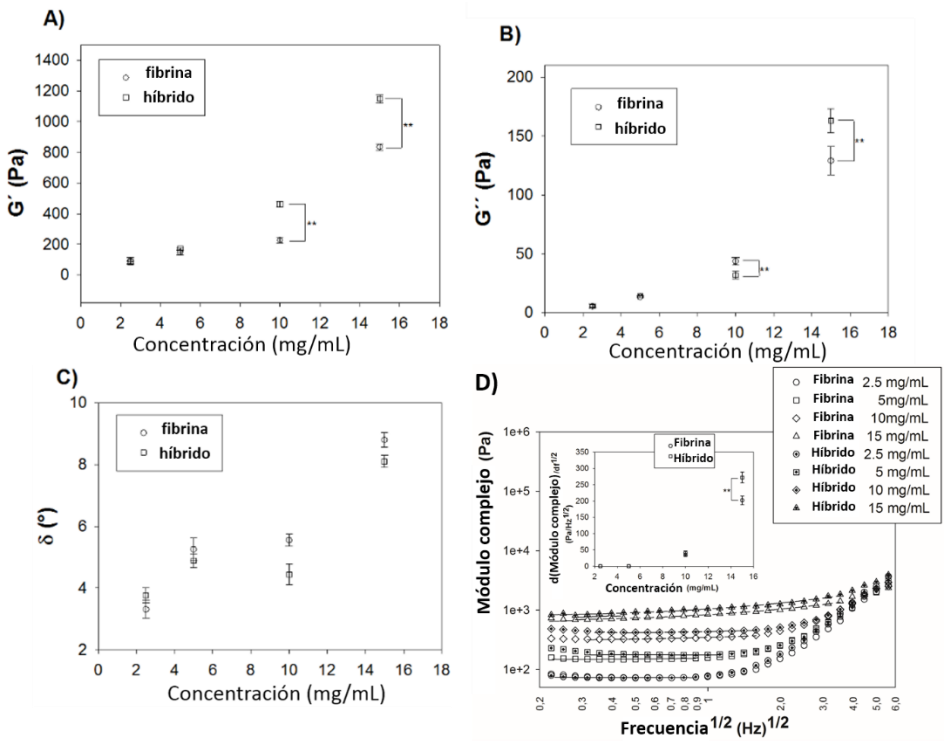

Figura 1. *Evolución de G', G'' y d para geles de fibrina (círculos) y ELR-FGs (cuadrados) como función de la concentración a una temperatura de 37°C.*

Se ha comprobado que este tipo de hidrogeles híbridos, ELR-FGs, poseen un comportamiento visco-elástico ya que el módulo complejo (|G*|) sigue una dependencia lineal respecto a $f^{1/2}$ (Figura 1, imagen D)[52]. La pendiente de esta línea nos indica la permeabilidad de estos geles y se puede comprobar que esta crece al aumentar la concentración. Este hecho se corroboró tras investigar la porosidad y microestructura de dichos geles. En las imágenes SEM (Figura 2) se puede comprobar cómo va variando la microestructura de dichos geles al ir aumentando la concentración. Se puede observar la estructura en fibras típica[18-20] de los geles de fibrina y como entrecruzadas con ellas se aprecian los ELRs. Esta presencia de ELRs es más evidente a concentraciones más altas, donde se puede ver que las hebras de fibrina están más próximas

y los ELRs producen un efecto de malla que interconecta estas hebras de fibrina.

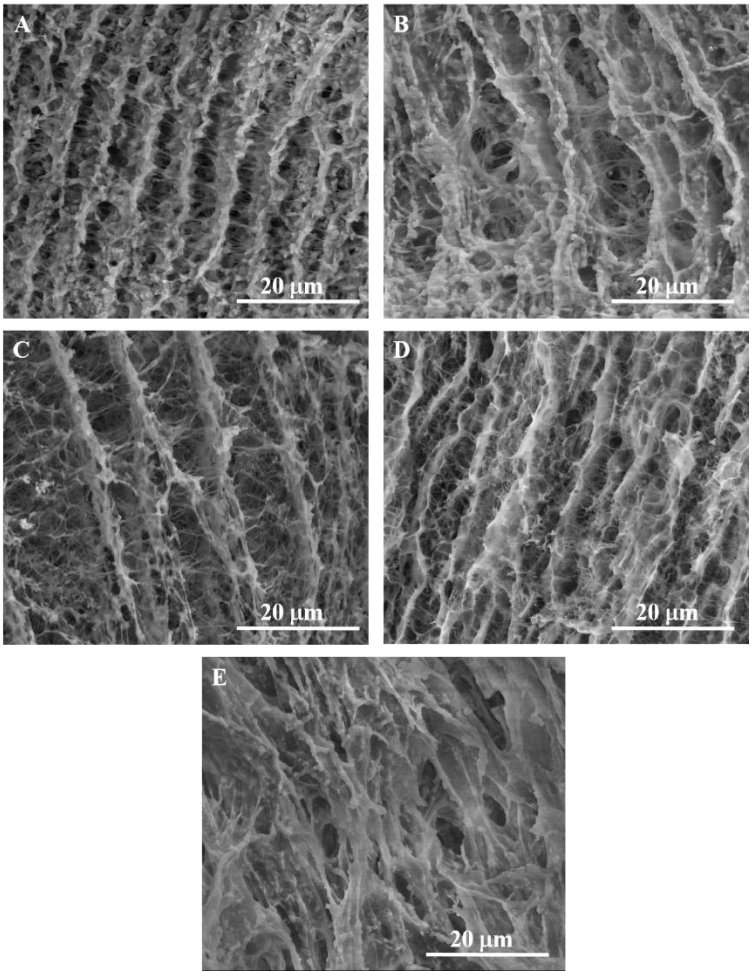

Figura 2. *Imágenes SEM de la microestructura de los ELR-FGs a distintas concentraciones (2.5, 5, 10 y 15 mg/mL, imágenes A, B, C y D respectivamente). Micrografía de un gel de fibrina de 10 mg/mL (E)*

Hay que reseñar que el tamaño de poro disminuye al aumentar la concentración, pasando de un valor de porosidad de entorno a un 90% para concentraciones de 2.5 mg/mL a un valor de entorno al 70% a concentraciones de 15 mg/mL, a 37°C. Estas medidas de porosidad e hinchamiento fueron obtenidas como se

detalla en la sección de materiales y métodos y sus valores están recogidos en la figura 3.

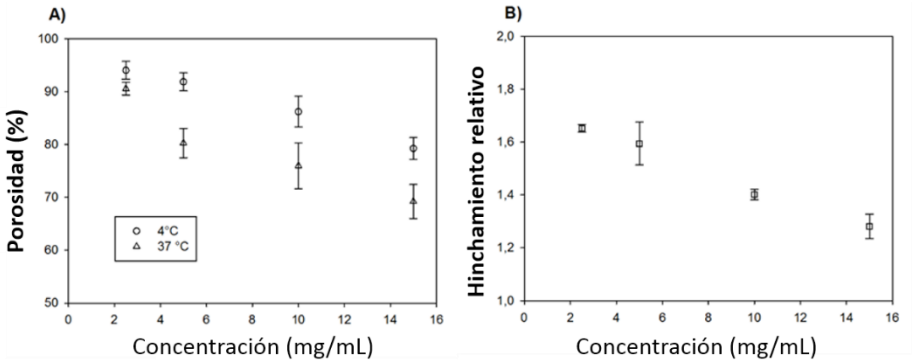

Figura 3. *Porosidad a 4 y 37 °C (A) e hinchamiento relativo (B) de los geles híbridos de ELRs y fibrina*

La presencia de ELR en estos geles quedó patente no solo en las imágenes SEM y en las propiedades reológicas de los mismos, si no que los ELRs aportaron su termosensibilidad a estos geles híbridos, como puede verse en la figura 4. Por debajo de la temperatura de transición de 34°C que se midió mediante calorimetría diferencial de barrido (Figura 4.c estos geles son más transparentes (Figura 4.A) mientras que por encima se vuelven más opacos (menisco más blanquecino en la imagen B de la figura 5).

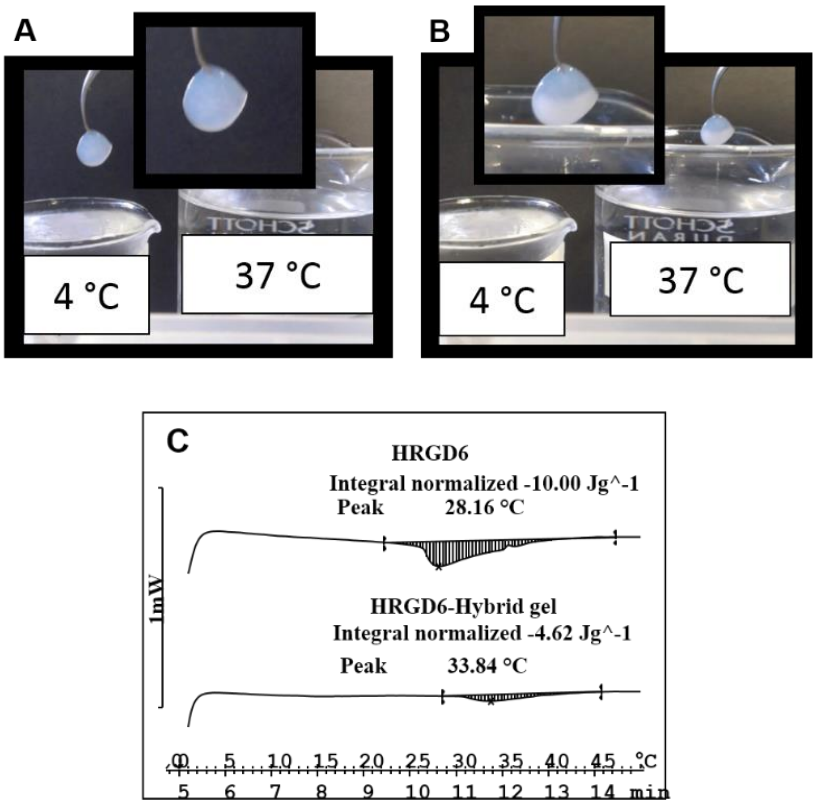

Figura 4. *Comportamiento termosensible de los ELR-FGs. (A) ELR-FG después de estar sumergido 1 minuto a 4°C. (B) ELR-FG tras ser parcialmente sumergido en agua a 37°C, se puede apreciar una "media luna" más blanquecina que es la parte que ha sido sumergida. (C) termograma del ELR HRGD6 (10 mg/mL) y del gel híbrido a la misma concentración (curva superior y curva inferior respectivamente).*

Por lo tanto queda patente que los ELRs han aportado su comportamiento termosensible a este nuevo material híbrido.

Después de esta caracterización física se continuó con la evaluación de la citocompatibilidad del material. Es claro que dicha caracterización es necesaria teniendo en cuenta que las aplicaciones más relevantes de estos hidrogeles pasarán por su combinación con células. Para ello, se embebieron 5 millones por mililitro de células de músculo liso ovinas en ELR-FGs de concentración 10 mg/mL. Se mantuvieron creciendo durante dos semanas durante las cuales se monitorizaron los niveles de glucosa,

lactato, CO_2, O_2 y pH, comprobándose que se mantenían en niveles en concordancia con los de un crecimiento celular normal. Transcurrido ese tiempo, los geles fueron fragmentados, incluidos en parafina, laminados y teñidos contra elastina, a-SMA, colágenos I, III (figura 6 filas 1, 2 3 y 4 respectivamente) y contra vimentina y miosina de cadena ligera (Figura 5, última fila, en este caso el cultivo celular se mantuvo durante 21 días). En dicha figura se puede ver, en comparación con los controles, cómo este tipo de hidrogeles ELR-FGs encapsulan y permiten un crecimiento normal de las células. Se puede observar también cómo las células crecen con normalidad adoptando su fenotipo característico, produciendo fibras de colágeno I y III al igual que a-SMA.

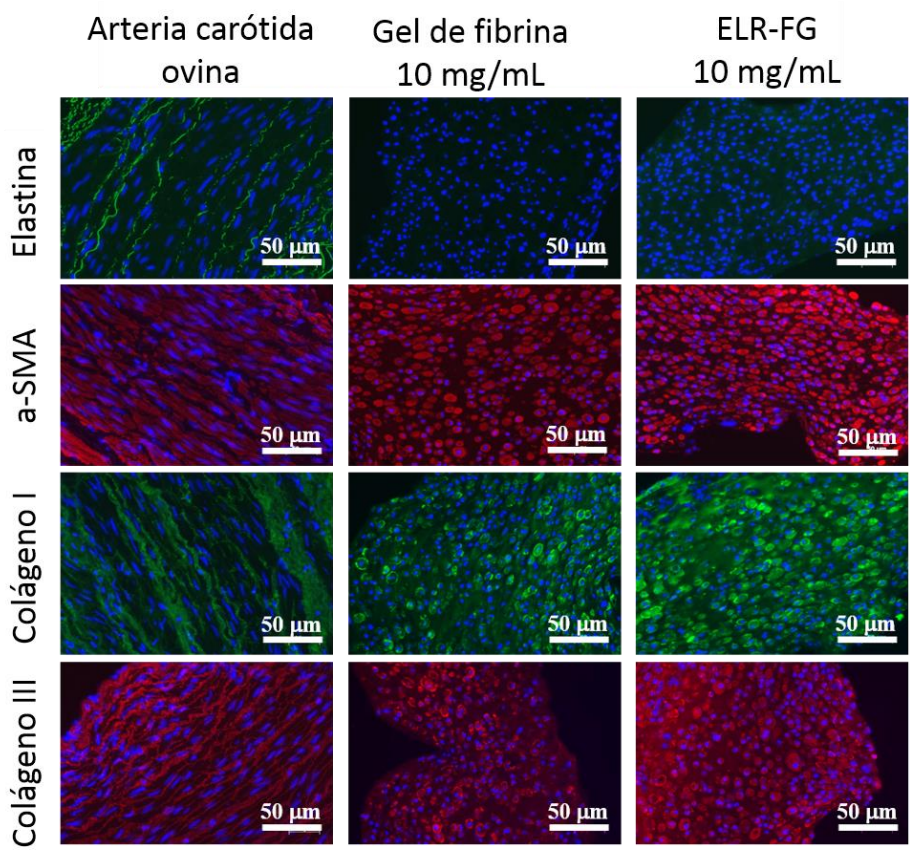

Figura 5. Imágenes de inmunotinciones contra elastina, a-SMA, colágeno I y colágeno III de un trozo de arteria carótida ovina (control positivo) y cultivos 3D de OUSMCs en geles de fibrina y en ELR-FGs.

Tras evaluar la citocompatibilidad de los hidrogeles ELR-FGs se procedió a formar y evaluar estructuras más complejas que simples discos, en concreto se moldearon válvulas aórticas, debido al interés que existe en el desarrollo de nuevas válvulas aórticas como ya se comentó en la introducción. Las válvulas obtenidas a partir de fibrina presentaban importantes problemas al presentar unas inadecuadas propiedades mecánicas para esta aplicación[55], por lo tanto se intentó desarrollar este tipo de prótesis con un nuevo material híbrido con propiedades mecánicas mejoradas con respecto a los geles de fibrina. Se diseñaron y prepararon dichas válvulas con y sin células, según se ha descrito en la sección de

materiales y métodos (cualquier pequeña variación de dicho método puede ser encontrada en el capítulo 2 de esta tesis). También se hicieron lo que denominamos "*bivalves*", en estas válvulas las valvas estaban hechas de geles híbridos ELR-FGs y las paredes de la válvula de gel de fibrina. Para este caso el método se modificó ligeramente, formándose primero las valvas y después las paredes. En la figura 6 se presentan a modo de ejemplo los resultados de una "bivalve", cómo se moldea y cómo las paredes son distintas a las valvas (teñidas con un colorante azul para una mejor visualización). Los resultados se pueden ver en el capítulo 2.

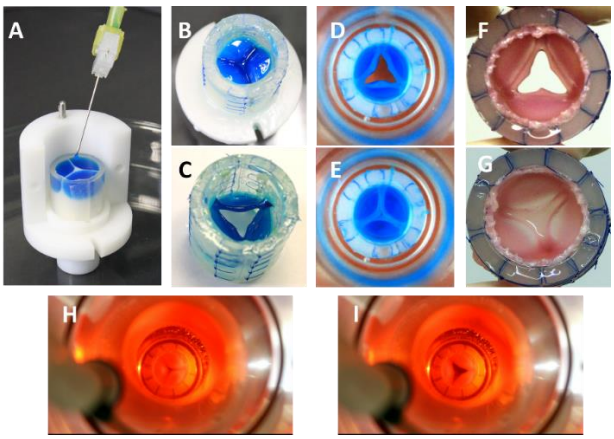

***Figura 6**. Detalle del proceso de formación una "bivalve" (A). Válvula en el molde con las valvas aun cerradas (B), teñidas en azul para una mejor visualización, y con las valvas ya abiertas (C). Válvula abierta (F) y cerrada (G) con células embebidas. Detalle de las válvulas en el bioreactor (D, E, H e I).*

Ambos tipos de válvulas acomodaron a las células perfectamente y estas se desarrollaron sin problema pero después de 21 días de cultivo en estático las valvas no llegaban a cerrar completamente, aunque si es cierto que se observaba una mejoría con respecto a los mismos dispositivos hechos sólo con geles de fibrina[56].

4.2. Geles de Recombinámeros Tipo Elastina mediante tecnología click, con o sin catalizador. Formación y caracterización.

En esta segunda parte de esta tesis se exploró la posibilidad de formar geles únicamente con ELRs en condiciones fisiológicas que nos asegurasen una total citocompatibilidad. Era deseable que las propiedades mecánicas de estos geles fuesen ajustables desde geles muy blandos a geles "duros". También era parte del objetivo de esta segunda apartado que estos geles pudiesen ser aplicados como hidrogel inyectables.

Para ello se pensó en reacciones tipo "click", es decir en una ciclo-adición de Hüisgen en la que un grupo alquino reaccionara con un grupo azida para dar un ciclo de triazol[53,57]. Primeramente se modificaron ELRs introduciéndoles cadenas alifáticas con un triple enlace terminal, y por otro lado se modificaron los grupos amino de las lisinas contenidas en ELRs para convertirlos en grupos azida y así poder llevar a cabo la reacción de ciclo-adición en presencia de un catalizador. En este caso se utilizó una sal de cobre (II) tal y como se muestra en la figura 7.

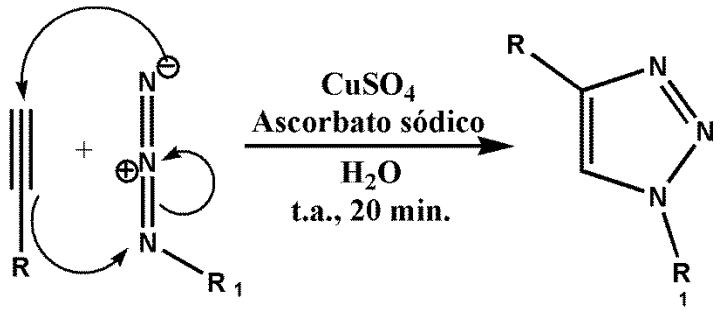

***Figura 7**. Reacción click con cobre.*

Se prepararon geles siguiendo el procedimiento descrito en la sección correspondiente del apartado de materiales y métodos y en el capítulo 3 de esta tesis. Se midieron las propiedades mecánicas de dichos geles al igual que su porosidad e hinchamiento, como ya se ha descrito anteriormente para los geles híbridos de fibrina y ELRs. Dichas porosidades variaban desde el 40% hasta el 98% en función de la concentración y la temperatura, disminuyendo al aumentar la concentración y presentando valores menores a 37°C. El comportamiento es análogo para el grado de inchamiento. Esto es debido a que las cadenas poliméricas se encuentran hidratadas y por lo tanto más extendidas permitiendo una mayor captación de agua lo que nos da como consecuencia mayores hinchamientos y porosidades mayores. Ver figura 8

La porosidad en estos geles disminuye al aumentar la concentración además de haber una reducción al tamaño del poro, y esto se produce no solo por la presencia de un mayor número de cadenas de polímero que se entrecruzan "dividiendo" así a los poros, sino a un aumento del espesor de la pared que rodea a esos poros.

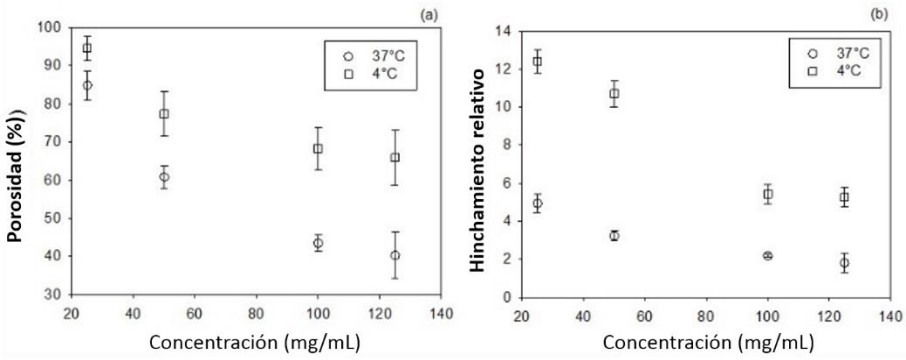

Figura 8. *Porosidad a 4 y 37 °C (A) e hinchamiento relativo (B), de los geles de click con cobre.*

En cuanto a las propiedades mecánicas estos geles muestran valores del G' y G'' que van desde 1kPa a cerca de los 10 kPa (Figura

1), aumentando al aumentar la concentración en el hidrogel y siendo mayores a 37°, es decir por encima de la T_t que a 4°C, por debajo de dicha temperatura. Los valores de la tangente de δ son muy bajos. Como conclusión a estos resultados decir que podemos modular sus propiedades mecánicas con la concentración y que son geles muy elásticos y con propiedades físicas mucho mayores que las encontradas para los geles híbridos ELR-FGs.

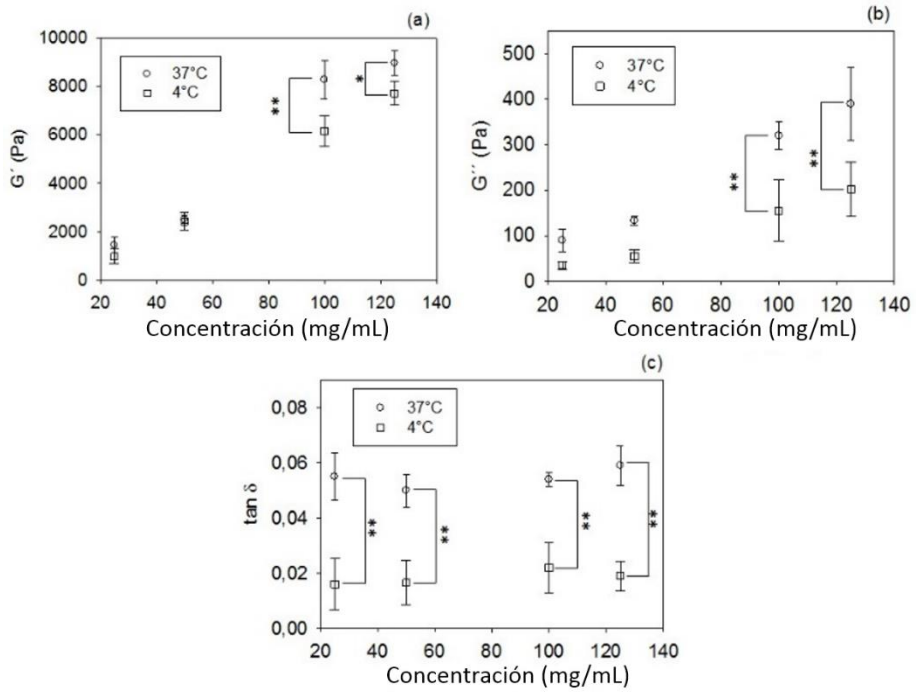

Figura 9. *Evolución de G', G'' y δcorregir de geles de click con cobre a 37°C y 4°C como función de la concentración.*

Estos geles demostraron ser adecuados para reproducir micro-estampados por el método de "replica molding"[50] reproduciendo distintas geometrías como surcos o pilares, y que se puede apreciar en la figura 10.

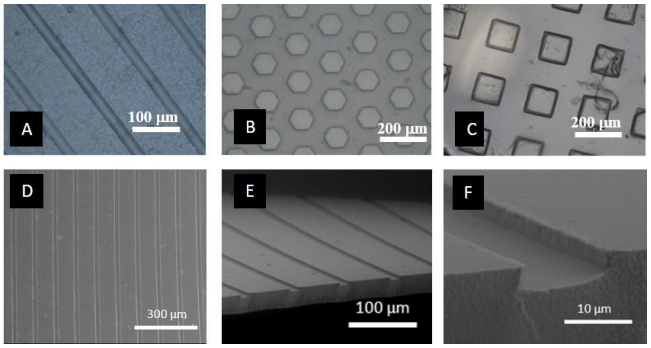

***Figura 10**. Imágenes de microscopía óptica (A, B, C) de diversos micro-estampados obtenidos por la técnica de réplica molding. Imágenes de microscopía electrónica de microsurcos (D) y detalle de los mismos (E, F).*

Como ya se ha descrito, el sistema catalizador utilizado fue una mezcla de ascorbato sódico y sulfato de cobre debido a que este sistema es menos tóxico que el que se puede obtener con otros metales de transición. Los geles se formaron con una proporción 12:1:3 entre ELR:cobre:ascorbato. Con esta relación entre los componentes se evaluó la viabilidad y proliferación de los hidrogeles para distintas líneas celulares (HFF1, HUVEC y MSC). Las células se embebieron en los geles y se pueden ver en diferentes planos focales mediante microscopía óptica. Las tres líneas crecieron y desarrollaron su morfología y estructuras habituales colonizando los geles. Se pueden ver células mesenquimales grandes y estiradas, los fibroblastos adoptan su típica disposición extendia y elongada mientras que las células endoteliales adoptan su morfología poliédrica habitual (Figura 11).

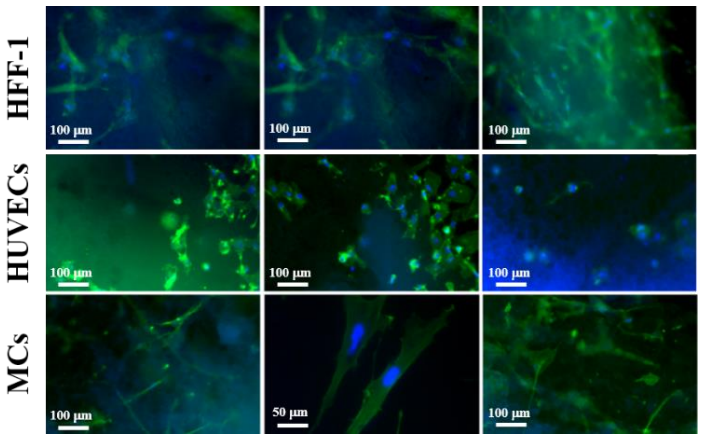

***Figura 11**. Imágenes de microscopía óptica a distintos planos focales de fibroblastos humanos primarios (HFF-1), células endoteliales humanas (HUVEC) y células mesenquimales humanas derivadas de tejido adiposo (MSC) embebidas en geles de click con cobre.*

Se realizaron estudios a más largo plazo (60 días) con MSC embebidas en el gel. En la figura 12 se pueden apreciar distintos planos focales y cómo pasados estos días las células colonizan completamente el material.

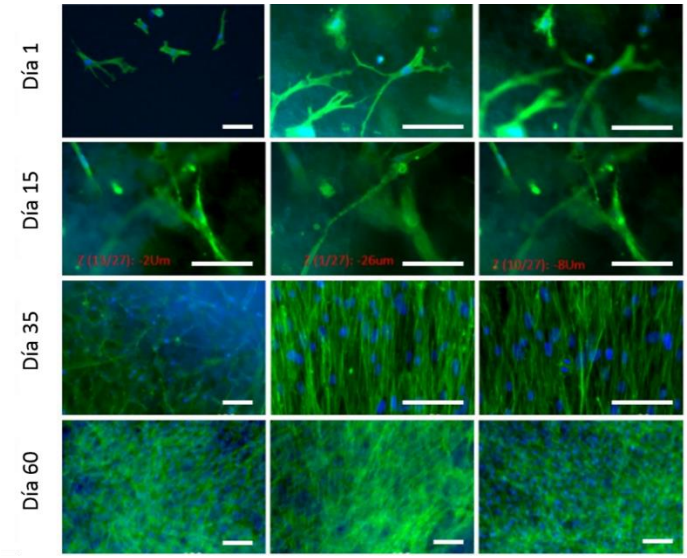

***Figura 12.** Imágenes de microscopía óptica a distintos planos focales de la colonización de células mesenquimales humanas de tejido adiposo (MSC) embebidas en geles de RGD de click con cobre en un periodo de tiempo de hasta 60 días. Escala 100 µm.*

Uno de los mayores problemas que tiene estos geles click catalizados por cobre es la complejidad a la hora de prepararlos pues es necesario preparar cuatro disoluciones distintas, dos disoluciones una con cada ELR otra de ascorbato sódico y otra con la sal de cobre. Estas disoluciones han de ser manejadas a la vez, y si se quieren incluir células tienen que resuspenderse en la disolución que no lleva cobre teniendo que ir en la de ascorbato, y además, aunque la concentración final de cobre en el gel es baja podría afectar a las células. Otro problema es la citotoxicidad del metal[58], que aunque como hemos visto es reducida puede tener cierto efecto en otras líneas celulares más sensibles. Por todo ello, se desarrolló un sistema en el que la reacción no necesitase de ningún tipo de agente externo evitando así cualquier sustancia que pudiese ser citotóxica. Para ello se necesitaba tener el grupo alquino activado de manera que pudiese reaccionar con el grupo azida en condiciones fisiológicas y sin catalizadores. Con el fin de tener el grupo alquino activado se modificaron los ELRs al nivel de las lisinas para que portasen grupos ciclooctinos en los que el triple enlace está lo suficientemente activado como para que la reacción se lleve a cabo obteniendo geles en tiempos cortos (de 1 a 25 minutos dependiendo de la concentración). Estas modificaciones están descritas en los apartados correspondientes de la sección de materiales y métodos. Una vez modificados los ELRs se pueden disolver en medio acuoso a baja temperatura y obtener geles mediante el simple mezclado de las dos disoluciones y sin necesidad de añadir nada más al sistema. Con este procedimiento se han obtenido geles de ELRs mediante tecnología click sin catalizador (ELRs-CFCGs) y con concentraciones de entre 50 a 150 mg/mL y en consecuencia con diferentes propiedades físicas. Este tipo de geles sin catalizador poseen unos valores de G’ y G’’ equiparables

a los de los geles de click con catalizador descritos anteriormente (Figura 13). Se alcanzaron valores desde 1.5 kPa hasta unos 8 kPa para el caso del módulo de almacenamiento y de entre 100 a 700 Pa para el caso del módulo de pérdidas, a 37°C. Los valores de la tangente de δ permanecen muy bajos para todas las concentraciones y a ambas temperaturas (4 y 37 °C), lo que indica que estos geles presentan también un comportamiento altamente elástico.

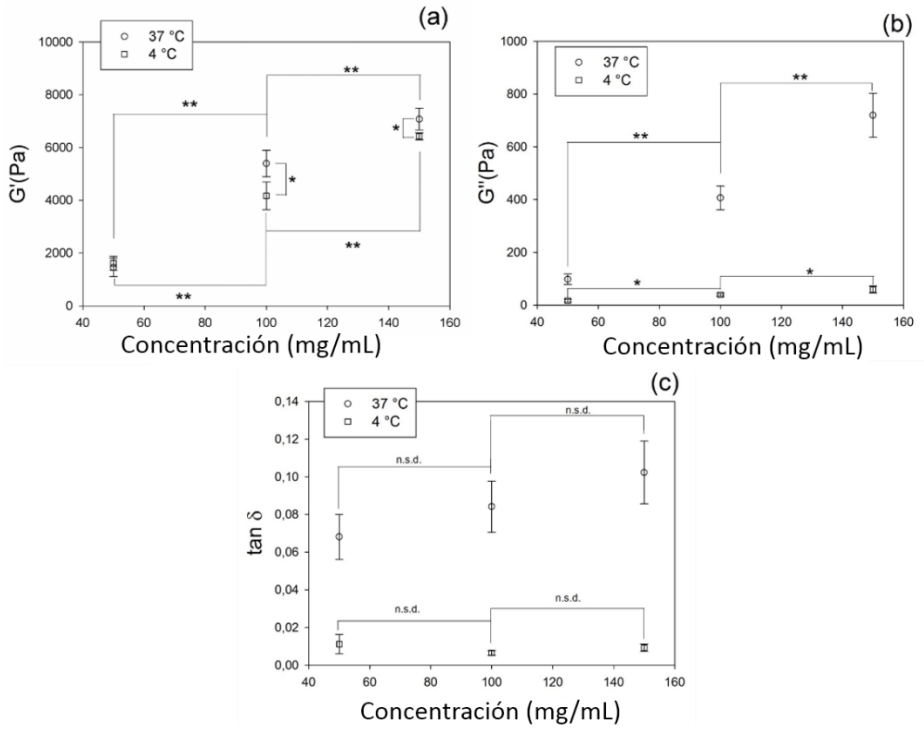

Figura 13. *Evolución de G', G'' y δ de geles de click sin catalizador a 37°C y 4°C como función de la concentración.*

De la misma forma que ocurría para los hidrogeles de click con catalizador, para este tipo de geles sin catalizador la porosidad decrece al aumentar la concentración y de igual forma ocurre con el hinchamiento. El comportamiento es similar a ambas temperaturas pero con valores más altos de porosidad e

hinchamiento en el caso de 4°C (Figura 14). Como se puede ver, estos ELR-CFCGs siguen un comportamiento análogo al de los geles con cobre y la explicación de la variación de la porosidad y el hinchamiento es totalmente análoga a la ya descrita en los geles formados con catalizador.

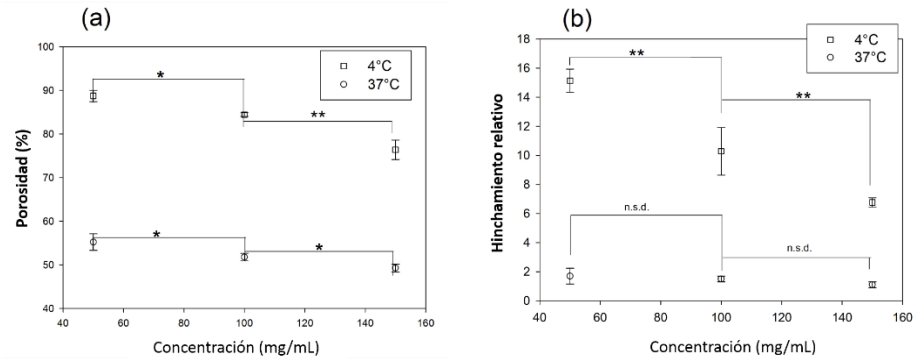

Figura 14. *Porosidad a 4 y 37 °C (A) e hinchamiento relativo (B) de los geles de click sin catalizador.*

Las microfotografías tomadas por SEM (Figura 15) nos permiten apreciar la micro estructura de estos geles, corroborándose lo descrito anteriormente.

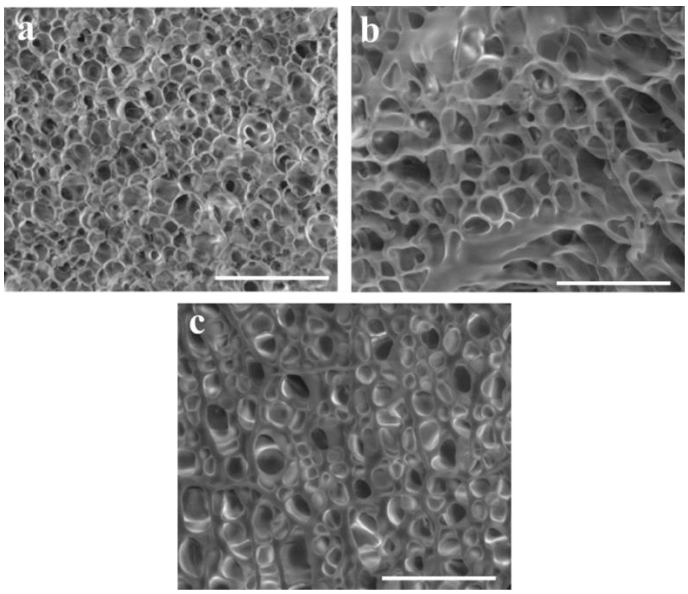

Figura 15. *Imágenes SEM de la microestructura de los ELR-CFCGs a distintas concentraciones (50, 100 y 150 mg/mL, imágenes A, B, y C respectivamente)*

Basándonos en estos estudios y en la variación del módulo complejo como función de la raíz cuadrada de la frecuencia (Figura 16) se ha propuesto un modelo poroviscoelástico para estos ELRs-CFCGs. De tal forma que a frecuencias muy bajas, un mecanismo poroelástico es el que domina los procesos de relajación, en el que la difusión del fluido a través del material tiene poca o nula influencia y sólo la reorganización de las cadenas de polímero es capaz de disipar la energía que se aplica. Mientras que por encima de una determinada frecuencia en el que el valor del módulo complejo varía de forma lineal con la raíz cuadrada de la frecuencia, denominado por otros autores como frecuencia de relajación poroelástica[59,60]. El mecanismo de relajación está dominado tanto por el flujo del fluido a través de los poros del gel como por fricciones entre el fluido y el sólido que forman el gel. La figura 16 trata de arrojar un poco más de luz a esta explicación. Podemos ver cómo por encima de una cierta frecuencia la variación del módulo complejo se asemeja a una recta mientras que por debajo de esa frecuencia esta variación no es lineal. Este modelo es se aplicó también a los hidrogeles de click con cobre y es extrapolable a los geles híbridos previamente estudiados.

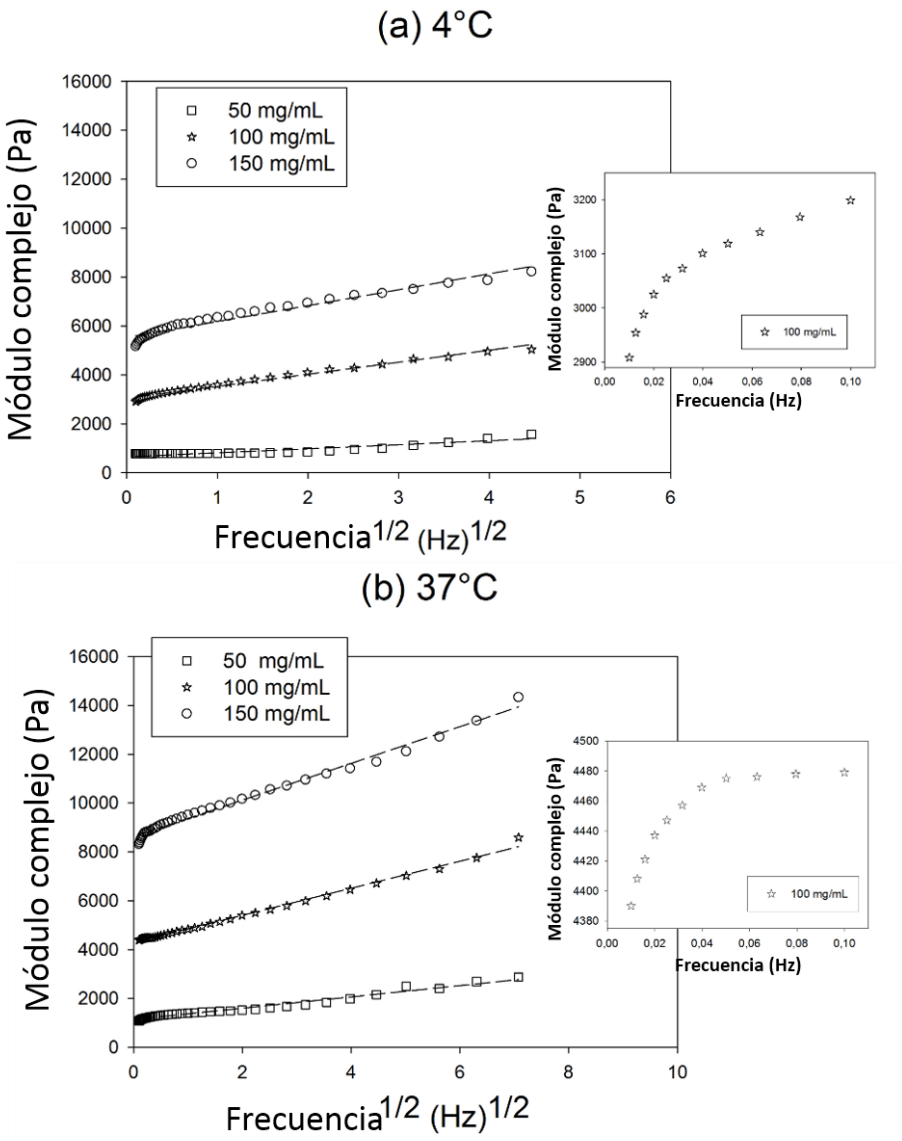

Figura 16. *Dependencia del módulo complejo con la raíz cuadrada de la frecuencia a 4°C (a) y 37°C (b) para distintas concentraciones. La línea punteada corresponde al ajuste de la zona lineal de la curva. En los insertos puede verse la evolución del módulo complejo para valores bajos de la frecuencia.*

Todas estas propiedades y valores del módulo elástico muy parecidos a los encontrados en tejidos naturales (ver tabla 1) hacen a estos ELRs-CFCGs unos candidatos muy adecuados e interesantes para aplicaciones biomédicas en el campo de la ingeniería de tejidos.

Tabla 1. *Valores del módulo elástico de diversos tejidos y células naturales y de los ELRs-CFCGs.*

Material	Módulo elástico
Capa adventicia[61]	4.7 ± 1.7 kPa
Cortex de riñón y médula[62]	~10 kPa
Núcleo pulposo[62]	~ 1 kPa
Condrocitos aislados[63]	0.6–4 kPa
ELRs-CFCGs	
(50 mg/mL a 37°C)	~ 1.8 kPa
(100 mg/mL a 37°C)	~ 5.7 kPa
(150 mg/mL a 37°C)	~ 7.5 kPa

4.3. Obtención de Nanogeles a partir de Recombinámeros tipo elastina mediante tecnología click sin catalizador. Estudio de la dependencia con la temperatura.

Una vez que hemos evaluado y caracterizado los ELRs-CFCGs macroscópicamente[52], nos centraremos en investigar la formación de nanogeles a partir de disoluciones diluidas de ELRs modificados y precursores de la reacción click. Para ello se prepararon disoluciones lo suficientemente diluidas para que las presunciones de homogeneicidad y ergodicidad[64] (la hipótesis de ergodicidad establece que, sobre un período prolongado de tiempo, el tiempo de permanencia en una dada región del espacio de fase de microestados con la misma energía es proporcional al volumen de la región, o sea todos los microestados accesibles son igualmente probables a lo largo de un período prolongado) sigan siendo válidas. Las concentraciones elegidas fueron 0.1, 0.5 y 1 mg/mL. Las

muestras se prepararon como se ha descrito en la sección de materiales y métodos (cualquier variación de este método está indicada en el capítulo 5 de esta tesis).

Tras mezclar las disoluciones de cada componente a distintas temperaturas se midieron las dimensiones, cargas superficiales y micro-reología de estructuras formadas por medio de técnicas de dispersión de luz láser y potencial Z.

Los nanogeles formados a 37°C mostraban un tamaño de unos 500 nm que, independientemente de la concentración, era mayor al tamaño de los nano-geles formados a 4°C, en torno a 100 nm. En cuanto a la carga en superficie de estos nanogeles, también se encuentran claras diferencias entre los dos procedimientos. Mientras que a 37°C se encuentra un valor de potencial Z en torno a +30 mV, independientemente de la concentración, para los nanogeles formados 4°C el valor del potencial Z varía desde los +15 mV hasta los +7 mV, decreciendo al aumentar la concentración.

Se comprobó que una vez formados los nanogeles (a 37 o a 4°C), al variar la temperatura de las suspensiones donde se encuentran variaba también su tamaño y su carga en superficie (Figura 17). Siendo estos cambios reversibles, es decir, al recuperar la temperatura de partida recuperaban también sus características iniciales [64].

.

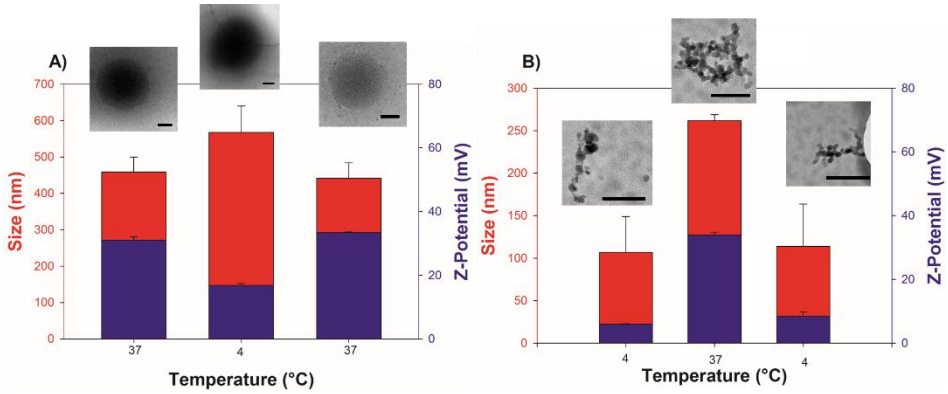

Figura 17. *Variación del tamaño y potencial Z como función de los cambios de temperatura para nanogeles formados a 37°C (A) y 4°C (B). Los insertos son imágenes de Crio-TEM y muestran la microestructura de los nanogeles a distintas temperaturas. Escala 100 nm*

En cuanto a la microreología[65], si prestamos atención a los valores de G' y G'' para los nanogeles formados a 4°C podemos ver que G'' es ligeramente mayor que G' independientemente de la concentración, lo que nos indica que la muestra es un fluido viscoelástico en todo el rango de frecuencias consideradas. En el caso de los nanogeles formados a 37°C, para los geles de menor concentración se observó que G' y G'' tenían valores similares alcanzando G' un plató en torno a 1000 rad/seg mientras que para la concentración de 1 mg/mL G' domina claramente sobre G'' y no se alcanza ese plató alcanzado para las concentraciones de 0.1 y 0.5 mg/mL. (Figura 18)

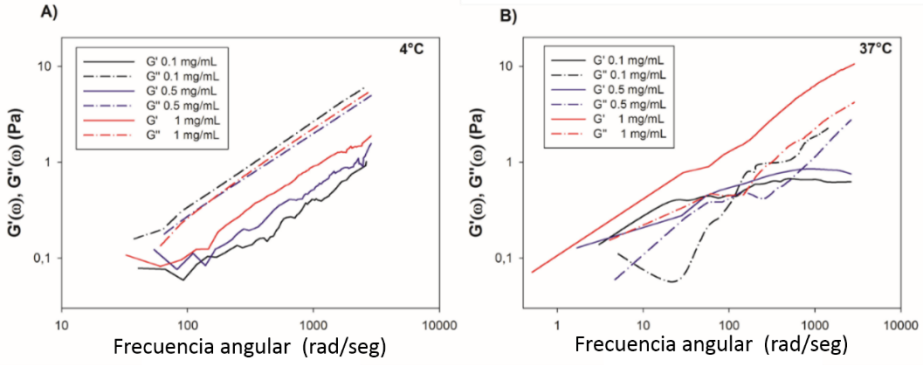

Figura 18. *Variación de G' y G'' como función de la frecuencia angular para nanogeles formados a 4°C (A) y 37°C (B).*

Tras analizar estos datos se propuso un mecanismo fractal de formación de los geles de tal forma que los nanogeles formados a diferentes temperaturas son y tienen propiedades diferentes y no pueden interconvertirse unos en otros, pero conservan el comportamiento termosensible de los ELRs que los forman.

Los nanogeles formados a 4°C, por encontrarse por debajo de su transición inversa presentan una conformación extendida y por tanto tienen homogéneamente distribuidas las lisinas (tanto por la superficie externa como por la parte interna), que son las que aportan la carga positiva, a lo largo del nanogel, lo que hace que tengan valores de potencial Z menores que los geles formados a 37°C, en que las cadenas de los ELRs se encontraban en una conformación plegada por encontrarse la disolución por encima de la T_t y en esta situación las partes más hidrofílicas quedan preferentemente expuestas hacia el exterior.

Por otro lado, estos valores disminuyen al aumentar la concentración, ya que al aumentar la concentración aumenta la cantidad de lisinas pero la relación de lisinas por unidad de superficie disminuye , por lo tanto baja el valor del potencial Z. En los geles formados por encima de la temperatura de transición el

valor del potencial Z se mantiene constante ya que tienen una distribución segregada de las lisinas, tienden a exponer todos los grupos amino de las lisinas hacia el exterior, por lo tanto aunque se aumente la concentración y por tanto el número de lisinas, al estar éstas expuestas hacia afuera, el valor del potencial Z se mantendrá prácticamente constante. Este modelo fractal se muestra en la figura 19. Se encontró que las estructuras formadas a diferentes temperaturas eran distintas tanto en tamaño, carga y propiedades micro-reológicas. Se produce un cambio en la estructura al cambiar la temperatura, pero la formada a 37°C no se convierte en la formada a 4°C y viceversa[66]

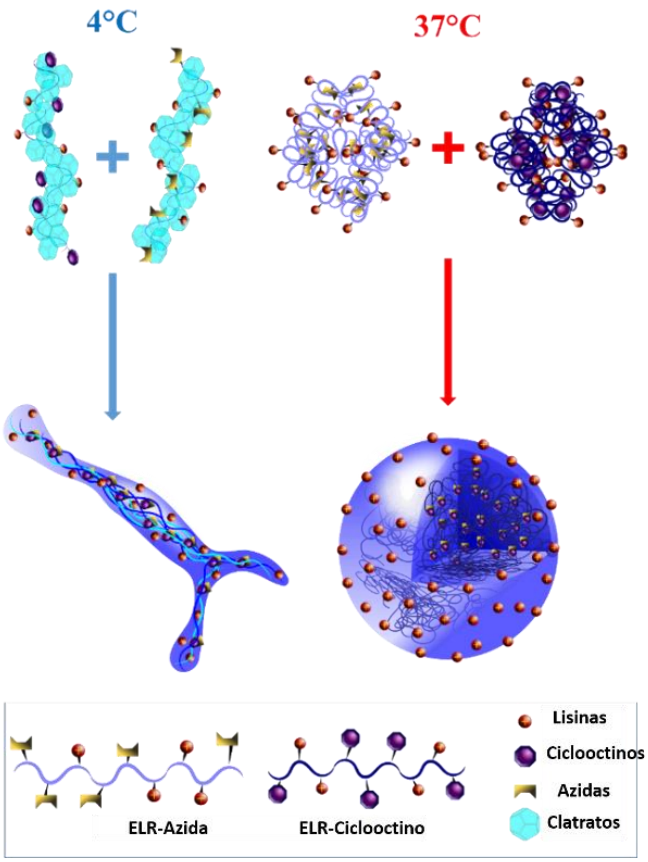

Figura 19. *Esquema de la formación fractal de los nanogeles formados a 4°C (A) y 37°C (B).*

Las diferentes propiedades de estos nanogeles nos permiten pensar en otras aplicaciones diferentes de las comentadas hasta ahora como puede ser encapsulación de principios activos, que dependiendo de la hidrofobicidad del mismo se podrían encapsular mejor en un tipo de nanogel o en otro (formado por encima o por debajo de la T_t).

4.4. Modificación de superficies mediante capas reactivas de Recombinámeros tipo elastina por tecnología click sin catalizador.

En la actualidad la mayor parte de los implantes y prótesis que se emplean para tratar defectos o lesiones son implantes no basados en materiales biológicos. La interacciób̀n entre la superficie del implante y el sistema biológico es crucial para evitar procesos inflamatorios, infecciones o incluso rechazo del implante. Por ello, la técnica del capa a capa (LBL de sus siglas en inglés layer by layer) es una técnica que se lleva utilizando desde los años 60 (en 1966 Ralph K. Iler introdujo este concepto[21]) para modificar diferentes sustratos. Si bien es verdad que prácticamente todos los autores se han basado en una sucesión de capas que se mantienen unidas mediante fuerzas electrostáticas, fuerzas hidrofóbicas, fuerzas de Van der Waals, puentes de hidrógeno[67-72] o incluso enlaces covalentes algunos con tecnología click con catalizador[73,74], en esta sección queremos describir la formación de una sucesión de capas que reaccionan químicamente con la capa anterior sin la necesidad de ningún tipo de catalizador o aditivo para que se produzca dicha reacción. Por otro lado, se han modificado para que porten una sonda fluorescente con el fin de visualizar mejor el proceso y también como demostración de que cada capa puede ser

modificada con diversas moléculas o principios activos de una forma sencilla.

El proceso de funcionalización de superficies es sencillo y se inicia con una primera etapa de limpieza y activación de los sustratos a utilizar (vidrio, poliestireno y titanio) mediante plasma. La biofuncionalización propiamente dicha, se realiza por sucesivas inmersiones en las disoluciones de los dos ELRs involucrados en el proceso de forma alternativa; de tal forma que una capa completa se obtiene tras una inmersión en ambos componentes. En este proceso se puede incluir una etapa de lavado entre cada inmersión, de esta forma se obtienen capas más finas que si no se realiza este paso intermedio de lavado. El tiempo necesario para formar una capa es de 2 minutos sin el proceso de lavado y de 5 minutos si incorporamos la etapa de lavado. Un tiempo tan corto y el uso de condiciones suaves y no citotóxicas nos permite utilizar este sistema en aplicaciones en que sea necesaria una encapsulación celular. Por medio de estos dos métodos obtenemos espesores en los recubrimientos de entorno a los 500 nm por capa, para el caso del proceso con lavado, y de entorno a las 2 micras para el caso del proceso sin la etapa de lavado (para más detalles ver el capítulo 6 de esta tesis). Una vez que tuvimos las superficies funcionalizadas, se procedió a caracterizarlas por distintas técnicas (FTIR, XPS, ángulo de contacto, microscopía óptica, de fluorescencia, SEM y AFM). La evolución en el recubrimiento de las superficies a nivel atómico fue evaluado mediante FTIR y XPS (ver resultados detallados en el capítulo 6 de esta tesis), en cuyos espectros podemos ver cómo las señales características de cada sustrato desaparecen dejando paso a las señales de los ELRs. Estos cambios a nivel atómico llevan asociados cambios en la hidrofobicidad. Esta hidrofobicidad se midió mediante la técnica de ángulo de contacto.

Se comprobó que las superficies se volvían muy hidrófilas, obteniéndose ángulos inferiores a 10°) después del lavado y activación con plasma y cómo tras la aplicación de la primera capa el valor del ángulo de contacto aumentaba hasta valores en torno a 80°, valor que aumentaba hasta unos 100° al alcanzar la 5 capa (Tabla 1).

Tabla 1. *Valores del ángulo de contacto (°) para los materiales estudiados y su variación con el número de capas.*

	Titanio		**Poliestireno**		**Vidrio**	
Comercial	67,3±5,2		43,9±7,1		49,5±4,7	
Activado	<8		<8		<8	
Nº Capas	**Lavado**	**Sin lavar**	**Lavado**	**Sin lavar**	**Lavado**	**Sin lavar**
1	80,9±6,2	88,1±4,6	79,5±3,0	93,8±3,6	86,2±2,8	92,4±3,2
2	89,7±3,3	96,0±2,1	97,6±2,9	95,5±3,5	89,0±5,3	95,0±3,1
5	90,5±3,6	99,8±1,1	99,1±1,6	99,1±3,6	93,4±2,1	100,2±3,6

Tanto la microscopía SEM como AFM (Figura 20) nos revelaron cambios en la topografía de la superficie de los sustratos con cada nueva capa. Podemos observar cómo se pasa de la micro-topografía típica de cada sustrato (aquí solo se muestra el titanio como ejemplo, el resto puede encontrarse en el capítulo 6 de esta tesis), a una superficie más rugosa que se va a suavizando con cada nueva capa.

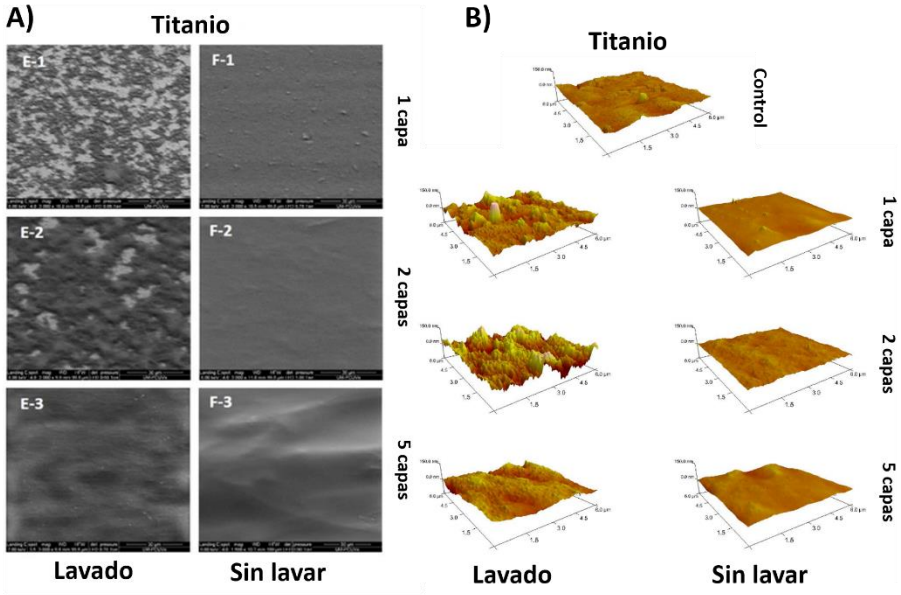

Figura 20. *Evolución de la microtopografía y rugosidad de las superficies de titanio después de cada nueva capa. Micrografías de SEM (A) y AFM (B).*

Las propiedades mecánicas de los sustratos también se ven afectadas con cada nueva capa. De esta forma, el módulo de Young (medido por AFM) decrece con cada nueva capa que se añade, obteniéndose materiales superficialmente más blandos donde el efecto del sustrato subyacente es cada vez menos notable. Ver figura 21.

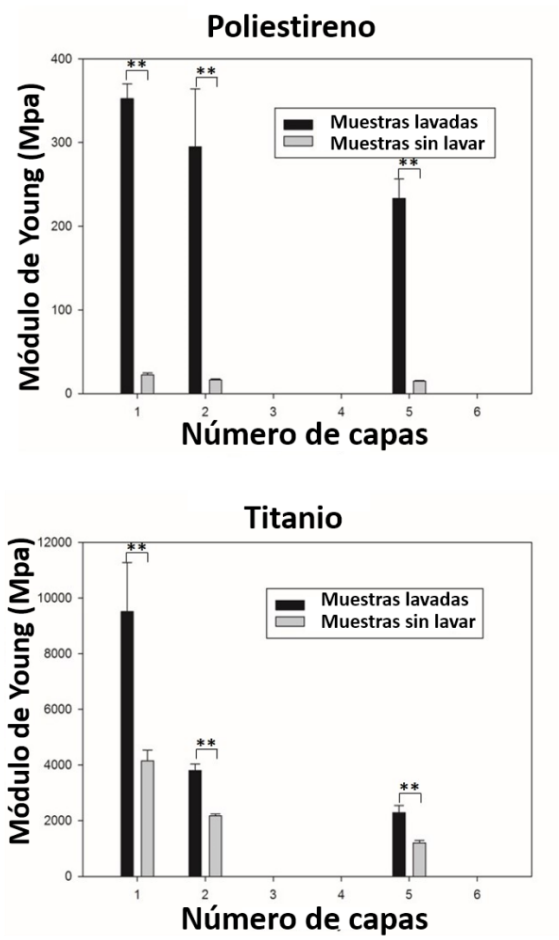

Figura 21. *Evolución del valor del módulo de Young, medido por AFM, de las superficies de poliestireno y titanio con el número de capas.*

Por lo tanto, podemos decir que hemos recubierto sustratos con muy diferentes composiciones químicas mediante la técnica LBL gracias a una deposición mediante inmersión de una sucesión de capas reactivas de ELRs. De esta forma hemos variado las propiedades mecánicas, químicas y topográficas de estos sustratos, a la vez que les hemos dotado de secuencias bioactivas. En este caso las secuencias bioactivas fueron de adhesión celular (RGD), que ayudan a una mejor integración y reducir los fenómenos de

rechazo en sistemas biológicos de potenciales implantes elaborados con estos materiales.

Como prueba de concepto se recubrieron bolas de agarosa de tamaño semejante a islotes pancreáticos que suelen tener tamaños comprendidos entre los 150 y 200 nm de diámetro, y estents coronarios.

En el primer caso se pretende demostrar que podemos obtener un recubrimiento total y efectivo estructuras esféricas, demostrando que esta tecnología podría ser eficaz para el recubrimiento de islotes pancreáticos, de tal forma que este recubrimiento de ELRs permita el intercambio de nutrientes y productos de desecho a través de la nano-capa de gel que hemos visto que se forma mediante esta técnica de LBL.

En el caso de los estents coronarios el objetivo consistió en conseguir un recubrimiento total de este tipo de estructuras que poseen un pequeño diámetro por ejemplo de 1.5 mm de tal forma que este recubrimiento fuese lo más fino posible, pudiésemos controlar su espesor y además incorporar secuencias bioactivas que favorezcan una perfecta endotelización disminuyendo así los procesos de reestenosis.

En ambos casos tanto las microscopías ópticas, de fluorescencia como de SEM revelaron un recubrimiento óptimo dese la primera capa, para este tipo de estructuras se utilizó un proceso de LBL sin el paso de lavado entre capas. Ver figura 22.

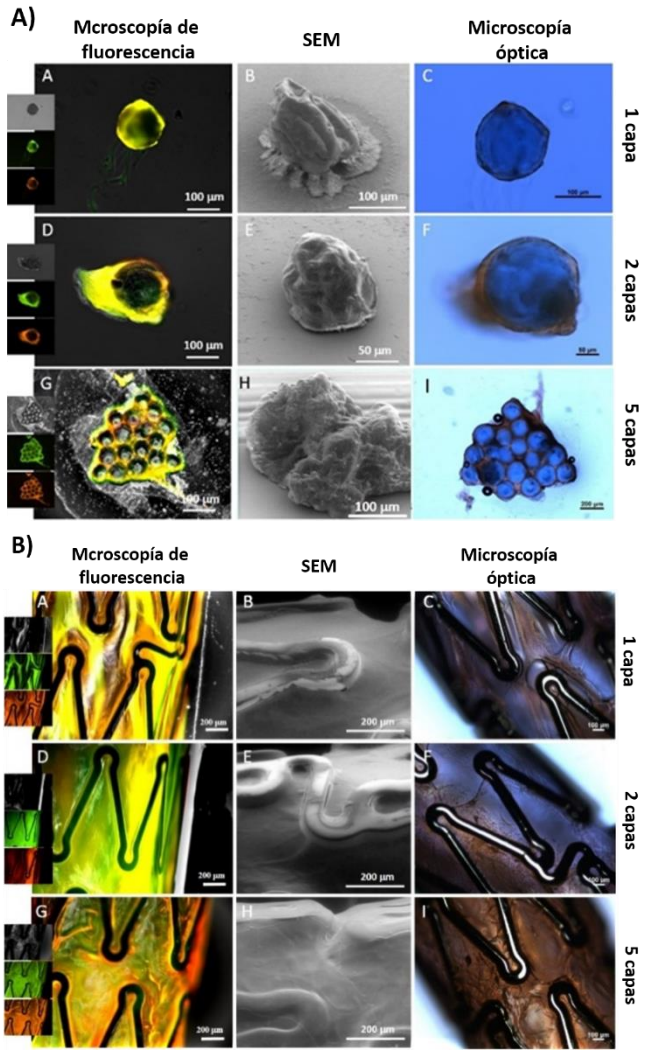

Figura 22. *Imágenes de microscopía de fluorescencia (columna izquierda), SEM columna central y microscopia óptica (columna derecha) del recubrimiento de bolas de agarosa (A) y stents coronarios (B) mediante la técnica de LBL. Los insertos pequeños de las imágenes de fluorescencia corresponden a los canales contrate de fases (arriba), verde (medio) y rojo (abajo).*

A modo de resumen, podemos decir que hemos recubierto sustratos con muy diferentes composiciones químicas mediante la técnica LBL gracias a una sucesión de capas reactivas por química click de ELRs. De esta forma hemos variado las propiedades mecánicas, atómicas y topográficas de estos sustratos, a la vez que les hemos dotado de secuencias bioactivas, en este caso secuencias

de adhesión celular RGD, que pueden ayudar a una mejor integración y reducir los fenómenos de rechazo de posibles implantes de estos materiales en sistemas biológicos. También se han recubierto estructuras más complejas como esferas o stents coronarios de forma efectiva lo que nos hace pensar que este tipo de tecnología de capa a capa mediante una serie de ELRs reactivos vía química click puede ser muy adecuada para bio-compatibilizar implantes coronarios y como medio de encapsulación celular gracias a las propiedades de citocompatibilidad de los materiales y la técnica empleada.

4.5. Stents recubiertos por Recombinámeros tipo Elastina: Un paso hacia un dispositivo totalmente biocompatible y no trombogénico para enfermedades cardiovasculares.

Uno de los mayores problemas que plantea la implantación de stents es la posibilidad de aparición de problemas derivados de la presencia del propio stent. Alguno de esos problemas son el re-estrechamiento de las paredes de los vasos sanguíneos afectados o la posibilidad de aparición de trombos dentro del estent por acumulación de plaquetas derivada de una reacción inmune del organismo[75-79]. En este apartado describiremos cómo hemos combinado estents metálicos con buenas propiedades mecánicas con recubrimientos de una capa de ELRs-CFCGs con el fin de biocompatibilizarlos y biactivarlos (descritos en el apartado 5.2 de esta tesis) [52].

Para ello se diseñó un molde especial donde se coloca el estent metálico y en el cual se inyecta las soluciones de los ELRs

modificados que van a formar el gel. Para un mayor detalle ver el apartado correspondiente en la sección materiales y métodos.

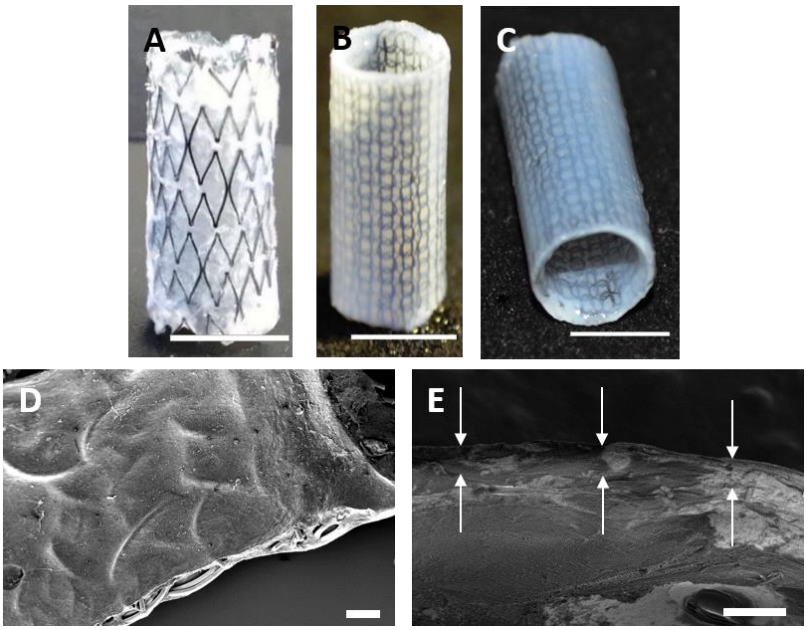

Figura 23. *Imágenes de distintos tipos de estents recubiertos con ELR-CFCGs (A, B, C), escala 5 mm. Detalles de SEM de la parte interna del estén después de ser recubierto (D) y del perfil para ver el espesor del gel (E), escala 200 μm.*

Una vez recubiertos estos estents con ELRs se sometieron a distintas pruebas mecánicas para testar su estabilidad. Se realizaron pruebas de prensado reduciendo el diámetro del estent recubierto hasta 2 mm (40% del diámetro original) durante 5 minutos, comprobándose que es estent recubierto recuperaba sus dimensiones originales sin daños en la estructura del gel, también se realizaron pruebas de resistencia a flujos elevados, para ello se colocaron estos estents recubiertos de ELRs-CFCGs en un circuito diseñado para proporcionar un flujo de 2.5 L/min a través del estent durante 24h. Mediante diferencia de pesada antes y después del test se demostró que el dispositivo había perdido menos del 0.1% en peso. Con este resultado junto con la observación al microscopio

(óptico y de barrido de electrones) se concluyó que estos dispositivos eran estables a flujos elevados, pudiendo soportar las condiciones fisiológicas del sistema circulatorio humano.

El siguiente aspecto que se evaluó fue la composición del gel para obtener una rápida y efectiva endotelización del interior del dispositivo. Para ello se testaron 3 tipos de ELRs-CFCGs en placas de 96 pocillos. Uno sin ningún tipo de secuencia bioactiva (VKVx24-CFCG), otro con una secuencia de adhesión celular general (HRGD6-CFCG) y el último con una secuencia de adhesión celular específica para células endoteliales (REDV-CFCG). Sobre estos ELR-CFCGs se sembraron 2500 HUVECS por pocillo y se midió su proliferación después de 1, 5 y 9 días. Para ello se realizaron curvas de calibrado (de 1000 a 10000 celulas por pocillo) con células del mismo tipo sembradas 24 horas antes de parar cada experimento. Se siguió la proliferación mediante tinción Live/Dead midiendo fluorescencia a 530 nm y 645 nm. La intensidad de fluorescencia a 530 nm fue convertida a número de células vivas mediante interpolación en las curvas de calibrado descritas anteriormente. Se comprobó cómo para el caso de los geles con secuencias bioactivas (RGD y REDV) la proliferación celular fue mucho mayor que para el caso del gel formado con el ELR de control (VKVx24). Y respecto a los dos geles con secuencias bioactivas el gel que contiene la secuencia RGD ofrecía una mayor proliferación que el gel con la secuencia REDV (Figura 24).

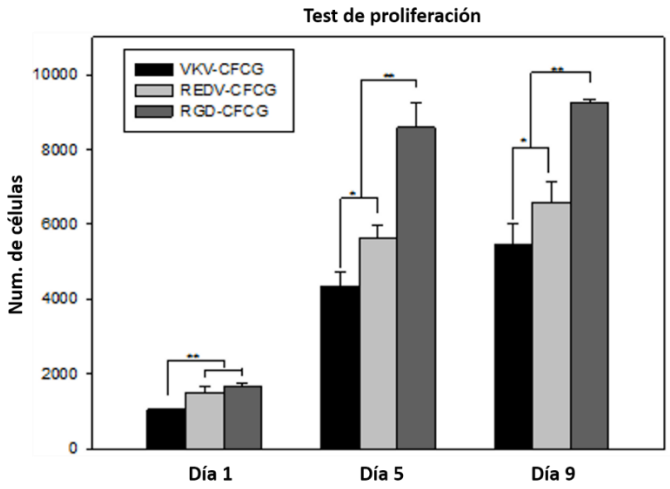

Figura 24. *Proliferación de células endoteliales humanas sobre distintos tipo de ELR-CFCGs a distintos tiempos.*

A la vista de este resultado se decidió descartar el gel sin secuencias bioactivas para el proceso de endotelización. Dicho proceso se llevó a cabo en estents recubiertos con HRGD6-CFCGs y con REDV-CFCGs y en dos etapas. La primera etapa consistió en una endotelización en estático para la cual se depositaron $10x10^6$/mL HUVECs en el interior del estent recubierto con los ELRs-CFCGs y dispuesto horizontalmente. Este se hizo girar un cuarto de vuelta, en torno a su eje longitudinal, cada 20 segundos. Este proceso se realizó durante 6 horas, para conseguir una distribución homogénea de las células en el interior de los estents recubiertos. Después de esta etapa se inició un proceso de endotelización en dinámico en el cual se hizo pasar un flujo de medio de cultivo apropiado a través del ELR-estent. De esta forma se pudo comprobar cómo después de 15 días se había conseguido una endotelización completa para el caso de los estents recubiertos con HRGD6-CFCGs, mientras que para el caso de los estents recubiertos con REDV-CFCGs las células no llegaban a formar una capa continua, como se puede ver en los resultados del capítulo 7.

Estos nuevos ELR-estents fueron sometidos a un test de trombogeneicidad dando como resultado una muy baja adhesión de plaquetas, como se pueden ver en las imágenes de fluorescencia (A) y de SEM (B) de la figura 25 (el color a las imágenes de SEM fue añadido mediante el uso de software informático, Corel draw, para una mejor visualización de los contornos). En dicha figura se puede ver cómo en los controles de GoreTex®, tanto de fluorescencia como de SEM, e incluso en el control de BMS en las imágenes de SEM, existe un gran número de plaquetas activadas adheridas al material, mientras que en nuestros ELRs-biostents, ya sean sin endotelizar o endotelizados (completamente o parcialmente), prácticamente no se aprecia esa adhesión de plaquetas activadas, lo que indica una baja respuesta a este test siendo este resultado muy prometedor para futuros ensayos in vivo.

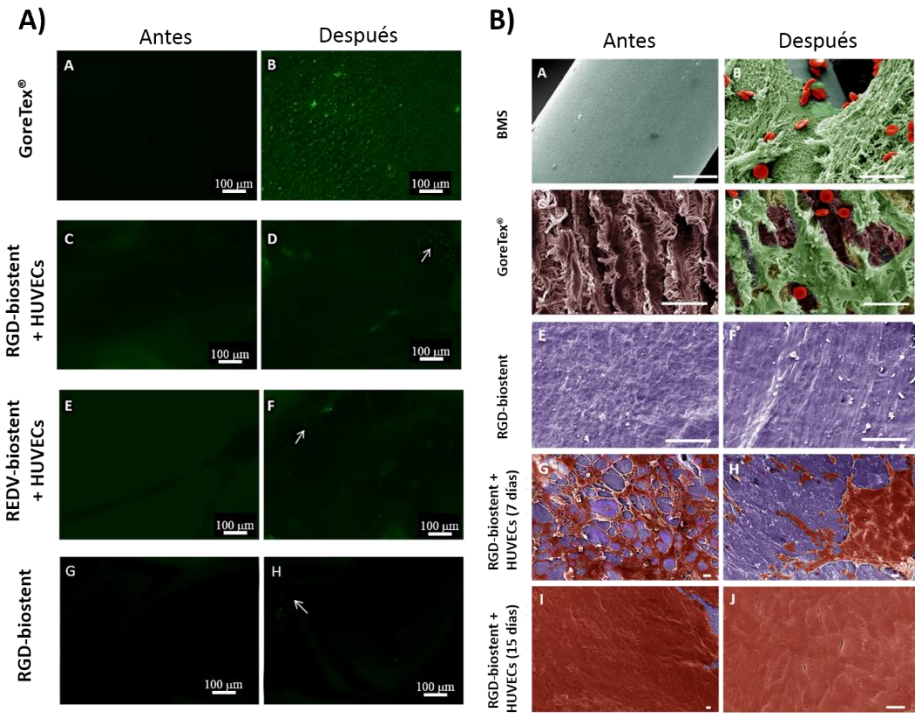

Figura 25. *Imágenes de inmunofluorescencia contra plaquetas activadas (A) y de SEM (B) en distintos materiales.*

Podemos entonces concluir que se abre una nueva vía a un nuevo tipo de dispositivo para el tratamiento de procesos de estenosis de los vasos sanguíneos, y que aunque aquí nos hemos centrado en vasos de calibres relativamente grandes podrían ser empleados también en vasos más pequeños simplemente variando las dimensiones iniciales del estent metálico utilizado. También se podrían incluir distintos principios activos dentro de los ERLs-CFCGs que recubren a los estents.

4.6. Válvulas aórticas de Recombinámeros tipo elastina, "EA-Valves".

En este último apartado se abordó la que quizá haya sido la aplicación más ambiciosa de los ELRs-CFCGs en esta tesis. El objetivo fue el diseño y preparación de válvulas aórticas hechas exclusivamente de ELRs que aportaran las propiedades mecánicas y actuaran como soporte celular hasta que las propias células colonizaran y desarrollaran sus propias estructuras y que a su vez reforzaran y potenciaran el constructo inicialmente preparado.

Actualmente la sustitución de una válvula aórtica sigue siendo un motivo de preocupación para médicos y pacientes ya que no se tiene un modelo de válvula que satisfaga todas las necesidades de biocompatibilidad, propiedades mecánicas y durabilidad deseadas para este tipo de implantes. Se han probado con válvulas artificiales mecánicas que nos pueden ofrecer las propiedades mecánicas deseadas pero que tarde o temprano dan problemas de biocompatibilidad al ser detectadas por el sistema inmune del propio anfitrión produciendo fallos en la apertura o cierre de la misma[80]. Se ha probado con válvulas humanas descelurarizadas[81,82] pero se han producido problemas de rechazo.

También se está explorando el campo de las válvulas hechas con biomateriales, como pueden ser las válvulas de geles de fibrina pero generalmente no ofrecen las propiedades mecánicas deseadas[55] y después de ser testadas in vitro se comprueba que no se consigue la coaptación de las tres valvas por lo que no se consigue un cierre óptimo de la válvula y por lo tanto no son completamente funcionales.

Después de la experiencia adquirida con los geles híbridos de fibrina y ELRs descritos en el primer apartado de los resultados de esta tesis, moldeando válvulas aórticas y tras comprobar las buenas propiedades mecánicas y de citocompatibilidad y la baja trombogeneicidad que tienen los ELRs-CFCGs el siguiente paso fue testar estos materiales en la formación de este tipo de válvulas. Para ello se siguió el proceso descrito en el apartado de materiales y métodos. Primero se llevó a cabo el moldeado de estás válvulas solo con ELRs-CFCGs sin células y se comprobó que se podían moldear y desmoldar de manera semejante a los ELRs-FGs. El único aspecto a tener en cuenta fue que el inicio del moldeo debe hacerse a baja temperatura para evitar la transición de los ELRs y por tanto su segregación de la disolución.

Posteriormente se moldearon válvulas aórticas hechas exclusivamente de ELRs (EA-valves) y con células musculares humanas procedentes de venas umbilicales (HUVSMCs) siguiendo el proceso descrito en el apartado de materiales y métodos y bajo condiciones totalmente estériles. Después de extraer la válvula del molde se mantuvo durante 7 días en condiciones de cultivo estático. Tras ese periodo se abrieron las valvas y se colocó la válvula dentro de un bioreactor capaz de simular el flujo sanguíneo y para comenzar el proceso de cultivo con una estimulación mecánica

adecuada. Este proceso de estimulación se empieza con condiciones suaves (20 pulsaciones por minuto) y se fueron incrementando paulatinamente hasta alcanzar las 45 pulsaciones por minuto). Tras dos semanas en régimen dinámico las valvas seguían cerrando completamente y no se apreciaba ni su contracción ni su retracción. La válvula se extrajo del bioreactor, y como se puede observar en las fotografías obtenidas (Figura 26) el tejido tenía buen aspecto y no se apreciaban roturas o deformaciones.

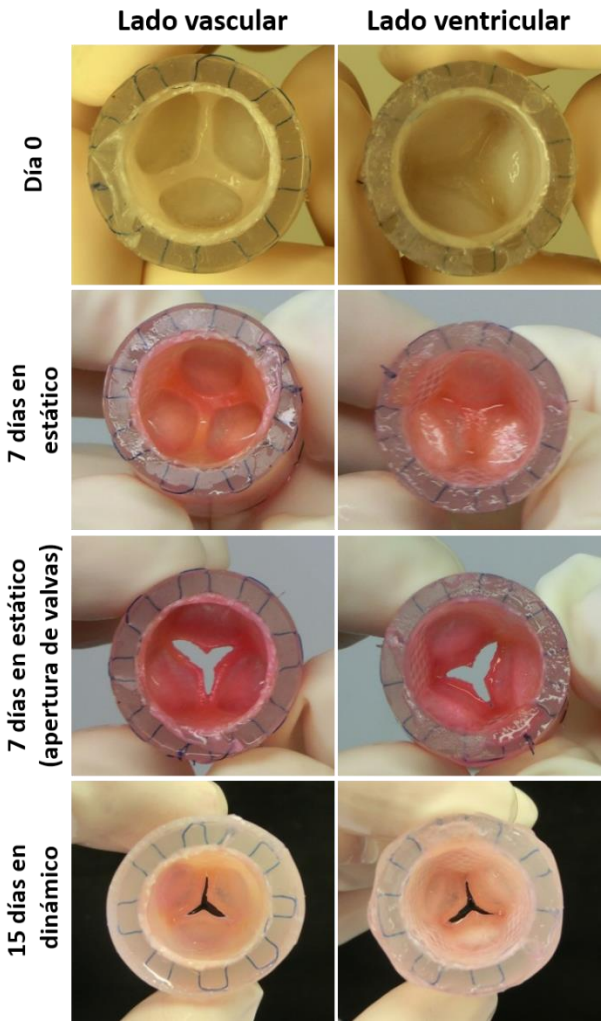

***Figura 26**. Fotografías de una EA-valve a lo largo del proceso de formación y cultivo celular.*

Antes de extraer la válvula del bioreactor y mediante un aparato de ecografía se comprobó cómo se alcanzaba la coaptación de las valvas en el momento en el que la válvula se cierra impidiendo el paso del fluido a través de ella. Ver figura 27

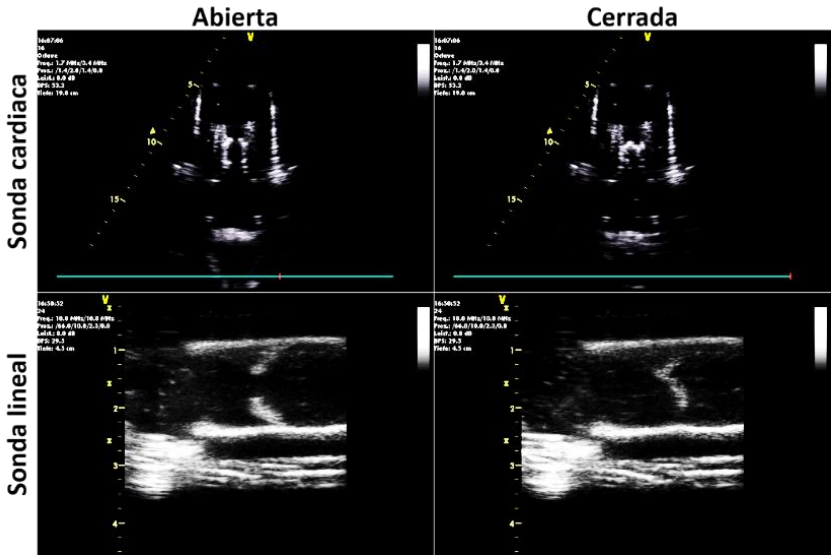

Figura 27. *Ecografías de la EA-valve dentro del bioreactor. Vista cardiaca (fila superior) y vista lineal (fila de abajo) de la válvula abierta (izquierda) y cerrada (derecha)*

También se tomaron fotografías y películas de cómo abrían (diástole) y cerraban (sístole) las valvas como se puede apreciar en la figura 28, la funcionalidad de la válvula parece ser bastante buena debido a que se consigue una completa apertura y cierre de la válvula, sin fisuras ni orificios. Se puede observar también cómo durante el proceso de apertura o cierre no se aprecia ningún tipo de deformación o movimiento parcial incompleto de ninguna de las válvulas.

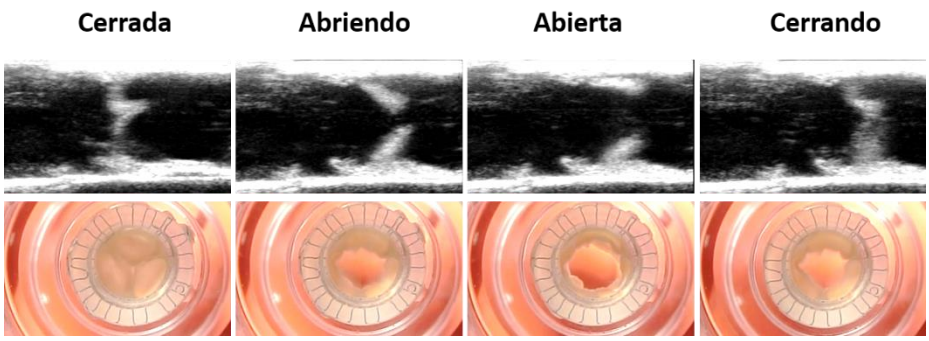

Figura 28. *Imágenes de ecografía y fotografías de la válvula durante el proceso de apertura y cierre en el bioreactor.*

Una vez acabado el proceso de cultivo, después de tres semanas la válvula fue cortada en trozos y sometidos dichos trozos a ensayos mecánicos, más concretamente ensayos de resistencia a rotura(Figura 29), e inmunohistoquímicos con tinciones contra colágenos I y III, elastina y α-SMA (Figura 30).

Los ensayos de resistencia a rotura se realizaron sobre trozos de las EA-valves sin células como control y sobre trozos de las EA-valves después de todo el proceso de cultivo descrito anteriormente. Se comprobó que si bien en las paredes de las válvulas no existían diferencias significativas debido principalmente a la presencia de la malla de tela que sujeta la estructura de la EA-valve y que hace que los valores de presión antes de romper sean parecidos, si se encontraban diferencias significativas en las valvas donde se triplica su resistencia para las muestras con células embebidas y cultivadas (Figura 29).

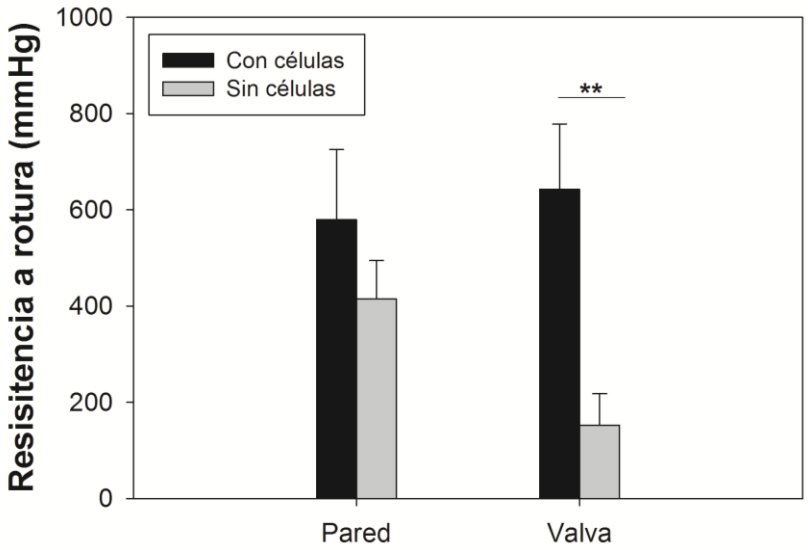

Figura 29. *Comparación entre los valores de presión durante el test de resistencia a rotura de una válvula con células o sin ellas, tanto en la pared como en las valvas.*

Este aumento en el valor de la tensión a la rotura de la valva es debido al nuevo tejido desarrollado por las células embebidas que habiendo producido nueva matriz extracelular con clara presencia de colágenos I y III al igual que α-SMA (Figura 30) le confieren una resistencia mecánica adicional a los ELRs que aportan flexibilidad. En la figura 30 se puede ver cómo en las valvas, tanto el colágeno I y III y a-SMA parecen adoptar una cierta alineación longitudinal a lo largo de la dirección del estrés de las valvas durante el movimiento de cierre y apertura de la valva. Incluso en el análisis de la elastina, en las valvas los propios ELRs parecen tener una cierta orientación longitudinal siguiendo la dirección de estrés. Esta orientación no es tan evidente en el caso de la pared de la EA-valve debido a que la pared no sufre la misma estimulación que las valvas y por consiguiente las células producen colágeno y a-SMA de forma desordenada.

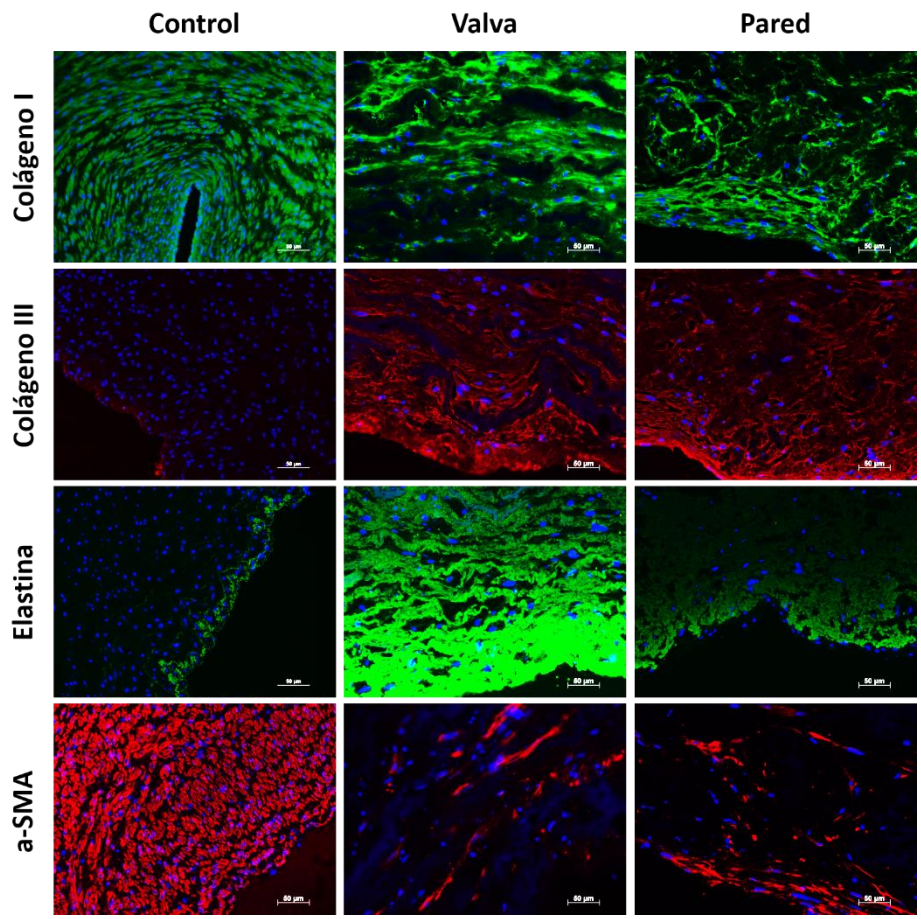

Figura 30. *Imágenes de inmunohistoquímica contra colágenos I y III, elastina y a-SMA de una arteria umbilical humana (control) y las valvas y pared de una EA-valve después del proceso de cultivo en dinámico.*

Como conclusión, por tanto podemos decir que se ha desarrollado un tipo de válvulas basadas en ELRs-CFCGs. Estos ELRs-CFCGs como hemos comprobado, en los anteriores apartados, han demostrado una muy baja trombogeneicidad y elevada citocompatibilidad, lo que unido a la buena funcionalidad in vitro de las e-valves después de 21 días de cultivo, pueden constituir una excelente aproximación para generar válvulas aórticas artificiales que puedan ser utilizadas para sustituir a las válvulas aórticas naturales dañadas o con baja funcionalidad.

Se concluye también que las excelentes propiedades mecánicas, se alcanzan gracias al desarrollo de nueva matriz extracelular por parte de las células embebidas dentro del biomaterial y de un tejido muy semejante al natural.

5. REFERENCIAS

(1) Lemons, B. D. R. S. H. J. S. E. In *Biomaterials Science (Third Edition)*; Lemons, B. D. R. S. H. J. S. E., Ed.; Academic Press: 2013, p xli.
(2) Norton, K. *Motion* **2007**.
(3) Griffith, L. G. *Annals of the New York Academy of Sciences* **2002**.
(4) Lemons, B. D. R. S. H. J. S. E. In *Biomaterials Science (Third Edition)*; Lemons, B. D. R. S. H. J. S. E., Ed.; Academic Press: 2013, p 1119.
(5) Lemons, B. D. R. S. H. J. S. E. In *Biomaterials Science (Third Edition)*; Lemons, B. D. R. S. H. J. S. E., Ed.; Academic Press: 2013, p 1337.
(6) Naderi, H.; Matin, M. M.; Bahrami, A. R. *Journal of biomaterials applications* **2011**, *26*, 383.
(7) Mironov, V.; Kasyanov, V.; Zheng Shu, X.; Eisenberg, C.; Eisenberg, L.; Gonda, S.; Trusk, T.; Markwald, R. R.; Prestwich, G. D. *Biomaterials* **2005**, *26*, 7628.
(8) Wertz, J. T.; Mauldin, T. C.; Boday, D. J. *ACS applied materials & interfaces* **2014**, *6*, 18511.
(9) Yao, W.; Xu, P.; Pang, Z.; Zhao, J.; Chai, Z.; Li, X.; Li, H.; Jiang, M.; Cheng, H.; Zhang, B.; Cheng, N. *International journal of nanomedicine* **2014**, *9*, 3963.
(10) Coşkun, G.; Karaca, E.; Ozyurtlu, M.; Özbek, S.; Yermezler, A.; Çavuşoğlu, İ. *Bio-Medical Materials and Engineering* **2014**, *24*, 1527.
(11) Yao, X.; Zhou, N.; Wan, L.; Su, X.; Sun, Z.; Mizuguchi, H.; Yoshioka, Y.; Nakagawa, S.; Zhao, R. C.; Gao, J.-Q. Q. *Biochemical and biophysical research communications* **2014**, *447*, 383.
(12) Shen, M.; Li, L.; Sun, Y.; Xu, J.; Guo, X.; Prud'homme, R. K. *Langmuir : the ACS journal of surfaces and colloids* **2014**, *30*, 1636.
(13) Chen, G. In *Methods in Cell Biology*; Matthieu, P., Manuel, T., Eds.; Academic Press: 2014; Vol. Volume 119, p 17.
(14) Chen, C.-H. H.; Shyu, V. B.; Chen, J.-P. P.; Lee, M.-Y. Y. *Biofabrication* **2014**, *6*, 15004.
(15) Wolf, M. T.; Dearth, C. L.; Sonnenberg, S. B.; Loboa, E. G.; Badylak, S. F. *Advanced drug delivery reviews* **2014**.
(16) Gasperini, L.; Mano, J. F.; Reis, R. L. *Journal of the Royal Society, Interface / the Royal Society* **2014**, *11*, 20140817.
(17) Janmey, P. A.; Winer, J. P.; Weisel, J. W. *Journal of the Royal Society, Interface / the Royal Society* **2009**, *6*, 1.
(18) Collet, J.-P.; Shuman, H.; Ledger, R. E.; Lee, S.; Weisel, J. W. *Proceedings of the National Academy of Sciences of the United States of America* **2005**, *102*, 9133.
(19) Guthold, M.; Liu, W.; Sparks, E. A.; Jawerth, L. M.; Peng, L.; Falvo, M.; Superfine, R.; Hantgan, R. R.; Lord, S. T. *Cell biochemistry and biophysics* **2007**, *49*, 165.
(20) Laurens, N.; Koolwijk, P.; de Maat, M. P. *Journal of thrombosis and haemostasis : JTH* **2006**, *4*, 932.
(21) Iler, R. K. *Journal of Colloid and Interface Science* **1966**.
(22) Humphries, M. J. *Biochemical Society transactions* **2000**, *28*, 311.

(23) Hynes, R. O. *Cell* **2002**, *110*, 673.
(24) Colognato, H.; Yurchenco, P. D. *Developmental dynamics : an official publication of the American Association of Anatomists* **2000**, *218*, 213.
(25) Mithieux, S. M.; Weiss, A. S. In *Advances in Protein Chemistry*; David, A. D. P., John, M. S., Eds.; Academic Press: 2005; Vol. Volume 70, p 437.
(26) Gauvin, R.; Guillemette, M.; Galbraith, T.; Bourget, J. M.; Larouche, D.; Marcoux, H.; Aube, D.; Hayward, C.; Auger, F. A.; Germain, L. *Tissue Eng Part A* **2011**, *17*, 2049.
(27) Huang, L.; McMillan, R. A.; Apkarian, R. P.; Pourdeyhimi, B.; Conticello, V. P.; Chaikof, E. L. *Macromolecules* **2000**, *33*, 2989.
(28) Dreher, M. R.; Simnick, A. J.; Fischer, K.; Smith, R. J.; Patel, A.; Schmidt, M.; Chilkoti, A. *J Am Chem Soc* **2008**, *130*, 687.
(29) Martin, L.; Alonso, M.; Girotti, A.; Arias, F. J.; Rodriguez-Cabello, J. C. *Biomacromolecules* **2009**, *10*, 3015.
(30) Herrero-Vanrell, R.; Rincon, A. C.; Alonso, M.; Reboto, V.; Molina-Martinez, I. T.; Rodriguez-Cabello, J. C. *Journal of Controlled Release* **2005**, *102*, 113.
(31) Urry, D. W. *Angewandte Chemie-International Edition in English* **1993**, *32*, 819.
(32) San Biagio, P. L.; Madonia, F.; Trapane, T. L.; Urry, D. W. *Chemical Physics Letters* **1988**, *145*, 571.
(33) Urry, D. W. *Journal of Physical Chemistry B* **1997**, *101*, 11007.
(34) Rodriguez-Cabello, J. C.; Alonso, M.; Perez, T.; Herguedas, M. M. *Biopolymers* **2000**, *54*, 282.
(35) Ribeiro, A.; Arias, F. J.; Reguera, J.; Alonso, M.; Rodriguez-Cabello, J. C. *Biophys J* **2009**, *97*, 312.
(36) Li, B.; Alonso, D. O. V.; Daggett, V. *Journal of Molecular Biology* **2001**, *305*, 581.
(37) Urry, D. W. *What sustains life? Consilient mechanisms for protein-based machines and materials*; Springer-Verlag: New York, 2006.
(38) Peppas, N. A. *J Control Release* **2000**, *68*, 135.
(39) Hoffman, A. S. *Adv Drug Deliv Rev* **2002**, *54*, 3.
(40) Kopecek, J. *Biomaterials* **2007**, *28*, 5185.
(41) Wichterle, O.; Lim, D. *Nature* **1960**, *185*, 117.
(42) Campoccia, D.; Doherty, P.; Radice, M.; Brun, P.; Abatangelo, G.; Williams, D. F. *Biomaterials* **1998**, *19*, 2101.
(43) Prestwich, G. D.; Marecak, D. M.; Marecek, J. F.; Vercruysse, K. P.; Ziebell, M. R. *J Control Release* **1998**, *53*, 93.
(44) Cappello, J.; Crissman, J.; Dorman, M.; Mikolajczak, M.; Textor, G.; Marquet, M.; Ferrari, F. *Biotechnology Progress* **1990**, *6*, 198.
(45) Lewis, R. V.; Hinman, M.; Kothakota, S.; Fournier, M. J. *Protein Expression and Purification* **1996**, *7*, 400.
(46) McPherson, D. T.; Morrow, C.; Minehan, D. S.; Wu, J.; Hunter, E.; Urry, D. W. *Biotechnol Prog* **1992**, *8*, 347.
(47) Cheng, S.; Google Patents: 1996.
(48) Mcgrath, K. P.; Tirrell, D. A.; Kawai, M.; Mason, T. L.; Fournier, M. J. *Biotechnology Progress* **1990**, *6*, 188.
(49) Won, J. I.; Barron, A. E. *Macromolecules* **2002**, *35*, 8281.
(50) Martin, L.; Alonso, M.; Moeller, M.; Rodriguez-Cabello, J. C.; Mela, P. *Soft Matter* **2009**, *5*, 1591.

(51) Girotti, A.; Reguera, J.; Rodriguez-Cabello, J. C.; Arias, F. J.; Alonso, M.; Matestera, A. *J Mater Sci Mater Med* **2004**, *15*, 479.
(52) González de Torre, I.; Santos, M.; Quintanilla, L.; Testera, A.; Alonso, M.; Rodríguez Cabello, J. C. *Acta Biomaterialia* **2014**, *10*, 2495.
(53) Huisgen, R. *Angewandte Chemie International Edition in English* **1963**, *2*, 565.
(54) Rabaud, M.; Lefebvre, F.; Piquet, Y.; Belloc, F.; Chevaleyre, J.; Roudaut, M.; Bricaud, H. *Thrombosis research* **1986**, *43*, 205.
(55) Flanagan, T. C.; Cornelissen, C.; Koch, S.; Tschoeke, B.; Sachweh, J. S.; Schmitz-Rode, T.; Jockenhoevel, S. *Biomaterials* **2007**, *28*, 3388.
(56) Jockenhoevel, S.; Zund, G.; Hoerstrup, S.; Chalabi, K.; Sachweh, J.; Demircan, L.; Messmer, B.; Turina, M. *European journal of cardio-thoracic surgery : official journal of the European Association for Cardio-thoracic Surgery* **2001**, *19*, 424.
(57) Kolb, H. C.; Finn, M. G.; Sharpless, K. B. *Angewandte Chemie International Edition* **2001**, *40*, 2004.
(58) Kennedy, D.; McKay, C.; Legault, M.; Danielson, D.; Blake, J.; Pegoraro, A.; Stolow, A.; Mester, Z.; Pezacki, J. *Journal of the American Chemical Society* **2011**, *133*, 17993.
(59) Han, L.; Frank, E. H.; Greene, J. J.; Lee, H. Y.; Hung, H. H.; Grodzinsky, A. J.; Ortiz, C. *Biophys J* **2011**, *100*, 1846.
(60) Lee, B.; Han, L.; Frank, E.; Chubinskaya, S.; Ortiz, C.; Grodzinsky, A. *Journal of Biomechanics* **2010**, *43*, 469.
(61) Yu, Q.; Zhou, J.; Fung, Y. C. *American Journal of Physiology - Heart and Circulatory Physiology* **1993**, *265*, H52.
(62) Erkamp, R.; Wiggins, P.; Skovoroda, A.; Emelianov, S.; O'Donnell, M. *Ultrasonic imaging* **1998**, *20*, 17.
(63) Freeman, P.; Natarajan, R.; Kimura, J.; Andriacchi, T. *Journal of orthopaedic research : official publication of the Orthopaedic Research Society* **1994**, *12*, 311.
(64) Dasgupta, B.; Weitz, D. *Physical review. E, Statistical, nonlinear, and soft matter physics* **2005**, *71*, 21504.
(65) Peters, R. *Google Patents* **2000**.
(66) González de Torre, I.; Quintanilla, L.; Pinedo-Martín, G.; Alonso, M.; Rodríguez-Cabello, J. C. *ACS Applied Materials & Interfaces* **2014**, *6*, 14509.
(67) Bertrand, P.; Jonas, A.; Laschewsky, A.; Legras, R. *Macromolecular Rapid Communications* **2000**, *21*, 319.
(68) Costa, R. R.; Custodio, C. A.; Arias, F. J.; Rodriguez-Cabello, J. C.; Mano, J. F. *Small* **2011**, *7*, 2640.
(69) Decher, G. *Science* **1997**, *277*, 1232.
(70) Hammond, P. T. *AIChE Journal* **2011**, *57*, 2928.
(71) Tang, Z.; Wang, Y.; Podsiadlo, P.; Kotov, N. A. *Advanced Materials* **2006**, *18*, 3203.
(72) Cameron, R. K.; Kim, W.; Georgina, K. S.; Angus, P. R. J.; Frank, C. *Small* **2009**, *5*.
(73) Yang, W.; Pranantyo, D.; Neoh, K.-G.; Kang, E.-T.; Teo, S.; Rittschof, D. *Biomacromolecules* **2012**, *13*, 2769.
(74) Bergbreiter, D. E.; Chance, B. S. *Macromolecules* **2007**.
(75) Curcio, A.; Torella, D.; Indolfi, C. *Circulation Journal* **2011**, *75*, 1287.
(76) Sigwart, U.; Puel, J.; Mirkovitch, V.; Joffre, F.; Kappenberger, L. *New England Journal of Medicine* **1987**, *316*, 701.

(77) Kornowski, R.; Hong, M. K.; Tio, F. O.; Bramwell, O.; Wu, H.; Leon, M. B. *Journal of the American College of Cardiology* **1998**, *31*, 224.
(78) Farb, A.; Sangiorgi, G.; Carter, A. J.; Walley, V. M.; Edwards, W. D.; Schwartz, R. S.; Virmani, R. *Circulation* **1999**, *99*, 44.
(79) Pfisterer, M.; Brunner-La Rocca, H.; Buser, P.; Rickenbacher, P.; Hunziker, P.; Mueller, C.; Jeger, R.; Bader, F.; Osswald, S.; Kaiser, C.; Investigators, B.-L. *Journal of the American College of Cardiology* **2006**, *48*, 2584.
(80) Alexiou, C.; McDonald, A.; Langley, S. M.; Dalrymple-Hay, M. J. R.; Haw, M. P.; Monro, J. L. *European Journal of Cardio-Thoracic Surgery* **2000**, *17*, 125.
(81) Dijkman, P. E.; Driessen-Mol, A.; Frese, L.; Hoerstrup, S. P.; Baaijens, F. P. *Biomaterials* **2012**, *33*, 4545.
(82) Syedain, Z. H.; Meier, L. A.; Reimer, J. M.; Tranquillo, R. T. *Annals of biomedical engineering* **2013**, *41*, 2645.

CHAPTER 1:

ELASTIN-LIKE HYDROGELS AND SELF-ASSEMBLED NANOSTRUCTURES FOR DRUG DELIVERY

JOSE CARLOS RODRIGUEZ-CABELLO,*
ISRAEL GONZALEZ DE TORRE AND GUILLERMO PINEDO

G.I.R. BIOFORGE (Group for Advanced Materials and Nanobiotechnology), Universidad de Valladolid, Edificio I + D, Paseo de Belen, 11, 47011-Valladolid, Spain

Rodriguez-Cabello, J. C.; Gonzalez de Torre, I.; Pinedo, G. CHAPTER 19 Elastin-like Hydrogels and Self-assembled Nanostructures for Drug Delivery. In Smart Materials for Drug Delivery: Volume 2; The Royal Society of Chemistry, 2013; Vol. 2, pp 180-198. DOI:10.1039/9781849734318-00180

1. INTRODUCTION

Nature has always provided humans with all classes of resources and, in particular, supplies a vast amount of protein-based materials that present outstanding properties. Nowadays, researchers of different disciplines such as materials science and biology are combining efforts in the design of advanced materials that exhibit naturally occurring properties. This has led to the birth of a new and evolving science called biomimicry or biomimetics. Mimicking natural sophisticated materials sets challenging goals and although significant progress has been made, there is still a lot to learn from the organizational principles employed by Nature. Translating these hierarchical concepts into synthetic, bio-inspired structures would lead to new, high-performance, types of products.

Material scientists are mimicking nature to obtain synthetic proteins with the properties of natural macromolecules. Protein based polymers offer a set of interesting physical, chemical and biological features. Their component units, the amino acids, provide a broad range of specific characteristics since they can be hydrophobic or hydrophilic, and bear aromatic, cationic, anionic or neutral groups. By changing the sequence design, complex secondary structures as different as a helices, β turns or β sheets can be obtained. This chapter provides an overview of the features and applications in drug delivery of elastin-like recombinamers (ELRs), a new family of protein-based polymers that mimic natural elastin.

2. ELASTIN-LIKE RECOMBINAMERS

Elastin is a major component of the extra-cellular matrix and it can be found in many tissues such as skin, lung, artery, ligament and cartilage, conferring them with elasticity. Recombinant techniques allow one to obtain protein-based materials that combine some features found in natural proteins together with other properties of technological interest. One of the most interesting protein- based materials is the family of the so-called elastin-like recombinamers (ELRs), which have recently focused the attention of many researchers due to their ability to form a variety of structures, such as nanoparticles, nanofibers, films or hydrogels[1-3]. This versatility along with biocompatibility, bioactivity and smart behaviour make ELRs unsurpassable candidates for biomedical applications, including implants and drug-delivery systems (DDSs)[4]. ELRs are genetically engineered biopolymers exhibiting stimuli-responsiveness, based on repeats of the pentapeptide sequence Val-Pro-Gly-Xaa-Gly, where Xaa is any natural amino acid except proline. The most widely studied is poly(VPGVG), namely poly(Val-Pro-Gly-Val-Gly). All functional ELRs present a reversible phase transition in response to changes in temperature[5]. In aqueous solution below a certain temperature, i.e. the transition temperature (T_t) or lower critical solution temperature (LCST), the polymer chains remain disordered, relatively extended with a random coil conformation and fully hydrated[6]. This hydro- phobic hydration is characterized by an ordered clathrate-like water structure surrounding the apolar moieties of the polymer. This structure is somewhat similar to that described for crystalline gas hydrates, although it is more heterogeneous and of varying

perfection and stability[7,8]. When temperature surpasses the T_t, according to Urry's model the polymer chains hydrophobically fold and undergo a conformational transition that leads to phase separation. That "coacervate" is composed of about of 63% water and 37% polymer[9]. In the folded state, the polymer chain adopts a dynamic, regular, non-random structure called a β spiral, which involves one type II β turn per pentamer stabilized by intra-spiral, inter-turn and inter-spiral hydrophobic contacts[5]. The process begins with the formation of filaments composed of three stranded dynamic polypeptide b-spirals, which grow up to hundreds of nanometers before settling into a visible separated state[5,10]. This process is completely reversible (i.e. lowering the temperature below T_t, the initial state is recovered) and has an associated latent heat, ΔHt.5

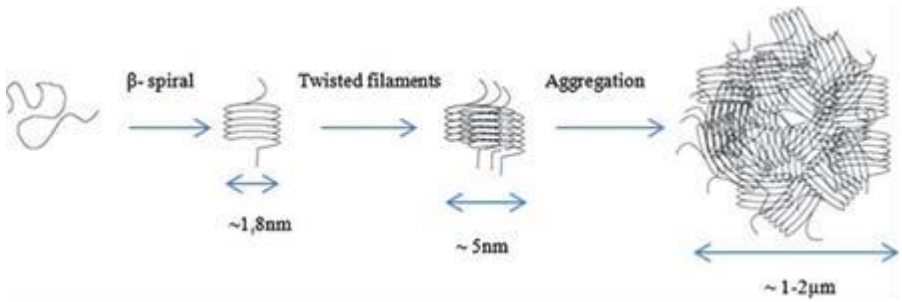

***Fig.1**. Steps of the inverse temperature transition of elastin-like polymers. From left to right: β-spiral structure, formation of twisted filaments or supercoil of β-spiral and aggregation into microaggregates.*

This ΔHt is the result of the combination of the disruption of the water structure and the folding and stabilization owing to the Van der Waals interactions[11]. One VPGVG is enough to permit the transition from random coil to ordered β turn, but higher molecular weight polymers are required to obtain materials presenting useful properties (Fig. 1)[12].

Common proteins undergo unfolding and denaturalization when temperature rises. The shift described above from a disordered to an ordered state upon heating is the base of the inverse temperature transition (ITT). At this point, the reader might think that this behaviour is not possible, because it seems to violate the second law of thermodynamics. However, this apparent mystery can be solved if the system as a whole, i.e. not only the protein but also the water surrounding it, is considered. When the system moves to the ordered state, the increase in order of the protein component is less than the decrease in order of the water component. Thus, the second law of thermodynamics is indeed satisfied.

It has been proven that the amino acids sequence has a great influence on the ITT of ELRs[13]. Substitutions of the amino acid at the fourth position (Xaa) of the pentamer modify the values of T_t, to an extent that depends on the polarity of the amino acid side chain. As a rule of thumb, an increase in the polarity decreases the hydrophobic hydration, which causes an increase in T_t and a decrease in ΔHt. The transition temperature can also be altered by physiological variables, such as pH, salt concentration or presence of certain ions and molecules[14].

As mentioned above, most of the ELRs are based on the general formula (VPGXG), where X represents any natural or modified amino acid except proline. All polymers with this general formula are functional, i.e. all show smart behaviour with sharp responsiveness. However, the achievement of functional ELRs by means of the substitution of any of the other amino acids in the pentamer is not so straightforward. For example, the proline cannot be substituted, and the first glycine cannot be replaced with any

natural amino acid other than L-alanine. This is because the type II β-turn per pentamer involves this glycine together with the proline in the folded state of the polymer.

The presence of bulky moieties in amino acids with L chirality impedes the formation of the b-turn, and the resulting polymer is not functional. Thus, the substitution by alanine is the only possibility reported that still leads to a functional polymer, though even in this case, the resulting polymer shows significantly different and out-of-trend mechanical and thermal properties. Another strategy for tuning the features of ELRs materials is to synthesize them through genetic engineering to obtain multiblock copolymers.

3. ELRS-BASED DRUG-DELIVERY SYSTEMS

The efficacy of pharmacological treatments is constricted by inadequate pharmacokinetics and/or systemic toxicity of some drugs[15]. Targeted drug delivery using a suitable carrier can increase the plasma half-life, minimize the systemic toxicity and improve the local efficacy of the therapeutic agent[16]. An alternative to systemic drug administration is the localized delivery from an immobile matrix that is implanted in the tissue of interest. Drug diffusion into the target organ or tissue reduces the need of repetitive administrations, and overcomes systemic barriers associated with the traditional delivery approaches.

A narrow control of the composition and the size of the carrier is crucial for the biocompatibility and effectiveness of the systemic target delivery. Thus, the possibility of synthesizing ELRs with accurate molecular weight and low polydispersity, biocompatibility

and controlled degradation makes them exceptional carriers for systemic and targeted drug delivery. Many DDSs based on ELRs have been designed in the form of nanoparticles (aggregates, micelles), films and hydrogel networks, which can regulate drug release through diffusion, erosion or swelling mechanisms (Fig. 2)[17].

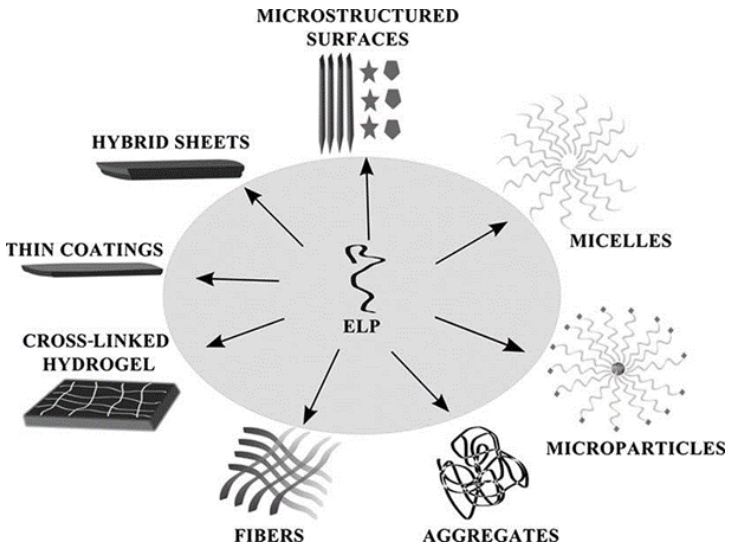

Fig. 2. *Some structures of elastin-based systems useful for drug delivery.*

3.1 ELRs-based Hydrogels

In the last four decades, hydrogels have been used for biomedical and pharmaceutical applications, mainly due to the high water content, resemblance of natural tissues, biocompatibility and stimuli-responsiveness of some of them[18,19]. In fact, they were the first biomaterials designed to be applied in the human body[20]. Hydrogels can be classified into two large groups according to the way the network is formed: reversible or physical, and permanent or chemical (Fig. 3). In a reversible or physical hydrogel the network is held together by molecular entanglements, Coulomb

forces, H-bonding or hydrophobic interactions[21,22]. Usually physical hydrogels are not homogeneous and present clusters of molecular entanglements (areas of high cross-linking density and low water swelling) and hydrophobically or ionically associated domains. Chain loops and free chain ends also create transitory network defects. Permanent or chemical hydrogels are covalently cross-linked networks and may contain clusters spread within regions of low cross-linking density and high water swelling. Free chain ends also cause defects in the gel and do not contribute to the elasticity of the networks.

Most traditional methods of synthesis do not permit an exact control of the sequence, the chain length and the three-dimensional structure and, thus, some deficiencies in the mechanical properties and delayed or slow response times to external stimuli might appear[23]. To overcome these problems many strategies have been developed and numerous polypeptide-based responsive hydrogels have been designed, including networks formed from block copolypeptides[24], recombinant segments of elastin, silk and collagen[7,25] and recombinant triblock copolymers of a random polypeptide sequence flanked by two coiled-coil blocks[26,27]. Protein segments can be introduced to provide degradability, temperature-induced phase transition and sensitivity to biologically active molecules[28-30]. All these strategies can provide very close control over the length and the molecular weight of the proteins that will form the hydrogel network. Hydrogels bearing functional proteins in their structures have huge potential applications in nanotechnology, microfabrication, tissue engineering and drug delivery.

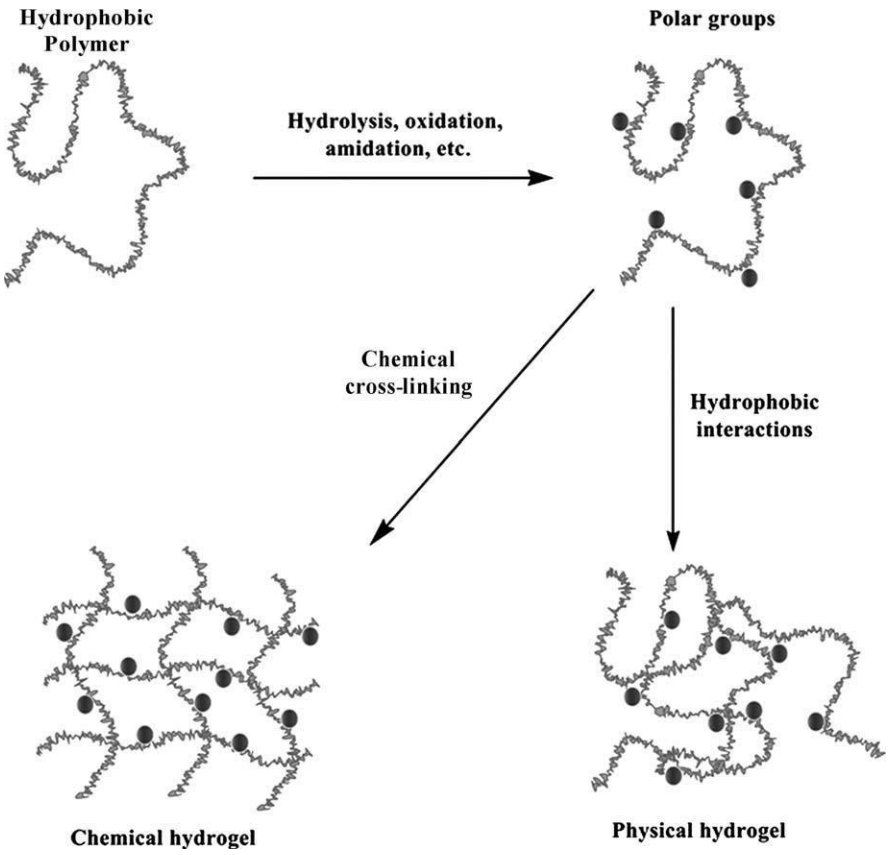

Fig. 3. *Schematic view of the formation of physical and chemical polymer hydrogels.*

ELRs can be cross-linked at exact places along the skeletal structure of the polypeptide[31,32]. Usually these cross-linking sites correspond to lysine residues spaced and repeated after a concrete number of amino acids, which can react with amine reactive molecules such as glutaraldehyde, disuccinimidyl suberate or hexamethylene diisocianate. Through chemoselective cross-linking of dried thin films of ELRs, the stiffness of the hydrogel network can be controlled[33].

Recently, click-chemistry has been applied to form ELRs networks avoiding the use of organic solvents[34]. Nevertheless,

hydrogels formed in water have less uniform structure. Presumably due to phase transitions, which do not occur in organic media.

3.1.1 Chemically Cross-linked ELRs Hydrogels

ELRs hydrogels are quite attractive due to the versatility of the genetic techniques to incorporate active amino acids as guest residue (X) in the elastin base unit (VPGXG) and to render biologically active sequences that can provide unique properties. The formed hydrogels maintain the sensitivity to environ- mental changes in temperature, pH and light exposition[35,36]. Four typical cross-linking strategies can be applied to obtain ELRs hydrogels, as follows (Fig. 4)[37].

a) Radical polymerization.

Chemically cross-linked hydrogel networks can be synthesized by radical polymerization of ELRs derivatized with polymerizable (vinyl, acrylic, alkyne) groups. The polymerization can be induced using chemical initiators like peroxides, which usually are not cytotoxic, or with UV light. The remnant chemical initiator and its degradation products have to be removed (usually by diffusion in an appropriate medium) from the hydrogel network before any in vivo.

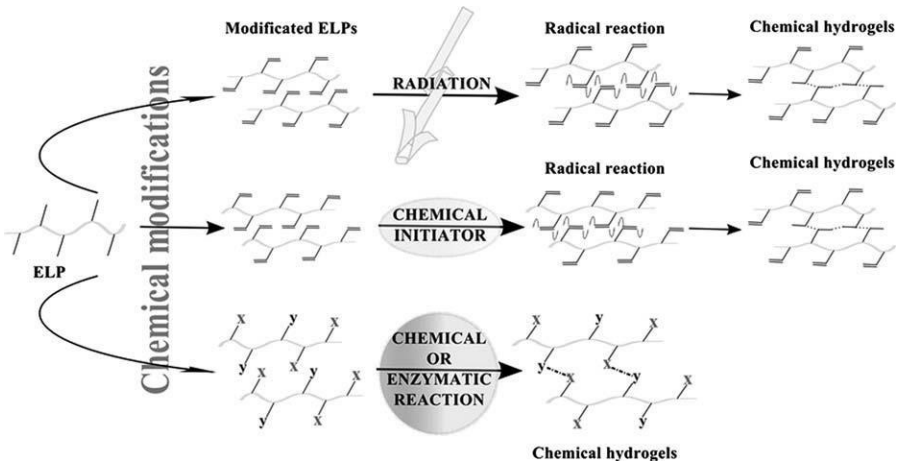

Fig. 4. *Typical strategies to cross-link elastin-like recombinamers (ELRs).*

b) Chemical reaction of complementary groups.

Functional groups of ELRs (amines, alcohols, tiols and acid groups) can be used for hydrogels formation through covalent bonds with complementary groups, involving, for example, the reaction of an aldehyde with an amine or with a hydrazide, or even a Michael reaction of an acrylate and a primary amine or a thiol to form a secondary amine or a sulfide[38]. Some different types of condensation reactions can also be applied to hydrogels formation, such as the Passerini condensation, in which a carboxylic acid and an aldehyde or ketone reacts with an isocyanide, or the Ugi condensation by adding an amine to the same reaction mixture to yield an a-(acylamino) amide[39,40]. Some of these reactions can be used for rapid cross-linking and in situ gelling due to the short reaction time (in certain cases even less than 6 minutes)[41] and the versatility to form different kinds of bonds[42,43]. Other cross-linkers can be used to slowly form hydrogel networks (gelling time greater than 30 minutes)[44]. Two typical procedures are used for ELRs chemical cross-linking. The first one consists of the prefunctionalization of the ELRs with a cross-linking agent, avoiding

the use of small molecules that could be cytotoxic. This procedure has the inconvenience of requiring one or more reactions to functionalize the ELRs, which involve the use of non-biocompatible solvents or cytotoxic chemical agents. Once the ELRs have been modified, the gelation reaction could be carried out in aqueous medium. The second procedure involves the direct reaction of functional groups (amines, alcohols, tiols and acids) of ELRs with homo- or hetero-bifunctionalized molecules. As a drawback, this kind of gelation process has to be carried out in non-biocompatible conditions (organic solvents or chemical compounds) and for this reason the gels obtained have to be washed intensely under biofriendly conditions.

c) High-energy irradiation.

Vinyl and other unsaturated groups can be polymerized when high-energy radiation, principally gamma radiation and electron beam, is applied. The radiation can induce radicals on ELRs derivatized with vinyl groups, for instance homolytic C-H bond dissociation, but may also cause the radiolysis of water molecules and the formation of hydroxyl radicals, which can react with ELRs chains to form macroradicals[45]. The reaction between the macroradicals on different chains of ELRs leads to the formation of covalent bonds. Usually, the irradiation is carried out in an inert atmosphere in order to avoid the macroradicals reacting with air oxygen. The greater the irradiation dose, the higher the cross-linking density and thus the smaller the degree of swelling that the VPGXG-based hydrogels can display in water. The degree of swelling also depends on temperature due to the sensitivity of the polymer[46,47].

Network formation by means of high-energy radiation has the advantage of occurring under mild conditions (room temperature and physiological pH) and in the absence of chemical crosslinkers, which could be toxic.

d) Cross-linking using enzymes.

The use of enzymes to trigger gelation of PEG-based hydrogels has been widely reported[48,49]. By contrast, information on ELRs is still quite scarce and only a few examples of ELRs cross-linked by transglutaminase[50] and collagen enzymatically cross-linked with tailored ELRs[51,52] can be found in the bibliography.

Transglutaminases catalyze the formation of bonds between glutamine and lysine residues of the proteins. These enzymes need Ca^{2+} ions for their activity[53]. The gelation reaction usually takes between 5 and 30 minutes, depending on the protein structure and the enzyme concentration. The enzyme-controlled gelations take place under mild conditions and are, therefore, very cell-friendly.

Both aqueous and organic media can be used to form ELRs networks, although the cross-linking in an organic solvent renders hydrogels with a more uniform structure due to the absence of transitions. Conversely, in water the behaviour of the ELRs molecules is governed by the LCST[31]. Some organic solvents, such as tris-succinimidyl aminotriacetato, can react with the lysine residues of different ELRs chains to form a network. The crosslinking confers the hydrogel with structural stability, being insoluble in water even upon cooling.

Concentration, molecular weight and lysine content of ELRs are key parameters for hydrogel formation. Below a critical concentration[33], the hydrogel network is not formed due to the lack

of inter-molecular contacts. ELRs with high molecular weight are more prone to establish an elevated number of intermolecular contacts that promote the network formation. ELRs with a high content in lysine are the most used to form hydrogel networks, because of the suitability of the amino group of lysine to form covalent bonds between ELRs chains.

The chemical cross-linking strategy has some important advantages, for instance the covalent bonds avoid hydrogel network dilution and prevent components diffusing out from the place where the hydrogel is implanted. Furthermore, relevant features of the hydrogel, such as gelation time, network pore size, stiffness and degradability, can be narrowly controlled through the nature and the concentration of the cross-linker agent. Labile chemical linkages can also be formed in order to be broken under physiological conditions, either enzymatically or chemically[37]. As a drawback, chemical cross-linking usually requires organic solvents and reagents that have to be exhaustively removed after synthesis of the network.

3.1.2 Physically Cross-linked ELRs Hydrogels

Several strategies can be applied to prepare physically crosslinked ELRs hydrogels. Some are described below.

a) *Cross-linking by ionic interactions.*

Polymers with acid groups can be cross-linked by calcium ions at room temperature and physiological pH.

These hydrogels can be destabilized by extraction of calcium ions using a chelating agent[54]. ELRs modified with monosaccharide residues can be cross-linked by means of ionic/coordination

interactions in the presence of potassium ions, since the ionic radius perfectly fits into the free space established by six oxygen atoms of the glucose residues of various polymer chains.

b) *Self-assembly of amphiphilic blocks and graft copolymers.*

Hydrogels can be obtained through aggregation among hydrophobic segments of multi- block copolymers of ELRs. The hydrophobic functionalities are provided by amino acids like alanine (Ala), leucine (Leu), isoleucine (Ile), valine (Val), phenylalanine (Phe), tryptophan (Thp), tyrosine (Tyr) and methionine (Met).

3.1.3 Applications of ELRs Hydrogels

The ELRs hydrogels are attractive for a wide range of purposes, for instance protein purification, biosensing, tissue engineering and mainly drug delivery. Many different therapeutic agents can be encapsulated in ELRs hydrogels, e.g. peptides, antibiotics, antitumor drugs, anti-inflammatory agents, and so on.

a) Anticancer Therapy.

Systemic administration of anticancer drugs has the problem that, although the active principle reaches the site of action, the healthy tissues are also exposed to the toxic action of the drug. To overcome this limitation, two peculiarities of tumours can be exploited: i) the irregularity of their vasculature, which leads to leaky sections, increasing the global permeability; and ii) the lack of a functional lymphatic system. Thus, the drugs diffuse better from blood vessels to tumour tissues than to healthy tissues and, once the drug is inside the tumour, it is not efficiently cleared. This enhanced retention and permeability effect (EPR) can be exploited

using ELRs to encapsulate drugs for targeted delivery, as demonstrated for example with doxorubicin[55]. Cell internalization of ELRs-based constructs can be increased using a cellpenetrating peptide and taking Elastin-like Hydrogels and Selfassembled Nanostructures for Drug Delivery benefit of the hyperthermia induced phase transition.

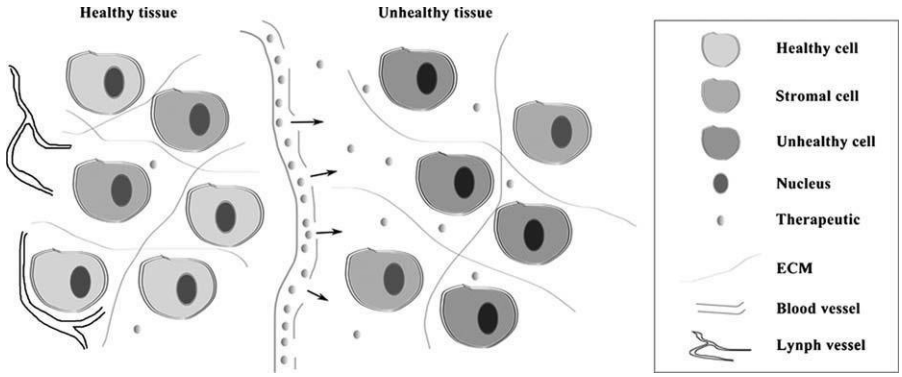

***Fig. 5**. Schematic view of the passive targeting of a systemic drug-delivery system to cancer cells, based on the differences between tumour and healthy tissue morphologies.*

The ELRs vector introduces doxorubicin into the cytoplasm and kills cells by apoptosis. When the treatment is combined with hyperthermia, the cytotoxicity rises up to 20-fold, which proves the usefulness of ELRs for the thermal targeting of doxorubicin. Xenografts of FaDu were used to evaluate in vivo the accumulation of ELRs in solid tumours grown in nude mice[56]. Greater tumour penetration and more homogeneous distribution were observed in thermally treated tumours, suggesting that the combination of temperature-sensitive ELRs with mild hyperthermia improve the anticancer therapy (Fig. 5).

b) Antimicrobial Therapy

Controlled release of antibiotics is another field of application of ELRs, particularly in orthopedics. It has been shown that vancomycin and cefazolin can be homogeneously entrapped in freeze-dried ELRs hydrogels, simply by pre-soaking the networks in drug solutions of different concentrations. The hydrogels can sustain the release of both drugs, keeping their bioactivity[57]. The size and the physico-chemical features of the encapsulated molecules strongly determine the entrapment efficiency and the subsequent release pattern. Drug loading of hydrogels using solutions with high drug concentration caused the networks to exhibit burst release of vancomycin, but not of cefazolin. The concentration of ELRs used to prepare the constructs also played an important role in the release rate of high-molecular-weight drugs: high ELR concentration prolonged the release of vancomycin, but in the case of cefazolin it did not significantly affect the process.

c) Peptide Delivery

Therapeutic peptides and proteins are susceptible to degradation by endogenous proteases located in the gastrointestinal tract and other tissues and exhibit a poor tissue and cellular membrane permeability. Thus, site specific and controlled delivery of these bioactive macromolecules is of great interest[58].

Some ELRs have been tested as carriers for delivery of therapeutic peptides. In particular, they have been attached to cellpenetrating peptides to enhance the intra-cellular delivery[59].

d) Gene Therapy

Gene therapy is a promising strategy for the treatment of many diseases, but the development of an efficient and safe gene delivery vector is still a great challenge[58]. Kim et al.[60] have developed an ELRs-mediated adeno-associated virus (AAV) delivery system for transduction to fibroblasts and human neural stem cells (hNSCs). The ELRs used in this study are based on the well-known pentapeptide sequence VPGVG and on a novel variant of the AAV; the AAV-v3.45. ELRs were absorbed on a tissue culture polystyrene surface (TCPS) and AAV-v3.45 was immobilized onto the ELRs. The amount of ELRs adsorbed on the TCPS determined the surface morphology, roughness and wettability, which are key factors in the modulation of cellular transduction.

ELR-mediated AAV delivery significantly enhanced the transfection efficiency in fibroblasts and hNSCs, which have great potential for use in tissue engineering and in neurodegenerative disorder treatments. In the case of nude plasmid DNA, the polymer concentration, the cure time of the hydrogels and the ionic strength of the medium had notorious influence on the diffusivity of the DNA through the networks[58].

3.2 ELRs Nanoparticles

ELRs block copolymers can form nano- or micro-sized structures that could be directly injected into the systemic circulation without the risk of blocking blood vessels[61-63]. The mimicking of natural elastin provides ELRs with the peculiarity of ‘‘hiding’’ from the immune system. In other words, the immune system just ignores these polymers because it is unable to distinguish them from natural elastin. Furthermore, the biodegradation products are just natural amino acids.

3.2.1 Preparation and Properties

ELRs leading to the formation of nanoparticles are normally synthesized as amphiphile diblock and triblock, namely one or more building blocks are hydrophilic and the other(s) hydrophobic. This is achieved by substituting the amino acid (X) in the guest position at the pentamer VPGXG. If X is glutamic acid (abbreviated as E), this block will be hydrophilic, but if X is valine and the third amino acid is substituted by alanine (abbreviated as A), the block will be hydrophobic. When an aqueous solution of an ELR multi-block copolymer is heated above the Tt, the copolymer chains orientate themselves in a way that the hydrophobic blocks are taken off from the aqueous environment in order to reach a state of minimum free energy. This process results in the formation of nanostructures with a core-corona structure, with the corona composed of the hydrophilic blocks and the core formed by the hydrophobic blocks. That is the case of the block copolymer comprising an E-block of [$(VPGVG)_2$-(VPGEG)-$(VPGVG)_2$] and Ablock of VPAVG monomer[64]. Both blocks are thermo-sensitive and, additionally, the E-block is pH responsive; at pH above the pK_a of the carboxylic acid group (i.e. 4.5), the glutamic acid is deprotonated and charged and the polymer loses the ITT, being ‘‘soluble’’ at any temperature. At acid pH, it is possible to obtain an amphiphilic block copolymer with the E-block soluble in water at any temperature, while the A-block becomes insoluble above the characteristic Tt. Under these conditions, the polymer shows polar and apolar domains and readily forms micelles. These ELRs micelles are good carriers for poorly soluble drugs entrapped within the hydrophobic cores.

Herrero-Vanrell et al.[4] characterized the self-assembly process of poly(VPAVG). This polymer aggregates at 30.7 °C forming nano-

or micro-structures, but does not re-dissolve until the temperature is undercooled down to 8.8 °C (Fig. 1.6). This hysteresis phenomenon is explained by the fact that during the cooling process, the reverse dissolution of the poly(VPAVG) aggregates is strongly hindered by the lack of water molecules between amide groups, which are directly bound together causing stabilization of the folded structure[65]. The hysteresis is a very interesting feature for drug delivery, as it allows the formation of drug-loaded particles at a certain temperature, and then the particles can be cooled down to the physiological temperature an injected into the patient. The size and the shape of the particles was characterized using dynamic light scattering (DLS), static light scattering (SLS) and transmission electron microscopy (TEM) techniques[66,67].

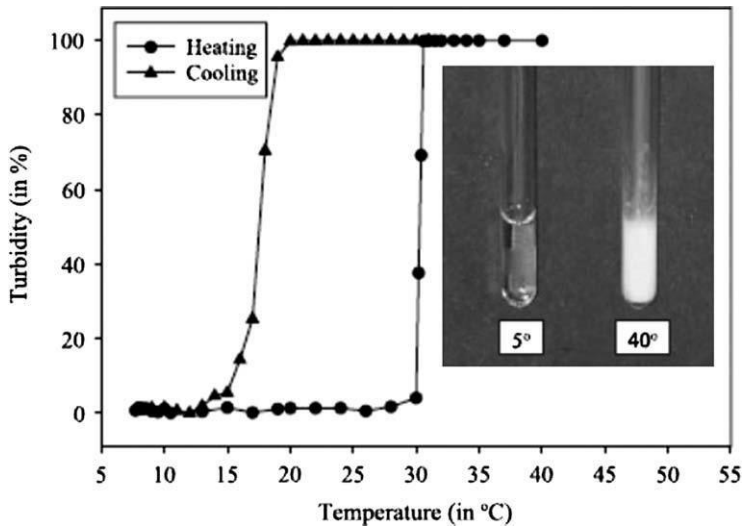

Fig. 6. *Turbidity vs. temperature profiles of poly(VPAVG) showing aggregation when the solution is heated, and dissolution when cooling down. The temperature at which turbidity reaches above 50% is assumed to be the transition temperature.*

3.2.2 Applications of ELRs Nanoparticles

Self-assembled ELRs particles have been tested for the delivery of a wide range of products, such as genes, proteins, therapeutic agents and so on. Bessa et al.[68] showed that recombinant ELR $(VPAVG)_{220}$ can render stable nanoparticles of 237.5 nm diameter suitable for the delivery of bone morphogenetic proteins (BMPs). The particles were formed exploiting the thermo-responsive self-assembly of the material, by resuspending lyophilized polymer in cold phosphate buffer saline (PBS) followed by incubation at 37 °C for 30 min. The growth factors were loaded into the particles by simple addition to the cold polymer solution. The particles encapsulated significant amounts of BMP-2 or BMP-14 with high efficiency as a result of the hydrophobic interactions between the polymer and the growth factors[68]. The release of both BMPs followed a two stage delivery profile, consisting of an initial rapid release in the first 24 h (due to a rapid swelling), followed by a slower release for 14 days. The growth factors retained their activity, as shown by the induction of alkaline phosphatase (ALP) activity and osteogenic mineralization in C2C12 cells.

Rodriguez Cabello's group also explored the use of self-assembled ELRs nanoparticles for controlled release of dexamethasone phosphate. Poly(VPAVG) formed particles above its transition temperature (30 °C), which kept their integrity until a strong cooling was applied. These nanoparticles were able to encapsulate important amounts of dexamethasone phosphate when the selfassembling process was carried out in a co-solution of polymer and drug. The release was sustained for about 30 days[4]. ELRs have also been reported as gene vectors. Chen et al.[69] have designed a polyplex based on K8-ELR (1-60) to transfect MCF-7

cells. The block copolymers were composed of a cationic block from oligolysine (VGK_8G) and an ELR block with 60 repetitive pentapeptide units [$(VPGXG)_{60}$; X being Val, Ala and Gly in a 5 : 2 : 3 ratio]. The cationic block provided the binding place for the plasmid DNA, in such a way that the pDNA remains in the core of the nanoparticles, while the ELR block forms a shell protecting the pDNA. K8-ELR (1-60) condensed pDNA at a cation to anion (N/P) ratio above 0.25 with a particle size (measured by DLS) ranging from 115.5–32.4 nm, showing minimal cytotoxicity and successful transduction of MCF-7 cells.

Recently, Sun et al.[70] have described a novel targeted drug carrier comprising the knob domain of a fibre protein from adenovirus 5 fused with an ELR diblock capable of self-assembling into a micellar structure. These polypeptide nanoparticles target a unique uptake mechanism, which is differentially expressed throughout the body. The chosen ELR diblock contained two motifs with different transition temperatures, which assemble into nanoparticles at physiological temperatures. It was demonstrated, by non-denaturing-PAGE, that the purified knobELRs form dimers and trimers, which is a property of the native knob/fibre protein. To examine the functionality of the knob-ELRs, their uptake was assessed in a hepatocyte cell line that expresses the adenovirus serotype 5 fibre and the knob receptor, the coxsackievirus and adenovirus receptor (CAR). It was found that both plain ELR and knob-ELR can attach to the outside of the cells. Nevertheless, more internalization and localization into lysosomes was attained by the knob-ELR complex. These results prove that large fusion proteins can be assembled by diblock ELR, without the need of bioconjugate chemistry, which simplifies the design of targeted drug carriers. ELRs micelles have also been evaluated as carriers of antitumoral

agents[71]. McDaniel et al.[72] conjugated the C-terminus of the ELRs with doxorubicin that self-assembled into nanostructures able to promote tumour regression on mouse model. The sequestration of doxorubicin within the core of the forming nanoparticles may limit the toxicity to healthy tissues while targeting the drug to the tumour via the EPR effect.

Electrospraying is also useful for generating ELRs nanoparticles with potential application in drug delivery. Wu et al.[73] reported the preparation of nanoparticles of 300–400 nm in diameter, dissolving ELRs in trifluoroethanol and doxorubicin in trifluoroethanol: ethanol 25:1 mixture. Two ELRs of different molecular weight were tested, with peptide sequence SKGPG-$(VGVPGIGVPGIGVPGEGVPGIGVPG)_8$WPC and SKGPG$(VGVPGIG-VPGIGVPGEGVPGIGVPG)_{32}$-WPC$(GGC)_7$. These sequences contained glutamic acid residues with the aim that the charged amino acids i) promote the formation of nanoparticles in electrospraying via Coulombic repulsion and ii) enable the tuning of the Tt and, thus, of the drug release rate as a function of pH (Fig. 1.7). During the electrospraying process, the solution is accelerated across a voltage gradient and the solvents are rapidly evaporated, leading to the formation of solid particles that can be collected from the target surface. Varying the experimental conditions (flow rate, spraying voltage) different morphologies could be achieved such as particles with tails, fibres and nanospheres. The morphology was also strongly affected by the molecular weight and the concentration of the ELR. Spherical particles were preferentially obtained using ELRs of low molecular weight. Once immersed in buffer medium, particles exposed to pH 6.5 and 7.5 rapidly dissolved in water, while the particles incubated at pH 2.5 remain as a coacervate phase. This caused the particles incubated at pH

5.5 or 7.5 and 37 °C below their T_t to display nearly complete release of doxorubicin after only 15 min. In contrast, particles incubated at pH 2.5 and 37 °C above their Tt reached a plateau of only 70% released. The other 30% of drug remained trapped in the ELR coacervate, but could be released upon return to solubility at pH 7.5.

An alternative to the administration of preformed particles consists in exploiting the thermal responsiveness of ELRs with Tt between 37 and 42 °C (limit temperature for mild hyperthermia) to form the particles into the body[72]. For example, a solution of ELR was injected into mice containing human[45] ovarian carcinoma, and the tumour was heated up to 42 °C in order to trigger the coacervation of ELR in the tumour. In this way, active targeting to solid tumours can be achieved just by focused local hyperthermia.

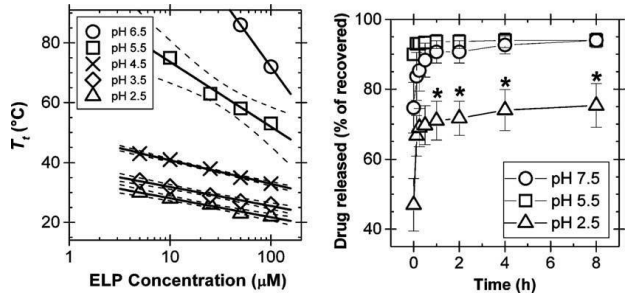

***Fig. 7**. pH-dependent transition temperature of lowmolecular-weight (17.8 kD) ELR as a function of concentration at pH 6.5 (circles), 5.5 (squares), 4.5 (crosses), 3.5 (diamonds) and 2.5 (triangles). A best-fit line and 95% confidence interval are presented. Cumulative drug release from the elastin-like recombinamer (ELR) nanoparticles at 37 °C (n ¼ 3) is shown in the plot on the right. *Significant (p = 0.05, ANOVA-Tukey) difference in comparison to either pH 7.5 or pH 5.5. Reproduced from Ref. 72.*

Recently, Martın et al.[64] have reported the possibilities of obtaining micelles and vesicles from the spontaneous selfassembly of ELRs. Three different ELRs (E50A40, E50A40E50 and E100A40) were investigated, all of them based on the same composing blocks but with different lengths and architecture. The E block was $[(VPGVG)_2\text{-}(VPGEG)\text{-}(VPGVG)_2]_n$ and the A block was $(VPAVG)_n$.

ELRs were solubilized in water at 4 °C, filtered through a 0.45 mm pore membrane and then heated up to 60 °C. The ELR E50A40 adopted micellar structure upon heating, while the other two ELRs self-assembled into hollow vesicles. Therefore, the molecular architecture of the ELRs, namely the block arrangements and lengths, is determinant for the self-assembled structure. The typical structure of these hollow vesicles is shown in Fig. 8. In aqueous solution the hydrophilic segment is expressed, both on the inside and the outside of the hydrophobic membrane, forming a hydrated hydrophilic corona. Theoretically, the elasticity, permeability and mechanical stability are determined by the membrane thickness, which can be controlled by the molecular weight of the hydrophobic block of the copolymer[74]. Compared to liposomes (see Chapters 2 and 3 in this book), the membrane of the hollow[40] vesicles is in general thicker, stronger and tougher due to the higher molecular weight of the components. Thus, these hollow vesicles may be more stable than conventional liposomes. Perhaps the most striking potential application of the ELRs vesicles is in the suitability of their inner cavity for the encapsulation of hydrophilic guest molecules, such as therapeutic agents. While micelles are adequate for the entrapment of hydrophobic molecules, the hollow vesicles can encapsulate hydrophilic ones in the cavity and hydrophobic molecules in the hydrophobic bilayer.

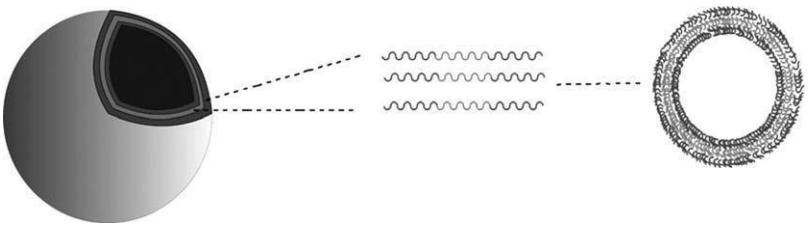

Fig. 8. *Structure of a hollow vesicle formed by self-assembly of an amphiphilic elastin-like recombinamer (ELR) triblock copolymer.*

An alternative to self-assembly to obtain hollow vesicles is the coating of polystyrene beads with ELRs, followed by cross-linking of the ELRs and the dissolution of the beads. Such hollow spheres have been tested by Dah et al.[75] as depots for gene delivery. One ELR, containing a hydrophobic block and a cross-linking block, was used. The hydrophobic block was composed of sequences derived from human exons 20 and 24, while the cross-linking domain was derived from exons 21 and 23. Briefly, the hollow spheres were obtained through three sequential processes: coating, crosslinking and dissolution of the core. Polystyrene beads were sulfonated to create negative surface charges and then used as a template. Sulfonate polystyrene beads were coated with the ELR and incubated in media with different concentrations of mTGase for cross- linking. Finally, polystyrene beads were dissolved using THF to obtain the hollow spheres. Polyplexes were prepared, using poly(2-dimethylaminoethylmethacrylate) (PDMAEMA)-block-poly ethylene glycol methyl ether methacrylate (PEGMEMA)/ethylene dimethacrylate (EDGMA) copolymer and pCMV-GLuc plasmid in PBS. A polyplex of pCMV-GFP was prepared following a similar procedure. The polyplexes may provide pDNA protection against endosomal degradation. Both pDNA and polyplexes were efficiently loaded inside the hollow spheres. The loading yield of pDNA was higher when the polyplex was used. The pDNA alone is loaded by diffusion and not through a charge interaction; in fact, both hollow spheres and pDNA are negatively charged. The high efficiency of polyplex loading is likely due to i) reduction of pDNA size when complexed with a polymer, ii) electrostatic interaction between positively charged polyplex and negatively charged hollow spheres and iii) diffusion. The release of polyplexes from the hollow spheres was minimal, but it remarkably increased after a protease and

elastase treatment. This high pDNA loading capability triggered by enzymes and the transfection ability of the released polyplexes highlight the interest of hollow spheres as nucleic acid depots.

4. CONCLUSION AND FUTURE PERSPECTIVES

Elastin-like recombinamers are excellent biocompatible candidates to form part of DDSs since they are ‘‘invisible’’ for the human immune system and can be easily degraded. The selfassembling property of ELRs in response to environmental changes makes them hugely attractive for the fabrication of nanodevices that can load the drug during the hydrophobic aggregation above T_t, target the drug to specific organs and tissues and modulate subsequent release. Finally, the carriers can degrade at a suitable rate if an appropriate amino acid sequence for the polymer is selected. Hydrophilic drugs can also be loaded within ELR hollow nanoparticles. Furthermore, the ELRs may be convenient to prepare injectable implants that form long-time biocompatible depots for easier treatment of diseases like diabetes or other chronic diseases. On the other hand, novel ELRs can provide more environmentally sensitive DDSs suitable for cancer treatment and gene therapy. Nevertheless, for these applications to become a reality much research is still needed.

5. REFERENCES

(1) Huang, L.; McMillan, R. A.; Apkarian, R. P.; Pourdeyhimi, B.; Conticello, V. P.; Chaikof, E. L. *Macromolecules* **2000**, *33*, 2989.

(2) Dreher, M. R.; Simnick, A. J.; Fischer, K.; Smith, R. J.; Patel, A.; Schmidt, M.; Chilkoti, A. *J Am Chem Soc* **2008**, *130*, 687.

(3) Martin, L.; Alonso, M.; Girotti, A.; Arias, F. J.; Rodriguez-Cabello, J. C. *Biomacromolecules* **2009**, *10*, 3015.

(4) Herrero-Vanrell, R.; Rincon, A. C.; Alonso, M.; Reboto, V.; Molina-Martinez, I. T.; Rodriguez-Cabello, J. C. *Journal of Controlled Release* **2005**, *102*, 113.

(5) Urry, D. W. *Angewandte Chemie-International Edition in English* **1993**, *32*, 819.

(6) San Biagio, P. L.; Madonia, F.; Trapane, T. L.; Urry, D. W. *Chemical Physics Letters* **1988**, *145*, 571.

(7) Urry, D. W. *Journal of Physical Chemistry B* **1997**, *101*, 11007.

(8) Rodríguez-Cabello, J. C.; Alonso, M.; Perez, T.; Herguedas, M. M. *Biopolymers* **2000**, *54*, 282.

(9) Urry, D. W.; Trapane, T. L.; Iqbal, M.; Venkatachalam, C. M.; Prasad, K. U. *Biochemistry* **1985**, *24*, 5182.

(10) Manno, M.; Emanuele, A.; Martorana, V.; San Biagio, P. L.; Bulone, D.; Palma-Vittorelli, M. B.; McPherson, D. T.; Xu, J.; Parker, T. M.; Urry, D. W. *Biopolymers* **2001**, *59*, 51.

(11) Rodríguez-Cabello, J. C.; Reguera, J.; Alonso, M.; Parker, T. M.; McPherson, D. T.; Urry, D. W. *Chem. Phys. Lett.* **2004**, *388*, 127.

(12) Reiersen, H.; Clarke, A. R.; Rees, A. R. *Journal of Molecular Biology* **1998**, *283*, 255.

(13) Ribeiro, A.; Arias, F. J.; Reguera, J.; Alonso, M.; Rodriguez-Cabello, J. C. *Biophys J* **2009**, *97*, 312.

(14) Li, B.; Alonso, D. O. V.; Daggett, V. *Journal of Molecular Biology* **2001**, *305*, 581.

(15) Satchi-Fainaro, R.; Duncan, R.; Barnes, C. In *Polymer Therapeutics II*; Springer Berlin / Heidelberg: 2006; Vol. 193, p 1.

(16) Langer, R.; Tirrell, D. A. *Nature* **2004**, *428*, 487.

(17) Langer, R.; Peppas, N. *Journal of Macromolecular Science, Part C: Polymer Reviews* **1983**, *23*, 61.

(18) Hoffman, A. S. *Adv Drug Deliv Rev* **2002**, *54*, 3.

(19) Peppas, N. A. *J Control Release* **2000**, *68*, 135.

(20) Kopecek, J. *Biomaterials* **2007**, *28*, 5185.

(21) Campoccia, D.; Doherty, P.; Radice, M.; Brun, P.; Abatangelo, G.; Williams, D. F. *Biomaterials* **1998**, *19*, 2101.

(22) Prestwich, G. D.; Marecak, D. M.; Marecek, J. F.; Vercruysse, K. P.; Ziebell, M. R. *J Control Release* **1998**, *53*, 93.

(23) Kopeček, J.; Yang, J. *Polymer International* **2007**, *56*, 1078.

(24) Nowak, A. P.; Breedveld, V.; Pakstis, L.; Ozbas, B.; Pine, D. J.; Pochan, D.; Deming, T. J. *Nature* **2002**, *417*, 424.

(25) Prince, J. T.; Mcgrath, K. P.; Digirolamo, C. M.; Kaplan, D. L. *Biochemistry* **1995**, *34*, 10879.

(26) Petka, W. A.; Harden, J. L.; McGrath, K. P.; Wirtz, D.; Tirrell, D. A. *Science* **1998**, *281*, 389.

(27) Xu, C.; Breedveld, V.; Kopecek, J. *Biomacromolecules* **2005**, *6*, 1739.

(28) Ulbrich, K.; Strohalm, J.; Kopecek, J. *Biomaterials* **1982**, *3*, 150.

(29) Wang, C.; KopecÌŒek, J. i.; Stewart, R. J. *Biomacromolecules* **2001**, *2*, 912.

(30) Miyata, T.; Asami, N.; Uragami, T. *Nature* **1999**, *399*, 766.

(31) McMillan, R. A.; Caran, K. L.; Apkarian, R. P.; Conticello, V. P. *Macromolecules* **1999**, *32*, 9067.

(32) McMillan, R. A.; Conticello, V. P. *Macromolecules* **2000**, *33*, 4809.

(33) Trabbic-Carlson, K.; Setton, L. A.; Chilkoti, A. *Biomacromolecules* **2003**, *4*, 572.

(34) Patterson, J.; Martino, M. M.; Hubbell, J. A. *Materials Today*, *13*, 14.

(35) Rodríguez-Cabello, J. C.; Alonso, M.; Guiscardo, L.; Reboto, V.; Girotti, A. *Advanced Materials* **2002**, *14*, 1151.

(36) Rodríguez-Cabello, J. C.; Reguera, J.; Girotti, A.; Alonso, M.; Testera, A. M. *Progress in Polymer Science* **2005**, *30*, 1119.

(37) Hennink, W. E.; van Nostrum, C. F. *Advanced Drug Delivery Reviews* **2002**, *54*, 13.

(38) Hoare, T. R.; Kohane, D. S. *Polymer* **2008**, *49*, 1993.

(39) de Nooy, A. E. J.; Masci, G.; Crescenzi, V. *Macromolecules* **1999**, *32*, 1318.

(40) de Nooy, A. E. J.; Capitani, D.; Masci, G.; Crescenzi, V. *Biomacromolecules* **2000**, *1*, 259.

(41) Shu, X. Z.; Ahmad, S.; Liu, Y.; Prestwich, G. D. *Journal of Biomedical Materials Research Part A* **2006**, *79A*, 902.

(42) Bulpitt, P.; Aeschlimann, D. *Journal of Biomedical Materials Research* **1999**, *47*, 152.

(43) Hiemstra, C.; van der Aa, L. J.; Zhong, Z.; Dijkstra, P. J.; Feijen, J. *Macromolecules* **2007**, *40*, 1165.

(44) Hahn, S. K.; Oh, E. J.; Miyamoto, H.; Shimobouji, T. *International Journal of Pharmaceutics* **2006**, *322*, 44.

(45) Peppas, N. A. *Hydrogels in medicine and pharmacy : vol.1 fundamentals*; CRC Press: Boca Raton, Fla., 1986.

(46) Lee, J.; Macosko, C. W.; Urry, D. W. *Macromolecules* **2001**, *34*, 4114.

(47) Lee, J.; Macosko, C. W.; Urry, D. W. *Biomacromolecules* **2001**, *2*, 170.

(48) Sperinde, J. J.; Griffith, L. G. *Macromolecules* **2000**, *33*, 5476.

(49) Sperinde, J. J.; Griffith, L. G. *Macromolecules* **1997**, *30*, 5255.

(50) McHale, M. K.; Setton, L. A.; Chilkoti, A. *Tissue Engineering* **2005**, *11*, 1768.

(51) Garcia, Y.; Hemantkumar, N.; Collighan, R.; Griffin, M.; Rodriguez-Cabello, J. C.; Pandit, A. *Tissue Eng Part A* **2009**, *15*, 887.

(52) Garcia, Y.; Collighan, R.; Griffin, M.; Pandit, A. *Journal of Materials Science: Materials in Medicine* **2007**, *18*, 1991.

(53) Westhaus, E.; Messersmith, P. B. *Biomaterials* **2001**, *22*, 453.

(54) Gacesa, P. *Carbohydrate Polymers* **1988**, *8*, 161.

(55) Bidwell, G. L., 3rd; Fokt, I.; Priebe, W.; Raucher, D. *Biochem Pharmacol* **2007**, *73*, 620.

(56) Liu, W.; Dreher, M. R.; Chow, D. C.; Zalutsky, M. R.; Chilkoti, A. *J Control Release* **2006**, *114*, 184.

(57) Adams, S. B.; Shamji, M. F.; Nettles, D. L.; Hwang, P.; Setton, L. A. *Journal of Biomedical Materials Research Part B: Applied Biomaterials* **2009**, *90B*, 67.

(58) Megeed, Z.; Cappello, J.; Ghandehari, H. *Advanced Drug Delivery Reviews* **2002**, *54*, 1075.

(59) Bidwell, G. L., 3rd; Raucher, D. *Adv Drug Deliv Rev* **2010**, *62*, 1486.

(60) Kim, J. S.; Chu, H. S.; Park, K. I.; Won, J. I.; Jang, J. H. *Gene Therapy* **2012**, *19*, 329.

(61) Gref, R.; Domb, A.; Quellec, P.; Blunk, T.; Müller, R. H.; Verbavatz, J. M.; Langer, R. *Adv. Drug Delivery Rev.* **1995**, *16*, 215.

(62) Douglas, S. J.; Davis, S. S.; Illum, L. *Crit. Rev. Ther. Drug Carrier Syst.* **1987**, *3*, 233.

(63) Kim, W.; Thévenot, J.; Ibarboure, E.; Lecommandoux, S.; Chaikof, E. *Angewandte Chemie International Edition* **2010**, *49*, 4257.

(64) Martín, L.; Castro, E.; Ribeiro, A.; Alonso, M.; Rodríguez-Cabello, J. C. *Biomacromolecules* **2012**, *13*, 293.

(65) Schmidt, P.; Dybal, J.; Rodriguez-Cabello, J. C.; Reboto, V. *Biomacromolecules* **2005**, *6*, 697.

(66) Brown, W. *Light scattering : principles and development*; Clarendon Press: Oxford, 1996.

(67) Burchard, W. *Static and dynamic light scattering from branched polymers and biopolymers*

Springer Berlin / Heidelberg, 1983; Vol. 48.

(68) Bessa, P. C.; Machado, R.; Nurnberger, S.; Dopler, D.; Banerjee, A.; Cunha, A. M.; Rodriguez-Cabello, J. C.; Redl, H.; van Griensven, M.; Reis, R. L.; Casal, M. *J Control Release* **2009**.

(69) Chen, T. H.; Bae, Y.; Furgeson, D. Y. *Pharm. Res.* **2008**, *25*, 683.

(70) Sun, G.; Hsueh, P.-Y.; Janib, S. M.; Hamm-Alvarez, S.; Andrew MacKay, J. *J. Controlled Release* **2011**, *155*, 218.

(71) Dreher, M. R.; Raucher, D.; Balu, N.; Michael Colvin, O.; Ludeman, S. M.; Chilkoti, A. *J Control Release* **2003**, *91*, 31.

(72) McDaniel, J. R.; Callahan, D. J.; Chilkoti, A. *Adv. Drug Delivery Rev.* **2010**, *62*, 1456.

(73) Wu, Y.; MacKay, J. A.; McDaniel, J. R.; Chilkoti, A.; Clark, R. L. *Biomacromolecules* **2009**, *10*, 19.

(74) Discher, B. M.; Won, Y. Y.; Ege, D. S.; Lee, J. C. M.; Bates, F. S.; Discher, D. E.; Hammer, D. A. *Science* **1999**, *284*, 1143.

(75) Dash, B. C.; Mahor, S.; Carroll, O.; Mathew, A.; Wang, W.; Woodhouse, K. A.; Pandit, A. *J. Controlled Release* **2011**, *152*, 382.

CHAPTER 2:

HYBRID ELASTIN-LIKE RECOMBINAMER-FIBRIN GELS: PHYSICAL CHARACTERIZATION AND *IN VITRO* CELL EVALUATION FOR CARDIOVASCULAR TISSUE ENGINEERING APPLICATIONS.

Israel González de Torre[1]*, Miriam Weber[2], Luis Quintanilla[1], Matilde Alonso[1], José Carlos Rodríguez Cabello[1], Stefan Jockenhoevel[2], Petra Mela[2]

1 BIOFORGE, CIBER-BBN, Campus "Miguel Delibes" Centro I+D, Universidad de Valladolid, Paseo Belén 11, 47011, Valladolid, Spain
2Tissue Engineering and Textile Implants, AME, Helmholtz Institute, RWTH Aachen, Germany

González de Torre, I.; Weber, M Quintanilla, L.; Alonso, M.; Rodríguez Cabello, J. C.; Jockenhoevel, S.; Mela, P. Hybrid elastin-like recombinamer-fibrin gels: physical characterization and in vitro cell evaluation for cardiovascular tissue engineering applications. Acta Biomaterialia Under review.

ABSTRACT:

Hybrid Elastin-Like Recombinamer-Fibrin Gels (ELR-FGs) have been prepared and characterized. The fibrin–ELRs ratio have been selected to maximize the complex modulus magnitude of the resulting ELR-FGs. The correlation between SEM micrographs, porosity, swelling ratio and rheological properties have been discussed. For several gel concentrations, a poroelastic mechanism has been suggested to explain the mechanical behavior of these Hybrid gels. Their cytocompatibility has been tested through 3D cell cultures of Ovine Umbilical Smooth Muscle Cells (OUSMCs). The cells developed their normal structures to form a natural extracellular matrix. As a proof of concept an artificial aortic valve was molded.

1. INTRODUCTION

There are many applications in the bioscience field where biomaterials are required, and depending on the particular needs of those applications the biomaterials should have specific properties. Anyway, biocompatibility, in some cases biodegradation, absence of toxic byproducts, suitable mechanical properties and cell-friendly behavior are always desired for a biomaterial. In particular, hydrogels have been widely employed as drug depots, scaffolds for tissue engineering, gene delivery or cell encapsulation among other applications. These gels must meet the specifications previously mentioned. Yet, many times some of these requirements are not completely satisfied by those hydrogels. Thus, the biomaterial scientists are continuously bringing to light new systems which match the needs of the specific application where it will be employed.

Elastin-Like Recombinamers (ELRs) are a kind of protean biomaterials which mimics certain sequences of natural elastin; they show extraordinary properties for the most cutting-edge applications in biomedicine and nanotechnology. These compounds are obtained by recombinant DNA technologies. The bioproduction of these protein-based polymers means a total knowledge of their structure and a complete control over the aminoacid sequences. ELRs can include different bioactive sequences[83], such as those governing cell adhesion, protease sensitiveness, etc. These ELRs exhibit outstanding biocompatibility, tunable mechanical properties, thermosentive behavior and strong self-assembly capabilities[83,84]. The thermosensitive behavior is characterized by a critical temperature in aqueous solution, the transition temperature

(T_t), which is associated with a conformational reorganization at the molecular level. Thus, whereas the polymer chains are soluble in water below certain T_t, above this temperature they self-assemble into nano- and micro-aggregates and become insoluble. This process is completely reversible.

Fibrin gels have been widely physically and biologically described[85,86], and employed for cartilage repair[86], nerve regeneration[87], soft tissues reconstruction (CMH), cardiovascular tissue engineering[56] or cell culture and differentiation[88] among others. They exhibit high biocompatibility as well as low mechanical stiffness[56], and the absence of elastin in cell cultures does not help to improve this lack on the mechanical properties of the fibrin gels.

The affinity of fibrinogen and fibrin for elastin was widely investigated for Rabaud et al[54] and the potential uses of these materials for tissue engineering have been reported[89-91]. Yet, the reaction between both materials was not completely controlled. In this paper, we postulate a covalent reaction between glutamines from fibrin and lysines from ELRs promoted by the XIIIa factor (transglutaminase). Specifically, an ELR which bear RDG adhesion sequences and lysines homogeneously distributed along polypeptide chain is cross-linked with fibrinogen in presence of transglutaminase, $CaCl_2$, and thrombin to obtain a novel hybrid gel that incorporates the bioactivity and mechanical properties of ELRs.

In these new hybrid gels, a detailed characterization is essential. In particular, the mechanical/viscoelastic properties of hydrogels have to be considered since these properties strongly correlate with material microstructure and functionality, even at a biological level. In this sense, it is well-known that rheological measurements, which have been employed for measuring the

mechanical and dynamic viscoelastic properties of the fibrin gel[92-95], are an adequate tool for characterizing these properties. A biphasic poro-viscoelastic (BPVE) model[96-98], which takes into account the viscoelastic behavior generated by both the flow-dependent frictional interactions (poroeslasticity) as well as the intrinsic (fluid-independent) viscoelastic nature of the porous solid-matrix, is essential for explaining the behavior of ELRs based hydrogels[99].

In the next pages we will focus our attention on the microstructural morphology and mechanical properties of those hybrid hydrogels, as well as their biological properties. In particular, the physical mechanism that dominates the viscoelastic behavior of hybrid gels in the frequency range considered in this work will be discussed. Thus, a new generation of ELR-Fibrin hybrid gels with high biocompatibility and synergetic outstanding mechanical properties of both materials, including the thermosensitive behavior and bioactive domains of ELRs, will be presented along with their potential uses as drug-delivery systems, scaffolds for tissue engineering. Due fibrin gels have been widely employed for vascular tissue engineering applications[56,100-102], quite interesting applications for these new ELR-FGs could be found in this field. Based on the mechanical properties that will be explained, and as a probe of concept, an aortic valve will be molded and in vitro evaluated.

2. EXPERIMENTAL

2.1.Materials

Fibrinogen, Human Plasma was purchased from CALBIOCHEM (EMD Biosciences), purity > 95%.

2.1.1. ELR bioproduction

The ELRs were constructed using standard genetic engineering techniques and purified using several cycles of temperature-dependent reversible precipitation, as described by Girotti et al.[51] The bio-produced polymer was purified by a series of centrifugations under and above its transition temperature. The ELRs obtained following this method were dialyzed against MilliQ (MQ) water and then lyophilized.

The ELR employed is HRGD6, previously characterized by Costa et al[103], a polymer containing a general adhesion sequence, RGD, whose amino acid sequence is

MGSSHHHHHHSSGLVPRGSHMESLLP $[(VPGIG)_2(VPGKG)(VPGIG)_2]_2AVTGRGDSPASS[(VPGIG)_2(VPGKG)(VPGIG)_2]_2$.

2.1.1.1. ELRs-Fibrin hybrid gels formation:

As is well-known, the reaction between γ-carboxy-amine group of a glutamine residue and the ε-amino group of a lysine residue is improved by the presence of the enzyme transglutaminase (Factor XIII) which is a Ca^{2+}-dependent enzyme. Two solutions were prepared for the ELRs-Fibrin hybrid gels formation: one with Fibrinogen and HRGD6 at a concentration of each component of 2.5 and 15 mg/mL to obtain a final

concentration of polymer between 5 and 30 mg/mL in TBS. The second solution contained 30% of thrombin and 30% of $CaCl_2$ in TBS. Both solutions were homogeneously mixed into the appropriated mold and kept at room temperature (r.t.) for at least 15 minutes. After this period the gel, with a total polymer concentration between 2.5 and 15 mg/mL, was already formed and could be easily handled. The enzymatic process to obtain the ELRs-Fibrin hybrid gels is outlined in Fig 1.

At least three replicates for each hybrid gels of each concentration were prepared and measured by any of the instrumental methods reported in this work.

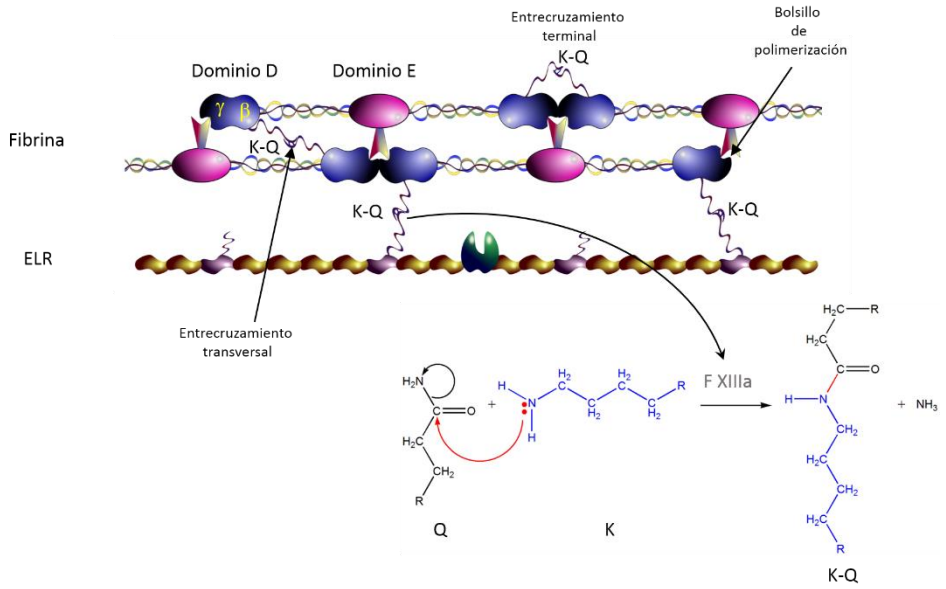

***Fig 1**. Scheme of ELRs-Fibrin hybrid gels formation.*

2.2.Experimental methods

2.2.1.1. Microstructural morphology:

Scanning electron microscopy (SEM) was employed to investigate the morphology of fibrin and hybrid gels. Thus, both,

the ELR-Fibrin hybrid gels and fibrin gels were immersed in MQ water at 37 °C for one day, then immediately they were dropped into liquid nitrogen, physically fractured, and immersed in liquid nitrogen again. Finally, they were freeze-dried. Images of lyophilized hydrogels were obtained by (FEI Quanta 200 FEG) with no prior coating procedures. SEM in low vacuum mode (~ 1 torr) and with water vapour as working gas was used to investigate the morphology of both hydrogels.

2.2.1.2. Porosity calculations and swelling ratio:

The following equation[29,104] was employed to estimate hydrogel porosity:

$$\text{Porosity } (\%) = ((W_1-W_2)/\rho_{water})x100/V_{hydrogel} \quad \text{(Eq.1)}$$

where W_1 and W_2 are the weight of the swollen and lyophilized gels, respectively, ρ_{water} is the density of pure water, and $V_{hydrogel}$ is the measured volume of the gel in the swollen state ($V_{hydrogel} = \pi r^2 h$, where r and h are the radius and height of the cylindrical sample, respectively). Excess surface water was removed with a filter paper before each measurement.

The volume change related to the phase-transition of the hydrogels in aqueous solution was quantified, at a fixed temperature, in terms of the equilibrium swelling ratio by weight, Q_w, defined as

$$Q_w(\%) = ((W_1-W_2)/W_2)x100 \quad \text{(Eq.2)}$$

All measurements were taken 24 h after soaking the hydrogel in MQ water at the selected temperature. Equilibrium was defined as the steady state at which there was no change in volume of the ELR-Fibrin hybrid gels.

Both porosity and the equilibrium swelling ratio were measured at 4 and 37 °C. Lyophilization (freeze-drying) was performed for water-swollen and hydrogels frozen in liquid nitrogen at the corresponding test temperature.

2.2.1.3. Rheological measurements:

A strain-controlled AR-2000ex rheometer (TA Instruments) was employed to perform rheological experiments. Disc-shaped swollen gel samples were placed between parallel plates of nonporous stainless steel (diameter = 12 mm) and the gap between the plates was adjusted using a normal force enough to prevent slippage. A gap higher than 1000 μm was always reached after the sample relaxed until equilibrium. Measurements were performed at 37 °C, with the sample temperature being controlled and maintained using a Peltier device.

Two different measurements were carried out in shear deformation mode. First, with the aim to determine the range of strain amplitudes over which the gels exhibited a linear region of viscoelasticity, dynamic shear modulus was measured as function of strain. Thus, a dynamic strain sweep (with amplitudes ranging between 0.1% and 20% and at a frequency of 1 Hz) was accomplished. And second, to obtain the dependence of the dynamic shear modulus and loss factor on frequency, dynamic frequency sweep (between 0.05 and 70 Hz at a fixed strain, selected within the hydrogel linear region) tests were performed. Rheological evaluation allowed the storage modulus (G'), loss modulus (G''), complex modulus magnitude |G*|, ($|G^*|^2 = (G')^2 + (G'')^2$), and the loss factor ($\tan \delta \equiv (G'')/(G')$, where δ is the phase angle between the applied stimulus and the corresponding response) as a function of strain amplitude or frequency.

2.2.1.4. Cycompatibility:

Hybrid ELRs-FGs were prepared in a final polymer concentration of 10 mg/mL and 11 million/mL of Ovine Umbilical Smooth Muscle Cells (OUSMCs) pass 5 were embedded inside the gels. For this purpose a solution of fibrinogen and HRGD6, at the desired proportion, in sterile TBS was prepared. Another solution of 15% of thrombin and 15 % of $CaCl_2$ and OUSMCs, at the desired concentration, in sterile TBS was prepared. Both solutions were co-injected using a two syringe system into a 24 well-plate to obtain 0.5 mL ELRs-Fibrin hybrid gels in a concentration of 10 mg/mL of polymer and 50% of ELR and with 2.8 million of OUSMCs embedded inside them.

As negative control, fibrin gels were prepared in a similar way as previously described for ELRs-Fibrin hydrogels, a solution of fibrinogen-ELR in sterile TBS was prepared. Another solution of 15% of thrombin and 15 % of $CaCl_2$ and OUSMCs, at the desired concentration, in sterile TBS was prepared (the final concentration of polymer was 10 mg/mL and 50% of ELR).

The gels were cultured for 15 days at 37°C and 5% CO_2 in bioreactor medium for fibroblasts. After these 15 days, the gels were removed from the well-plate and cut into pieces. These pieces were dried and prepared to be embedded in paraffin, cut into slices with a microtome and lately staining against elastin, collagen I and III, α Smooth Muscle Actin (αSMA), Myosin Light Chain Kinase (MLCK) , αSMA, and Vimentin.

2.2.1.5. Aortic valve formation:

A sterile solution of fibrinogen and HRGD6 in TBS was prepared (30 mg of fibrinogen and 30 mg of HRGD6 in 3 mL of TBS). A solution of 30% of thrombin and 30% of $CaCl_2$ in sterile TBS was prepared (3 mL) (final concentrations: fibrinogen-ELR 10 mg/mL, thrombin 15%, $CaCl_2$ 15%).

60 millions of Miofibroblasts were suspended into the thrombin/$CaCl_2$ sterile solution. A sterilized aortic valve mould of 19 mm was used to cast the valve, and a net was stitched up to a silicon ring, which was placed inside the mould. Both solutions were simultaneously injected into the mould; once the solutions were mixed inside the mould with the cells, the mould was quickly closed to avoid any leaking, and this was kept closed at r.t., under sterile conditions for 45 minutes. Next, the valve was removed from the mould and was placed into a bioreactor. One litre of bioreactor medium for fibroblasts was added. The valve was cultivated under static conditions for 7 days. BGA analyses were carried out along this period in a blood-gas analyser (Radiometer ABL520 and EML 100; Radiometer Medical A/S, Copenhagen, Denmark). Finally, the valve was removed from the bioreactor under sterile conditions. The leaflets were opened with the help of a scalpel.

After the medium was substituted by new bioreactor medium for fibroblasts, a dynamic cultivation cycle of seven days was started. The stimulation program was based on the procedure described by Flanagan et al[105]. The starting parameters of the dynamic cultivation were set at a frequency of 40 beats per minute (bpm). BGA analyses were carried out every two days. Two days after start the dynamic cultivation period, the frequency was raised till 80 bpm. After fifteen days the bioreactor medium was removed

from the bioreactor and one liter of Phosphate Saline Buffer (PBS) x1 was added to wash the valve. The PBS was also removed, and then, the valve was extracted from the bioreactor.

Some pieces from the leaflets and from the wall of the valve were cut off, dried and embedded into parafilm cut into slices with a microtome and lately staining against elastin, collagen I and III, α Smooth Muscle Actin (αSMA).

2.2.1.6. Immunohistochemical analysis:

Immunohistochemistry was performed on Bodian's-fixed, paraffin-embedded sections of hybrid gels and artificial valve. Non-specific sites on tissue and construct sections were blocked and the cells permeabilized with 5% normal goat serum (NGS) in 0.1% Triton x100-PBS. Sections were incubated for 60 min. at 37°C with the following primary antibodies: 1:400 mouse mono- clonal anti-alpha smooth muscle actin (a-SMA); 1:500 mouse monoclonal anti-type I collagen; 1:150 rabbit anti-type III collagen (DPC Biermann); 1:200 Rabbit polyclonal Elastin (Fitzgerald Industries International, EEUU); 1:150 mouse mono-clonal anti-vimentin; anti-Miosin Ligth Chain Kinase (MLCK). Then, sections were incubated for 1 h at 37°C with either rhodamine or fluorescein-conjugated goat-anti-mouse or goat-anti-rabbit secondary antibodies (1:400; Molecular Probes, Leiden, The Netherlands) for elastin staining. The samples were incubated 60 min. at 37°C with 1:1000 streptavidin TRITC (Acris Antibodies GmbH. Herford, Germany) or 1:400 Alexa Fluor 488 (Molecular Probes). Cells were counterstained with DAPI nucleic acid stain (Molecular Probes). 5% NGS in 0.1% Triton x 100-PBS was used as diluent for all antibodies. As negative controls, samples were incubated in diluent and the secondary antibody. Samples were viewed using an optical

microscope equipped for epi-illumination (Nikon ES400; Nikon Instruments Inc., Melville, NY, USA). Images were acquired using a 3-chip cooled CCD colour camera (Hamamatsu C5810; Hamamatsu Photonics KK, Hamamatsu City, Japan).

2.2.1.7. Statistical analysis:

Values are reported as mean ± SD (n = 3). Statistical analysis was evaluated by one way analysis of variance using the Holm-Sidak method. A p value lower than 0.05 was considered to be statistically significant. (**) $p < 0.001$, (*) $p < 0.05$. $p>0.05$ indicates no significant differences (n.s.d.).

3. RESULTS AND DISCUSSION

3.1.Rheological characterization.

After the linear viscoelastic region of the hydrogel has been obtained by a strain sweep (up to 6 – 7 %, see Figure XX in Supporting Information), several dynamic frequency sweep measurements at a fixed strain selected within this linear region (1% in this case) have been carried out.

First, the optimal ELR fibrin ratio in the hydrogel must be determined. This value was selected according to the criterion of maximizing |G*|, while an elastic behaviour is maintained (G´>>G´´ and a low value of δ). As can be seen in Fig. 1, this criterion is satisfied about an ELR percentage of 50%. This proportion was chosen providing the corresponding rheological parameters at 1 Hz G´= 500 Pa, G´´ = 30 Pa, and δ = 3°. These values indicate a high elastic behaviour of hydrogels. In

consequence, the same proportion of fibrin and ELR polymer was always used in the following hydrogels described in this work.

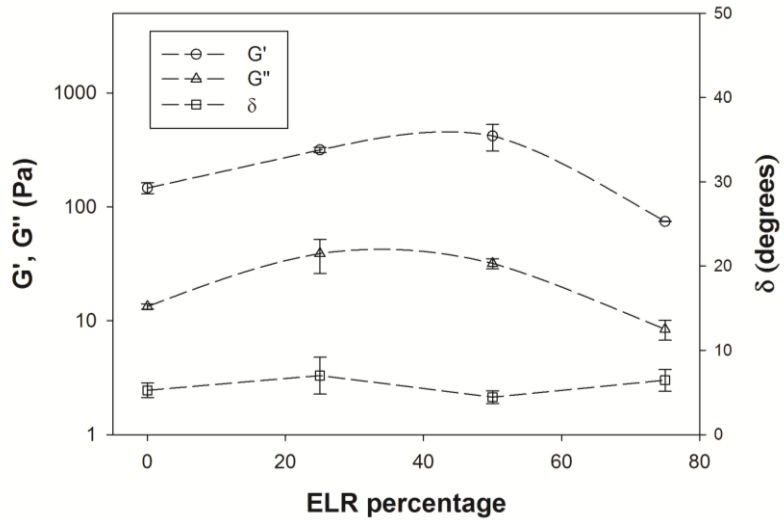

***Fig. 2**. Evolution of Storage (G') and Loss (G'') moduli, and δ as function of the ELRs proportion in hybrid ELR-FGs at a frequency of 1 Hz. These values have been obtained from dynamic frequency sweeps at 37°C using a strain amplitude of 1%.*

Next, the dynamic response of several ELR-FGs at several concentration (ranging from 2.5 mg/mL to 15 mg/mL) is obtained by frequency sweep measurements (Fig.3).

No significant dependence of |G*| on the frequency (Fig.3 (A)) is observed up to 1 Hz and 2 Hz for ELRs concentrations of 2.5 and 5 mg/mL, respectively. For higher concentrations (10 and 15 mg/mL), a frequency dependence is found in the frequency range up to 5 and 10 Hz, respectively. For all concentrations, |G*| shows a strong increase at higher frequencies. The phase angle, δ, only shows a noticeable frequency dependence for frequencies beyond 10 Hz (Fig.3 (B)).

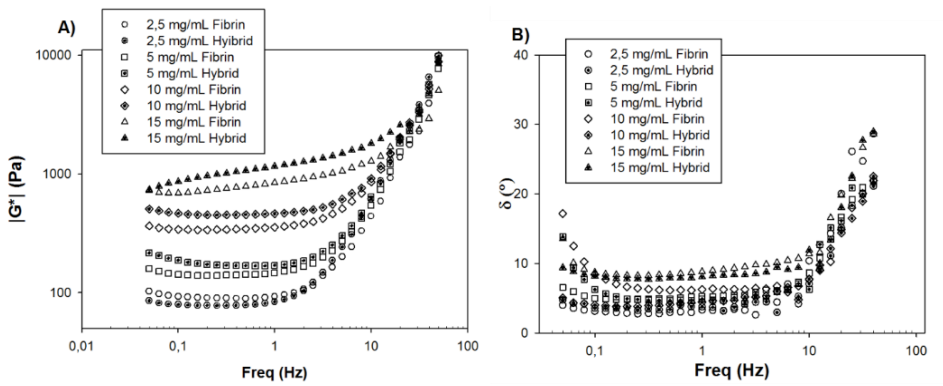

Fig.3. *Evolution of complex modulus magnitude, A), and phase angle (δ), B), as function of the frequency for several concentrations of hybrid ELR-FGs (cross hair symbols) and fibrin gels (open symbols). Each curve corresponds to the average of three different samples.*

In Fig.4, storage and loss moduli along with the phase angle have been plotted as a function of the ELR concentration at a fixed frequency (1 Hz). Both G´ and G´´ (Fig. 4 (A) and (B) respectively) increase when concentration does. Moreover, G´ >> G´´ for the considered concentration range. Quite similar values are obtained for the lower concentrations (2.5 and 5 mg/mL), but for higher concentrations both G´ and G´´ are higher for the ELR-FG than for the fibrin one, and the difference in G´ and G´´ becomes statistically significant. These results agree with bibliography since Sun et al.[106] have reported an increase of G´ with the fibrin concentration in fibrin hydrogels.

As far as δ is concerned (Fig.4 (C)), an increase with concentration is found for both types of hydrogels. Anyway, the low values obtained are agreed with a high elastic hydrogel behaviour throughout the concentration range considered. In conclusion, the presence of ELRs in the hybrid gels increases the mechanical properties of these gels with respect to the fibrin gels.

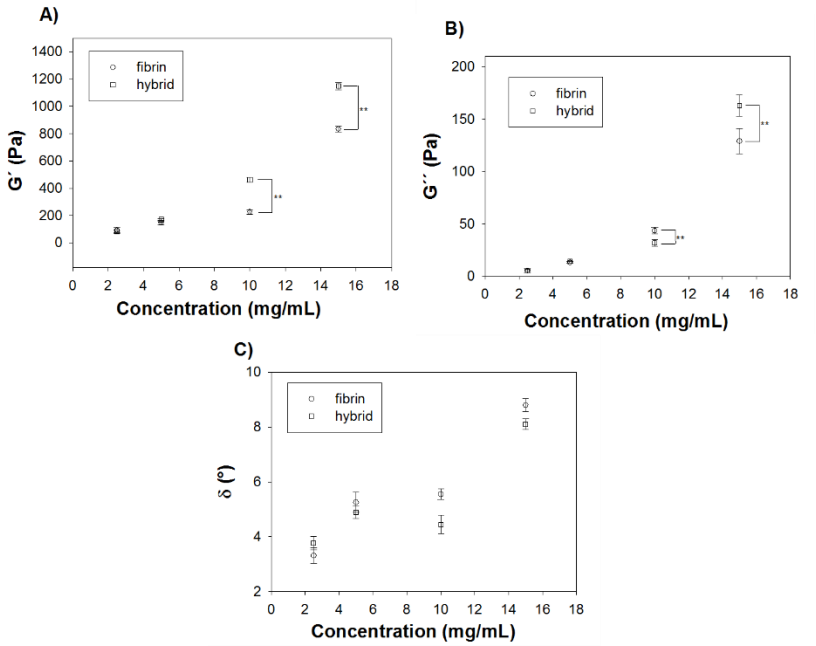

Fig 4. *Evolution of G′, G″ and δ for Fibrin gels (circles) and ELR-FGs (squares) as function of the gel concentration at a fixed temperature of 37°C.*

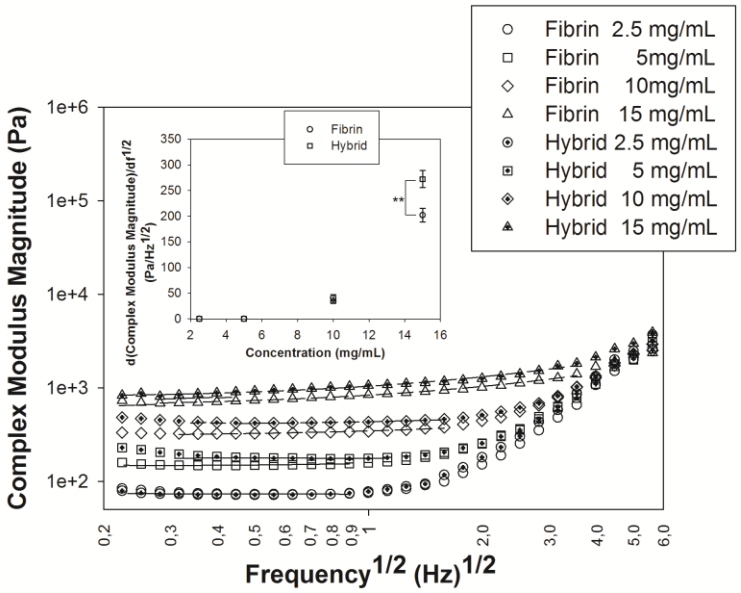

Fig.5. *Dependence of the magnitude of the complex modulus on f½ at 37°C for every kind of gel and concentration analyzed in this work. A log-log scale has been used. The dashed line corresponds to the least-square linear regression of the linear region. In every case R2 is always better than 0.990. The slope of these curves has been plotted in the inset as a function of concentration in the range 2.5–15 mg/mL. Each curve corresponds to the average of three different samples measured.*

To provide an insight in the physical mechanisms that determines the frequency dependence of |G*|, the evolution of |G*| has been plotted as a function of $f^{1/2}$ on Fig. 5. For 2.5 and 5 mg/mL concentrations, a plateau in |G*| values is observed up to about 1 $Hz^{1/2}$. However, for higher concentrations, a linear dependence of |G*| on $f^{1/2}$ is found. It has been recently reported a similar behaviour in Elastin-Like Catalyst Free Click Gels[99] where this linear dependence was related to a poroelastic mechanism that dominates the viscoelastic behaviour in this frequency range. The slope is related to the gel permeability that is a macroscopic measure of the ease with which a fluid can flow through the gel matrix. When the ELRs concentration increases, permeability decreases[99]. For the concentration of 15 mg/mL a higher slope is found for the ELR-FGs, corresponding to a higher hindrance in the fluid flow through the gel structure. These results obtained from the rheological measurements will be correlated with SEM micrographs in its corresponding sub-section.

3.2.Thermosensitive behaviour

As previously mentioned, ELRs exhibit some special thermal features which make them very interesting polymers for biomedical applications. One of these properties is their temperature sensitiveness, characterized by their T_t. Below this temperature, the polymeric chains of the ELRs suffer a hydrophobic hydration, which means that the ELRs chains are completely hydrated by clathrates formed by water molecules. Above T_t, the chains of ELRs adopt a more ordered structure excluding the water that forms those clathrates. This process makes them precipitate. Thus, this thermal sensitiveness could be present in our hybrid gels.

In order to prove this thermosensitive behaviour DSC and organoleptic assays were performed. For these tests, 12 mm diameter and 3 mm high disc-shaped hybrid gels (10 mg/mL) were formed. These gels were immersed in cold distilled water (4°C) for one minute. Then, the gels were partially immersed in a warm distilled water bath (37°C) for one minute. A change in the transparency of the gels was clearly evident as can be observed in the picture sequence of the Fig. 6 (A, B). This thermosensitive behaviour was corroborated by DSC measurements, which showed an increment in the T_t of the hybrid gel with respect to the ELR of more than 5°C. Therefore, the thermosensitive properties of the ELRs have inherited by our hybrid gels.

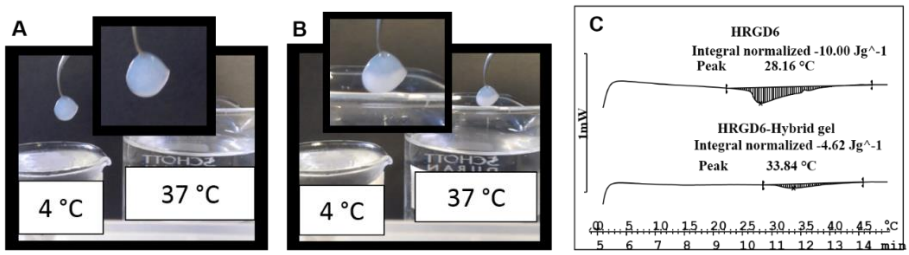

Fig 6. *Thermosensitive behaviour of the ELR-FGs. (A) Hybrid ELR-FG after 1 minute of immersion at 4°C. (B) Hybrid ELR-FG after partial immersion during 1 minute at 37°C water. A white half-moon can be seen in the lower part of the gel due the transition of the ELRs. (C) Thermogram of ELR (10 mg/mL) (upper curve) and ELR-FG (10 mg/mL) (lower curve) in MilliQ water.*

3.3.Microscopic structure

SEM micrographs were accomplished to investigate the microscopic structure of fibrin and hybrid gels for several recombinamer concentrations (Fig. 7).

As is well-known, fibrin gels show a compact fibrin network microstructure[85,107], as can be seen in Fig 7 E, which shows our 10 mg/mL fibrin gel control.

On the contrary, hybrid gels showed a microscopic structure where the mixture of both biopolymers is evident. For the lowest concentration (2.5 mg/mL, Fig 7 (A)) fibrin strands (each visible strand comprises multiple fibrin fibres) are clearly observed. Moreover, thin elastin fibres can be also found, and some of them are in the perpendicular direction to the fibrin strands. A significant pore size of several microns must be noted. When concentration increases (5 mg/mL, Fig 7 (B)), a similar structure is detected, but fibrin strands are closer and the elastin fibres give rise to a web-like structure. Finally, for higher concentration (10 and 15 mg/mL, Fig 7 (C and D)) a mesh-like structure and a significant pore size reduction is observed.

SEM micrographs confirm the higher hindrance in the fluid flow through the gel structure suggested from rheological measurements (see inset in fig 5) owing to the decrease in the pore size and more compact structure when recombinamer concentration increase.

In Fig. 7 (F) the ratio |G*|/concentration as a function of the polymer concentration has been plotted for both the fibrin and the hybrid gels. Both curves show a similar dependence. Two regions are detected in the graph. First, a plateau up to a concentration lower than 10 mg/mL with similar values for the fibrin and hybrid gels. Second, for higher concentrations a significant increase of the concentration-normalized complex modulus magnitude is observed, higher for the hybrid gel. Therefore, a synergetic interaction between fibrin and elastin can be suggested for these concentrations.

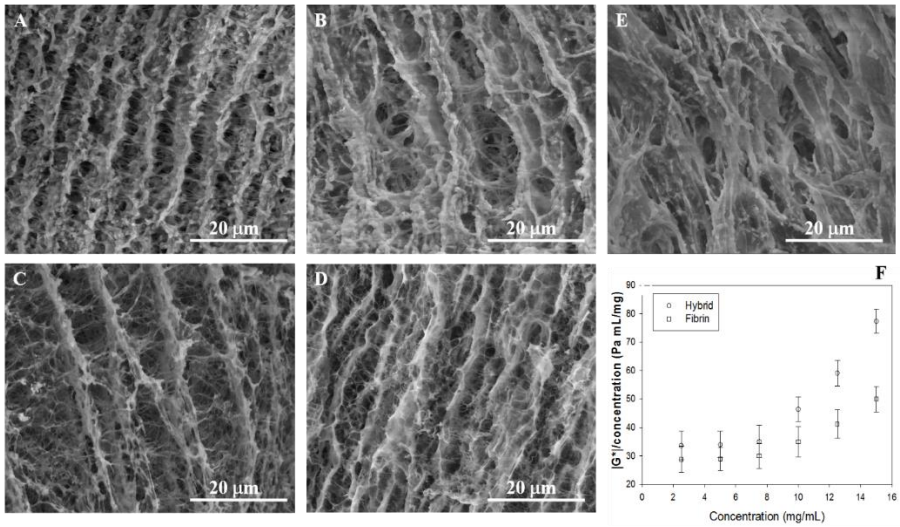

***Fig 7**. SEM pictures of the microstructure of ELR-FGs for concentrations 2.5, 5, 10 and 15 mg/mL (A, B, C, D), at several magnifications. Fibrin gel control of 10 mg/mL (E). Variation of the normalized |G*| versus concentration for ELR-FGs (circles) and fibrin gels (squares). A 1% strain amplitude and a frequency of 1 Hz were used for the rheological measurements (F).*

To provide a comprehensive overview of the microscopic structure of the ELR-FGs, porosity and swelling ratio studies were carried out. Fig 8A shows the dependence of the porosity of the hybrid gels as function of concentration. Porosity decreases when concentration increases at both temperatures. Porosity at low temperature (4°C) is higher than at normal physiological temperature (37°C). A similar porosity behaviour was already observed for Elastin-Like Recombinamers Catalyst Free Click Gels by González de Torre et al.[99]. In any case, at 4°C and 37°C, these ELR-FGs exhibit a high porosity, which is one of the main factors to improve the flow of nutrients inside the scaffold and to facilitate the cell colonization of the gels[108-110]. The relative swelling ratio ($Q_{4°C}/Q_{37°C}$) for hybrid gels at 4°C and at 37°C is showed in Fig.8B. As could be expected, the relative swelling ratio decreases when concentration increases. When the concentration increases, the number of polymers chains does, and the number of cross-linked

chains increases too. This rising in the number of cross-linked chains produce a reduction in the swelling capability of the gels.

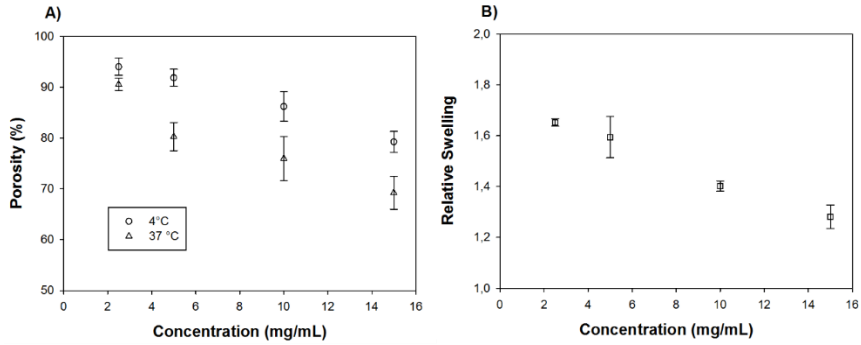

Fig 8. *(A) Porosity of the ELRs-FGs at both temperatures 4°C and 37 °C. (B) Relative equilibrium swelling ratio between 4°C and 37°C.*

The presence of ELRs in these ELR-FGs was corroborated by Immunofluorescence staining with streptavidin TRIC (red stain) and Alexa Fluor 488 (green stain). Several samples of Fibrin gels, ELR-FGs and ovine carotid artery (this last as control) were stained as described in the experimental section with both stains. As can be observed in Fig 9, natural elastin in ovine carotid artery samples is arranged in thin, ordered layers. In ELR-FGs the presence of ELRs appears as a continuous and homogeneous background (green or red, depending of the stain) along the gel, since hybrid gels were formed from homogeneous solutions of fibrin and ELRs, where no segregation was observed. The presence of some bright dots indicate ELRs agglomerations, typical behavior of unreacted ELRs above their Tt, adopting a folded structure[111,112]. In the case of fibrin gels no presence of elastin is founded, as expected.

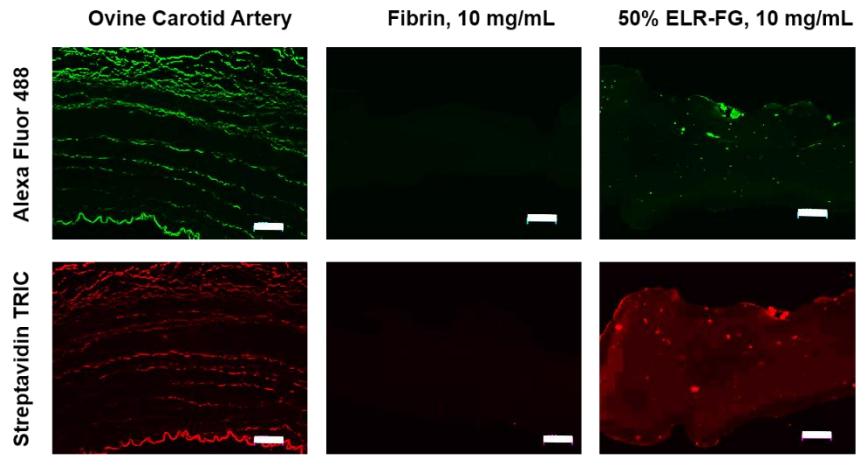

Fig.9. *Optic microscopy pictures for Alexa Fluor 488 (upper row) and Straptavidin TRIC (lower row) immunostaining for ovine carotid artery (control), fibrin gels and ELR-FGs samples.*

3.4.Cytocompatibility

After physical characterization, some cell assays were performed to test the biocompatibility and cell-friendly behavior of these new ELR-FGs. For this purpose five million/mL of OUSMCs (pass 5) were seeded embedded inside 10 mg/mL ELR-FGs. After 15 days of culture, in which levels of glucose, lactate, CO_2, O_2 and pH were monitored and normal values (data not shown) that matches with healthy cells were found, gels were cut into pieces, embedded into paraffin, cut into slices and stained against elastin, a-SMA, collagen I and III. As control, a piece of ovine carotid artery was treated under the same conditions than the ELR-FGs samples. While in natural tissue, elastin, collagen and a-SMA are ordered in fibers, in Fibrin and in ELR-FGs the presence of a-SMa, and collagen I and III is clearly evident, but they doesn't adopt a regular ordered structure. Based on pictures in Fig 10, the production of collagen I and III, and a-SMA in ELR-CGs is at least as good as in Fibrin gels, but in none of them ordered structures are found. Moreover, while in fibrin gels there is no presence of elastin, a soft green background

in our ELR-FGs demonstrates the presence of the ELRs. As expected, ELRs are not ordered as in natural tissue, but the ELR presence improves the mechanical properties of the scaffold, as it was found in the rheological characterization of these new ELR-FGs. Therefore, immunostainings for MLC, a-SMA and Vimentin were carried out and as can be observed in the lower row in Fig 10, cells grew in a total healthy way, developing their habitual structures of the extracellular matrix. So we can conclude that these ELR-FGs are suitable for cell cultures and tissue engineering applications.

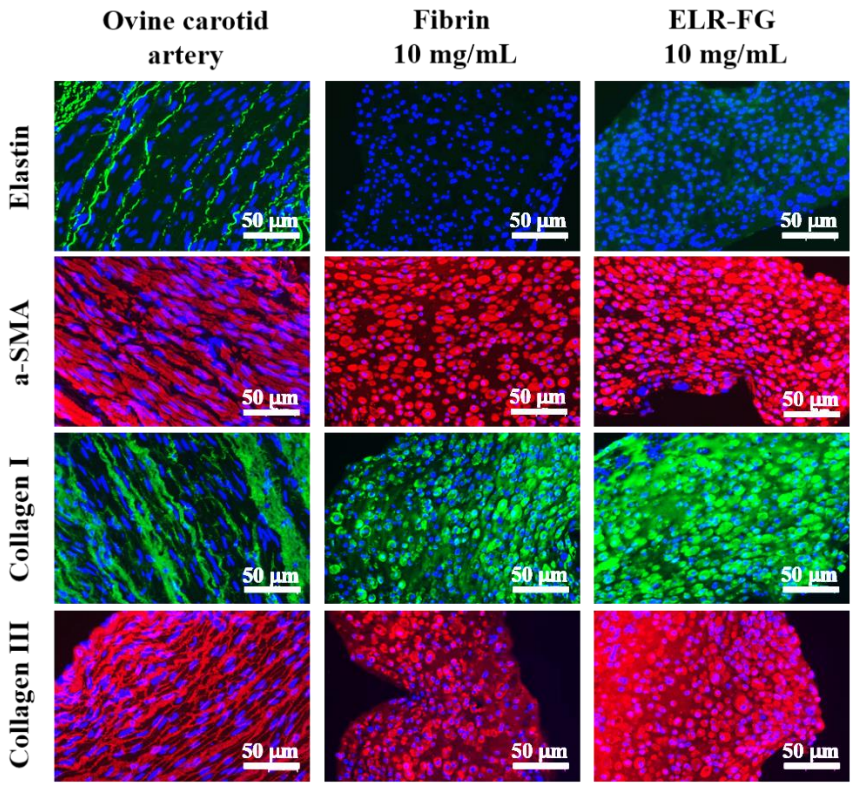

Fig.10 *Elastin, a-SMA, Collagen I and Collagen III immunostaining images for Ovine carotid artery (positive control) and 3D cultures of OUSMCs in Fibrin and ELR-FGs*.

3.5.Potential cardiovascular tissue application for hybrid ELR-FGs

Fibrin gels have been widely applied in the tissue engineering world, specifically for cartilage regeneration[113-116], in the neurological field[117,118], for spinal cord regeneration[119] and, of course in the cardiovascular field[102,105,120]. One of these latter applications is the construction of aortic valves, and although important improvements have been reached in the modeling, some drawbacks still have to be surmounted such as construction and conditioning into bioreactor systems[101]. One of those drawbacks is the mechanical properties of the fibrin gels used to mold those valves.

In this work, we tried to mold one of these aortic valves with our new ELR-FGs that have improved mechanical properties with respect to the fibrin gels, as has been demonstrated in the rheological study. In this section, our intention is not to get a completely functional aortic valve, our aim is to mold an aortic valve as proof of concept, to show that the material satisfied the requirements of the molding process, accommodation into the bioreactor and possess a cell-friendly behavior. To accomplish this endeavor, the procedure depicted by Flanagan et al.[105] was followed under the conditions described in the material section.

Fig.11 shows images from several steps in the aortic valve molding and accommodation process. Pictures A, B and C show the mold parts and their assemble process prior to molding. Picture D illustrate the moment of the injection of the ELR-FG solution into the closed mold. Picture E (closed valve) and F (open valve) show the valve after one week of static culture. Pictures G and H depict the valve inside the bioreactor during the dynamic culture process.

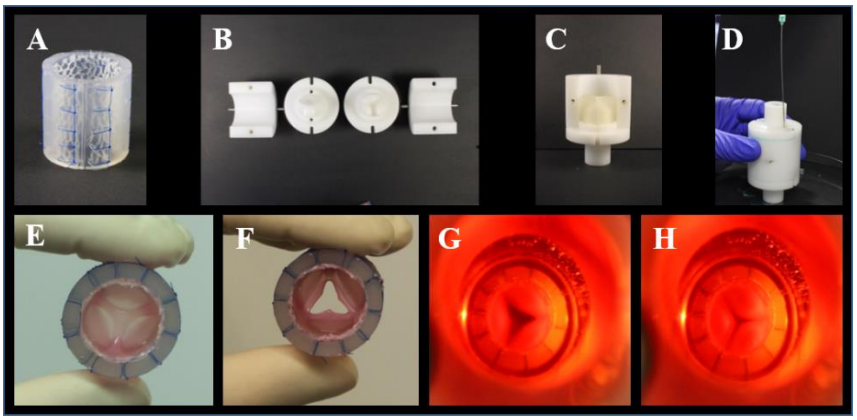

Fig.11. *Images corresponding to several steps in the aortic valve molding and accommodation process.*

Valve construction and accommodation was carried out as previously described. The valve was removed from the bioreactor after 15 days of dynamic culture. Along this culture time, BGA tests were carried out every two days: the glucose and lactate level started at 5.0 mmol/L and 1.4 mmol/L, respectively, and at the end it was 3.3 mmol/L and 4.8 mmol/L, respectively. pH was kept at 7.35 and CO_2 and O_2 pressures were always around 43 and 150 mmHg respectively. The glucose consumption and the increase of the lactate levels means a normal growing of the OUSMCs. Even when the valve after those 15 days didn't close completely, the overall appearance of the ELR-FG valve was good. This appreciation was corroborated by immunostaining evaluation of the wall and leaflets of the valves. The valves were cut into pieces embedded in paraffin and stained against elastin, collagen I and III, α Smooth Muscle Actin (αSMA) as described in the material section. In basis of the immunopictures in Fig. 12, OUSMCs developed more amount of αSMA in the leaflets than in the wall of the engineered ELRR-FG aortic valve. This higher production of αSMA can be attributed to a

higher stimulation of the leaflets with respect to walls. Moreover, collagen I and III were normally produced, in both walls and leaflets, which means a correct production of normal extracellular matrix by OUSMCs. The soft green background in the pictures of immunostaining against elastin, of the valve (walls and leaflets) can not be attributed to a new produced elastin by the cells. This background should be assigned to the ELRs introduced in the valve formation, as previously showed in the cytocompatibility section.

Therefore, we can conclude that, even when this particular application have to be improved, these new ELR-FGs are suitable for aortic valves scaffolds, letting the cells develop their own environment in a normal and healthy way.

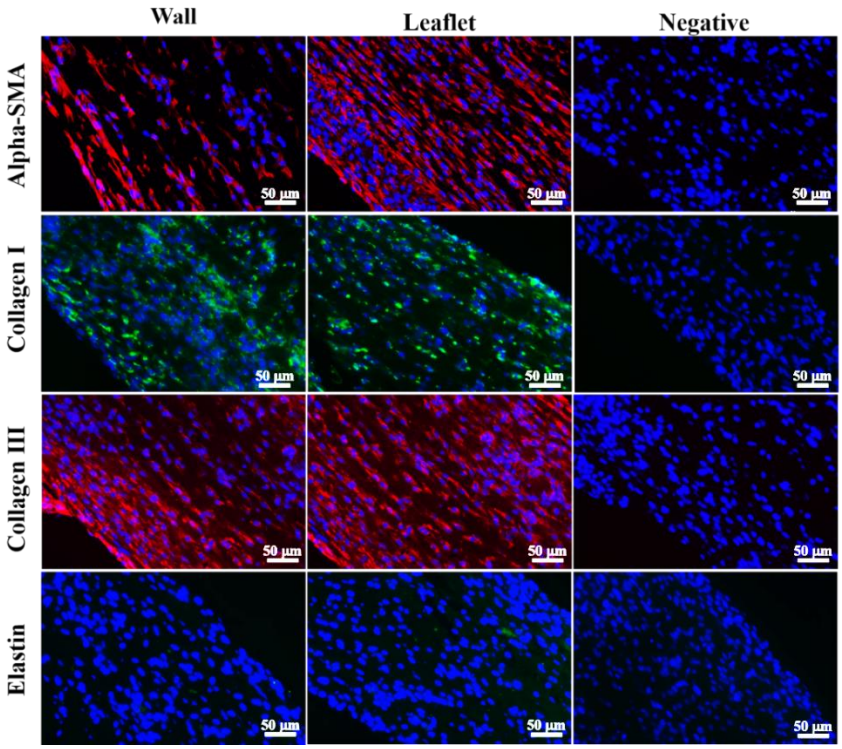

Fig.12. *Elastin, a-SMA, Collagen I and Collagen III immunostaining images for engineered ELR-FGs aortic valve (leaflets and walls) with OUSMCs. Right column, negative controls.*

4. CONCLUSIONS

A new hybrid material formed by Elastin-Like Recombinames (ELRs) and Fibrin was presented in the previous pages. These hybrid gels can include bioactive sequences provided by ELRs, specifically in this work, the cell adhesion sequence RGD has been included. From the mechanical point of view, this material is easy formed and handled, and combines the outstanding properties of the ELRs with the well-known mechanical properties of the fibrin gels, improving the elastic properties with respect to fibrin gels. These ELR-FGs have been mechanically characterized by rheology exhibiting higher storage and loss moduli than fibrin gels for higher concentrations. Since a linear dependence of $|G^*|$ on $f^{1/2}$ has been found in the frequency range of 0.05-10 Hz for all concentrations, a poroelastic mechanism dominates the viscoelastic behaviour in this range. Their microstructure was investigated under microscopy (SEM and light microscopy) and porosity and swelling tests were carried out. The thermosensitive behavior was evaluated by DSC and organoleptic assays.

Their cytocompatibility was evaluated by 3D cell cultures where OUSMCs were seeded inside the gels and after 15 days the cells not only had colonized the whole gels, but they had developed their normal structures to form the extracellular matrix, as immuno-assays revealed. As proof of concept, an artificial aortic valve was molded and cultured for a total of 21 days. The OUSMCs seeded inside the valve grew normally and in a healthy way developing their natural structures to build the extra cellular matrix, what is a promising starting point to apply these new ELR-FGs not only for cardiovascular tissue engineering applications, but also in

other tissue engineering fields due to their mechanical properties and cytocompatibility.

5. ACKNOWLEDGMENTS

We acknowledge financial support from the EU through the European regional development fund (ERDF) NMP3-LA-2011-263363, HEALTH-F4-2011-278557, PITN-GA-2012-317304), from the MINECO (MAT-2010-15982, MAT2010-15310, PRI-PIBAR-2011-1403 and MAT2012-38043-C02-01), the JCyL (projects VA152A12-2, VA244U13 and VA155A12-2), the CIBER-BBN, and the JCyL and the Instituto de Salud Carlos III under the "Network Center of Regenerative Medicine and Cellular Therapy of Castilla and Leon".

6. REFERENCES

(1) Lemons, B. D. R. S. H. J. S. E. In *Biomaterials Science (Third Edition)*; Lemons, B. D. R. S. H. J. S. E., Ed.; Academic Press: 2013, p xli.

(2) Norton, K. *Motion* **2007**.

(3) Griffith, L. G. *Annals of the New York Academy of Sciences* **2002**.

(4) Lemons, B. D. R. S. H. J. S. E. In *Biomaterials Science (Third Edition)*; Lemons, B. D. R. S. H. J. S. E., Ed.; Academic Press: 2013, p 1119.

(5) Lemons, B. D. R. S. H. J. S. E. In *Biomaterials Science (Third Edition)*; Lemons, B. D. R. S. H. J. S. E., Ed.; Academic Press: 2013, p 1337.

(6) Naderi, H.; Matin, M. M.; Bahrami, A. R. *Journal of biomaterials applications* **2011**, *26*, 383.

(7) Mironov, V.; Kasyanov, V.; Zheng Shu, X.; Eisenberg, C.; Eisenberg, L.; Gonda, S.; Trusk, T.; Markwald, R. R.; Prestwich, G. D. *Biomaterials* **2005**, *26*, 7628.

(8) Wertz, J. T.; Mauldin, T. C.; Boday, D. J. *ACS applied materials & interfaces* **2014**, *6*, 18511.

(9) Yao, W.; Xu, P.; Pang, Z.; Zhao, J.; Chai, Z.; Li, X.; Li, H.; Jiang, M.; Cheng, H.; Zhang, B.; Cheng, N. *International journal of nanomedicine* **2014**, *9*, 3963.

(10) Coşkun, G.; Karaca, E.; Ozyurtlu, M.; Özbek, S.; Yermezler, A.; Çavuşoğlu, İ. *Bio-Medical Materials and Engineering* **2014**, *24*, 1527.

(11) Yao, X.; Zhou, N.; Wan, L.; Su, X.; Sun, Z.; Mizuguchi, H.; Yoshioka, Y.; Nakagawa, S.; Zhao, R. C.; Gao, J.-Q. Q. *Biochemical and biophysical research communications* **2014**, *447*, 383.

(12) Shen, M.; Li, L.; Sun, Y.; Xu, J.; Guo, X.; Prud'homme, R. K. *Langmuir : the ACS journal of surfaces and colloids* **2014**, *30*, 1636.

(13) Chen, G. In *Methods in Cell Biology*; Matthieu, P., Manuel, T., Eds.; Academic Press: 2014; Vol. Volume 119, p 17.

(14) Chen, C.-H. H.; Shyu, V. B.; Chen, J.-P. P.; Lee, M.-Y. Y. *Biofabrication* **2014**, *6*, 15004.

(15) Wolf, M. T.; Dearth, C. L.; Sonnenberg, S. B.; Loboa, E. G.; Badylak, S. F. *Advanced drug delivery reviews* **2014**.

(16) Gasperini, L.; Mano, J. F.; Reis, R. L. *Journal of the Royal Society, Interface / the Royal Society* **2014**, *11*, 20140817.

(17) Janmey, P. A.; Winer, J. P.; Weisel, J. W. *Journal of the Royal Society, Interface / the Royal Society* **2009**, *6*, 1.

(18) Collet, J.-P.; Shuman, H.; Ledger, R. E.; Lee, S.; Weisel, J. W. *Proceedings of the National Academy of Sciences of the United States of America* **2005**, *102*, 9133.

(19) Guthold, M.; Liu, W.; Sparks, E. A.; Jawerth, L. M.; Peng, L.; Falvo, M.; Superfine, R.; Hantgan, R. R.; Lord, S. T. *Cell biochemistry and biophysics* **2007**, *49*, 165.

(20) Laurens, N.; Koolwijk, P.; de Maat, M. P. *Journal of thrombosis and haemostasis : JTH* **2006**, *4*, 932.

(21) Iler, R. K. *Journal of Colloid and Interface Science* **1966**.

(22) Humphries, M. J. *Biochemical Society transactions* **2000**, *28*, 311.

(23) Hynes, R. O. *Cell* **2002**, *110*, 673.

(24) Colognato, H.; Yurchenco, P. D. *Developmental dynamics : an official publication of the American Association of Anatomists* **2000**, *218*, 213.

(25) Mithieux, S. M.; Weiss, A. S. In *Advances in Protein Chemistry*; David, A. D. P., John, M. S., Eds.; Academic Press: 2005; Vol. Volume 70, p 437.

(26) Gauvin, R.; Guillemette, M.; Galbraith, T.; Bourget, J. M.; Larouche, D.; Marcoux, H.; Aube, D.; Hayward, C.; Auger, F. A.; Germain, L. *Tissue Eng Part A* **2011**, *17*, 2049.

(27) Huang, L.; McMillan, R. A.; Apkarian, R. P.; Pourdeyhimi, B.; Conticello, V. P.; Chaikof, E. L. *Macromolecules* **2000**, *33*, 2989.

(28) Dreher, M. R.; Simnick, A. J.; Fischer, K.; Smith, R. J.; Patel, A.; Schmidt, M.; Chilkoti, A. *J Am Chem Soc* **2008**, *130*, 687.

(29) Martin, L.; Alonso, M.; Girotti, A.; Arias, F. J.; Rodriguez-Cabello, J. C. *Biomacromolecules* **2009**, *10*, 3015.

(30) Herrero-Vanrell, R.; Rincon, A. C.; Alonso, M.; Reboto, V.; Molina-Martinez, I. T.; Rodriguez-Cabello, J. C. *Journal of Controlled Release* **2005**, *102*, 113.

(31) Urry, D. W. *Angewandte Chemie-International Edition in English* **1993**, *32*, 819.

(32) San Biagio, P. L.; Madonia, F.; Trapane, T. L.; Urry, D. W. *Chemical Physics Letters* **1988**, *145*, 571.

(33) Urry, D. W. *Journal of Physical Chemistry B* **1997**, *101*, 11007.

(34) Rodriguez-Cabello, J. C.; Alonso, M.; Perez, T.; Herguedas, M. M. *Biopolymers* **2000**, *54*, 282.

(35) Ribeiro, A.; Arias, F. J.; Reguera, J.; Alonso, M.; Rodriguez-Cabello, J. C. *Biophys J* **2009**, *97*, 312.

(36) Li, B.; Alonso, D. O. V.; Daggett, V. *Journal of Molecular Biology* **2001**, *305*, 581.

(37) Urry, D. W. *What sustains life? Consilient mechanisms for protein-based machines and materials*; Springer-Verlag: New York, 2006.

(38) Peppas, N. A. *J Control Release* **2000**, *68*, 135.

(39) Hoffman, A. S. *Adv Drug Deliv Rev* **2002**, *54*, 3.

(40) Kopecek, J. *Biomaterials* **2007**, *28*, 5185.

(41) Wichterle, O.; Lim, D. *Nature* **1960**, *185*, 117.

(42) Campoccia, D.; Doherty, P.; Radice, M.; Brun, P.; Abatangelo, G.; Williams, D. F. *Biomaterials* **1998**, *19*, 2101.

(43) Prestwich, G. D.; Marecak, D. M.; Marecek, J. F.; Vercruysse, K. P.; Ziebell, M. R. *J Control Release* **1998**, *53*, 93.

(44) Cappello, J.; Crissman, J.; Dorman, M.; Mikolajczak, M.; Textor, G.; Marquet, M.; Ferrari, F. *Biotechnology Progress* **1990**, *6*, 198.

(45) Lewis, R. V.; Hinman, M.; Kothakota, S.; Fournier, M. J. *Protein Expression and Purification* **1996**, *7*, 400.

(46) McPherson, D. T.; Morrow, C.; Minehan, D. S.; Wu, J.; Hunter, E.; Urry, D. W. *Biotechnol Prog* **1992**, *8*, 347.

(47) Cheng, S.; Google Patents: 1996.

(48) Mcgrath, K. P.; Tirrell, D. A.; Kawai, M.; Mason, T. L.; Fournier, M. J. *Biotechnology Progress* **1990**, *6*, 188.

(49) Won, J. I.; Barron, A. E. *Macromolecules* **2002**, *35*, 8281.

(50) Martin, L.; Alonso, M.; Moeller, M.; Rodriguez-Cabello, J. C.; Mela, P. *Soft Matter* **2009**, *5*, 1591.

(51) Girotti, A.; Reguera, J.; Rodriguez-Cabello, J. C.; Arias, F. J.; Alonso, M.; Matestera, A. *J Mater Sci Mater Med* **2004**, *15*, 479.

(52) González de Torre, I.; Santos, M.; Quintanilla, L.; Testera, A.; Alonso, M.; Rodríguez Cabello, J. C. *Acta Biomaterialia* **2014**, *10*, 2495.

(53) Huisgen, R. *Angewandte Chemie International Edition in English* **1963**, *2*, 565.

(54) Rabaud, M.; Lefebvre, F.; Piquet, Y.; Belloc, F.; Chevaleyre, J.; Roudaut, M.; Bricaud, H. *Thrombosis research* **1986**, *43*, 205.

(55) Flanagan, T. C.; Cornelissen, C.; Koch, S.; Tschoeke, B.; Sachweh, J. S.; Schmitz-Rode, T.; Jockenhoevel, S. *Biomaterials* **2007**, *28*, 3388.

(56) Jockenhoevel, S.; Zund, G.; Hoerstrup, S.; Chalabi, K.; Sachweh, J.; Demircan, L.; Messmer, B.; Turina, M. *European journal of cardio-thoracic surgery : official journal of the European Association for Cardio-thoracic Surgery* **2001**, *19*, 424.

(57) Kolb, H. C.; Finn, M. G.; Sharpless, K. B. *Angewandte Chemie International Edition* **2001**, *40*, 2004.

(58) Kennedy, D.; McKay, C.; Legault, M.; Danielson, D.; Blake, J.; Pegoraro, A.; Stolow, A.; Mester, Z.; Pezacki, J. *Journal of the American Chemical Society* **2011**, *133*, 17993.

(59) Han, L.; Frank, E. H.; Greene, J. J.; Lee, H. Y.; Hung, H. H.; Grodzinsky, A. J.; Ortiz, C. *Biophys J* **2011**, *100*, 1846.

(60) Lee, B.; Han, L.; Frank, E.; Chubinskaya, S.; Ortiz, C.; Grodzinsky, A. *Journal of Biomechanics* **2010**, *43*, 469.

(61) Yu, Q.; Zhou, J.; Fung, Y. C. *American Journal of Physiology - Heart and Circulatory Physiology* **1993**, *265*, H52.

(62) Erkamp, R.; Wiggins, P.; Skovoroda, A.; Emelianov, S.; O'Donnell, M. *Ultrasonic imaging* **1998**, *20*, 17.

(63) Freeman, P.; Natarajan, R.; Kimura, J.; Andriacchi, T. *Journal of orthopaedic research : official publication of the Orthopaedic Research Society* **1994**, *12*, 311.

(64) Dasgupta, B.; Weitz, D. *Physical review. E, Statistical, nonlinear, and soft matter physics* **2005**, *71*, 21504.

(65) Peters, R. *Google Patents* **2000**.

(66) González de Torre, I.; Quintanilla, L.; Pinedo-Martín, G.; Alonso, M.; Rodríguez-Cabello, J. C. *ACS Applied Materials & Interfaces* **2014**, *6*, 14509.

(67) Bertrand, P.; Jonas, A.; Laschewsky, A.; Legras, R. *Macromolecular Rapid Communications* **2000**, *21*, 319.

(68) Costa, R. R.; Custodio, C. A.; Arias, F. J.; Rodriguez-Cabello, J. C.; Mano, J. F. *Small* **2011**, *7*, 2640.

(69) Decher, G. *Science* **1997**, *277*, 1232.

(70) Hammond, P. T. *AIChE Journal* **2011**, *57*, 2928.

(71) Tang, Z.; Wang, Y.; Podsiadlo, P.; Kotov, N. A. *Advanced Materials* **2006**, *18*, 3203.

(72) Cameron, R. K.; Kim, W.; Georgina, K. S.; Angus, P. R. J.; Frank, C. *Small* **2009**, *5*.

(73) Yang, W.; Pranantyo, D.; Neoh, K.-G.; Kang, E.-T.; Teo, S.; Rittschof, D. *Biomacromolecules* **2012**, *13*, 2769.

(74) Bergbreiter, D. E.; Chance, B. S. *Macromolecules* **2007**.

(75) Curcio, A.; Torella, D.; Indolfi, C. *Circulation Journal* **2011**, *75*, 1287.

(76) Sigwart, U.; Puel, J.; Mirkovitch, V.; Joffre, F.; Kappenberger, L. *New England Journal of Medicine* **1987**, *316*, 701.

(77) Kornowski, R.; Hong, M. K.; Tio, F. O.; Bramwell, O.; Wu, H.; Leon, M. B. *Journal of the American College of Cardiology* **1998**, *31*, 224.

(78) Farb, A.; Sangiorgi, G.; Carter, A. J.; Walley, V. M.; Edwards, W. D.; Schwartz, R. S.; Virmani, R. *Circulation* **1999**, *99*, 44.

(79) Pfisterer, M.; Brunner-La Rocca, H.; Buser, P.; Rickenbacher, P.; Hunziker, P.; Mueller, C.; Jeger, R.; Bader, F.; Osswald, S.; Kaiser, C.; Investigators, B.-L. *Journal of the American College of Cardiology* **2006**, *48*, 2584.

(80) Alexiou, C.; McDonald, A.; Langley, S. M.; Dalrymple-Hay, M. J. R.; Haw, M. P.; Monro, J. L. *European Journal of Cardio-Thoracic Surgery* **2000**, *17*, 125.

(81) Dijkman, P. E.; Driessen-Mol, A.; Frese, L.; Hoerstrup, S. P.; Baaijens, F. P. *Biomaterials* **2012**, *33*, 4545.

(82) Syedain, Z. H.; Meier, L. A.; Reimer, J. M.; Tranquillo, R. T. *Annals of biomedical engineering* **2013**, *41*, 2645.

(83) Rodríguez-Cabello, J. C.; Martín, L.; Alonso, M.; Arias, F. J.; Testera, A. M. *Polymer* **2009**, *50*, 5159.

(84) Wright, E. R.; Conticello, V. P. *Advanced Drug Delivery Reviews* **2002**, *54*, 1057.

(85) Zhao, H.; Ma, L.; Zhou, J.; Mao, Z.; Gao, C.; Shen, J. *Biomedical materials (Bristol, England)* **2008**, *3*, 15001.

(86) Haugh, M.; Thorpe, S.; Vinardell, T.; Buckley, C.; Kelly, D. *Journal of the mechanical behavior of biomedical materials* **2012**, *16*, 66.

(87) Carriel, V.; Garrido-Gómez, J.; Hernández-Cortés, P.; Garzón, I.; García-García, S.; Sáez-Moreno, J.; Del Carmen Sánchez-Quevedo, M.; Campos, A.; Alaminos, M. *Journal of neural engineering* **2013**, *10*, 26022.

(88) Willerth, S.; Faxel, T.; Gottlieb, D.; Sakiyama-Elbert, S. *Stem cells (Dayton, Ohio)* **2007**, *25*, 2235.

(89) San-Galli, F.; Deminière, C.; Guérin, J.; Rabaud, M. *Biomaterials* **1996**, *17*, 1081.

(90) Riquet, M.; Carnot, F.; Gallix, P.; Callise, D.; Lefebvre, F.; Rabaud, M. *Biomaterials* **1990**, *11*, 518.

(91) Bonzon, N.; Carrat, X.; Deminiére, C.; Daculsi, G.; Lefebvre, F.; Rabaud, M. *Biomaterials* **1995**, *16*, 881.

(92) Roberts, W.; Kramer, O.; Rosser, R.; Nestler, F.; Ferry, J. *Biophysical chemistry* **1974**, *1*, 152.

(93) Gerth, C.; Roberts, W.; Ferry, J. *Biophysical chemistry* **1974**, *2*, 208.

(94) Nelb, G.; Gerth, C.; Ferry, J. *Biophysical chemistry* **1976**, *5*, 377.

(95) Rosser, R.; Roberts, W.; Ferry, J. *Biophysical chemistry* **1977**, *7*, 153.

(96) Mak, A. F. *J Biomech Eng* **1986**, *108*, 123.

(97) Mak, A. F. *Biorheology* **1986**, *23*, 371.

(98) Kalyanam, S.; Yapp, R. D.; Insana, M. F. *J Biomech Eng* **2009**, *131*, 081005.

(99) González de Torre, I.; Santos, M.; Quintanilla, L.; Testera, A.; Alonso, M.; Rodríguez Cabello, J. C. *Acta Biomaterialia* **2014**.

(100) Cholewinski, E.; Dietrich, M.; Flanagan, T.; Schmitz-Rode, T.; Jockenhoevel, S. *Tissue engineering. Part A* **2009**, *15*, 3645.

(101) Jockenhoevel, S.; Chalabi, K.; Sachweh, J.; Groesdonk, H.; Demircan, L.; Grossmann, M.; Zund, G.; Messmer, B. *The Thoracic and cardiovascular surgeon* **2001**, *49*, 287.

(102) Ye, Q.; Zünd, G.; Benedikt, P.; Jockenhoevel, S.; Hoerstrup, S.; Sakyama, S.; Hubbell, J.; Turina, M. *European journal of cardio-thoracic surgery : official journal of the European Association for Cardio-thoracic Surgery* **2000**, *17*, 587.

(103) Costa, R.; Custódio, C.; Arias, F.; Rodríguez-Cabello, J.; Mano, J. *Small (Weinheim an der Bergstrasse, Germany)* **2011**, *7*, 2640.

(104) Zeng, X.; Ruckenstein, E. *Industrial & Engineering Chemistry Research* **1996**, *35*, 4169.

(105) Flanagan, T.; Cornelissen, C.; Koch, S.; Tschoeke, B.; Sachweh, J.; Schmitz-Rode, T.; Jockenhoevel, S. *Biomaterials* **2007**, *28*, 3388.

(106) Sun, Y.; Giraudier, O.; Garde, V. L. *Biopolymers* **2005**, *77*, 257.

(107) Jockenhoevel, S.; Flanagan, T. C. *Cardiovascular Tissue Engineering Based on Fibrin-Gel-Scaffolds*, 2011.

(108) Lawrence, B.; Madihally, S. *Cell adhesion & migration* **2008**, *2*, 9.

(109) Pamula, E.; Bacakova, L.; Filova, E.; Buczynska, J.; Dobrzynski, P.; Noskova, L.; Grausova, L. *Journal of materials science. Materials in medicine* **2008**, *19*, 425.

(110) Chan, G.; Mooney, D. *Trends in biotechnology* **2008**, *26*, 382.

(111) Rodríguez-Cabello, J. C.; Reguera, J.; Girotti, A.; Alonso, M.; Testera, A. M. *Progress in Polymer Science* **2005**, *30*, 1119.

(112) Schmidt, P.; Dybal, J.; Rodriguez-Cabello, J. C.; Reboto, V. *Biomacromolecules* **2005**, *6*, 697.

(113) Eyrich, D.; Brandl, F.; Appel, B.; Wiese, H.; Maier, G.; Wenzel, M.; Staudenmaier, R.; Goepferich, A.; Blunk, T. *Biomaterials* **2007**, *28*, 55.

(114) Lee, K.; Kim, J.; Young, K.; Lee, Y.; Park, Y.; Kim, Y.; Cho, H. *Knee surgery, sports traumatology, arthroscopy : official journal of the ESSKA* **2013**, *21*, 1251.

(115) Lee, J.-M.; Im, G.-I. *Biomaterials* **2012**, *33*, 2016.

(116) Park, S.-H.; Gil, E.; Cho, H.; Mandal, B.; Tien, L.; Min, B.-H.; Kaplan, D. *Tissue engineering. Part A* **2012**, *18*, 447.

(117) Mooney, R.; Tawil, B.; Mahoney, M. *Tissue engineering. Part A* **2010**, *16*, 1607.

(118) Uibo, R.; Laidmäe, I.; Sawyer, E.; Flanagan, L.; Georges, P.; Winer, J.; Janmey, P. *Biochimica et biophysica acta* **2009**, *1793*, 924.

(119) Tsai, E.; Dalton, P.; Shoichet, M.; Tator, C. *Biomaterials* **2006**, *27*, 519.

(120) Nakatsu, M.; Davis, J.; Hughes, C. *Journal of visualized experiments : JoVE* **2007**, 186.

CHAPTER 3:

BIOCOMPATIBLE ELASTIN-LIKE CLICK GELS: DESIGN, SYNTHESIS AND CHARACTERIZATION

Ana M. Testera[1,2], Alessandra Girotti[1,2], Israel González de Torre[1,2], Luis Quintanilla[1,2], Mercedes Santos[1,2], Matilde Alonso[1,2], José Carlos Rodríguez-Cabello[1,2].
1 Bioforge group, University of Valladolid, Edificio I+D, Paseo de Belén, 11, 47011 Valladolid, Spain
2 Biomedical Research Networking center in Bioengineering, Biomaterials and Nanomedicine (CIBER-BBN), Valladolid, Spain

Testera, A.; Girotti, A.; González de Torre, I.; Santos, M; Alonso, M.; Rodríguez Cabello, J. C. Elastin-like recombinamer catalyst-free click gels: Characterization of poroelastic and intrinsic viscoelastic properties. Journal of Materials Science: Materials in Medicine. Just acepted. 2014 (11)

Abstract

Elastin-like recombinamer click gels (ELR-CGs) for biomedical applications, such as drug delivery or tissue engineering, have been developed by taking advantage of the click reaction (CuAAC) in the absence of traditional crosslinking agents. ELRs are functionalized with alkyne and azide groups using conventional chemical techniques to introduce the reactivity required to carry out the 1,3-dipolar cycloaddition under mild biocompatible conditions, with no toxic by-products and in short reaction times. Hydrogels with moduli in the range 1000−10,000 Pa have been synthesized, characterized, and tested *in vitro* against several cell types. The cells embedded into ELR-CGs possessed high viability and proliferation rate. The mechanical properties, porosity and swelling of the resulting ELR-CGs can easily be tuned by adjusting the ELR concentration. We also show that it is possible to replicate different patterns on the hydrogel surface, thus allowing the use of this type of hydrogel to improve applications that require cell guidance or even differentiation depending on the surface topography.

1. INTRODUCTION

New biomaterials are currently required to satisfy the needs and expectations of researchers in the bioscience and biotechnology fields. The desirable features of such materials include biocompatibility, specific mechanical properties, cell-friendly behaviour, non-toxic degradation products, and ease of handling. The development of functional materials often involves the generation of well-defined micro- and nanopatterned surfaces. The design and development of systems with a well-defined topographical biochemical activity and controlled mechanical properties is a hot research topic due to their potential biomedical applications[1,2]. Cell behaviour can be conditioned by a specific and well-defined topography of the material surface, either alone or in combination with specific bioactivity, thus leading to a promising strategy for controlling cellular organization and function in tissue engineering[3,4]. For instance, topographical patterns have been used to facilitate cell adhesion[5], direct cell migration[6], enhance cell proliferation[7], and control cell differentiation[8], and, according to the work of Engler et al. [9], surface stiffness can also be used to modify the cell phenotype.

Elastin-like recombinamers (ELRs) are protein-based polymers obtained by recombinant DNA technologies, thus allowing the bioproduction of protein polymers with well-defined, complex and controlled sequences. ELRs can include different bioactive sequences[10], such as those for cell adhesion and proliferation or sequences sensitive to enzymes[11]. These materials are based on the repetition of short peptides considered to be building blocks in natural elastin[12]. The wide range of interesting properties

exhibited by this family of polymers, for instance their extraordinary biocompatibility, excellent mechanical properties (similar to those of natural elastin), acute self-assembly and thermosensitive behaviour, should be highlighted[10-13]. The latter is characterized by a critical temperature, known as the transition temperature in aqueous solution (Tt), which is associated with the occurrence of a conformational reorganization in this material. Thus, whereas the polymer chains are soluble in water below Tt, above this temperature they form nano- and micro-aggregates and become insoluble in a completely reversible process.

The Cu(I)-catalysed 1,3-dipolar cycloaddition reaction (CuAAC) between azides and alkynes, which is prob ably the most prominent example of "click chemistry" [14,15], was discovered independently in 2002 by the groups of Meldal[16], and Sharpless[17] and is compatible with most functional groups present in proteins and peptides, thereby ruling out the need for protecting groups. This Hüisgen reaction combines high specificity with quantitative yield, a lack of side reactions and toxic by-products, short reaction times, and high tolerance towards other functional groups present in the molecule. As alkynes and azides are remarkably stable within biological systems, click chemistry has been widely employed in drug discovery[18], bioconjugation with proteins[19] and DNA[20], cell surface labelling[21], surface modifications with ELRs[22], amongst other molecules, and for hydrogel synthesis[23,24]. Some studies have provided evidence of the potential use of ELR-based hydrogels as a scaffold to promote tissue regeneration in vitro due to their low endotoxicity[24], low cytotoxicity and absence of antigenic properties upon implantation[25-27]. In particular, in the field of cartilage tissue engineering, the synthesis and accumulation of a cartilaginous

matrix for both encapsulated cartilage cells[28] and human adipose tissue-derived stem cells[29] in vitro has been reported.

In this paper elastin-like recombinamer-click gels (ELR-CGs) are obtained under mild, physiological conditions by exploiting the advantageous properties of the click reaction. Specifically, two modified ELRs including azide or alkyne groups in their structure are processed to obtain chemically covalently cross-linked hydrogels, which are characterized by scanning electron microscopy (SEM), porosity, equilibrium swelling ratio, and rheological properties. The porous structure and favourable thermoresponsiveness of the resulting ELR-CGs are also evaluated. Topographically micropatterned structures with different features are processed by a biocompatible, simple and straightforward method known as the replica moulding[30-32] procedure, which opens up the future possibility of controlling cellular organization and function in tissue engineering as well as the development of cell-based biomedical systems. Finally, the cytocompatibility of these new ELR-CGs will be demonstrated by way of viability assays with several cell lines (HFF-1, MSCs and HUVECs). This cytocompatibility will be demonstrated using both surface and 3D cultures.

2. MATERIALS AND METHODS.

All reagents used were of analytical grade. They were purchased from Aldrich Co. and used as received.

2.1.ELR bioproduction.

The ELRs used herein were constructed using standard genetic-engineering techniques. Thus, they were produced using

cellular systems for genetically engineered protein biosynthesis in Escherichia coli and purified using several cycles of temperature-dependent reversible precipitations[33]. The purity and molecular weight of the ELRs were verified by sodium dodecyl sulfate polyacrylamide gel electrophoresis (SDS-PAGE) and matrix-assisted laser desorption/ionization time-of-flight (MALDI-TOF) mass spectroscopy using a Voyager STR apparatus from Applied Biosystems. Amino acid composition analysis was also performed. Additional characterization of ELRs was accomplished using infrared spectroscopy, differential scanning calorimetry (DSC) and nuclear magnetic resonance (NMR) techniques.

The two ELRs employed were VKVx24, a structural polymer lacking a bioactive sequence and with the amino acid sequence:

MESLLP VG VPGVG [VPGKG(VPGVG)5]23 VPGKG VPGVG VPGVG VPGVG VPGV, and HRGD6, a polymer containing the adhesion sequence (RGD) and with the amino acid sequence [34]:

MGSSHHHHHHSSGLVPRGSHMESLLP [(VPGIG)2(VPGKG)(VPGIG)2]2AVTGRGDSPASS[(VPGIG)2(VPGKG)(VPGIG)2]2.

2.2.Chemical modification of ELRs.

The ELRs were chemically modified by transformation of the ε-amine group present in the lateral chain of the lysine residue to bear the groups required for hydrogel formation using click chemistry techniques. The specific modifications are described below.

2.3.Synthesis of azide-bearing ELRs.

A substitution reaction was carried out using triflic azide as nucleophile. Triflic azide solution was freshly prepared in situ prior

to each reaction as previously described by Lundquist et al. [35] NaN3 (5 eq.) was dissolved in 14 mL of Milli-Q water and 17.5 mL of CH2Cl2 added. The reaction mixture was cooled in an ice-water bath and a solution of triflic anhydride (1 eq.) added dropwise at 4ºC while stirring. The resulting mixture was stirred vigorously at 0ºC for 1 h and then at room temperature for another hour. The crude reaction mixture was decanted and the aqueous phase washed with dichloromethane (2 x 10 mL). The combined organic phases were then washed with saturated Na2CO3 solution (10 mL). The resulting azide-containing solution was employed directly without further purification. A solution containing triflic azide was added dropwise to a solution of the ELRs (2g,VKVx24 or HRGD6, 1 eq.) in 24 mL of milli-Q water with sodium carbonate (1.5 eq) and copper(II) sulfate (0.01 eq) at 0ºC. Methanol (4 mL) was then added and the reaction allowed to run overnight at room temperature. The organic solvents were subsequently eliminated under reduced pressure and the polymer purified by dialysis at 4ºC, followed by lyophilisation to yield a white solid. The transformation was corroborated by MALDI-TOF, IR spectroscopy, amino-acid composition determination, and DSC (Data not shown).

2.4.Synthesis of acetylene-bearing ELRs.

Chemical modification of the ELR (VKVx24 or HRGD6) was carried out to obtain an ELR with a pendant alkynyl group. Thus, pentynoic anhydride was synthesized from pentynoic acid (2 eq.) in a 1:1 mixture (v/v) of dichloromethane and diethyl ether in the presence of dicyclohexylcarbodiimide (1 eq.). Ten equivalents of pentinoic anhydride and five equivalents of ethylendiaminecarbodiimide (EDAC) were added to a solution of ELR (1 eq.) in 5mL of trifluoroethanol (TFE). The reaction mixture

was stirred for 3 days at room temperature. After this time the functionalized polymer was precipitated into diethyl ether, washed with additional diethyl ether fractions, and dried under reduced pressure. The modified ELR was solubilized in cold water, purified by exhaustive dialysis against water (3 x 25 L), and lyophilized to yield a white product (89%). Chemical characterization of the polymer by MALDI-TOF and 1H NMR spectroscopy confirmed total conversion of the free amine group of the biopolymer (data not shown).

2.5.ELR-CHG formation.

Different amounts of ELR-alkyne and modified ELR-azide were dissolved in milli-Q water to a final polymer concentration of 25, 50, 100 and 125 mg/mL with an alkyne/azide molar ratio of 1:1. After mixing the above aqueous solutions, sodium ascorbate and aqueous copper(II) sulfate (CuSO4) solution were added as reagents to initiate the crosslinking reaction between the alkyne and azide groups at 4ºC. An azide: copper(II): ascorbate molar ratio of 12:1:3 (optimization process not shown) was used for all reactions. The mixture was vigorously stirred and injected into moulds (diameter: 13.5 mm; height: 2 mm) at 4ºC for 5 min, and then 1 h at r.t., in order to finish the gelification process. Finally, all hydrogels were carefully removed and washed with milli-Q water.

The chemical process for obtaining ELR-CG hydrogels from ELRs is summarised in the scheme shown in Fig. 1. It should be noted that covalent crosslinking is based on the reaction between azide and alkyne groups. Three replicates for each concentration of each hydrogel were prepared for analysis using any of the instrumental methods reported in this work. A preliminary

characterization based on IR spectroscopy and DSC was performed (data not shown).

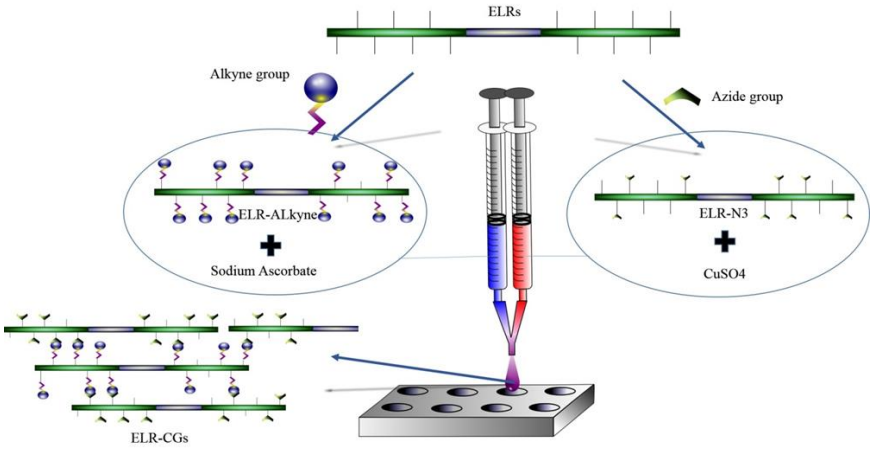

***Fig. 1**. Scheme showing ELR-CG formation as bi-component system.*

2.6.Micropatterned hydrogels fabricated by replica moulding.

The replica moulding method was carried out using micropatterned polydimethylsiloxane (PDMS) substrates as moulds. The PDMS prepolymer and curing agent were thoroughly mixed at a 10/1 (w/w) ratio then degassed for 1 h. The mixture was then cast onto different patterned silicon masters with different topographical features. Specifically, hexagonal pillars (width (w) = 100 μm, spacing (s) = 100 μm), square pillars (w = s = 40 μm and w = s = 100 μm), and grooves (w = 20 μm, s = 100 μm). The step height of the micro-features was 5 μm for the pillars and grooves. The mixture was cured at 65°C for 1 h, then the PDMS was carefully peeled off from the silicon wafer and used as a mould. Micropatterned hydrogels were obtained in a one-step process by pouring the mix of aqueous polymer solutions (concentration = 50 mg/mL) with sodium ascorbate and CuSO4 solution, in the proportions previously described, on top of the PDMS mould, at

4ºC. After heating the system from 4 to 25 ºC, then leaving it at this temperature for 1 hour, the hydrogels were peeled off. Their surface topography was observed, with no prior treatment or manipulation, by optical microscopy, using a Nikon ECLIPSE 80i light microscope, and by scanning electron microscopy (SEM) in low vacuum mode.

2.7.Cell culture.

Paraformaldehyde (ref. P6148) and Triton X-100 (ref. T9284) were purchased from Sigma-Aldrich. Normal Human Adipose-Derived Mesenchymal Stem Cells (hMSCs, ref R7788-115) basal medium Dulbecco's modified Eagle's medium (DMEM, ref 31966-021), fetal bovine serum (FBS ref. 16000-044), penicillin streptomycin solution (ref. SV30010), trypsin-EDTA (ref. SV30010), DPBS (ref. 14190-136), HEPES (ref. 15630049), Trypan Blue stain 0.4% (ref. 15250061), Alexa Fluor 488 phalloidin (ref. A12379), LIVE/DEAD® Viability/Cytotoxicity Kit for mammalian cells (ref. L3224), Alamar Blue® (ref. DAL1025) and DAPI (ref. D21490) were supplied by Invitrogen . Human umbilical vein endothelial cells (HUVECs; cat. no. cc-2517) and endothelial growth medium (EGM; Clonetic, cat. no. cc-3124) were purchased from Lonza (Lonza Walker). Human foreskin fibroblasts HFF-1 (SCRC-1041) were purchased from the American Type Culture Collection (ATCC, USA). All cell culture plastic-ware and consumables were acquired from NUNC.

hMSCs and HFF1 were cultured in DMEM supplemented with 100 U·mL-1 penicillin, 0.1 mg·mL-1 streptomycin and 10% or 15% FBS. HUVECs were grown in complete endothelial growth medium. Cells were incubated at 37 ºC in a 5% CO2 humidified

environmental chamber and their medium was replaced every two days.

2.8.Cell viability assays.

2x105 HFF1 and 5x104 MSCs/mL were embedded inside ELR-CGs at a concentration of 50 mg/mL, as described previously. Metabolic activity was evaluated using the Alamar Blue® assay. The relative number of metabolically active cells was evaluated using the Alamar Blue® assay according to the manufacturer's guidelines. Twenty-four hours after seeding the cells, the hydrogels were washed twice with DPBS and incubated in 10% Alamar Blue solution in DMEM for 2 h at 37 °C and under a 5% CO2 atmosphere. Subsequently, 70 µL of the reduced medium was transferred to a 96-well plate. The hydrogels were washed twice with DPBS, and the corresponding growth medium added and incubated again in order to determine the cell number at different times. Fluorescence (excitation: 560 nm; emission: 590 nm) was measured using a SpectraMax M5e (Molecular Devices) microplate reader. The fluorimetric reduction of 10% Alamar Blue® reagent in the culture medium by the cells expressed as fluorescence emission intensity units, was measured at regular time intervals.

Samples for phase-contrast epifluorescence or SEM were fixed in 4% paraformaldehyde for 40 min. The staining was carried out before permeabilization of the samples with 0.2% Triton X-100, and stained with the fluorescent dyes Phalloidin-Alexa Fluor488R and DAPI, as indicated in the text.

2.9.Microstructural Morphology.

SEM in low vacuum mode (~ 1 torr) and with water vapour as working gas was used to investigate the morphology of both

hydrogels and micropatterned hydrogels. ELR-CG hydrogels were immersed in milli-Q water below (at 4 °C) and above (at 37 °C) the Tt for 1 day, instantaneously plunged into liquid nitrogen, physically fractured, and immersed in liquid nitrogen again. Finally, the hydrogels were freeze-dried. Images of lyophilized hydrogels were obtained by SEM (FEI Quanta 200 FEG) without any coating procedures. Hydrogel microstructural details, such as pore size and pore wall thickness, were quantitatively evaluated using the ZEN software (Blue Edition, 2012) from Carl Zeiss Microscopy based on the micrographs.

Structured hydrogels were peeled off from the mould after gelification and their surface topography observed without any treatment or manipulation.

2.10. Porosity and Swelling Ratio calculations.

The following equation[36,37] was employed to estimate hydrogel porosity:

$$\text{Porosity } (\%) = ((W1-W2)/\rho water)\cdot 100/Vhydrogel \quad \text{(Equ. 1)}$$

where W1 and W2 are, respectively, the weight of swollen and lyophilized gel, ρwater is the density of pure water, and Vhydrogel is the measured volume of the gel in the swollen state (Vhydrogel = πr2h, where r and h are, respectively, the radius and height of the cylindrical sample). Excess surface water was removed with a filter paper before each measurement.

The equilibrium swelling ratio by weight, Qw, was used to quantify the volume change related to the phase transition of the hydrogels in aqueous solution.

$$Qw\ (\%) = ((W1-W2)/W2)\cdot 100 \quad \text{(Equ. 2)}$$

Both, porosity and equilibrium swelling ratio, were measured at 4° and 37°C. All measurements were taken 24 h after soaking the hydrogel in MQ water at the chosen temperature. Equilibrium was defined as the steady state at which there was no change in volume of the ELR-CG. Lyophilization or freeze-drying was performed with hydrogels previously frozen in liquid nitrogen and swollen in water at the corresponding test temperature.

2.11. Rheological measurements.

Rheological experiments were performed using a strain-controlled AR-2000ex rheometer (TA Instruments) with the hydrogel immersed in water. Cylindrical swollen gels were placed between parallel, nonporous stainless-steel plates (diameter = 12 mm) and the gap between the plates adjusted using a normal force of around 0.2 N in order to prevent slippage. A gap higher than 1000 μm was always reached after the sample relaxed until equilibrium. Measurements were carried out at 4°C and at 37°C. Two types of measurements were performed in shear deformation mode. First of all, the range of strain amplitudes for which gels exhibit a linear region of viscoelasticity was determined. A dynamic strain sweep (with amplitudes ranging between 0.1% and 20%) was carried out at a frequency of 1 Hz to measure the dynamic shear modulus as a function of strain. Second, in order to measure the dependence of the dynamic shear modulus and loss factor on frequency, dynamic frequency sweep tests were accomplished. Specifically, a frequency sweep between 0.01 Hz and 10 Hz at a fixed strain (corresponding to the hydrogel linear region) was selected. Thus, the storage modulus, G´, the loss modulus, G´´, the complex modulus magnitude, |G*| (|G*|2 = (G´)2 + (G´´)2), and the loss factor, tan δ (tan δ ≡ G´´/G´, where δ is the phase

angle between the applied stimulus and the corresponding response) as a function of strain amplitude or frequency were obtained.

2.12. Statistical analysis.

Data are reported as mean ± SD (n = 3). Error bars represent the standard deviation calculated from tests of triplicate measurements for each hydrogel at each recombinamer concentration. Statistical analysis was evaluated by a one-way analysis of variance using the Holm-Sidak method. A p value lower than 0.05 was considered to be statistically significant. (**) $p < 0.001$, (*) $p < 0.05$, and $p>0.05$ indicates no significant differences (n.s.d.).

3. EXPERIMENTAL RESULTS AND DISCUSSION

3.1.SEM measurements.

SEM micrographs of ELR-CG hydrogels at 37°C have been included in Fig. 2. A homogeneous 3D structure with high interconnectivity and a thin pore wall is observed for the lowest polymer concentration. Interconnectivity provides a noticeable advantage in tissue engineering applications, thereby favouring cell migration and nutrient delivery. The structure becomes denser and more compact, with a thicker pore wall, with increasing polymer concentration. As a consequence, porosity qualitatively decreases. A predominantly closed-pore structure is observed at higher concentrations, whereas an open-pore structure is found for low polymer concentrations.

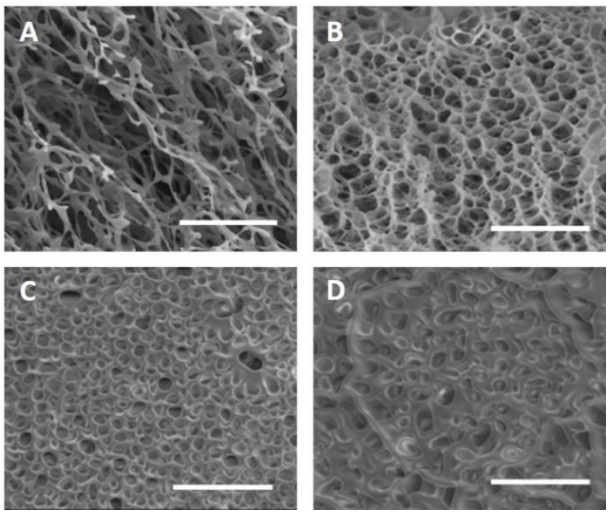

***Fig. 2**. Representative SEM micrographs for several polymer concentrations of ELR-CG hydrogels: 25 mg/mL (a), 50 mg/mL (b), 100 mg/mL (c), and 125 mg/mL (d) at 37°C. Scale bar: 20 μm*

Both the mean pore size and mean pore wall thickness were evaluated and the results at 37°C are included in Table 1. Pore geometry is predominantly circular or ellipsoidal, with pore size decreasing as ELR concentration increases. The pore wall thickness tends to increase as the recombinamer concentration increases. Both effects affect the porosity of the gels as defined in Equ. 1, as will be demonstrated below.

Table 1. *Mean pore size and mean pore wall thickness at 37°C for the ELR-CG evaluated using the ZEN software (Blue Edition, 2012) from Carl Zeiss Microscopy. 30 measurements taken in three different sample regions were averaged to calculate the mean and standard deviation values. $p < 0.05$ for pairwise multiple comparison between different concentrations.*

ELR-CG	Pore size (μm)	Wall Thickness (μm)
25 mg/mL	3.3 ± 0.7	0.4 ± 0.1
50 mg/mL	2.7 ± 0.3	0.5 ± 0.2
100 mg/mL	2.4 ± 0.3	1.1 ± 0.6
125 mg/mL	1.7 ± 0.4	2.1 ± 1.1

3.2.Porosity and Swelling Ratios

The dependence of the ELR-CG hydrogel porosity on polymer concentration is plotted in Fig. 3 (a). In agreement with the SEM micrographs, hydrogel porosity decreases at both temperatures (37°C and 4°C) as concentration increases. Porosity is higher at 4°C than at 37°C for a given concentration, although a high porosity is found at both temperatures. Specifically, a porosity value of around 70-75% is found at 4°C for a recombinamer concentration of 50 mg/mL. Furthermore, these results show that the hydrogel matrix retains the thermoresponsive nature of the original ELR. As can be seen from Fig. 3 (b), the equilibrium hydrogel swelling ratio at a given temperature decreases as the concentration increases. Although this trend is similar at both temperatures, in agreement with the literature[38] it is more evident at 4°C. As the concentration increases, the number of polymer chains and the number of cross-linked chains also increases. Consequently, the ability of the hydrogel to swell is reduced.

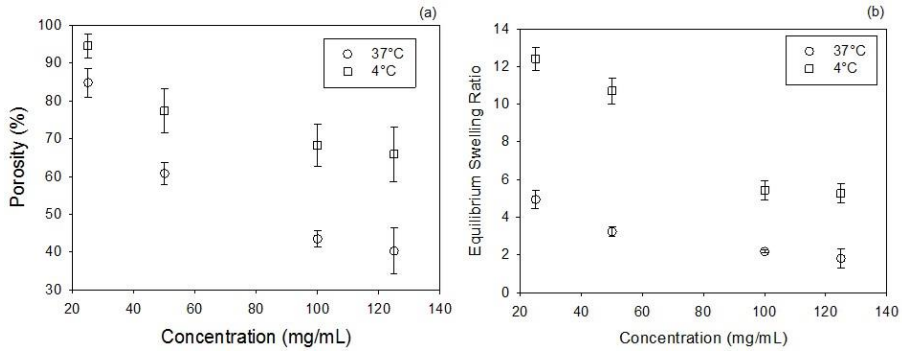

Fig. 3. *Evolution of porosity (a) and equilibrium swelling ratio (b) as a function of polymer concentration for the ELR-CHG hydrogels at 4°C and 37°C. Data are reported as mean ± SD (n = 3).*

Porosity and equilibrium swelling of the 125 mg/mL ELR-CG hydrogel at both temperatures are quite similar to the values found for the 100 mg/mL hydrogel. Covalent crosslinking requires both the presence of the reactive groups responsible for chain crosslinking and their accessibility. Moreover, a Cu(I) ion must be present to catalyse the ELR-CGs formation. At the highest concentration, where the number of polymer chains is very high, steric hindrance may limit the interaction between the groups that take part in the crosslinking process.

3.3.Rheological measurements.

The viscoelastic mechanical properties of hydrogels have been determined by rheological measurements in the linear viscoelastic range using a strain of 1%. The evolution of G´, G´´, and tan δ with frequency at 4° C and 37° C has been also obtained, and both G´ and G´´ are frequency-dependent (data not shown). A similar frequency-dependence has been reported for biological tissue (e.g., liver[39] and uterus[40]) and newly synthesized materials[41,42].

The values of G´, G´´, and tan δ as a function of polymer concentration are plotted in Fig. 4 at a fixed frequency of f = 1 Hz.

As G´ is much larger than G´´, the storage modulus is the dominant contribution to |G*|. The value of G´ at 1 Hz is in the range 1-10 kPa, tending towards the higher end of this range at the highest concentrations used. As such, the hydrogel exhibits a high degree of elasticity and the material can therefore be included in the category of "hard hydrogel". G´ and G´´ increase with polymer concentration at both temperatures. However, the G´ value for the highest concentration shows some saturation (Fig. 4 (a)). The same trend is observed at 4°C and 37°C. The porosity and swelling ratio results showed similar behaviour for this specific concentration.

Relatively similar values of G´ are found at both temperatures. Specifically, almost identical values are obtained at 4 and 37°C for concentrations of 25 and 50 mg/mL. For higher concentrations, G´ is higher at 37°C. These results can be explained by taking into account the high porosity observed for these samples[37].

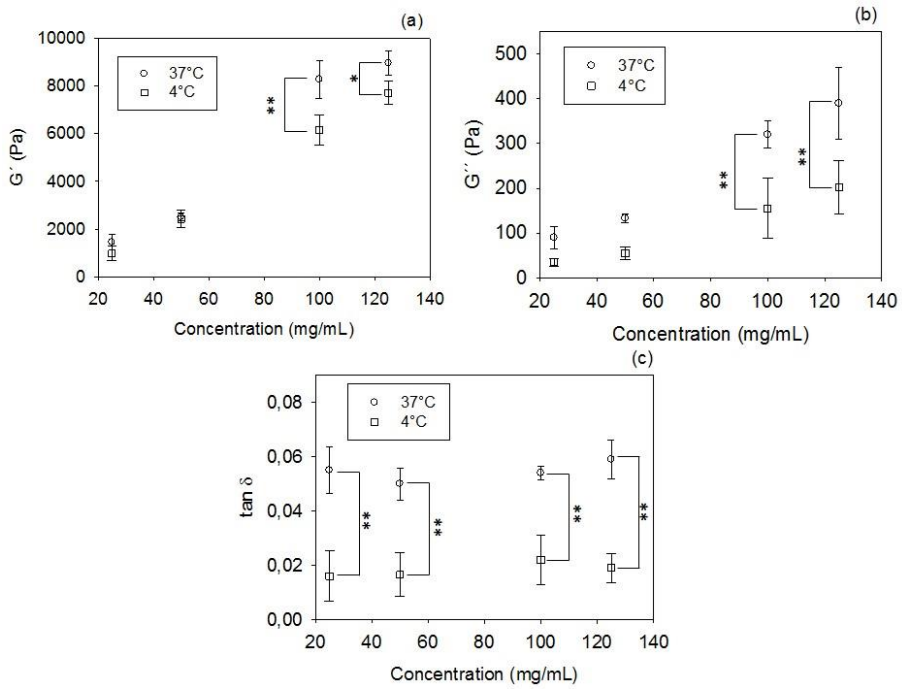

Fig. 4. *Evolution of G´ (a), G´´ (b), and tan δ (c) as a function of hydrogel polymer concentration at a fixed frequency of 1 Hz at 4° and 37°C. Data are reported as mean ± SD (n = 3). Statistical analysis was performed using an analysis of variance with the Holm-Sidak method. (**) p<0.001, (*) p<0.05*

Biomaterials with elastic moduli in the 1-10 kPa range are of widespread interest as many native tissues, for instance pig adventitial layer (4.7 ± 1.7 kPa) [43], canine kidney cortex and medulla (~10 kPa), and nucleus pulpous and eye lens (~1 kPa) [44], have moduli in this range. The moduli of isolated chondrocytes without cell-associated pericellular matrix have been reported to be in the range 0.6–4 kPa[45]. As far as the loss factor is concerned, no noticeable dependence on polymer concentration at a given temperature is observed from Fig. 4 (c). Tangent values of around 0.02 (at 4°C) and 0.06 (at 37°C) correspond to phase angles of about 1° and 3°, respectively. These values agree with the values for human bone (typically between 0.02 and 0.04) at physiological frequencies (around 10-2 – 103 Hz) [46]. Very low phase angles

are characteristic of highly elastic, energy-storing hydrogels. At 4°C these angles suggest low contact between the polymer chains. At 37°C the hydrogels are contracted and shed water, thus meaning that far less water is present to lubricate chain reorientation in response to an applied strain. Values of tan δ at this temperature suggest that some portion of the load is transferred between interacting ELP chains by friction[38]. Our experimental results agree with the literature[47,48] as, in general, tan δ does not correlate with either porosity or pore size.

3.4.Micropatterning of the ELR-CGs.

It is well known that surface topography induces and controls cell behaviour[49,50] and organization. As such, spatial control of the surface of materials for cell applications is a crucial factor to be taken into consideration when designing a device that will emulate the natural cell environment[51]. In light of this, several micropatterned gels, obtained by the replica moulding method, have been prepared for a recombinamer concentration of 50 mg/mL. Optical micrographs of the four different patterns obtained at 37°C, as described previously, are shown in Fig. 5.

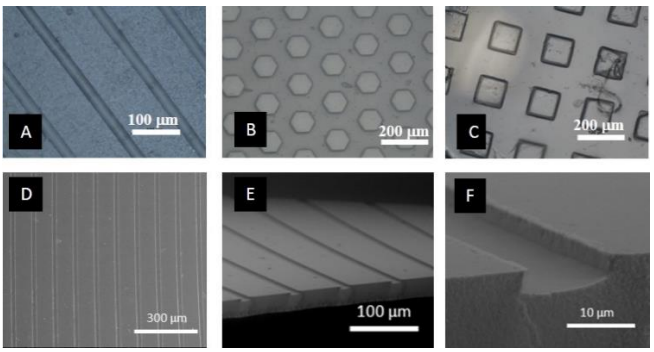

Fig. 5*. Optical micrographs of micro-structured ELR-CGs at 37°C (recombinamer concentration: 50 mg/mL) after demoulding. (A) 100 µm periodic grooves with w = 20 µm, (B) 100 µm periodic hexagonal pillars with w = 100 µm, (C) 100 µm periodic square pillars with w = 100 µm. (D, E, and F): SEM details of the micropatterned gel obtained in low vacuum mode for 100 µm periodic grooves with a width of 20 µm, and a step height (h) of 5 µm*

The replication quality with respect to the original silicon masters is high, and the homogeneity over the whole area is remarkable. In light of these results, we can conclude that total control of the surface topography of these ELR-CHGs is possible using the simple replica moulding method.

3.5.Bioactivity.

To evaluate the cytocompatibility of these new ELR-CGs, a polymer concentration of 50 mg/mL was chosen to form hydrogels with storage modulus values similar to those found in many natural tissues, as mentioned above. Moreover, at this concentration the hydrogel combines high porosity, which is important for a good cell colonization of the material, with easy handling.

With the aim of determining the influence of the bioactive sequences in the backbone structure of the ELRs that form the ELR-CGs on cell adhesion and proliferation, two kinds of ELR-CGs were prepared: one lacking a bioactive sequence (VKV-CG) and the second including the well-known RGD cell-adhesion sequence (RGD-CG).

SEM pictures of the RGD-CGs surfaces after fibroblast seeding showed that the presence of RGD in the ELR backbone results in a strong adhesion of seeded cells that spread well on the hydrogel surfaces, as can be seen from Fig. 6. These findings corroborate those previously observed for films or nanofibre RGD-ELR scaffolds[22,52,53]. The first picture shows the gel surface prior to cell deposition, whereas pictures B and C show details of the surface after cell adhesion. Cells can be observed as a soft tissue covering the RGD-CG surface.

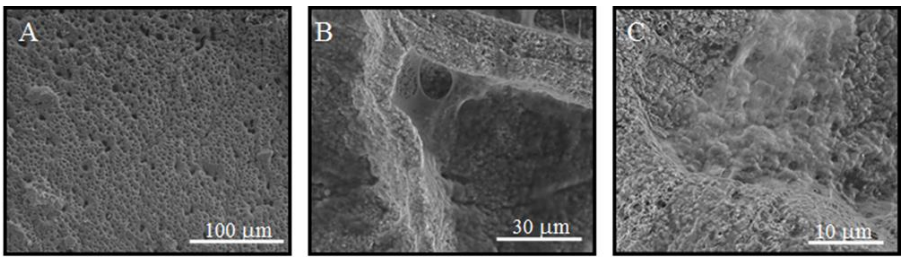

Fig. 6 *SEM details of RGD-CGs prior to (A) and after (B and C) HFF-1 cell colonization*

ELR-CGs would allow the co-seeding of cellular and polymeric suspensions to form a hydrogel with embedded cells within a few minutes. In order to corroborate the viability of this process, gels were prepared and HFF-1 cells embedded inside the ELR-CGs as described previously. Metabolic activity tests were performed every three days for eighteen days with the aim of evaluating the viability and proliferation of the embedded cells. As can be seen in Fig. 7, the viability of the HFF1 cells in RGD-CGs is clearly higher than in VKV-CGs for the whole culture time. The cells cultured in control CGs showed a lower metabolic activity that did not increase substantially during the experimental time. In contrast, fibroblasts embedded in RGD-CGs showed a sigmoidal growth, with slow growth in the first eight days, logarithmic growth between days nine and twelve, and stabilization until the end of the experiments. Although the presence of RGD in the molecule backbone of these scaffolds has no influence on the number of cells as they are encapsulated in the CGs, it is well known that binding between cell-surface receptors and ECM protein motifs activates the intracellular signalling pathways that strongly influence a cell's behaviour and fate[54].

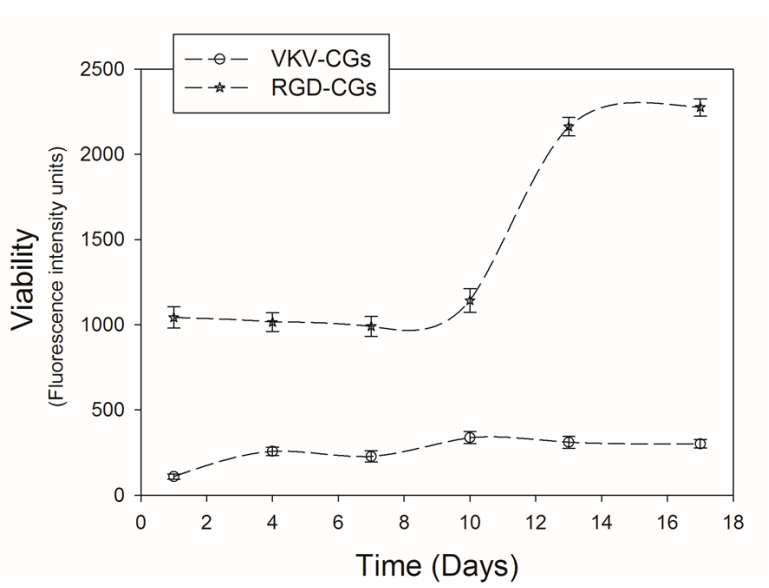

Fig. 7. *Dependence of viability of HFF-1 cells on two different substrates containing or lacking the bioactive sequence RGD (VKV-CGs and RGD-CGs) over 18 days. Error bars represent standard error (n=4).*

In order to assess the ability of ELR-CGs to sustain different cell types, the development and phenotype of human primary cell cultures in click-hydrogels was evaluated. Primary cells were chosen as the model as they produce more physiologically relevant data than other cell lines. A one-week ELR-CGs culture of fibroblast, endothelial and mesenchymal stem cells was evaluated by optical fluorescent microscopy after hydrogel fixation and specific staining of the cytoskeletal actin (green) and nucleus (blue). As can be seen in Fig. 8, the embedded cells present in different focal planes have the typical morphology of their respective cell types, in other words large mesenchymal stem cells, extended, elongated and fibrous fibroblasts that can provide long cytoplasmic processes, and a polyhedral morphology for HUVECs.

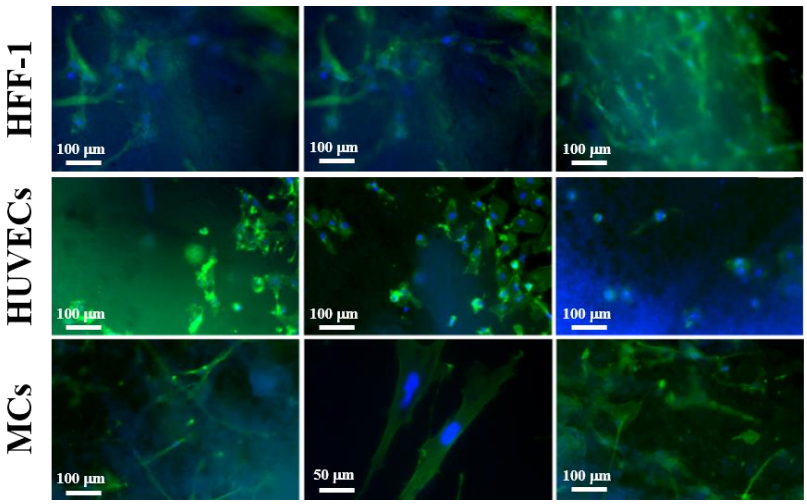

Fig. 8. *Human primary fibroblasts (HFF1), human primary umbilical vein endothelial cells (HUVEC) and human adipose-derided tissue mesenchymal stem cells (MSC) embedded inside RGD-CGs after seven days of culture.*

MSCs are pluripotent cells that are able to differentiate into multiple cells types widely utilized in both tissue engineering and regenerative medicine. Long-term culture studies were carried out with MSCs embedded inside RGD-CGs obtained as described previously, with cells seeded on standard polystyrene cell culture being used as controls. The metabolic activity of these cells was measured for 60 days. As can be seen from Fig. 9, cell growth shows a sigmoidal behaviour, with slow growth for the first 10-15 days. This first phase is followed by a logarithmic growth phase from day 20 onwards. The delayed growth in the ELR-CG observed in the first phase is compensated in this second phase and is followed by a higher metabolic stability of the cells in the last stationary phase in the ELR-CG than for the control.

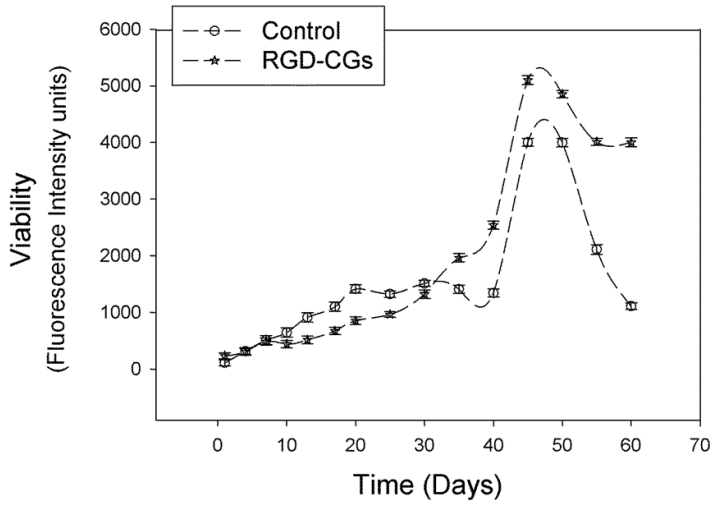

Fig. 9 *Dependence of MSC viability in RGD-CGs over 60 days. Comparison of growth on standard plastic tissue culture and cells embedded inside ELR-CGs. Error bars represent standard error (n=4).*

Fig. 10 shows a morphological analysis of the MSCs embedded in the three-dimensional structure. Although the texture, consistency and thickness of the gel partially hinder viewing, embedded cells can be analysed in different focal planes in which we can see extended and elongated cells with long cytoplasmic processes. Colonization of the hydrogel is almost complete after 60 days, thus indicating that the scaffolds are capable of supporting the long-term culture of embedded cells. The protein nature of the ELR-CGs could allow the cell-mediated remodeling of the artificial scaffold due to the proteases action during the new extracellular matrix synthesis, permitting the cell proliferation, and thus, a quite total colonization of the scaffolds. Cells showed a well-spread morphology, with large extensions and numerous pseudopodia, and their cytoskeleton actin filaments (green stained) were well organized in stress fibres, thereby indicating a strong adhesion.

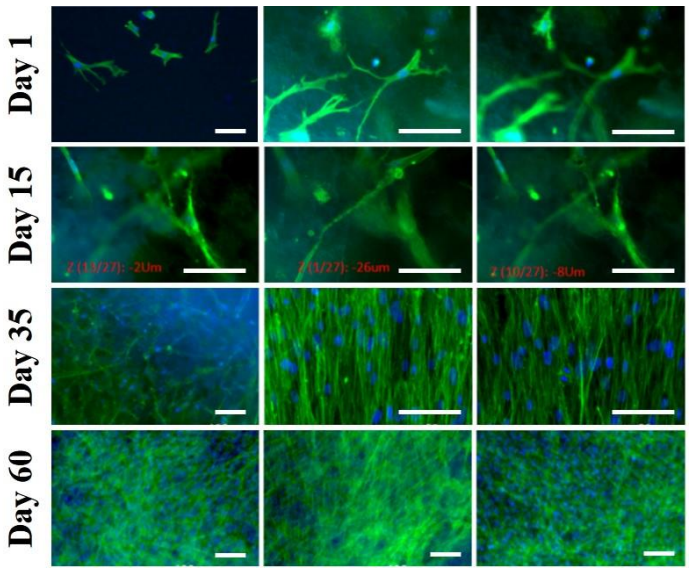

***Fig. 10**. Optical microscope pictures of RGD-CG colonization by MSCs in several focal planes for up to 60 days. Scale bars: 100 μm.*

4. CONCLUSIONS

In this paper two elastin-like recombinamers (ELRs), namely a structural ELR (VKVx24) and an ELR containing the RGD cell-adhesion sequence (HRGD6) have been chemically modified at the amino groups of the lysine residues to bear azide and alkyne groups that react in the presence of Cu(I) to yield novel and highly biocompatible elastin-like recombinamer-click hydrogels (ELR-CGs). These ELR-CGs have been designed, synthesized, and characterized, and their cytocompatibility has also been tested. Special attention has been paid to their microstructural morphology and mechanical properties, and the correlation between SEM micrographs, porosity, swelling ratio, rheological measurements and concentration has been determined. We have reported a simple, fast, water-based method for obtaining micropatterned ELR-CGs under mild, physiological conditions by replica moulding. This ELR-CGs system enables the highly reproducible fabrication of

different microstructured surfaces and can be used as a substrate with a well-controlled microtopography for studying spatially controlled cell behaviour. Injectable hydrogels present several important therapeutic advantages as regards the minimally invasive implantation technique, reducing the pain associated with conventional surgical procedures. The possibility of co-injection of cells as therapeutic agents that remain embedded and confined at the administration site is another great benefit of this approach.

Studies of the medium- and long-term viability have revealed a good cytocompatibility with respect to several human primary cell types (HFF-1, MSCs and HUVECs) in both surface and 3D cultures. As such, we can conclude that our ELR-CGs are able to maintain and expand cell cultures in time and are therefore suitable scaffolds for tissue engineering.

Several polymer concentrations and temperatures have been used to obtain gels with fully tuneable properties with potential applications as drug-delivery systems or scaffolds for tissue engineering.

5. ACKNOWLEDGEMENTS

We acknowledge financial support from the EU via the European regional development fund (ERDF), from the MINECO (MAT-2010-15982, MAT2010-15310, PRI-PIBAR-2011-1403 and MAT2012-38043), the JCyL (projects VA049A11, VA152A12 and VA155A12), the CIBER-BBN, and the JCyL and the Instituto de Salud Carlos III under the "Network Center of Regenerative Medicine and Cellular Therapy of Castilla and Leon".

6. REFERENCES

1. Mitragotri S, Lahann J. Physical approaches to biomaterial design. Nat Mater 2009;8(1):15-23.

2. Raghavan S, Chen CS. Micropatterned Environments in Cell Biology. Advanced Materials 2004;16(15):1303-1313.

3. Curtis A, Wilkinson C. Topographical control of cells. Biomaterials 1997;18(24):1573-1583.

4. Falconnet D, Csucs G, Michelle Grandin H, Textor M. Surface engineering approaches to micropattern surfaces for cell-based assays. Biomaterials 2006;27(16):3044-3063.

5. Curtis A, Wilkinson C. Topographical control of cells. Biomaterials 1997;18(24):1573-83.

6. Mata A, Boehm C, Fleischman AJ, Muschler G, Roy S. Analysis of connective tissue progenitor cell behavior on polydimethylsiloxane smooth and channel micro-textures. Biomedical Microdevices 2002;4(4):267-275.

7. Mata A, Kim EJ, Boehm CA, Fleischman AJ, Muschler GF, Roy S. A three-dimensional scaffold with precise micro-architecture and surface micro-textures. Biomaterials 2009;30(27):4610-4617.

8. Dalby MJ, Gadegaard N, Tare R, Andar A, Riehle MO, Herzyk P, Wilkinson CD, Oreffo RO. The control of human mesenchymal cell differentiation using nanoscale symmetry and disorder. Nat Mater 2007;6(12):997-1003.

9. Engler AJ, Sen S, Sweeney HL, Discher DE. Matrix Elasticity Directs Stem Cell Lineage Specification. Cell 2006;126(4):677-689.

10. Rodríguez-Cabello JC, Martín L, Alonso M, Arias FJ, Testera AM. "Recombinamers" as advanced materials for the post-oil age. Polymer 2009;50(22):5159-5169.

11. Arias FJ, Santos M, Fernandez-Colino A, Pinedo G, Girotti A. Recent Contributions of Elastin-Like Recombinamers to Biomedicine and Nanotechnology. Current Topics in Medicinal Chemistry 2014;14(6):819-836.

12. Rincón A, Molina-Martinez I, de Las Heras B, Alonso M, Baílez C, Rodríguez-Cabello J, Herrero-Vanrell R. Biocompatibility of elastin-like polymer poly(VPAVG) microparticles: in vitro and in vivo studies. Journal of biomedical materials research. Part A 2006;78(2):343-351.

13. Wright ER, Conticello VP. Self-assembly of block copolymers derived from elastin-mimetic polypeptide sequences. Advanced Drug Delivery Reviews 2002;54(8):1057-1073.

14. Kolb HC, Finn MG, Sharpless KB. Click Chemistry: Diverse Chemical Function from a Few Good Reactions. Angewandte Chemie International Edition 2001;40(11):2004-2021.

15. Meldal M, Tornøe CW. Cu-Catalyzed Azide−Alkyne Cycloaddition. Chemical Reviews 2008;108(8):2952-3015.

16. Tornøe CW, Christensen C, Meldal M. Peptidotriazoles on Solid Phase: [1,2,3]-Triazoles by Regiospecific Copper(I)-Catalyzed 1,3-Dipolar Cycloadditions of Terminal Alkynes to Azides. The Journal of Organic Chemistry 2002;67(9):3057-3064.

17. Rostovtsev VV, Green LG, Fokin VV, Sharpless KB. A Stepwise Huisgen Cycloaddition Process: Copper(I)-Catalyzed Regioselective "Ligation" of Azides and Terminal Alkynes. Angewandte Chemie International Edition 2002;41(14):2596-2599.

18. Uterine adenomyosis in the infertility clinic. Hum. Reprod. Update 2003;9(2):139.

19. Baskin JM, Prescher JA, Laughlin ST, Agard NJ, Chang PV, Miller IA, Lo A, Codelli JA, Bertozzi CR. Copper-free click chemistry for dynamic in vivo imaging. Proceedings of the National Academy of Sciences 2007;104(43):16793-16797.

20. Wenge U, Ehrenschwender T, Wagenknecht H-A. Synthesis of 2'-O-Propargyl Nucleoside Triphosphates for Enzymatic Oligonucleotide Preparation and "Click" Modification of DNA with Nile Red as Fluorescent Probe. Bioconjugate Chemistry 2013;24(3):301-304.

21. Laughlin ST, Baskin JM, Amacher SL, Bertozzi CR. In vivo imaging of membrane-associated glycans in developing zebrafish. Science 2008;320(5876):664-7.

22. Pierna M, Santos M, Arias FJ, Alonso M, Rodríguez-Cabello JC. Efficient Cell and Cell-Sheet Harvesting Based on Smart Surfaces Coated with a Multifunctional and Self-Organizing Elastin-Like Recombinamer. Biomacromolecules 2013;14(6):1893-1903.

23. Ossipov DA, Hilborn J. Poly(vinyl alcohol)-Based Hydrogels Formed by "Click Chemistry". Macromolecules 2006;39(5):1709-1718.

24. Jiang Y, Chen J, Deng C, Suuronen EJ, Zhong Z. Click hydrogels, microgels and nanogels: Emerging platforms for drug delivery and tissue engineering. Biomaterials 2014;35(18):4969-4985.

25. Urry DW, Pattanaik A, Xu J, Woods TC, McPherson DT, Parker TM. Elastic protein-based polymers in soft tissue augmentation and generation. J Biomater Sci Polym Ed 1998;9(10):1015-48.

26. Urry DW, Parker TM, Reid MC, Gowda DC. Biocompatibility of the Bioelastic Materials, Poly(GVGVP) and Its γ-Irradiation Cross-Linked

Matrix: Summary of Generic Biological Test Results. Journal of Bioactive and Compatible Polymers 1991;6(3):263-282.

27. Lampe KJ, Antaris AL, Heilshorn SC. Design of three-dimensional engineered protein hydrogels for tailored control of neurite growth. Acta biomaterialia 2013;9(3):5590-5599.

28. Betre H, Setton LA, Meyer DE, Chilkoti A. Characterization of a Genetically Engineered Elastin-like Polypeptide for Cartilaginous Tissue Repair. Biomacromolecules 2002;3(5):910-916.

29. Betre H, Ong SR, Guilak F, Chilkoti A, Fermor B, Setton LA. Chondrocytic differentiation of human adipose-derived adult stem cells in elastin-like polypeptide. Biomaterials 2006;27(1):91-99.

30. Tejeda-Montes E, Smith KH, Poch M, López-Bosque MJ, Martín L, Alonso M, Engel E, Mata A. Engineering membrane scaffolds with both physical and biomolecular signaling. Acta Biomaterialia 2012;8(3):998-1009.

31. Martin L, Alonso M, Moller M, Rodriguez-Cabello JC, Mela P. 3D microstructuring of smart bioactive hydrogels based on recombinant elastin-like polymers. Soft Matter 2009;5(8):1591-1593.

32. Martin L, Arias FJ, Alonso M, Garcia-Arevalo C, Rodriguez-Cabello JC. Rapid micropatterning by temperature-triggered reversible gelation of a recombinant smart elastin-like tetrablock-copolymer. Soft Matter 2010;6(6):1121-1124.

33. Rodriguez-Cabello JC, Girotti A, Ribeiro A, Arias FJ. Synthesis of genetically engineered protein polymers (recombinamers) as an example of advanced self-assembled smart materials. Methods in molecular biology (Clifton, N.J.) 2012;811:17-38.

34. Costa RR, Custodio CA, Arias FJ, Rodriguez-Cabello JC, Mano JF. Layer-by-Layer Assembly of Chitosan and Recombinant Biopolymers into Biomimetic Coatings with Multiple Stimuli-Responsive Properties. Small 2011;7(18):2640-2649.

35. Lundquist, Pelletier JC. Improved Solid-Phase Peptide Synthesis Method Utilizing α-Azide-Protected Amino Acids. Organic Letters 2001;3(5):781-783.

36. Zeng X, Ruckenstein E. Control of Pore Sizes in Macroporous Chitosan and Chitin Membranes. Industrial & Engineering Chemistry Research 1996;35(11):4169-4175.

37. Martin L, Alonso M, Girotti A, Arias FJ, Rodriguez-Cabello JC. Synthesis and characterization of macroporous thermosensitive hydrogels from recombinant elastin-like polymers. Biomacromolecules 2009;10(11):3015-22.

38. Trabbic-Carlson K, Setton LA, Chilkoti A. Swelling and Mechanical Behaviors of Chemically Cross-Linked Hydrogels of Elastin-like Polypeptides. Biomacromolecules 2003;4(3):572-580.

39. Kiss MZ, Varghese T, Hall TJ. Viscoelastic characterization of in vitro canine tissue. Phys Med Biol 2004;49(18):4207-18.

40. Kiss MZ, Hobson MA, Varghese T, Harter J, Kliewer MA, Hartenbach EM, Zagzebski JA. Frequency-dependent complex modulus of the uterus: preliminary results. Phys Med Biol 2006;51(15):3683-95.

41. Oliveira MB, Song W, Martin L, Oliveira SM, Caridade SG, Alonso M, Rodriguez-Cabello JC, Mano JF. Development of an injectable system based on elastin-like recombinamer particles for tissue engineering applications. Soft Matter 2011;7(14):6426-6434.

42. González de Torre I, Santos M, Quintanilla L, Testera A, Alonso M, Rodríguez Cabello JC. Elastin-like recombinamer catalyst-free click gels: Characterization of poroelastic and intrinsic viscoelastic properties. Acta Biomaterialia 2014;10(6):2495-2505.

43. Yu Q, Zhou J, Fung YC. Neutral axis location in bending and Young's modulus of different layers of arterial wall. American Journal of Physiology - Heart and Circulatory Physiology 1993;265(1):H52-H60.

44. Erkamp RQ, Wiggins P, Skovoroda AR, Emelianov SY, O'Donnell M. Measuring the elastic modulus of small tissue samples. Ultrason Imaging 1998;20(1):17-28.

45. Freeman PM, Natarajan RN, Kimura JH, Andriacchi TP. Chondrocyte cells respond mechanically to compressive loads. Journal of Orthopaedic Research 1994;12(3):311-320.

46. Buechner PM, Lakes RS, Swan C, Brand RA. A Broadband Viscoelastic Spectroscopic Study of Bovine Bone: Implications for Fluid Flow. Annals of Biomedical Engineering 2001;29(8):719-728.

47. Spiller KL, Laurencin SJ, Charlton D, Maher SA, Lowman AM. Superporous hydrogels for cartilage repair: Evaluation of the morphological and mechanical properties. Acta Biomaterialia 2008;4(1):17-25.

48. Ghosh S, Gutierrez V, Fernández C, Rodriguez-Perez MA, Viana JC, Reis RL, Mano JF. Dynamic mechanical behavior of starch-based scaffolds in dry and physiologically simulated conditions: Effect of porosity and pore size. Acta Biomaterialia 2008;4(4):950-959.

49. Curtis A, Wilkinson C. Topographical control of cells.pdf. Biomaterials 1997;18:1573-1583.

50. Falconnet D, Csucs G, Grandin H, Textor M. Surface engineering approaches to micropattern surfaces for cell-based assays. Biomaterials 2006;27(16):3044-3063.

51. Martin L, Javier Arias F, Alonso M, Garcia-Arevalo C, Rodriguez-Cabello JC. Rapid micropatterning by temperature-triggered reversible gelation of a recombinant smart elastin-like tetrablock-copolymer. Soft Matter 2010;6(6):1121-1124.

52. Garcia-Arevalo C, Pierna M, Girotti A, Arias FJ, Rodriguez-Cabello JC. A comparative study of cell behavior on different energetic and bioactive polymeric surfaces made from elastin-like recombinamers. Soft Matter 2012;8(11):3239-3249.

53. Ozturk N, Girotti A, Kose GT, Rodríguez-Cabello JC, Hasirci V. Dynamic cell culturing and its application to micropatterned, elastin-like protein-modified poly(N-isopropylacrylamide) scaffolds. Biomaterials 2009;30(29):5417-5426.

54. Yannas IV. Emerging rules for inducing organ regeneration. Biomaterials 2013;34(2):321-330.

CHAPTER 4:

ELASTIN-LIKE RECOMBINAMERS CATALYST-FREE CLICK HYDROGELS I: CHARACTERIZATION OF POROELASTIC AND INTRINSIC VISCOELASTIC PROPERTIES

Israel González de Torre[1]; Ana Testera[1]; Luis Quintanilla[1]; Mercedes Santos[1]; MatildeAlonso[1]; Jose-Carlos Rodriguez-Cabello[1].

1 BIOFORGE, CIBER-BBN, Campus "Miguel Delibes" Centro I+D, Universidad de Valladolid, Paseo Belén 11, 47011, Valladolid, Spain

González de Torre, I.; Santos, M.; Quintanilla, L.; Testera, A.; Alonso, M.; Rodríguez Cabello, J. C. Elastin-like recombinamer catalyst-free click gels: Characterization of poroelastic and intrinsic viscoelastic properties. Acta Biomaterialia 2014, 10 (6), 2495-2505.
DOI:10.1016/j.actbio.2014.02.006

Abstract:

ELR Catalyst-Free Click Gels (ELR-CFCGs) have been prepared and characterized by modifying both a structural ELR (VKV x 24) and a biofunctionalized ELR bearing RGD cell-adhesion sequences (HRGD6) to bear the reactive groups needed to form hydrogels via a click reaction. Prior to formation of the ELR-CFCGs, azide-bearing and cyclooctyne-modified ELRs were also synthesised. Subsequent covalent crosslinking was based on the reaction between these azide and cyclooctyne groups, which takes place under physiological conditions and without the need for a catalyst. The correlation among SEM micrographs, porosity, swelling ratio, and rheological measurements have been carried out. The storage and loss moduli at 1 Hz are in the range 1–10 kPa and 100 – 1000 Pa, respectively. The linear dependence of $|G^*|$ on $f^{1/2}$ and the peak value of $tan\ \delta$ were considered to be consistent with a poroelastic mechanism dominating the frequency range 0.3–70 Hz. The discrete relaxation spectrum was obtained from stress-relaxation measurements (t > 5s). The good fit of the relaxation modulus to decrease exponential functions suggests that an intrinsic viscoelastic mechanism dominates the transients. Several recombinamer concentrations and temperatures were tested to obtain gels with fully tuneable properties that could find applications in the biomedical field.

1. INTRODUCTION

New biomaterials that meet the needs and expectations of researchers in the field of bioscience are currently the subject of numerous studies. Depending on their final applications, these materials should have specific properties, although some characteristics, such as biocompatibility, specific mechanical properties, cell-friendly behavior, absence of toxic degradation products, and ease of handling, are desirable for all of them.

Elastin-Like Recombinamers (ELRs) show extraordinary properties for the most cutting-edge applications in biomedicine and nanotechnology. These compounds are obtained by recombinant DNA technologies, thus allowing the bioproduction of these protein-based polymers with well-defined, complex and totally controlled sequences. ELRs can include different bioactive sequences[1], such as those governing cell adhesion, protease sensitiveness, etc. Exceptional biocompatibility, excellent mechanical properties similar to those of natural elastin, strong self-assembly capabilities and response to different stimuli are some of the outstanding properties showed by these materials [1, 2]. The response to thermal stimulus is characterized by a critical temperature, known as the temperature transition in aqueous solution, T_t, which is associated with a conformational reorganization at the molecular level. Thus, whereas the polymer chains are soluble in water below T_t, above this temperature they self-assemble into nano- and micro-aggregates and become insoluble. This process is completely reversible.

"Click chemistry", which was introduced by Sharpless in 2001[3], and specifically the Huisgen 1,3-dipolar cycloadition of azides and alkynes[4], has been shown to be stereospecific, easy to perform in aqueous solution under mild conditions, and provides high reaction yields. Two reasons support the use of azides and terminal alkynes for biomedical applications. First, their stability within biological systems, and second, their limited side product formation. As a result of these advantages, this reaction has been widely employed in drug discovery [5], bioconjugation with proteins[6] and DNA[7], cell surface labeling[8], and surface modifications with ELRs[9], among other molecules. However, as this reaction requires the use of a transition metal ion, usually Cu^{+}, as a catalyst to initiate the reaction, some cytotoxicity problems have been reported[10]. As an improvement to conventional "click chemistry", the use of activated alkyne groups, such as cyclooctyne derivatives, has allowed these reactions to be carried out without the need for a catalyst[11].

Hydrogels provide an excellent platform for tissue engineering and regenerative medicine strategies. One particularly relevant use of hydrogels is in the form of injectable administration. This application requires a liquid compound that can pass through the narrow hole of a syringe needle but, once in position, stabilizes to form the hydrogel. Hydrogel crosslinking can be carried out by using the click chemistry due to its strictly physiological conditions and no harmful compounds required. This technique was first reported as an efficient chemoselective cross-linking method for hydrogel synthesis by Ossipov et al.[12] in 2006.

Since novel materials to be used in biomedical applications should mimic natural materials, a detailed characterization of the

former is essential. In particular, the mechanical/viscoelastic properties of hydrogels have to be considered since these properties strongly correlate with material microstructure and functionality, even at a biological level. In this sense, it is well-known that rheological measurements are an adequate tool for characterizing these properties.

With the aim to explain the mechanical behavior of biological materials, several models have been proposed in order to more realistically take into account their complex structure. In the case of cartilage, although a triphasic theory can be found in the literature[13], the biphasic model developed by Mow et al.[14, 15] consisting of a solid organic matrix with a movable interstitial fluid phase, which is predominately water, flowing throughout this matrix is usually employed. These authors adapted Biot's poroelasticity theory[16] and proposed the biphasic poroelastic (BPE) model to account for the rheological behavior of cartilage. Thus, a purely elastic solid-matrix phase is assumed, and the elastic modulus of the matrix and its hydraulic permeability play a fundamental role. However, a flow-independent (intrinsic) viscoelastic behavior has also been demonstrated in cartilage[17], thus leading to the proposal of a biphasic poro-viscoelastic (BPVE) model[18-20] that takes into account the viscoelastic behavior generated from the flow-dependent frictional interactions as well as the intrinsic viscoelastic nature of the porous solid-matrix. This latter model has become essential for explaining the behavior of soft tissues and hydrogels.

The main objective of this work is the search for a suitable hydrogel intended for biomedical applications and based on novel precursors, such as ELRs. Moreover, an advanced "click chemistry"

approach will be used in order to avoid the use of copper ions or any other catalyst that may cause biosafety concerns. To accomplish this goal, both a structural non-biofunctionalized ELR (VKVx24) and a bioactive ELR bearing RGD cell-adhesion sequences (HRGD6) have been used. Both these ELRs were modified to bear the two different reactive groups needed to form hydrogels via a click reaction.

Special attention will be given herein to the microstructural morphology and mechanical properties of those novel injectable hydrogels, whereas their biological properties will be evaluated in a forthcoming paper. The viscoelastic behavior of hydrogels is discussed on the basis of the BPVE model, and the contribution of both the fluid-dependent (poroelasticity) and fluid-independent viscoelasticity is taken into account in this work. Different strategies for modulating the properties of the hydrogel as a function of recombinamer concentration and temperature will also be considered. Thus, a new generation of ELR-based gels with fully tunable properties will be presented along with their potential uses as drug-delivery systems, scaffolds for tissue engineering, and as injectable systems to form gels *in situ* inside the body directly where they are needed.

2. EXPERIMENTAL SECTION

2.1. Materials

All chemicals were of analytical grade. They were purchased from Aldrich Co. and used as received. Cyclooctyne was purchased from SynAffix. B.V. Heyendaalseweg 1356525 AJ Nijmegen. The Netherlands.

2.1.1. ELR bioproduction

The ELRs were constructed using standard genetic engineering techniques and purified using several cycles of temperature-dependent reversible precipitation, as described by Girotti et al.[21] The bio-produced polymer was purified by a series of centrifugations under and above its transition temperature. The ELRs obtained in this manner were dialyzed against MilliQ (MQ) water and then lyophilized.

Two ELRs were employed. The first of these is VKVx24, a structural polymer with no bioactive sequence whose amino acid sequence is

MESLLP VG VPGVG $[VPGKG(VPGVG)_5]_{23}$ VPGKG VPGVG VPGVG VPGVG VPGV.

The second is HRGD6, a polymer containing a general adhesion sequence (RGD) whose amino acid sequence is

MGSSHHHHHHSSGLVPRGSHMESLLP $[(VPGIG)_2(VPGKG)(VPGIG)_2]_2$AVTGRGDSPASS$[(VPGIG)_2(VPGKG)(VPGIG)_2]_2$.

The purity and molecular weight of these ELRs were verified by sodium dodecyl sulfate polyacrylamide gel electrophoresis (SDS-PAGE) and matrix-assisted laser desorption/ionization time-of-flight (MALDI-TOF) mass spectroscopy in a Voyager STR (Applied Biosystems). An amino acid composition analysis was also performed. Additional characterization of ELRs was accomplished by infrared spectroscopy, Differential Scanning Calorimetry (DSC) and Nuclear Magnetic Resonance (NMR) techniques. HRGD6 has been previously characterized by Costa et al[22], and the

characterization results for VKVx24 are provided as Supporting Information (Figures 1 – 5 and Table 1).

The ELRs obtained were chemically modified at their lysine amino acids to bear the reactive groups necessary for subsequent "click chemistry" reactions.

2.1.2. Chemical modification of the ELRs

The ELRs were chemically modified by transformation of the ε-amine group present in the lateral chain of the lysine residue to bear the groups to be used in the hydrogel formation process. These modifications are described in greater detail below.

2.1.3. Synthesis of azide-bearing ELRs

Although azido-modified amino acids can be introduced by single or multisite protein engineering replacement strategies [23-25], the degree of site specificity provided by these laborious methods is not always needed. This led us to investigate the possibility of applying the relatively mild and easy-to-perform diazo transfer reaction to amines in order to introduce azides directly at the lysine positions of proteins. The diazo transfer reaction is carried out in CH_2Cl_2, with trifluoromethanesulfonyl azide (TfN_3) as reagent and catalyzed by Cu(II)[26-28]. The results show that this method is suitable for use with ELRs, providing an azide conversion in the range 70–90% (see Supporting Information, Figures 6(A), 7(A), 8(A)).

A substitution reaction was carried out using triflic azide as nucleophilic reagent. The triflic azide solution was freshly prepared *in situ* prior to each reaction as previously described by Lundquist et al.[29] Thus, NaN_3 (5.143 g, 7.91 mol, 100 eq) was dissolved in

14 mL of doubly distilled water and 17.5 mL of CH_2Cl_2 added. The reaction mixture was cooled in an ice-water bath, and a solution of triflic anhydride (2.26 mL, 1.58 mmol, 20 eq, 4.46 g) was added dropwise at 4ºC while stirring. The resulting mixture was stirred vigorously at 0ºC for 1 h and then at room temperature (r.t.) for a further hour. The crude reaction mixture was then washed with MQ water, (2 x 10 mL) and saturated Na_2CO_3 solution (2 x 10 mL). The resulting azide-containing solution was used immediately without further purification.

A solution of triflic azide was added dropwise at 0ºC to a solution of the elastin like-recombinamer HRGD6 (2 g, 0.791 mmol NH_2, 1 eq) in 24 ml of doubly distilled water containing sodium carbonate (1.188 mol, 1.5 eq) and copper(II) sulfate (0.01 eq). A 4 mL aliquot of methanol was added and the reaction run overnight at r.t. The organic solvents were then removed under reduced pressure. The recombinamer was purified by dialysis at 4ºC and then lyophilized. Transformation was corroborated by infrared spectroscopy, MALDI-TOF, and DSC in PBS at pH 7 (see Supporting Information, Figures 7(A), 8(A), 9(A), respectively).

2.1.4. Cyclooctyne-modified ELRs

A solution of (1*R*,8*S*,9*S*)-bicyclo[6.1.0]non-4-yn-9-ylmethyl succinimidyl carbonate (0.12 mmol) in DMF was added to a solution of the ELR in DMF (0.008 mmol in 5 mL) at r.t. and the resulting mixture stirred at r.t. for 48 hours. After this time, 15 mL of diethyl ether was added to the mixture to give a white precipitate. The supernatant was removed and the solid was washed with acetone (3x15 mL), dried under reduced pressure, redissolved in cold MQ water (4°C, 20 mL), dialyzed against MQ water (3x25 L), and then

lyophilized to yield 510 mg of a white recombinamer (ELR-cyclooctyne) in which 60% of the amine groups had been substituted (^{1}H NMR in DMSO-d_6, see Supporting Information, Figure 6 (B)).

Additional characterization of cyclooctine-modified ELRs by FTIR, MALDI-TOF, and DSC is shown in Supporting Information, Figures 7 (B), 8 (B), and 9 (B), respectively.

2.1.5. ELR-CFCG formation

Catalyst-free click reactions require an azide group that will react with an activated alkyne group, in our case a cyclooctyne group. Solutions of the ELR-cyclooctyne and ELR-azide were prepared in MQ water (at the desired concentration and with a molar ratio of 1:1) and kept at 4 °C for at least 24 h. ELR-CFCGs with final recombinamer concentrations of 50, 100 and 150 mg/mL were obtained by simply mixing these two solutions at 4 °C inside the appropriate mold (diameter: 13.5 mm; height: 2 mm). After 20 minutes at 4 °C, the gels were completely formed and could be removed from the mold.

The chemical process followed to obtain ELR-CFCGs from the ELRs is summarized in the scheme shown in Fig. 1. It should be pointed out that covalent cross-linking is based on the reaction of azide and cyclooctyne groups. Three replicates for each concentration of each hydrogel were performed for analysis by any of the instrumental methods used in this work.

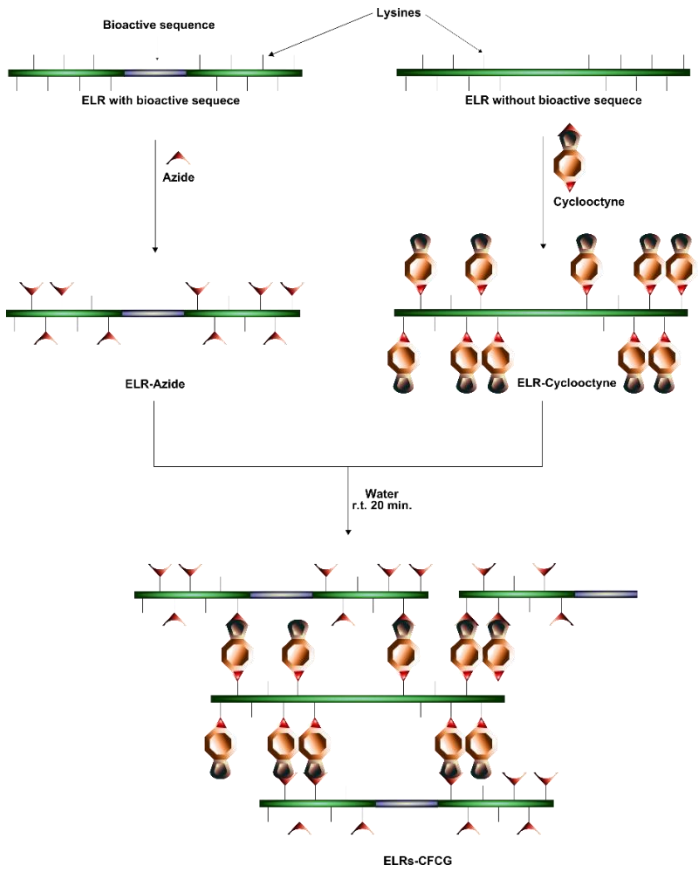

***Fig. 1**. Scheme showing ELR-CFCG formation. r.t. stands for room temperature.*

2.1.6. Preliminary ELR-CFCG characterization

A preliminary characterization of the hydrogels was carried out based on IR spectroscopy and DSC (Fig. 10 and Fig. 11, respectively, in the Supporting Information).

In agreement with literature reports[30-33], the azide band (~ 2100 cm^{-1}) either does not appear in the IR spectra or appears in only a residual percentage, thus indicating a high yield for the cross-linking reaction. As for the DSC results, a characteristic transition-phase temperature of about 26.5–27.5 °C was found irrespective of the recombinamer concentration.

2.2. Instrumental methods

2.2.1. Microstructural morphology

Scanning electron microscopy (SEM) was used to investigate the hydrogel morphology. Thus, the ELR-CFCGs were immersed in MQ water below (4 °C) and above (37 °C) the hydrogel T_t for one day, then immediately dropped into liquid nitrogen, physically fractured, and immersed in liquid nitrogen again. Finally, they were freeze-dried. Images of lyophilized hydrogels were obtained by SEM (JEOL, JSM-820) with no prior coating procedures. Morphological details (such as pore size and pore wall thickness) were evaluated quantitatively using the ZEN (Blue Edition, 2012) software package (Carl Zeiss Microscopy).

2.2.2. Microstructural morphology

The following equation [34, 35] was employed to estimate hydrogel porosity:

$$Porosity\ (\%) = ((W_1-W_2)/\rho_{water}) \cdot 100/V_{hydrogel} \quad \text{(Eq. 1)}$$

where W_1 and W_2 are the weight of the swollen and lyophilized gels, respectively, ρ_{water} is the density of pure water, and $V_{hydrogel}$ is the measured volume of the gel in the swollen state ($V_{hydrogel} = \pi r^2 h$, where r and h are the radius and height of the cylindrical sample, respectively). Excess surface water was removed with a filter paper before each measurement.

The volume change related to the phase-transition of the hydrogels in aqueous solution was quantified in terms of the equilibrium swelling ratio by weight, Q_w, defined as

$$Q_w(\%) = ((W_1-W_2)/W_2)\cdot 100 \quad \text{(Eq. 2)}$$

All measurements were taken 24 h after soaking the hydrogel in MQ water at the selected temperature. Equilibrium was defined as the steady state at which there was no change in volume of the ELR-CFCG.

Both porosity and the equilibrium swelling ratio were measured at 4 and 37 °C. Lyophilization (freeze-drying) was performed for water-swollen hydrogels frozen in liquid nitrogen at the corresponding test temperature.

2.2.3. Rheological measurements

Rheological experiments were performed using a strain-controlled AR-2000ex rheometer (TA Instruments) with the hydrogel submerged in water. Cylindrical swollen gel samples were placed between parallel plates of nonporous stainless steel (diameter = 12 mm) and the gap between the plates was adjusted using a normal force of 0.2 N in order to prevent slippage. A gap higher than 1000 μm was always reached after the sample relaxed until equilibrium. Measurements were carried out at 4 and 37 °C, with the sample temperature being controlled and maintained using a Peltier device.

Several measurements were performed in shear deformation mode. Initially, the range of strain amplitudes over which the gels exhibited a linear region of viscoelasticity was determined. To this end, a dynamic strain sweep (with amplitudes ranging between 0.1% and 20%) was carried out at a frequency of 1 Hz to measure the dynamic shear modulus as a function of strain. Secondly, dynamic frequency sweep tests were performed to determine the dependence of the dynamic shear modulus and loss factor on frequency. Specifically, a frequency sweep of between 0.01 and 70

Hz at a fixed strain (corresponding to the hydrogel linear region) was selected. Finally, in order to determine the transient evolution of the relaxation modulus, a stress relaxation test was undertaken. At least two specific biomedical applications explain these latter measurements. First, hydrogels developed to repair joint cartilage are more effective if their stress relaxation behavior matches that of the native tissue since such behavior affects load transfer and nutrient transport[36, 37]. The second application concerns the upregulated release of drugs from a hydrogel and for a period of time [38, 39]. The drug-release profile would be greatly affected by how stress evolves over this period[40].

In a stress relaxation test, a shear strain is applied to the hydrogels at t = 0 s and maintained constant up to the end of the measurement while recording the corresponding relaxation modulus, namely the ratio of the shear stress required to maintain a fixed strain to this same strain, as a function of time. In our measurements, a final time of 1800 s was selected in order to determine long-term hydrogel behavior, although a final time of 3600 s was used in some experiments. Due to the transient response of the rheometer, our transients show the evolution of the hydrogel relaxation modulus for $t > 5$ s. As such, no values are obtained for relaxation processes faster than that time.

Rheological measurements provide the storage modulus (G') and the loss modulus (G'') as a function of strain or frequency at a fixed temperature. The complex modulus magnitude $|G^*|$ ($|G^*|^2 = (G')^2 + (G'')^2$), and the loss factor ($\tan \delta = G''/G'$, where δ is the phase angle between the applied stimulus and the corresponding response) are also obtained. Moreover, the transient evolution of the relaxation modulus, $G(t)$, is registered.

2.2.4. Statistical analysis

Data are reported as mean ± SD (n = 3). Statistical analysis was evaluated by one way analysis of variance using the Holm-Sidak method. A p value lower than 0.05 was considered to be statistically significant. (**) $p < 0.001$, (*) $p < 0.05$, and $p>0.05$ indicates no significant differences (n.s.d.).

3. EXPERIMENTAL RESULTS

3.1.SEM results

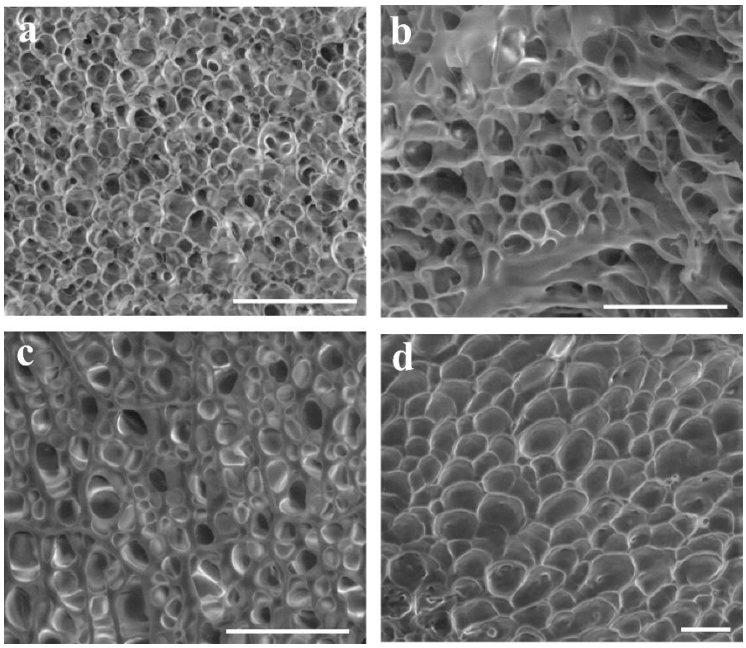

***Fig. 2**. Representative SEM micrographs of ELR-CFCGs for several recombinamer concentrations: 50 mg/mL (a), 100 mg/mL (b), and 150 mg/mL (c) at 37 °C. Picture (d) corresponds to 100 mg/mL at 4 °C. Scale bar: 20 µm.*

SEM micrographs of ELR-CFCGs at 37 °C can be found in Fig. 2. A homogeneous pore structure with high interconnectivity and a thin pore wall is observed for the lowest recombinamer concentration. Such interconnectivity provides a notable advantage in terms of tissue engineering. As the recombinamer concentration

increases, the structure becomes denser and more compact, with a thicker pore wall. As a result, inspection of the SEM micrographs shows that porosity qualitatively decreases. Generally speaking the pore geometry is predominantly circular or ellipsoidal. Moreover, whereas an open-pore structure is found for low recombinamer concentrations, a predominantly closed-pore structure is observed at higher concentrations.

Two morphological parameters have to be taken into consideration for further quantitative analysis: the mean pore size and the mean pore wall thickness. Both these parameters have been evaluated using the ZEN software package (Blue Edition, 2012) from Carl Zeiss Microscopy and the results obtained at 37 °C are included in Table 1. Statistical significance of these data was calculated and p remains always lower than 0.05 for pairwise multiple comparisons between different concentrations. The mean pore size decreases when recombinamer concentration increases. As for the mean pore wall thickness, this parameter increases with concentration.

Table 1. *Mean pore size and mean pore wall thickness for the ELR-CFCGs at 37 °C as evaluated using the ZEN software package (Blue Edition, 2012) from Carl Zeiss Microscopy. 30 measurements taken in three different sample regions have been averaged to calculate the mean and standard deviation values. $p < 0.05$ for pairwise multiple comparison between different concentrations. Statistical analysis was evaluated by analysis of variance using the Holm-Sidak method.*

37 °C	Pore size (μm)	Wall Thickness (μm)
50 mg/mL	4.5 ± 0.6	0.2 ± 0.1
100 mg/mL	4.0 ± 0.5	0.8 ± 0.2
150 mg/mL	3.1 ± 0.7	1.1 ± 0.5

Since the characteristic phase-transition temperature is about 26.5–27.5 °C, the 100 mg/mL hydrogels are completely

expanded at 4 °C (Fig. 2 (d)), thus resulting in a substantial increase in mean pore size (10.2 ± 3.5 μm) relative to that at 37 °C. Moreover, as a result of this higher pore size, porosity is higher at 4 °C than at 37 °C. These results show that the hydrogel matrix retains the thermo-responsive nature of the original ELRs.

3.2.Porosity and Swelling Ratios

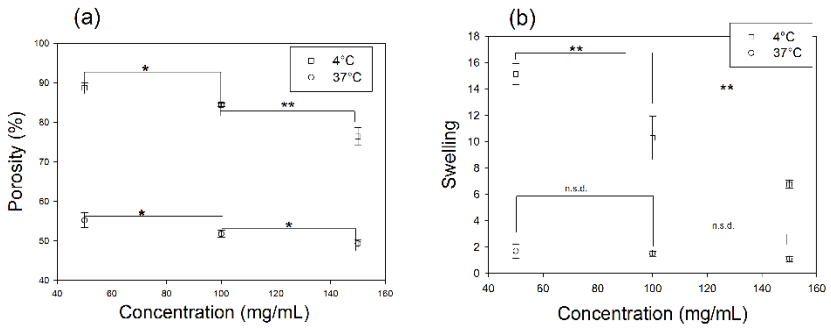

***Fig 3**. Evolution of porosity (a) and equilibrium swelling ratio (b) as a function of recombinamer concentration for the ELR-CFCGs at 4 and 37 °C. Data are reported as mean ± SD (n=3). Statistical analysis was evaluated by analysis of variance using the Holm-Sidak method. (**) p<0.001, (*) p<0.05, (n.s.d.) no significant differences.*

Fig. 3 (a) shows the dependence of ELR-CFCG porosity (estimated from equation 1) on recombinamer concentration, with porosity decreasing as concentration increases. The same trend is found at 4 and 37 °C. Porosity is higher at 4 than at 37°C for any given concentration,. All these findings agree with the previous SEM conclusions. At 4°C porosity values higher than 75% are found, with a value of around 90% being obtained for the lowest recombinamer concentration.

As can be seen in Fig. 3 (b), the equilibrium hydrogel swelling ratio at 4°C, decreases as the concentration increases. Yet, no significant dependence on the concentration is observed at 37°C under our experimental conditions. These results agree with bibliography [31].

3.3.Rheological results

The viscoelastic mechanical properties of the hydrogel can be determined by rheological measurements over the linear viscoelastic range, thereby providing information under conditions close to the unperturbed material state. Accordingly, in compliance with the principle of small deformation rheology [41-43], each hydrogel was tested over its respective linear viscoelastic range. |*G**| was found to remain independent of the strain amplitude (linear viscoelastic behavior) up to values of about 7–8 % (see Fig. 12 in Supporting Information). In order to ensure that measurements were carried out within the linear viscoelastic region, all subsequent rheological tests were performed for 1% strain.

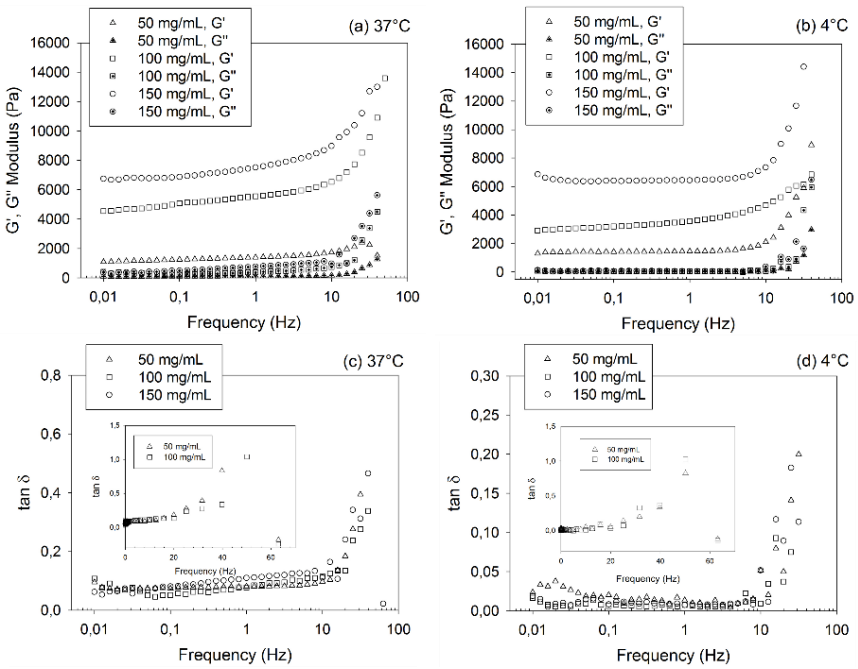

***Fig. 4**. Frequency dependence of the storage (G') and loss (G'') moduli for ELR-CFCGs at 37 (a) and 4 °C (b). Evolution of the loss factor (tan δ) as a function of frequency at 37 (c) and 4°C (d). The results obtained for every recombinamer concentration analyzed have been included. The inset in Figures (c) and (d) shows the peak value of tan δ for the recombinamer concentrations 50 and 100 mg/mL. Each curve corresponds to the average of three different samples measured.*

Fig 4 shows the dependence of *G'*, *G''*, and tan δ on frequency at 4 and 37 °C for all ELR-CFCGs studied. Both *G'* and *G''* increase with frequency. A similar frequency dependence has also been reported for biological samples (e.g., liver[44], and uterine[45] tissue) and newly synthesized materials of similar composition, such as RGD-containing ELR microparticles[46].

As far as the loss factor is referred, tan δ increases markedly for frequencies higher than 10 Hz until a peak value is observed at around 50 Hz (see the insets of Fig. 4 (c) and (d)) irrespective of recombinamer concentration and temperature. At lower frequencies (0.01 – 10 Hz), whereas no significant dependence on frequency was found for the 50 mg/mL recombinamer concentration at 37°C, the loss factor slightly increases for higher concentrations.

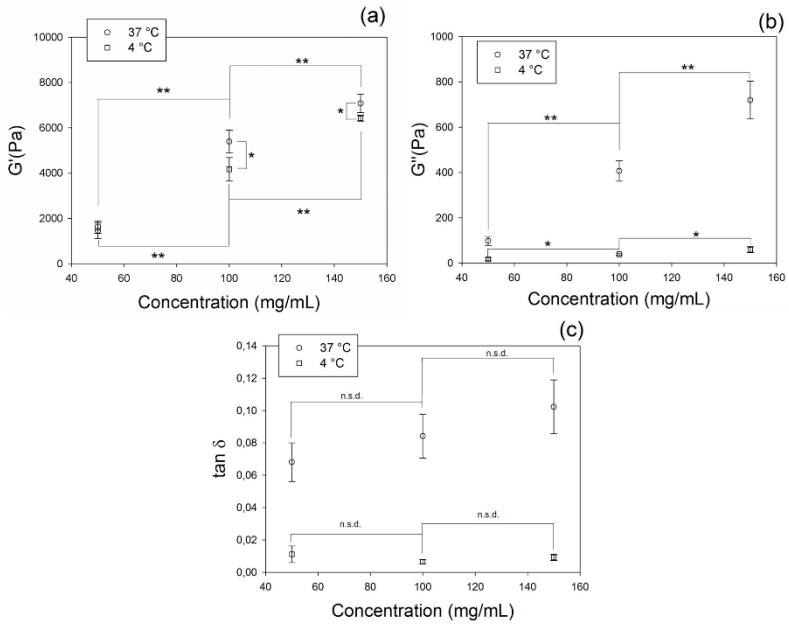

Fig. 5*. Evolution of G' (a), G'' (b), and tan δ (c) as a function of hydrogel recombinamer concentration at a fixed frequency of 1 Hz at 4 and 37 °C. Data are reported as mean ± SD (n=3). Statistical analysis was evaluated by analysis of variance using the Holm-Sidak method. (**) p<0.001, (*) p<0.05, (n.s.d.) no significant differences.*

Focusing on a fixed frequency of 1 Hz, *G'*, *G''* and *tan δ* values have been plotted in Fig. 5 as function of recombinamer concentration.

The gel strength can be estimated from the magnitude of G' and the significant difference between *G'* and *G''* (*G'* >> *G''*), which means that the storage modulus is the major contributor to |*G**|. At 1 Hz, the value of *G'* falls in the range 1-10 kPa and is around 7 kPa for the highest concentration (150 mg/mL). The hydrogel is therefore of the hard category and displays a high degree of elasticity.

Both *G'* and *G''* increase with recombinamer concentration. Relatively similar values of the storage modulus are found at both temperatures for a given concentration. No significant difference is found for the concentration of 50 mg/mL at 4°C and 37°C ($p>0.05$) for *G'*, while this modulus is slightly higher at 37°C than at 4°C for higher concentrations. The high porosity of these samples (see Fig. 3 (a)) may explain these results. Similar experimental results have been found in a previous work[35].

As far as the loss factor is concerned (Fig. 5 (c)), a constant value of about 0.01 (~ 0.5°) and 0.08 (~ 5°) are found at 4 and 37°C, respectively, for ELR-CFCGs. These experimental results agree with those found in literature [47, 48] as, in general, tan δ does not correlate with either porosity or pore size. At both temperatures phase angles are very low, which is characteristic of highly elastic, energy storing hydrogels. Higher values of tan δ are found at 37 °C than at 4 °C. The hydrogels are contracted at 37 °C and therefore have lower water content, thus meaning that less water is available to lubricate chain reorientation in response to an applied strain. Additionally, and probably more importantly, the ELR

chains are able to withstand extensive interchain hydrophobic contacts at temperatures above the characteristic phase transition temperature[31].

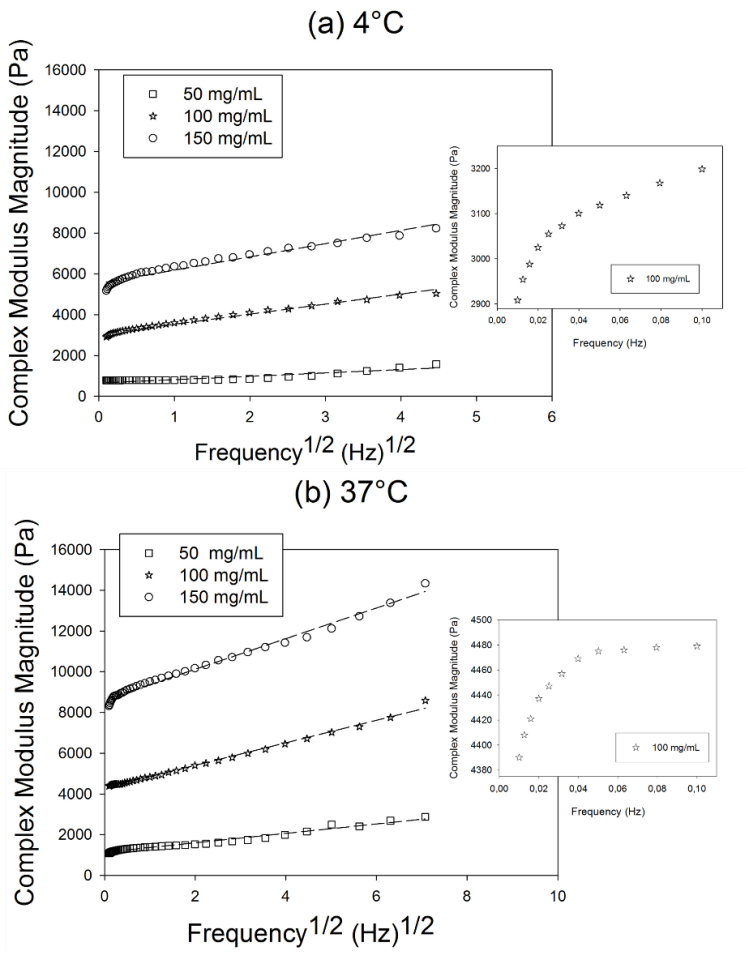

Fig. 6. *Dependence of the magnitude of the complex modulus on f½ at 37 (a) and 4 °C (b) for every recombinamer concentration analyzed in this work. The dashed line corresponds to the least-square linear regression of the linear region. In every case R2 is always better than 0.990. In both (a) and (b) |G*| has been plotted in the inset as a function of frequency in the range 0.01–0.1 Hz. Each curve corresponds to the average of three different samples measured.*

The dependence of $|G^*|$ on $f^{1/2}$ has been plotted in Fig. 6, for all ELR-CFCGs studied. Two different regions are observed at both temperatures. Thus, whereas a non-linear relationship with $f^{1/2}$ is found at low frequency (around 0.01–0.3 Hz), there is a frequency

range in which a linear relationship is observed (roughly in the range 0.3–30 Hz) irrespective of recombinamer concentration and temperature. This linear dependence is lost at frequencies higher than 30 Hz.

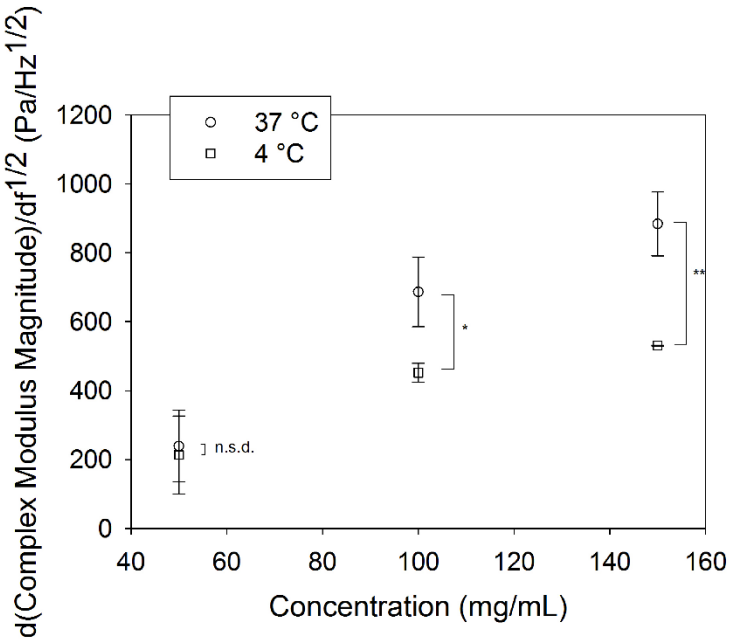

Fig. 7. *Dependence of d \|G*\|/dƒ1/2 on the recombinamer concentration at 4 and 37 °C. Data are reported as mean ± SD (n=3). Statistical analysis was evaluated by analysis of variance using the Holm-Sidak method. (**) p<0.001, (*) p<0.05, (n.s.d.) no significant differences.*

The slope can be calculated using the least-squares fitting of the experimental data in the linear region (Fig. 7). This value depends on both the recombinamer concentration and temperature. Thus, the slope increases with concentration at a fixed temperature. No significant differences are found between the slope at 4°C and 37°C for the concentration of 50 mg/mL ($p > 0.05$), whereas a higher slope is obtained at 37°C than at 4°C for higher concentrations.

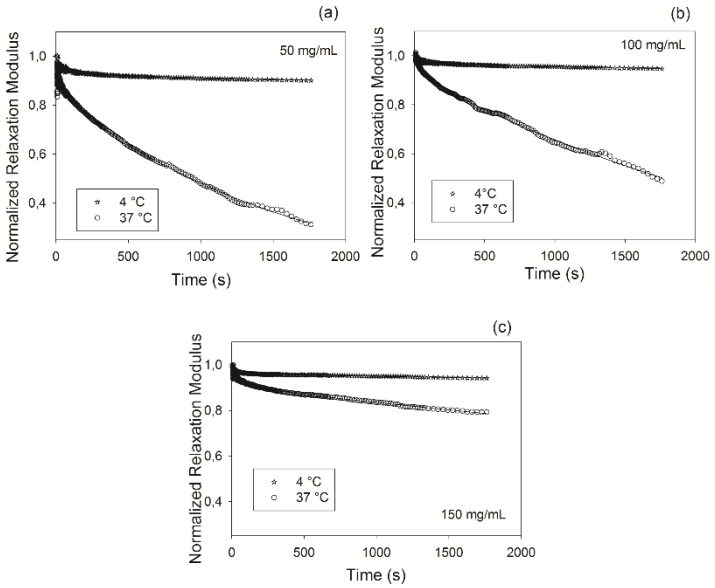

***Fig. 8**. Normalized relaxation modulus transients at 4 and 37°C for ELR-CFCGs. Transients are shown from 5 s to 1800 s. Strain amplitude of 1% was used in all cases. Each curve corresponds to the average of three different samples measured. The solid lines correspond to the numerical fitting of the experimental data to (Eq. 3) (R2 is always better than 0.990).*

Normalized relaxation modulus transients [G(t)/G(5s)] for the ELR-CFCGs studied herein are shown in Fig. 8. Transients were measured for a strain amplitude of 1% at 4 and 37°C for different recombinamer concentrations. Since transients are registered up to 1800 s, a long-term behavior of the ELR-CFCGs is determined.

G(t) shows a decreasing dependence on time. The rate of stress relaxation changes with temperature: transients are faster at 4 °C than at 37 °C; therefore they are more stabilized at low temperature than at high temperature after 1800 s. An estimate of the transient "amplitude" can be obtained from the normalized relaxation modulus at the end of the transient, i.e., *G*(1800s)/*G*(5s), and it is related to the percentage (relative to the peak value, *G*(5s)) by which the sample relaxes. A noticeable temperature-dependence of this parameter is found.

4. DISCUSSION

First of all, values of moduli and loss factor experimentally obtained in our hydrogels should be compared with those found in the bibliography. Biomaterials with elastic modulus in the range 1-10 kPa are of widespread interest as many native tissues also have moduli in this range. Among the data reported in the literature, for example, the moduli of some native tissues have been included in Table 2.

Table 2. *Elastic moduli of different native tissues along with that of the hydrogel proposed in this work are shown for comparison.*

Material	Elastic modulus
pig adventitial layer [49]	4.7 ± 1.7 kPa
canine kidney cortex and medulla [50]	~10 kPa
nucleus pulposus and eye lens [50]	~ 1 kPa
isolated chondrocytes [51]	range 0.6–4 kPa
Hydrogel proposed in this work	
(50 mg/mL at 37°C)	~ 1.8 kPa
(100 mg/mL at 37°C)	~ 5.7 kPa
(150 mg/mL at 37°C)	~ 7.5 kPa

The use of isolated cells without cell-associated pericellular matrix in Reference [51] should be noted. The goal in cell-based tissue engineering is to produce a new material with properties that mimic those of healthy tissue in order to restore physiological function upon maturation. Thus, the novel, non-dense cell-populated matrix shows a modulus lower than that of mature natural tissue (for bovine humeral head joint cartilage[52], the

aggregate modulus is around 0.6 MPa in a confined compression test and the shear modulus about 0.17 MPa from torsional shear), although this will increase once cells colonize the artificial matrix and generate their own natural structure.

As for the loss factor, Buechner et al.[53] collected a series of tan δ values for bone in the frequency range 10^{-7}–10^{7} Hz. At frequencies experienced physiologically by living bone (around 10^{-2}–10^{3} Hz), the values for human bone typically vary in the range 0.02 and 0.04. This range is of a similar magnitude to the values found in our hydrogels.

In order to discuss the different physical mechanisms contributing to the viscoelastic behavior of the hydrogel, the evolution of $|G^*|$ on $f^{½}$ is considered (Fig. 6). A similar behavior has been found in previous measurements and poroelastic models of the dynamic stiffness of native cartilage [54-57]. This evolution has also been found in a tissue-engineered matrix surrounding individual chondrocytes under different culture conditions[58]. Moreover, the phase angle δ (f) showed a peak value close to a characteristic frequency in these studies[57]. Both experimental results were considered to be consistent with a fluid-dependent viscoelastic mechanism (poroelasticity). Based on the linear poroelasticity theory[59], the characteristic poroelastic diffusion time is $\tau_p \sim L^2/Hk^2$ where L is the characteristic length over which the fluid flows, H is the elastic modulus, and k is the hydraulic permeability of the material.

The poroelastic relaxation frequency, $f_p \equiv 1/\tau_p$, has been estimated by Lee et al.[58] and Han et al.[57] to be around 50–90 Hz ($\tau_p \sim$ 10–20 ms) and 130 Hz ($\tau_p \sim$ 8 ms) for tissue-engineered matrix surrounding individual chondrocytes and native cartilage,

respectively, based on AFM-based indentations in the frequency range of 1–316 Hz in response to an imposed oscillatory deformation. The poroelastic mechanism dominates for frequencies close to f_p or lower. Lee [58] reported a value of the complex modulus magnitude in the range 1–20 kPa for frequencies in the range 1–100 Hz, similar to the values found in our hydrogels. In the Han work [57], δ (f) peaks at around 130 Hz corresponding to the characteristic poroelastic relaxation frequency. As a result, we suggest that in the frequency range over which |G*| is proportional to $f^{½}$, viscous drag of interstitial fluid (water) through the porous recombinamer network and fluid-solid frictional interactions due to fluid pressurization dominate. According to the dependence of tan δ on frequency plotted in the insets of Fig. 4 (c) and (d) for the ELR-CFCGs studied herein, an f_p value of around 50 Hz ($\tau_p \sim 20$ ms) is estimated.

It has been found experimentally that the storage modulus decreases as porosity increases [35, 47, 48]. Two reasons have been proposed to explain this behavior. First, the increased porosity allows for greater displacement of interstitial fluid from within the hydrogel pores, thereby resulting in higher strain at lower stresses. And second, the reduction in solid hydrogel content. Moreover, as the permeability of a hydrogel is a macroscopic measure of the ease with which fluid can flow through the matrix, permeability decreases as the matrix becomes denser and more compact. Since it has been reported[47] that permeability increases with porosity, G' decreases as permeability increases. As such, taking into account that G' is the dominant contributor to $|G^*|$, we suggest that the slope change observed for different concentrations and temperatures (Fig. 7) corresponds to a permeability change in the hydrogel, which decreases as the recombinamer concentration

increases. The lower slope found at 4 than at 37 °C for higher concentrations indicates a higher hydrogel permeability when the material is completely expanded at 4 °C. The SEM micrograph shown in Fig. 2 (d) supports this proposal.

When a fluid-independent viscoelastic mechanism (intrinsic viscoelasticity) dominates the relaxation modulus, *G(t)*, the time evolution of this parameter can be described by the equation[20, 60, 61]

$$G(t) = G_{equ} + \Sigma^{n}_{i=1} G_i \exp(-t/\tau_i) \qquad \text{(Eq. 3)}$$

based on a series of decreasing exponential functions, where τ_i and G_i are the relaxation time constant and the weight or degree of contribution of the τ_i -type relaxation to the overall relaxation process, respectively, and G_{equ} is the equilibrium modulus $(\lim_{t\to\infty} G(t) = G_{equ})$.

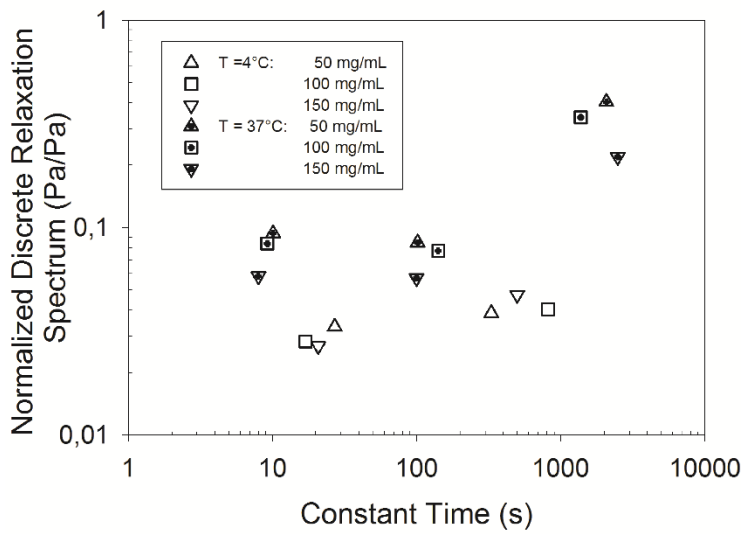

***Fig. 9**. Normalized discrete relaxation spectrum for ELR-CFCGs. Mean values have been used (n = 3), but bar errors have been omitted for clarity. Statistical analysis was evaluated by analysis of variance using the Holm-Sidak method. p-parameter was always higher than 0.05 (n.s.d) for pairwise multiple comparison between time constants in a constellation.*

Numerical fitting of the experimental data to this equation is carried out to obtain both G_{equ} and the discrete relaxation spectrum (namely, the weight of each relaxation process as a function of its corresponding time constant, Fig. 9). Actually, a normalized spectrum is calculated since each transient has been normalized to its corresponding peak value. At 37 °C this fitting needed three relaxation processes, whereas at 4 °C only two of them were required.

At a given temperature, and as a result of the different orders of magnitude of these constants, the overall relaxation process is mainly dominated by each time constant within the corresponding time range. In physical terms, a constant represents the time it takes the relaxation process to reach 63% of its asymptotic value.

Equivalent time constants are grouped into a constellation that is independent of recombinamer concentration under our experimental conditions. Statistical analysis confirms that there are no significant differences ($p > 0.05$) among the time constants in each constellation. At a fixed temperature, the relative weights for the various relaxation processes should also be taken into account. Moreover, higher weights are obtained at 37 °C than at 4 °C. The combination of time constants and weights of the various relaxation processes that contribute to the overall transient results in transients that are more stabilized at 4 °C than at 37 °C. The transient tail is mainly dominated by the relaxation process characterized by the longest time constant. At 37 °C, the longest time constant constellation is about 1500 s. As our transients are only recorded up to a time relatively similar to this constant (1800 s), the final transient time was extended up to 3600 s (results not

shown), thereby confirming the value of this time constant for ELR-CFCGs.

Since a good fitting of the transients was obtained, we suggest that the fluid-independent viscoelasticity whereby dissipation is related to the relaxation, reconfiguration and conformational mobility of recombinamer chains seems to be consistent with the dominant mechanism in these transients. A similar approach was used by Han et al.[57], who hypothesized that the intrinsic viscoelastic behavior dominates AFM-based force-relaxation transients (for $t >> \tau_p$) on the basis of their fitting of these transients to decreasing exponential functions.

These ideas can be used to provide further insight into the low frequency range in the dynamic frequency tests. In this frequency range (0.01–0.3 Hz), which corresponds to small variations in sinusoidal load with periods ranging from 3 to 100 s, a nonlinear dependence of $|G^*|$ on $f^{½}$ (and also on f, see the insets in Fig. 6 (a) and (b)) is observed. Thus, the dominant mechanism seems not to be poroelasticity. Since the above periods for the dynamic strain fall within the time range of our transients, an intrinsic viscoelastic behavior might be suggested.

In consequence, poroelasticity and intrinsic viscoelasticity dominate on different frequency (time) scales. At very low frequencies ($f << f_p$), the fluid has time to flow slowly and freely with minimal pressure buildup throughout the porous matrix. As such, it does not contribute significantly to the viscoelastic behavior, which is dominated by the intrinsic viscoelasticity. The increase in modulus with frequency may reflect the more difficult reaction of the conformational mobility of the chains. As the frequency increases ($f < f_p$), the time available for fluid flow

decreases, thus meaning that both the water and matrix incompressibility play a significant role in the module increase and poroelasticity becomes the dominant mechanism for viscoelasticity. At frequencies around the poroelastic relaxation frequency ($f \sim f_p$), pore fluid pressures increase, thus leading to a peak value in the loss factor. Although a significant pressure could arise in the fluid at frequencies well above f_p ($f >> f_p$), essentially negligible fluid flow would occur due to the short time available, thereby resulting in negligible energy dissipation[53].

The trend of the transients with temperature can be linked to the phase transition of the hydrogel matrix that occurs at T_t. Thus, whereas no order in the recombinamer chains is found at 4 °C, at 37 °C the chains fold and assemble hydrophobically, adopting a regular and non-random structure, thus meaning that the constraints for chain reorganizations are notably increased. The lack of order at low temperature favors chain rearrangement and reconformation and allows the equilibrium stress to be reached rapidly. In contrast, at high temperature the regular structure and the presence of intermolecular hydrophobic contacts hinder chain movement, thereby slowing the relaxation process. The presence of constraints hampers and complicates the relaxation process and may give rise to a higher number of relaxation processes at 37 °C than at 4°C. These arguments are in agreement with polymer dynamic theory[59], which predicts that stress relaxation should proceed faster in more compliant (i.e., less stiff) materials.

In accordance with these proposals, along with the differences found in the discrete relaxation spectrum at 4 °C and 37 °C, we suggest that the overall relaxation processes at low and

high temperature are qualitatively different and not a mere quantitative evolution associated with the temperature change.

5. CONCLUSIONS

In this paper, a novel and potentially highly biocompatible ELR Catalyst-Free Click Gels (ELR-CFCGs) have been prepared, and characterized in detail. They are based on a two component system in which the need of any catalyst is avoided, improving the biocompatibility of the click reaction. A structural ELR (VKV x 24) and an ELR having a RGD cell adhesion sequence (HRGD6) have been successfully chemically modified to bear the reacting groups needed to form the hydrogels via a click reaction based on the crosslinking reaction of azide and cyclooctine groups.

The correlation among SEM micrographs, porosity, swelling ratio, and rheological measurements have been carried out. Fully tunable hydrogel properties have been obtained based on the impact of the recombinamer concentration and temperature on the microstructure of these hydrogels. Rheological measurements were accomplished to determine the mechanical properties of the hydrogels. From dynamic and stress relaxation rheological measurements, we have demonstrated that poroelasticity and intrinsic viscoelasticity dominates in a different frequency (time) scale.

Although further biocompatibility studies are currently in progress, ELRs-CFCGs are presented as very promising candidates for biomedical applications such as drug delivery, tissue engineering, and as injectable systems for regenerative medicine or in situ drug delivery depots.

6. ACKNOWLEDGMENTS

We acknowledge financial support from the EU through the European regional development fund (ERDF), from the MINECO (MAT-2010-15982, MAT2010-15310, PRI-PIBAR-2011-1403 and MAT2012-38043), the JCyL (projects VA049A11, VA152A12 and VA155A12), the CIBER-BBN, and the JCyL and the Instituto de Salud Carlos III under the "Network Center of Regenerative Medicine and Cellular Therapy of Castilla and Leon".

7. REFERENCES

[1] Rodríguez-Cabello JC, Martín L, Alonso M, Arias FJ, Testera AM. "Recombinamers" as advanced materials for the post-oil age. Polymer 2009;50:5159-69.

[2] Wright ER, Conticello VP. Self-assembly of block copolymers derived from elastin-mimetic polypeptide sequences. Advanced Drug Delivery Reviews 2002;54:1057-73.

[3] Kolb HC, Finn MG, Sharpless KB. Click Chemistry: Diverse Chemical Function from a Few Good Reactions. Angewandte Chemie International Edition 2001;40:2004-21.

[4] Huisgen R. 1,3-Dipolar Cycloadditions. Past and Future. Angewandte Chemie International Edition in English 1963;2:565-98.

[5] Matthew W, John M, Ying-Chuan L, Steven MS, William L, Arthur JO, et al. Inhibitors of HIV-1 Protease by Using In Situ Click Chemistry. Angewandte Chemie 2006;118.

[6] Baskin JM, Prescher JA, Laughlin ST, Agard NJ, Chang PV, Miller IA, et al. Copper-free click chemistry for dynamic in vivo imaging. Proceedings of the National Academy of Sciences 2007;104:16793-7.

[7] Wenge U, Ehrenschwender T, Wagenknecht H-A. Synthesis of 2'-O-Propargyl Nucleoside Triphosphates for Enzymatic Oligonucleotide Preparation and "Click" Modification of DNA with Nile Red as Fluorescent Probe. Bioconjugate Chemistry 2013;24:301-4.

[8] Laughlin ST, Baskin JM, Amacher SL, Bertozzi CR. In vivo imaging of membrane-associated glycans in developing zebrafish. Science 2008;320:664-7.

[9] Pierna M, Santos M, Arias FJ, Alonso M, Rodríguez-Cabello JC. Efficient Cell and Cell-Sheet Harvesting Based on Smart Surfaces Coated with a Multifunctional and Self-Organizing Elastin-Like Recombinamer. Biomacromolecules 2013;14:1893-903.

[10] Kennedy DC, McKay CS, Legault MCB, Danielson DC, Blake JA, Pegoraro AF, et al. Cellular Consequences of Copper Complexes Used To Catalyze Bioorthogonal Click Reactions. Journal of the American Chemical Society 2011;133:17993-8001.

[11] Jewett JC, Bertozzi CR. Cu-free click cycloaddition reactions in chemical biology. Chemical Society Reviews 2010;39:1272-9.

[12] Dmitri AO, Jöns H. Poly(vinyl alcohol)-Based Hydrogels Formed by "Click Chemistry". Macromolecules 2006;39.

[13] Lai WM, Hou JS, Mow VC. A triphasic theory for the swelling and deformation behaviors of articular cartilage. J Biomech Eng 1991;113:245-58.

[14] Mow VC, Kuei SC, Lai WM, Armstrong CG. Biphasic creep and stress relaxation of articular cartilage in compression? Theory and experiments. J Biomech Eng 1980;102:73-84.

[15] Armstrong CG, Lai WM, Mow VC. An analysis of the unconfined compression of articular cartilage. J Biomech Eng 1984;106:165-73.

[16] Biot MA. General theory of three dimensional consolidation.

[17] Hayes WC, Bodine AJ. Flow-independent viscoelastic properties of articular cartilage matrix. Journal of Biomechanics 1978;11:407-19.

[18] Mak AF. The apparent viscoelastic behavior of articular cartilage--the contributions from the intrinsic matrix viscoelasticity and interstitial fluid flows. J Biomech Eng 1986;108:123-30.

[19] Mak AF. Unconfined compression of hydrated viscoelastic tissues: a biphasic poroviscoelastic analysis. Biorheology 1986;23:371-83.

[20] Kalyanam S, Yapp RD, Insana MF. Poro-viscoelastic behavior of gelatin hydrogels under compression-implications for bioelasticity imaging. J Biomech Eng 2009;131:081005.

[21] Girotti A, Reguera J, Rodriguez-Cabello JC, Arias FJ, Alonso M, Matestera A. Design and bioproduction of a recombinant multi(bio)functional elastin-like protein polymer containing cell adhesion sequences for tissue engineering purposes. J Mater Sci Mater Med 2004;15:479-84.

[22] Costa R, Custódio C, Arias F, Rodríguez-Cabello J, Mano J. Layer-by-layer assembly of chitosan and recombinant biopolymers into biomimetic coatings with multiple stimuli-responsive properties. Small (Weinheim an der Bergstrasse, Germany) 2011;7:2640-9.

[23] Wang L, Schultz P. Expanding the genetic code. Angewandte Chemie (International ed in English) 2004;44:34-66.

[24] Schoffelen S, Lambermon M, van Eldijk M, van Hest J. Site-specific modification of Candida antarctica lipase B via residue-specific incorporation of a non-canonical amino acid. Bioconjugate Chem 2008;19:1127-31.

[25] Kodama K, Fukuzawa S, Nakayama H, Kigawa T, Sakamoto K, Yabuki T, et al. Regioselective carbon-carbon bond formation in proteins with palladium catalysis; new protein chemistry by organometallic chemistry. Chembiochem : a European journal of chemical biology 2006;7:134-9.

[26] Chiara JL, Martín Lomas M, Vasella A, Witzig C. Convenient Synthesis of 2-Azido-2-deoxy-aldoses by Diazo Transfer. Helvetica Chimica Acta 2004;74:2073-7.

[27] Beckmann H, Wittmann V. One-pot procedure for diazo transfer and azide-alkyne cycloaddition: triazole linkages from amines. Organic letters 2007;9:1-4.

[28] Pothukanuri S, Winssinger N. A highly efficient azide-based protecting group for amines and alcohols. Organic letters 2007;9:2223-5.

[29] Lundquist, Pelletier JC. Improved Solid-Phase Peptide Synthesis Method Utilizing α-Azide-Protected Amino Acids. Organic Letters 2001;3:781-3.

[30] McMillan RA, Conticello VP. Synthesis and Characterization of Elastin-Mimetic Protein Gels Derived from a Well-Defined Polypeptide Precursor. Macromolecules 2000;33:4809-21.

[31] Trabbic-Carlson K, Setton LA, Chilkoti A. Swelling and Mechanical Behaviors of Chemically Cross-Linked Hydrogels of Elastin-like Polypeptides. Biomacromolecules 2003;4:572-80.

[32] Koschella A, Hartlieb M, Heinze T. A "click-chemistry" approach to cellulose-based hydrogels. Carbohydrate Polymers 2011;86:154-61.

[33] Xu X-D, Chen C-S, Wang Z-C, Wang G-R, Cheng S-X, Zhang X-Z, et al. "Click" chemistry for in situ formation of thermoresponsive P(NIPAAm-co-HEMA)-based hydrogels. Journal of Polymer Science Part A: Polymer Chemistry 2008;46:5263-77.

[34] Zeng X, Ruckenstein E. Control of Pore Sizes in Macroporous Chitosan and Chitin Membranes. Industrial & Engineering Chemistry Research 1996;35:4169-75.

[35] Martin L, Alonso M, Girotti A, Arias FJ, Rodriguez-Cabello JC. Synthesis and characterization of macroporous thermosensitive hydrogels from recombinant elastin-like polymers. Biomacromolecules 2009;10:3015-22.

[36] Mow VC, Holmes MH, Michael Lai W. Fluid transport and mechanical properties of articular cartilage: a review. Journal of Biomechanics 1984;17:377-94.

[37] Marijnissen WJCM, van Osch GJVM, Aigner J, van der Veen SW, Hollander AP, Verwoerd-Verhoef HL, et al. Alginate as a chondrocyte-delivery substance in combination with a non-woven scaffold for cartilage tissue engineering. Biomaterials 2002;23:1511-7.

[38] Lee KY, Peters MC, Anderson KW, Mooney DJ. Controlled growth factor release from synthetic extracellular matrices. Nature 2000;408:998-1000.

[39] Kim B-S, Nikolovski J, Bonadio J, Mooney DJ. Cyclic mechanical strain regulates the development of engineered smooth muscle tissue. Nat Biotech 1999;17:979-83.

[40] Lee KY, Rowley JA, Eiselt P, Moy EM, Bouhadir KH, Mooney DJ. Controlling Mechanical and Swelling Properties of Alginate Hydrogels Independently by Cross-Linker Type and Cross-Linking Density. Macromolecules 2000;33:4291-4.

[41] Meyvis TKL, Stubbe BG, Van Steenbergen MJ, Hennink WE, De Smedt SC, Demeester J. A comparison between the use of dynamic mechanical analysis and oscillatory shear rheometry for the characterisation of hydrogels. International Journal of Pharmaceutics 2002;244:163-8.

[42] Kavanagh GM, Ross-Murphy SB. Rheological characterisation of polymer gels. Progress in Polymer Science 1998;23:533-62.

[43] Tschoegl NW. The phenomenological theory of linear viscoelastic behavior : an introduction. Berlin ; New York: Springer-Verlag; 1989.

[44] Kiss MZ, Varghese T, Hall TJ. Viscoelastic characterization of in vitro canine tissue. Phys Med Biol 2004;49:4207-18.

[45] Kiss MZ, Hobson MA, Varghese T, Harter J, Kliewer MA, Hartenbach EM, et al. Frequency-dependent complex modulus of the uterus: preliminary results. Phys Med Biol 2006;51:3683-95.

[46] Oliveira MB, Song W, Martin L, Oliveira SM, Caridade SG, Alonso M, et al. Development of an injectable system based on elastin-like recombinamer particles for tissue engineering applications. Soft Matter 2011;7:6426-34.

[47] Spiller KL, Laurencin SJ, Charlton D, Maher SA, Lowman AM. Superporous hydrogels for cartilage repair: Evaluation of the morphological and mechanical properties. Acta Biomaterialia 2008;4:17-25.

[48] Ghosh S, Gutierrez V, Fernández C, Rodriguez-Perez MA, Viana JC, Reis RL, et al. Dynamic mechanical behavior of starch-based scaffolds in dry and physiologically simulated conditions: Effect of porosity and pore size. Acta Biomaterialia 2008;4:950-9.

[49] Yu Q, Zhou J, Fung YC. Neutral axis location in bending and Young's modulus of different layers of arterial wall. American Journal of Physiology - Heart and Circulatory Physiology 1993;265:H52-H60.

[50] Erkamp RQ, Wiggins P, Skovoroda AR, Emelianov SY, O'Donnell M. Measuring the elastic modulus of small tissue samples. Ultrason Imaging 1998;20:17-28.

[51] Freeman PM, Natarajan RN, Kimura JH, Andriacchi TP. Chondrocyte cells respond mechanically to compressive loads. Journal of Orthopaedic Research 1994;12:311-20.

[52] Soltz MA, Ateshian GA. A Conewise Linear Elasticity mixture model for the analysis of tension-compression nonlinearity in articular cartilage. J Biomech Eng 2000;122:576-86.

[53] Buechner PM, Lakes RS, Swan C, Brand RA. A Broadband Viscoelastic Spectroscopic Study of Bovine Bone: Implications for Fluid Flow. Annals of Biomedical Engineering 2001;29:719-28.

[54] Frank EH, Grodzinsky AJ. Cartilage electromechanics—II. A continuum model of cartilage electrokinetics and correlation with experiments. Journal of Biomechanics 1987;20:629-39.

[55] Kim YJ, Bonassar LJ, Grodzinsky AJ. The role of cartilage streaming potential, fluid flow and pressure in the stimulation of chondrocyte biosynthesis during dynamic compression. J Biomech 1995;28:1055-66.

[56] Soltz MA, Ateshian GA. Interstitial fluid pressurization during confined compression cyclical loading of articular cartilage. Ann Biomed Eng 2000;28:150-9.

[57] Han L, Frank Eliot H, Greene Jacqueline J, Lee H-Y, Hung H-Hwa K, Grodzinsky Alan J, et al. Time-Dependent Nanomechanics of Cartilage. Biophysical journal 2011;100:1846-54.

[58] Lee B, Han L, Frank EH, Chubinskaya S, Ortiz C, Grodzinsky AJ. Dynamic mechanical properties of the tissue-engineered matrix associated with individual chondrocytes. J Biomech 2010;43:469-76.

[59] Grodzinsky AJ, Frank EH. Fields, forces, and flows in biological systems. London ; New York: Garland Science; 2011.

[60] Suh JK, Bai S. Finite element formulation of biphasic poroviscoelastic model for articular cartilage. Journal of Biomechanical Engineering 1998;120:195-201.

[61] Strange DGT, Fletcher TL, Tonsomboon K, Brawn H, Zhao X, Oyen ML. Separating poroviscoelastic deformation mechanisms in hydrogels. Applied Physics Letters 2013;102:031913-4.

8. SUPPORTING INFORMATION

8.1.Materials

8.1.1. ELR bioproduction

ELR production was carried out using genetic-engineered protein biosynthesis in Escherichia Coli, while its purification was performed with several cycles of temperature-depending reversible precipitations as described elsewhere[1].

1 Girotti, A.; Reguera, J.; Arias, J.; Alonso, M.; Testera, A.M. and Rodríguez-Cabello, J.C. "Influence of the Molecular Weight on the Inverse Temperature Transition of a Model Genetically Engineered Elastin-like pH-Responsive Polymer". Macromolecules (2004), 37, 3396-3400

8.2.Instrumental methods

8.2.1. Amino acid analysis

The aminoacid composition was determined by the Technical-Scientific Service at the University of Barcelona (Spain) by HCl hydrolysis, derivatization by the AccQ-Tag Waters method and subsequent analysis by HPLC with UV detection for quantification. Each sample has been analyzed by triplicate.

8.2.2. Proton nuclear magnetic resonance 1H- and 13C-NMR Spectroscopy

NMR analysis was carried out using a 400 MHz Agilent Technologies equip with an Agilent MR console 400 and a One NMR probe. The measurements were carried out at 298 K with samples of 20–30 mg of the modified elastin like recombinamers, purified, and dissolved in DMSO-d6. Chemical shifts (δ) are given in ppm.

The nondeuterated dimethyl sulfoxide peaks at d ¼ 2.5 ppm and d ¼ 39.51 ppm were used as internal reference for 1H and 13C NMR spectra, respectively.

8.2.3. Fourier Transform Infrared Spectroscopy (FTIR).

FTIR analysis was conducted with a Bruker FTIR spectrophotometer (Bruker, USA). For each spectrum, a 512-scan interferogram was collected at single beam absorption mode with a 2 cm-1 resolution within the 4000- 600 cm-1 region. For each sample several FTIR absorption spectra were collected. Five measurements were averaged to obtain the final FTIR absorption spectrum of the sample. Residual water vapour absorption was interactively subtracted from the sample spectra.

Spectral calculations were performed by the OPUS (version 4.2) software (MATTSON INSTRUMENT, INC.).

8.2.4. Matrix-Assisted Laser Desorption/Ionization Time-of-Flight Mass Spectroscopy (MALDI-TOF)

Molecular weights were determined by matrix-assisted laser desorption/ionization mass spectroscopy (MALDI-MS), which was performed on a PE Biosystems Voyager-DE Instrument equipped with a nitrogen laser (337 nm) operating in the positive ion mode

with the delayed extraction. The ELR samples for MALDI-MS measurements were prepared in an aqueous 50% (v/v) acetonitrile solution containing 0.1% (v/v) trifluoroacetic acid, using sinapinic acid matrix.

8.2.5. Differential Scanning Calorimetry (DSC) measurements

DSC experiments were performed on a Mettler Toledo 822e DSC with a liquid nitrogen cooler accessory.

Both temperature and enthalpy were calibrated with an indium standard at the same experimental conditions used for the studied materials. Water solutions of mELRs at 50 mg mL-1 were prepared at different values of pH. In a typical DSC run, 20 µL of the solution was placed inside a standard 40 µL aluminium pan hermetically sealed. The same volume of water was placed in the reference pan. As for ELR-hydrogel analysis, 20 mg of the hydrated hydrogel was placed in the sample pan. To account for the exact amount of polymer in the assayed hydrogel, the sample was lyophilized and weighted after DSC run.

All samples were equilibrated for 10 min at 0ºC inside the sample chamber just before the beginning of each experiment, and then, heated from 0 to 60 ºC at a heating rate of 5ºC/min. The scans were run under a nitrogen atmosphere.

8.3.Characterization of materials

8.3.1. Characterization of VKVx24

8.3.1.1. DSC

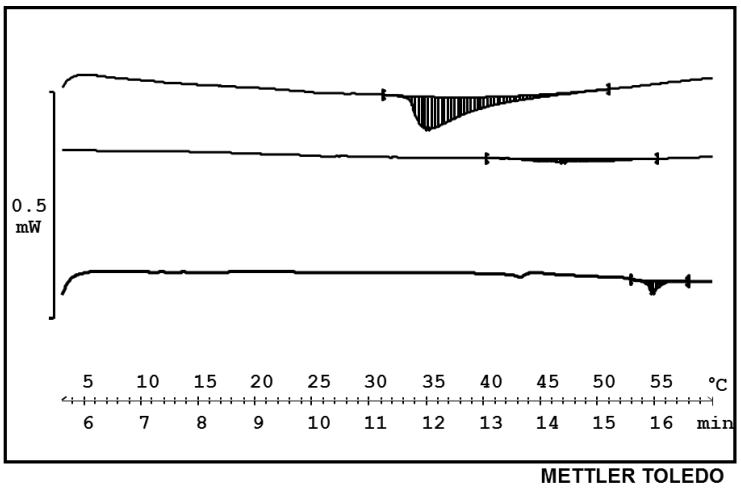

Fig. 1. *DSC thermograms for several pH values of the solution in Milli-Q water: 11.9, 10.3 and 6.6 (from top to bottom).*

8.3.1.2. FTIR

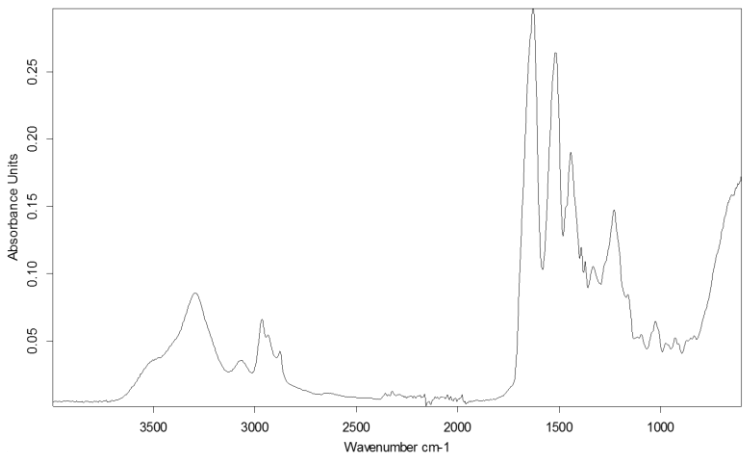

Fig. 2

8.3.1.3. Aminoacid analysis

	Molar ratio					Molar ratio				
	experimental	teoric				experimental	teoric			
Asx					Cys					
Ser	1.56	1			Tyr					
Glx	3.02	1			Val	257.75	266			
Gly	294.66	288			Met	1.75	1			
His					Lys	25.84	24			
Arg					Ile	3.26	2			
Thr					Leu					
Ala					Phe					
Pro	144.74	145								
n.d. undetermined										

Table 1

8.3.1.4. MALDI-TOF

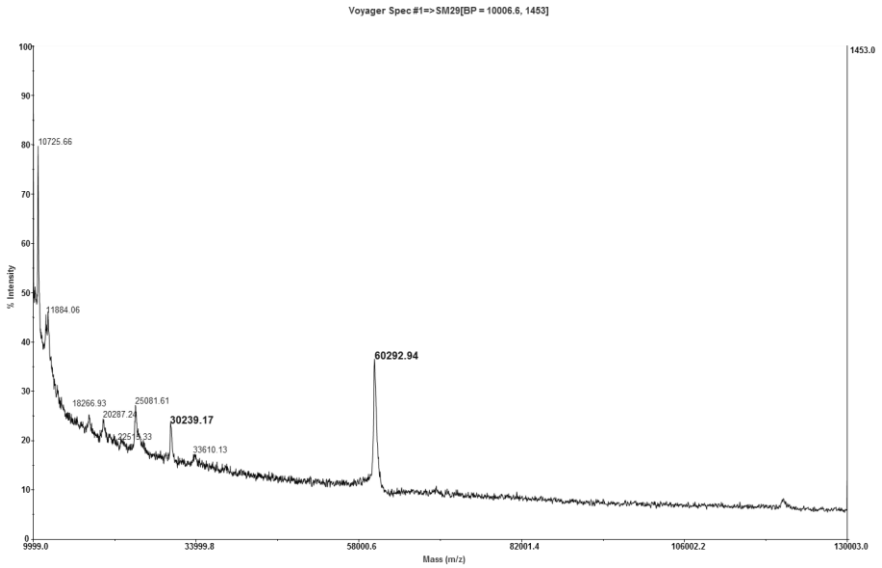

Fig. 3

8.3.1.5. NMR

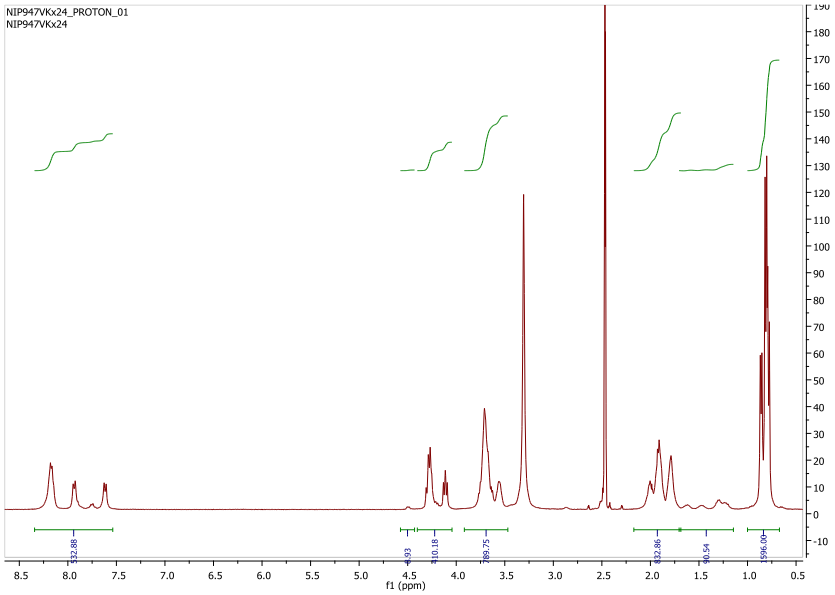

Fig. 4

8.3.1.6. SDS

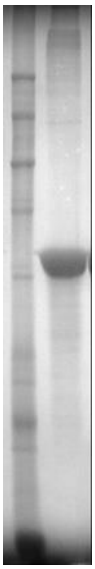

Fig. 5

8.3.2. Characterization of modified-ELRs

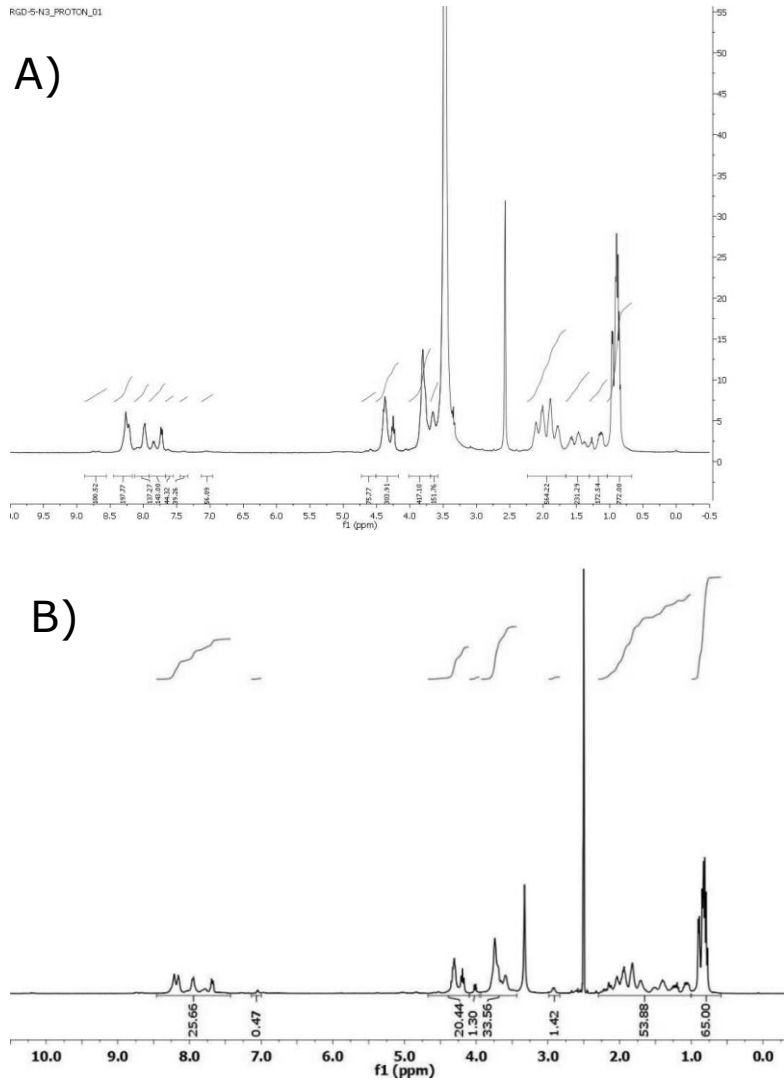

Fig. 6 *^{1}H-NMR (DMSO-d6) spectrum for A) RGD-N3, B) VKVx24-cyclooctine.*

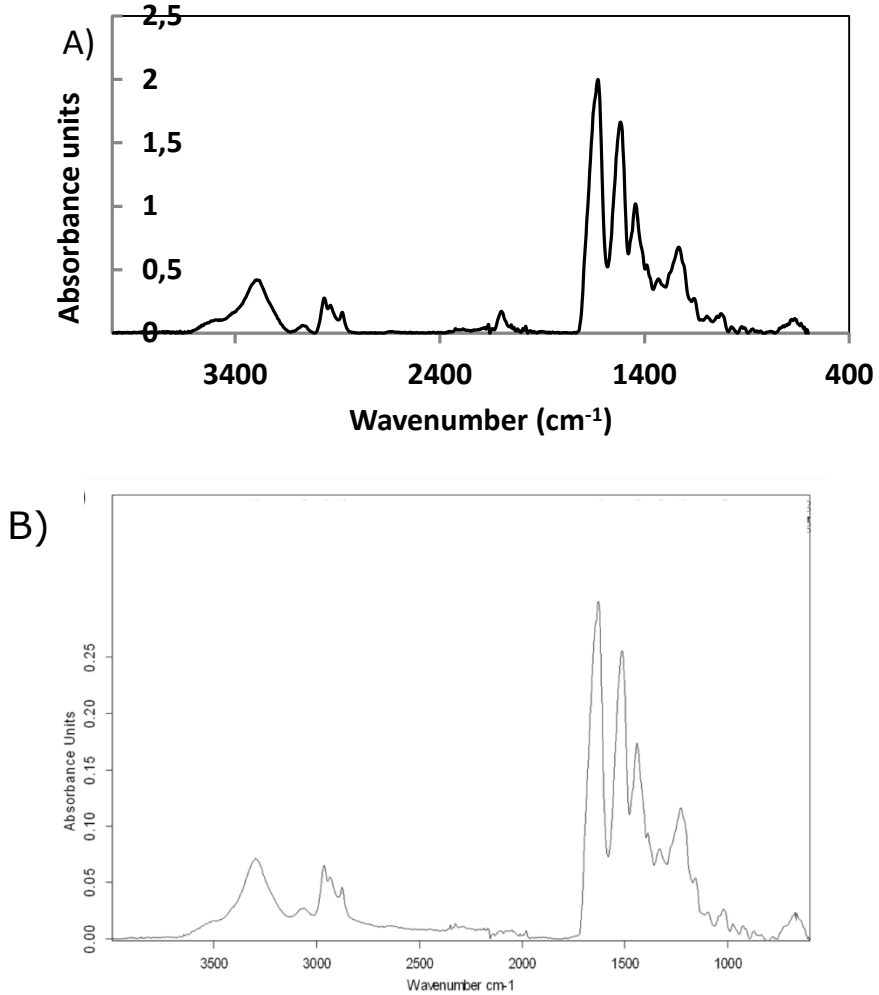

Fig. 7 *FTIR spectrum for A) RGD-N3, B) VKVx24-cyclooctine.*

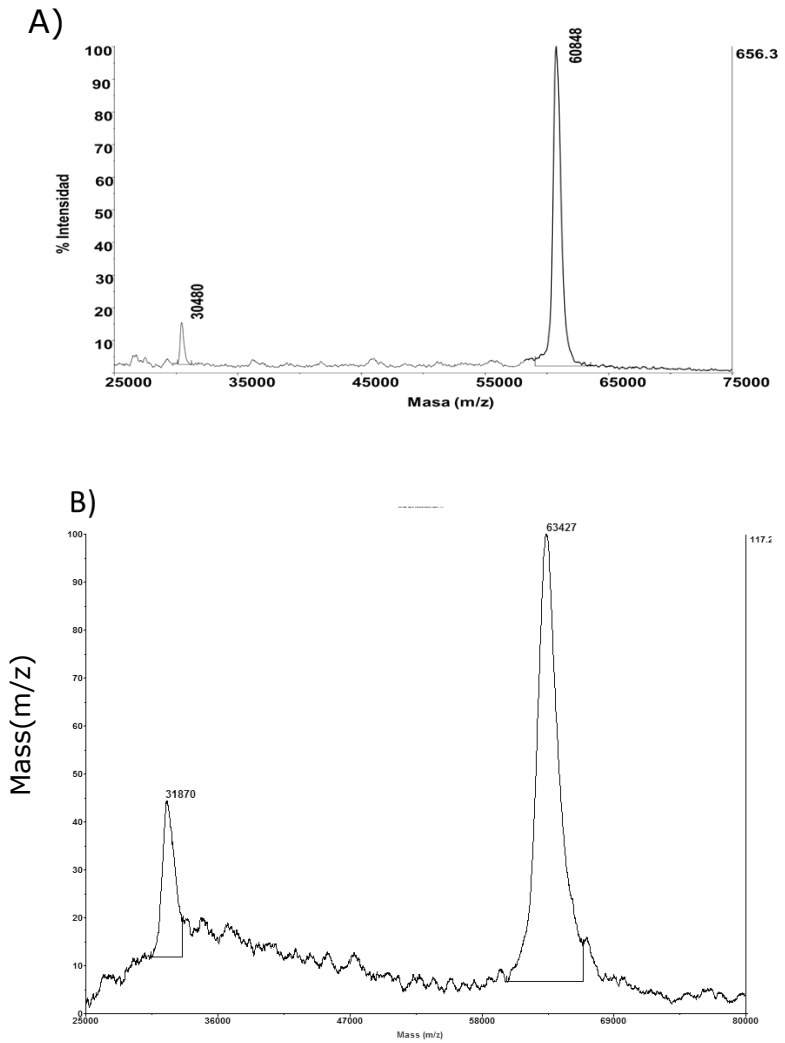

Fig. 8 *MALDI-TOF for A) RGD-N3, B) VKVx24-cyclooctine.*

A)

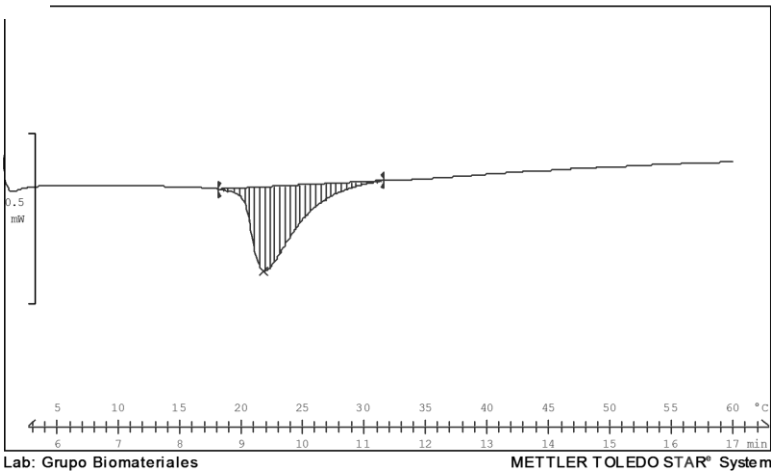

B)

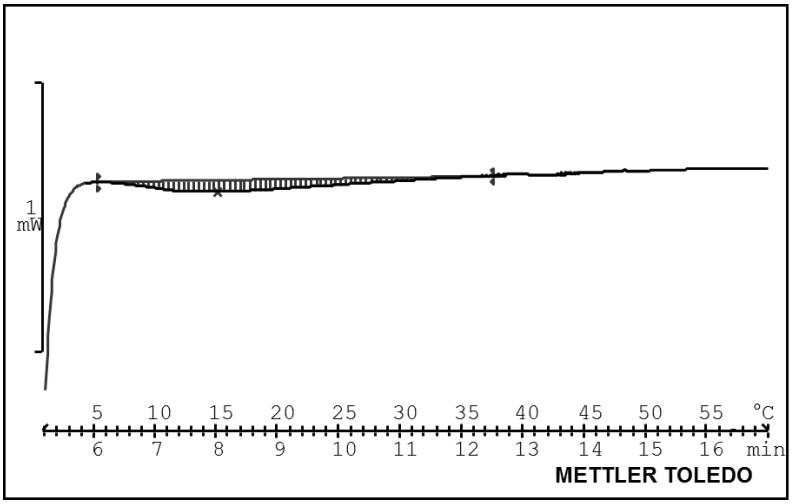

Fig. 9 *DSC thermograms for A) RGD-N3 (Tt = 21.8ºC), B) VKVx24-cyclooctine (Tt = 15.2°C). Same pH≈7 has been used.*

8.3.3. c. Characterization of ELR-CFCGs

8.3.3.1. FTIR results

Dried ELR-CFCGs were analyzed by FTIR. From the IR spectra of the formed hydrogels (Fig. 5), the peak intensity of azide pendant groups decreased dramatically, indicating that only very few azide pendant groups existed after the click coupling reaction and that azides were quantitatively transformed into triazoles by reacting with cyclooctine. In addition, it was reported2-4 that very few residual azide pendant groups would not affect biomedical applications.

[2] Crescenzi, V.; Cornelio, L.; Di Meo, C.; Nardecchia, S.; Lamanna, R. Biomacromolecules 2007, 8, 1844–1850.

[3] Wang, Q.; Chan, T. R.; Hilgraf, R.; Fokin, V. V.; Sharpless, K. B.; Finn, M. G. J Am Chem Soc 2003, 125, 3192–3193.

[4] Link, A. J.; Tirrell, D. A. J Am Chem Soc 2003, 125, 11164–11165.

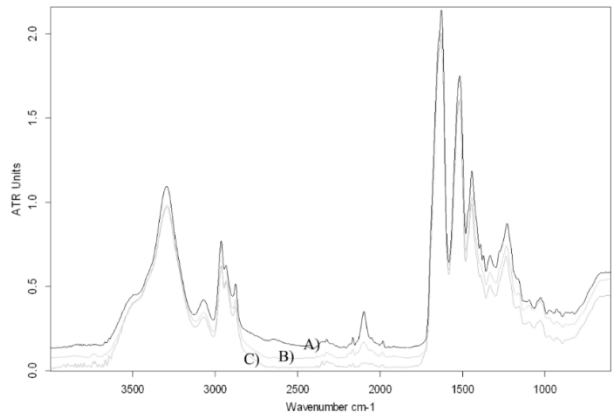

Fig. 10 *IR spectrum for A) HRGD6-N3 (reference), B) ELRs-CFCG 50 mg/mL, and C) ELRs-CFCG 150 mg/mL.*

8.3.3.2. DSC results

An endotherm peak associated to the phase transition of the recombinamer is observed for the ELR-CFCGs (Fig. 6), and then, the gel retains the thermo-responsiveness characteristics of the ELRs. This transition is characterized by the peak temperature, T_t, and the enthalpy involved in the phase transition: 26.5 – 27.5 °C and 8-10 J/gr, respectively. A similar result has been already reported in the bibliography for a ELR chemical hydrogel containing REDV[29]. The dense hydrogel cross-linked network leads to a decrease in chain mobility and partial loss of the conformational freedom, hindering the chain folding that takes place as the ELR is heated above its T_t. This hindered chain mobility causes also a noticeable broadening in the endotherm peak.

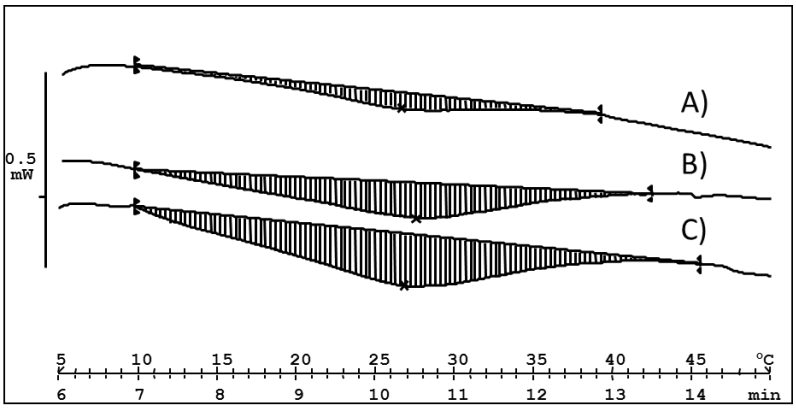

Fig. 11 *DSC thermograms of ELR-CFCGs for several recombinamer concentrations: A) 50 mg/mL, B) 100 mg/mL, and C) 150 mg/mL.*

5 Laura Martín, Matilde Alonso, Alessandra Girotti, F. Javier Arias and J. Carlos Rodríguez-Cabello."Synthesis and Characterization of Macroporous Thermosensitive Hydrogels from Recombinant Elastin-Like Polymers", Biomacromolecules, 2009, 10 (11), 3015–3022.

8.3.3.3. Rheological results

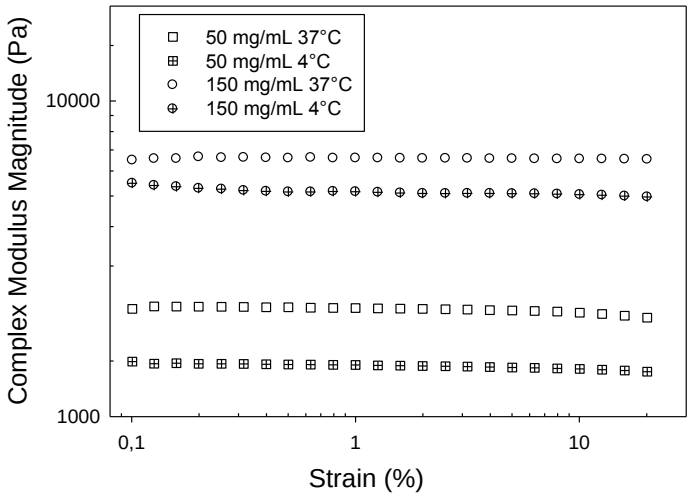

Fig. 12. *Complex module magnitude at a frequency of 1 Hz as a function of the strain amplitude at 4°C and 37°C for ELR-CFCGs with recombinamer concentrations of 50 mg/mL and 150 mg/mL.*

CHAPTER 5:

NANOGEL FORMATION FROM DILUTE SOLUTIONS OF CLICKABLE ELASTIN-LIKE RECOMBINAMERS AND ITS DEPENDENCE ON TEMPERATURE: TWO FRACTAL GELATION MODES.

Israel González de Torre[1]*, Luis Quintanilla[1], Guillermo Pinedo-Martín[1], Matilde Alonso[1], José Carlos Rodríguez-Cabello[1].

1 BIOFORGE, CIBER-BBN, Campus "Miguel Delibes" Centro I+D, Universidad de Valladolid, Paseo Belén 11, 47011, Valladolid, Spain.

González de Torre, I.; Quintanilla, L.; Pinedo-Martín, G.; Alonso, M.; Rodríguez-Cabello, J. C. Nanogel Formation from Dilute Solutions of Clickable Elastin-like Recombinamers and its Dependence on Temperature: Two Fractal Gelation Modes. ACS Applied Materials & Interfaces 2014, 6 (16), 14509-14515.
DOI: 10.1021/am503651y

ABSTRACT:

Diluted, complementary, click-reactive elastin-like recombinamer (ELR) solutions have been prepared and mixed at two different temperatures, one below and one above the characteristic transition temperature (T_t) of these chemically modified ELRs. FTIR measurements, size, aspect ratio, zeta potential and microrheological measurements have been carried out on the nanostructures formed under these dilute conditions as a way to better understand the relationship between the final macroscopic properties of ELR-based hydrogels and the molecular conditions governing the initial stages of the chemical crosslinking process that occurs, especially its dependence on the preparation temperature relative to T_t. As a result, two different fractal modes of gel formation have been found at the two temperatures studied (above and below T_t). Thus, when the reaction mixture is prepared below T_t, essentially one-dimensional linear nanogels with a high aspect ratio are obtained. In contrast, 3D nanogels are formed above T_t, with spherical shapes predominating. These different structures seem to reflect the two molecular organizations of the single components of the mixture under these conditions, namely extended chains below T_t and a spherical arrangement above T_t. In addition to the interest in these nanogels as models for understanding the formation of microscopic structures and differential macroscopic properties under more conventional hydrogel-formation conditions, these nanogels are of interest due to their thermoresponsiveness and biocompatibility, which provide them with potential uses for drug delivery and other biomedical applications in living systems.

1. INTRODUCTION

New materials, many of which are intended for use as gels, especially in the bioscience fields, are continuously coming to the fore.

Elastin-like recombinamers (ELRs) are proteinaceous biomaterials based on the repetition of certain sequences from natural elastin[1,2]. These compounds are designed and produced by recombinant DNA technology, thus allowing complete control of their structure and amino acid sequence. ELRs can include different bioactive sequences[3], such as those governing protease sensitivity or cell adhesion, etc. These ELRs exhibit cell friendly behavior, tunable mechanical properties, thermal sensitivity and an ability to self-assemble[3,4]. All these properties are interesting for the most cutting-edge applications in the fields of nanotechnology and biomedicine. Their thermal sensitivity is characterized by a critical temperature in aqueous solution, known as the transition temperature (T_t), which is associated with a conformational reorganization at the molecular level. Thus, whereas the polymer chains are soluble in water below T_t, they self-assemble into nano- and microaggregates above this temperature, becoming insoluble. This process is completely reversible.

We have recently, designed, synthesized, and bioproduced elastin-like recombinamer catalyst-free click gels (ELR-CFCGs), the characterization of which has been reported in detail elsewhere[5]. The temperature dependence of these gels exhibits two different mechanical behaviors, thereby mimicking the thermosensitive behavior of the single ELRs that form the hydrogel. This dual behavior suggested to us the presence of two different processes

during gel formation depending on whether hydrogel formation was carried out above or below the T_t of each component. In particular, RGD-azide and VKVx24-cyclooctyne (T_t of 21 and 15°C, respectively[5]) have been used in this work.

Although hydrogels have been widely studied in the literature, our understanding of the early stages of gel formation requires further studies in order to gain a better insight into the relationship between the final properties of the hydrogel and the conditions present during the early stages of the cross-linking reaction, when the initial gel seeds start to appear. These initial stages are equivalent to the conditions existing under dilute conditions where, because of the low quantity of reagent mass, the hydrogels formed are unable to grow above the nano-aggregate level and are therefore models for the initial emerging structures found under more conventional conditions. In addition, these entities are interesting in and of themselves. Some recent studies have been devoted to the topic of nano- and microgels[6-8].

Microrheology involves the use of several techniques to study the rheological properties of solutions, nanoparticles and, in general, soft materials by studying the motion of colloidal probes dispersed within the samples[9-12]. Several experimental methods for measuring the dynamics of those probes have been proposed in the literature[12]. However, whereas active microrheology involves external forces acting on the microparticles used as probes (tracers), passive microrheology make use of the thermal (Brownian) motion of these tracers. In addition to early microrheological measurements on cross-linked polymer systems[13-15], the microrheology of cross-linked polyacrylamide networks[16],

poly(vinyl alcohol) hydrogels[17], microtubule networks[18], and F-actin networks[19-21] has been reported in the literature.

In this work, the size and surface charge (zeta potential) of the nanogels emerging from dilute click-chemistry cross-linking ELR solutions have been correlated with the viscoelastic properties of these solutions obtained using passive microrheology.

2. MATERIAL AND METHODS

2.1. Sample preparation

Details regarding the compositions of the ELRs used in this work, as well as the chemical modifications used to obtain their clickable derivatives (ELR-Azide and ELR-cyclooctyne), can be found elsewhere[5]. The range of concentrations analyzed in this work was chosen to represent dilute solutions far from the sol-gel transition. As such, the samples are homogeneous and ergodic assumptions remain valid[16]. Three different concentrations (0.1, 0.5, and 1 mg/mL) of each modified ELR were prepared, filtered (using a 0.45 μm PVDF syringe filter) and kept overnight at 4°C. They were then mixed (at 4 or 37°C) to obtain the desired concentration of click solutions. These solutions were maintained at 4 or 37°C for 24 hours. A pH of 7.1 was achieved when both components were mixed at the appropriate concentrations in mQ water.

Samples for FTIR were prepared from 50 mL of a 1 mg/mL click solution. Nanogels were collected after centrifugation at 10000 r.p.m., they were frozen and lyophilized.

All measurements were carried out over at least three different samples, and results shown in graphs without standard deviation are representative values of at least three samples.

In order to verify the stability of the nanogels, measurements were carried out at 1, 3 and 5 days. Due to no noticeable differences were found along this period, experimental results correspond to measurements after five days.

Values in text are given as media and standard deviation.

2.2. Experimental techniques

2.2.1. FTIR

FTIR analysis was conducted with a Bruker FTIR spectrophotometer (Bruker, USA). For each spectrum, a 1024-scan interferogram was collected at single beam absorption mode with a 2 cm^{-1} resolution within the 4000-600 cm^{-1} region. For each sample several FTIR absorption spectra were collected. Five measurements were averaged to obtain the final FTIR absorption spectrum of the sample. Residual water vapor absorption was interactively subtracted from the sample spectra.

Spectral calculations were performed by the OPUS (version 4.2) software (MATTSON INSTRUMENT, INC.).

Dynamic light scattering, Zeta potential, and microrheology measurements were performed using a Zetasizer Nano ZSP (Malvern Instruments) equipped with a 10 mW He−Ne laser at a wavelength of 633 nm.

2.2.2. Dynamic Light Scattering.

For DLS measurements, samples were introduced into polystyrene cuvettes and stabilized for 5 min at the desired temperature of 4 or 37 °C.

The DLS autocorrelation functions were measured at 4 and 37°C for all three concentrations. The autocorrelation functions were used to obtain the size distribution and polydispersity index. DLS measurements were performed using a non-invasive back-scattering[22] configuration.

2.2.3. Z Potential.

The ζ potential of the solutions was monitored at 4 and 37°C. The ζ-potential values, which were determined using the Smolukowski equation relating ionic mobility to surface charge, were obtained as the average of 10 repeated measurements. ζ measurements were performed using phase analysis light scattering[23].

2.2.4. Cryo-Transmission Electron Microscopy (Cryo-TEM).

Cryo-TEM measurements were accomplished using a JEOL JEM-FS2200 electron microscope operating at an accelerating voltage of 200 kV. Stabilized click solutions at 4°C and 37°C for several concentrations were placed on a preheated plasma-treated carbon-coated copper grid, followed by cryovitrification of the sample using a Gatan Cryoplunge CP3. A zero-loss mode was used to improve image contrast.

2.2.5. Microrheology.

Passive microrheology was based on Dynamic Light Scattering with improved single scattering detection[22].

Prior to the microrheology measurements, a careful selection of the tracer has to be made[9,24]. Two different tracer particles for DLS-based microrheology were considered in this work: surface-sulfonated polystyrene spheres with a mean diameter of 1101 nm ± 23 nm, and surface-carboxylated melamine resin particles with a mean diameter of 1020 nm ± 40 nm.

Polystyrene tracer particles were purchased from Thermo Scientific (catalog number 4011A, nominal diameter 1.1 μm, density = 1.05 g/cm^3). Surface-carboxylated melamine resin particles were purchased from microParticles GmbH (catalog number MF-COOH-particles, nominal diameter 1.0 μm, density = 1.51 g/cm^3).

The tracer particles were added to the click solutions and allowed to fully disperse for at least 12 h prior to taking any measurement. The particle concentration for the microrheological measurements was selected to ensure that the light-scattering process was dominated by the particles, thus meaning that a single, narrow peak was observed in the light-scattering experiment. For each experiment, 10 μL of tracer was added to 500 μL of sample[25].

3. RESULTS AND DISCUSSION

3.1. FTIR measurements

Following the literature[5], an evaluation of the effectiveness of the click reaction was based on the evolution of the azide band (~ 2100 cm^{-1}). As can be seen in fig. 1C, this band only appears in a residual percentage in the IR spectrum of the nano gels, indicating a high yield for the cross-linking reaction.

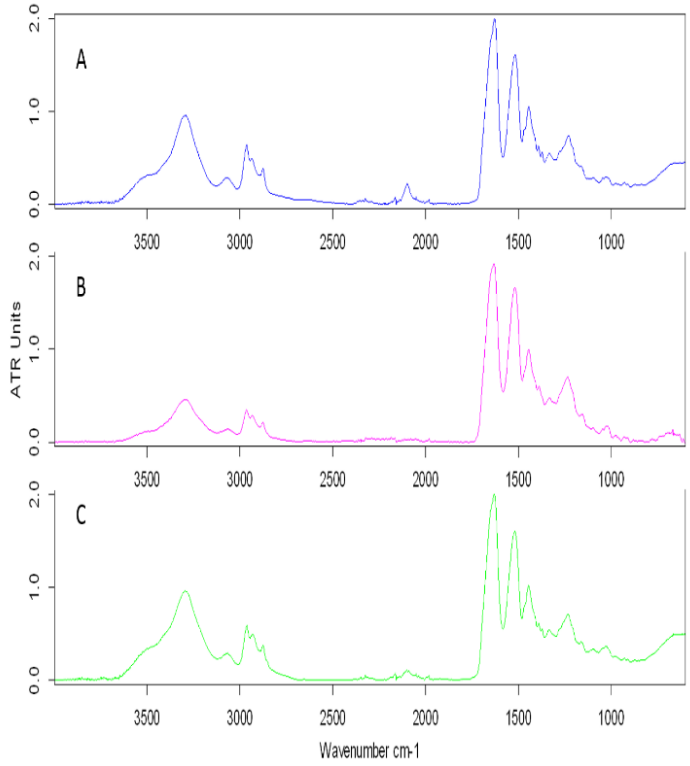

Fig. 1 *FTIR spectra for (A) RGD-azide, (B) VKVx24-cyclooctyne and (C) 1 mg/mL nanogel (1024 scans, 2 cm-1 resolution). Each curve is representative of five measured spectra.*

3.2. DLS and Zeta-potential measurements, and cryo-TEM micrographs

Size-distribution measurements for the nanogels present in our clickable solutions were performed by DLS below and above the T_t. Bimodal size distributions were found at both temperatures (Fig. 2), with a mean structure hydrodynamic diameter of 50 and 400 nm for the two lowest concentrations. These values are slightly higher (100 and 500 nm) for the 1 mg/mL solution at both temperatures. As can be seen from Fig. 2, at 4°C the majority of the nanogel population has a size distribution of less than 100 nm. This trend is opposite at 37°C. However, these hydrodynamic diameters must be taken with caution as the polydispersity value is high (0.325 and 0.300 at 4 and 37°C, respectively) and DLS is less accurate under these conditions.

As control, the same size measurements for each unmodified (RGD and VKVx24) and modified ELR (RGD-azide and VKVx24-cyclooctyne) solutions (1 mg/mL) were carried out at both temperatures. At 4°C no stable structures were found (PDI close to 1) for both kind of ELRs (unmodified and modified). At 37°C, a single size distribution of 160±18 nm (PDI~0.3) was found for both unmodified ELRs. In the case of modified ELRs, again a single size distribution of 228±20 nm (PDI= 0.17) and 298±30.6 nm (PDI=0.14) was obtained for RGD-azide and VKVx24-cyclooctyne, respectively. Unmodified ELRs solutions were mixed at both temperatures. While at 4°C a PDI=1 was found, at 37°C a single size distribution of 127.5±7.4 nm (PDI=0.24) was obtained.

At 4°C, the structures found in the nanogels were completely new with respect to the unmodified and modified ELR control solutions. At 37°C, the dominant structure (around 500 nm) can be

also related to a reaction between the azide and cyclooctyne groups due to the size of these structures are not present in the control solutions (prior or after their mixture).

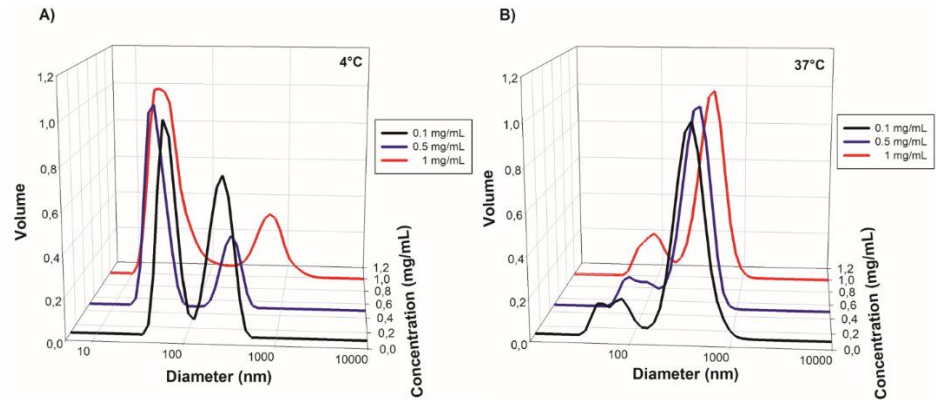

Fig. 2*. Normalized size distribution as a function of polymer concentration at 4 (A) and 37°C (B). The ratio of the volume to the peak volume of each measurement is used. Each curve corresponds to the average of three different samples measured.*

The size and shape of the nanogels were further evaluated by cryo-TEM. As can be seen in Fig. 3, the observed structures are completely different when obtained below (Fig. 3A) and above (Fig. 3B) their T_t. Thus, whereas the structures adopt an anisotropic geometry with a quasi-linear shape at 4°C, these structures adopt a spherical shape at 37°C. As can be seen from Figure 3, the size of the observed structures is in good agreement with the size distribution obtained by DLS.

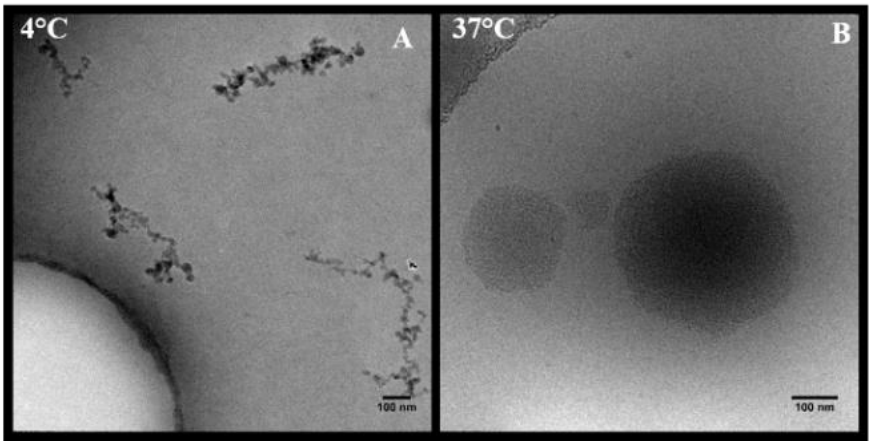

***Fig. 3**. Cryo-TEM micrographs of click nano-gels at 4 (A) and 37°C (B).*

Zeta-potential measurements (Fig. 4) also revealed two different trends in the distribution of the effective surface charge. The charge in these ELRs is mainly derived from the positively charged lysine side chains (epsilon amine group), which are not modified during cyclooctyne or azide addition. Thus, whereas a constant value of about +26 mV was found for all concentrations at 37°C, at 4°C this value decreased from +15 to +6 mV as a function of the concentration. According to the literature[26-29], these values suggest the presence of nano-gels with high and low stability at 37 and at 4°C, respectively.

As control, zeta potential measurement of unmodified ELR solutions (1 mg/mL) and their mixture were carried out at 4°C and 37°C. A value of about +15 mV was found for every solution at both temperatures. As for modified ELRs (RGD-azide, VKVx24-cyclooctyne), zeta potential values of +1.81±0.6 mV and -15.5±0.6 mV were obtained at 4°C, respectively. At 37°C 24.7±0.6 mV and -37.1±0.7 mV were obtained, respectively.

These value are different from the obtained zeta potential values found for the nanogels at the same concentration.

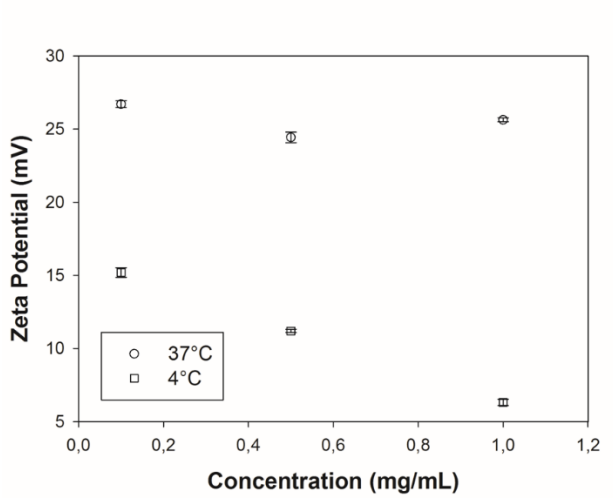

***Fig. 4**. Zeta potential (ζ) for the nanogels as a function of recombinamer concentration.*

To evaluate the potential reversibility of the nanogels as a function of temperature size and zeta potential measurements were carried out after 3 temperature cycles. As can be seen in fig. 5, size and zeta potential values are reversible for a specific nanogel (formed at 37°C (fig.5.A) or formed at 4°C (fig. 5 B)). But these values are completely different between nanogels formed at different temperatures. Cryo-TEM insert pictures show the effect of the temperature on the structure of each nanogel. Thus, the structure of a nanogel formed below its T_t cannot evolve to the structure of a nanogel formed above the T_t.

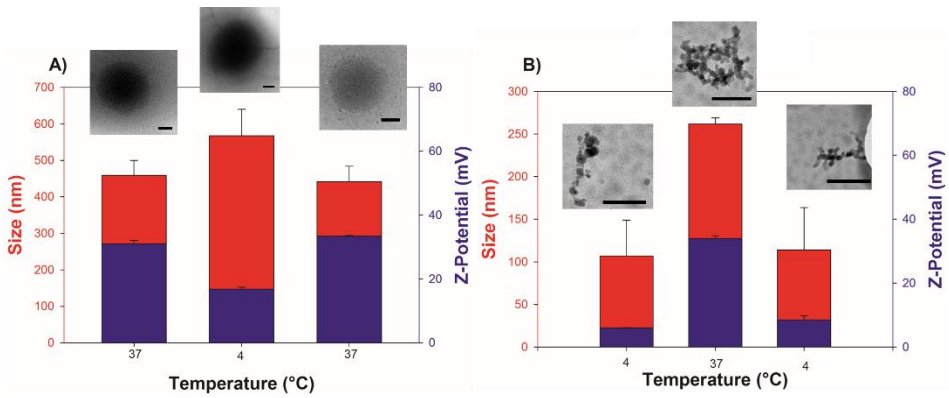

Fig. 5. *Effect of temperature on zeta potential (blue) and size (red) for nanogels formed at 37°C (A) and 4 °C (B). Cryo TEM insert has been included to show the nanogel structure at each temperature. Scale bars: 100 nm*

3.3. Microrheology measurements

To test the bulk response of the click-reactive ELR solution, the assumption of continuum viscoelasticity must be satisfied. As a result, the probe size has to be larger than the relevant length scale of the nanogels. Moreover, a minimization of tracer-matrix interactions, the extent of which is estimated by zeta potential measurements, is required.

In order to select the best candidate as a tracer for this system, tracer particles of two different compositions, namely polystyrene and melamine, were tested by adding them to the click-reactive ELR solution. This selection was made on the basis of the degree of interaction between the ELR gels and the tracer. The tracers were added to the same concentration as the ELR concentration and the zeta potential was then measured at 37°C for the solutions with tracer. Polystyrene particles gave rise to a 30-35% change compared to the previous zeta potential for the click-reactive ELR solution obtained without tracer, whereas only a 5-7%

change was found for melamine particles. These findings are in agreement with literature data for similar systems[19,25]. As a result, melamine resin particles were used for the microrheological measurements in this work.

In a microrheological experiment, the mean square displacement (MSD) provides a quantitative insight into the thermal motion of tracer particles. This MSD is obtained from the autocorrelation function when DLS is used to follow the tracer.

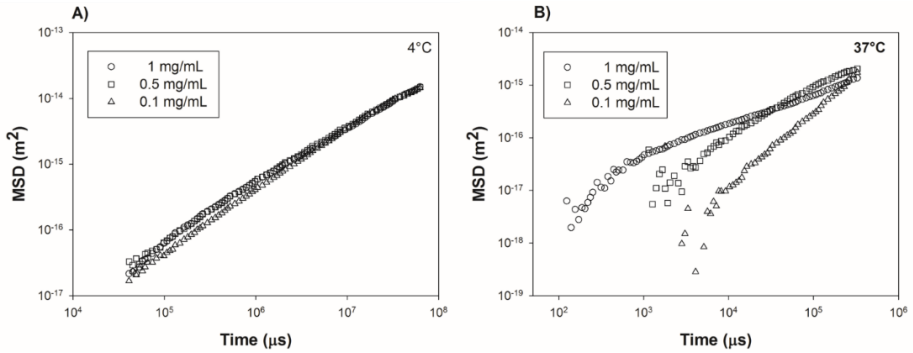

Fig. 6. *Mean square displacement (MSD) of the tracer particles for several recombinamer concentrations at 4 (A) and 37°C (B). Each curve corresponds to the average of three different measurements.*

In Fig. 6, the MSD for the three concentrations considered has been plotted as a function of time at 4 and 37°C. As can be seen from this figure, a linear response was found at both temperatures on a log-log scale. Relatively similar slopes (close to 1) are observed for the three recombinamer concentrations studied at 4°C, thus indicating a purely diffusive motion for the tracer. However, at 37°C the slope decreases as the concentration increases. According to the literature, this corresponds to a subdiffusive behavior[25]. The motion of the tracer particles is hampered by the slight increase in the size of the nanogels at 1 mg/mL and, as a result, the MSD slope decreases, thus reflecting an increase in the magnitude of their complex modulus[30].

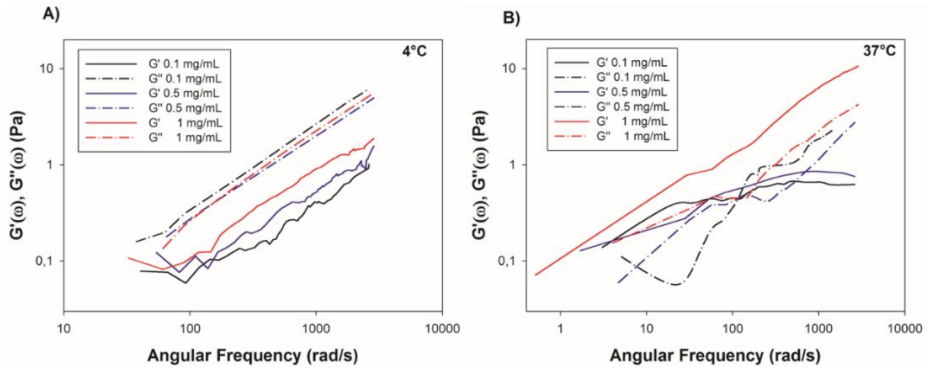

***Fig. 7**. Storage (G´) and loss (G´´) moduli as a function of angular frequency at 4 (A) and 37°C (B) for the studied concentrations (0.1, 0.5 and 1 mg/mL). Each curve corresponds to the average of three different samples.*

Using the generalized Stokes-Einstein relationship[9,24], the viscoelastic moduli were calculated using the method described by Mason[24]. The dependence of the storage (G´) and loss (G´´) moduli on angular frequency has been plotted in Fig. 7. G´ and G´´ were frequency-dependent in the range considered at both temperatures. At 4°C, G´´ is higher than G´, thus indicating that the sample is a viscoelastic fluid over the entire range of frequencies considered. No significant changes were found for G´´ with recombinamer concentration, although G´ increased slightly with concentration at frequencies higher than 200 rad/s. At 37°C, similar G´ values were obtained for the concentrations of 0.1 and 0.5 mg/mL, and a plateau seems to be reached at around 1000 rad/s. Furthermore, for each concentration, G´ dominates over G´´ up to a frequency of around 100 and 900 rad/s, respectively, at which point a crossover occurs. In contrast, G´ clearly dominates over G´´ for a concentration of 1 mg/mL, and no crossover is found in the frequency range analyzed. G´ is higher for this latter concentration than for lower concentrations, and no plateau is observed.

A schematic representation of the proposed mechanism governing the formation and thermal behavior of these nanogels is summarized in Fig. 8. ELRs show a lower critical solution temperature (LCST) behavior in which the ELR molecule is water soluble below T_t, with hydrophobic hydration being the characteristic and predominant hydration mode. The clathrate-like structure of water molecules surrounding the apolar ELR moieties, which is characteristic of hydrophobic hydration, gives rise to a relatively extended chain with no conformational order[31]. The ELR chains do not assemble under these conditions and remain extended in solution, in this particular case with positively charged lysine residues distributed homogeneously along the backbone. In contrast, this hydrophobic hydration no longer exists at 37°C, above their T_t, and the ELR chains undergo a self-aggregation process dominated by an extensive number of hydrophobic associations and segregation of those aggregated domains from solution. For the particular amphiphilic compositions of the ELRs employed herein, in which apolar domains coexist with polar ones, the resulting molecular arrangement is spherical, with the apolar domains forming a core in an attempt to hide from the aqueous environment, with the polar domains (charged lysines) exposed in the shell.

As the LCST behavior of ELRs is an intrinsic property, the tendency shown by the isolated chains prior to cross-linking must still be present and preserved in the cross-linked state. Below T_t, the cross-linked ELR chain tends to be hydrated and extended, whereas above T_t the cross-linked chain shows a folded globular state with extensive inter- and intrachain hydrophobic contacts. These two molecular arrangements appear to govern the way in which the newly formed gel structures grow. Thus, below T_t the

nanogels adopt a linear structure, which is coincident with the main structure at a molecular level and a certain degree of self-orientation driven by the formation of cross-linking reactions in these extended chains in a zipper-like manner, whereas at temperatures above T_t the newly formed gel nanoparticles show a spherical geometry following the globular organization at the molecular level. As such, the geometry observed at the nanometric level appears to be a fractal image of that observed at the molecular level.

The observed zeta potential values are also in agreement with this general description. Thus, below T_t the positively charged lysines are not segregated from the rest of the molecular domains but remain relatively evenly distributed, with no particular preference for being in the core or the shell of the newly formed nanogels. As such, the zeta potential is relatively low and decreases as the concentration increases due to the fact that the proportion of lysines exposed on the outer surface of the nanogels with respect to the total number of lysines within the nanogel decreases. In contrast, the nanogels obtained at a temperature above T_t are dominated by segregation of the apolar and polar domains. At the water-gel interphase, the latter would clearly tend to be exposed towards the water side, thus increasing the zeta potential and making it practically independent of the concentration.

The effect of the temperature changes on zeta potential and size of nanogels formed at 4 °C and 37°C can be seen in fig. 5. As can be deducted from these results, the structures formed at different temperatures (37°C and 4°C) cannot converted one into the other. But, for a given formation temperature each fractal can evolve reversibly to other structures. Nanogels formed at 37°C

exhibit a spherical shape, which evolves to a bigger sphere at 4°C due to the ELRs transition temperature. Covalent crosslinking bonds prevent from the spherical shape of the structure to be lost. And the original size is recovered when the temperature is increased to the initial temperature of 37°C.

At 4°C, nanogels show a linear structure that becomes globular at 37°C, where some aggregation of these new globular structures can be observed, recovering the linear structure when temperature decreases again to 4°C.

This differential behavior is also supported by the microrheology measurements. Below T_t, the complex viscoelastic modulus is dominated by the loss modulus (G''). As such, the mechanical properties of these nanogels are related to those of a viscoelastic fluid, a state which is compatible with the existence of a number of ELR chains that are fully hydrated and loose, with very few intermolecular interactions other than the crosslinks that give coherence to the nanogel. The mechanical properties would be affected by water diffusing in and out the hydrogel, which results in deformation and explains the high contribution of the loss modulus. However, above T_t, the chains experience a high number of intra- and intermolecular hydrophobic contacts, which result in consolidation of the solid continuous phase and the emergence of a more purely elastic behavior, where G' clearly dominates over G''.

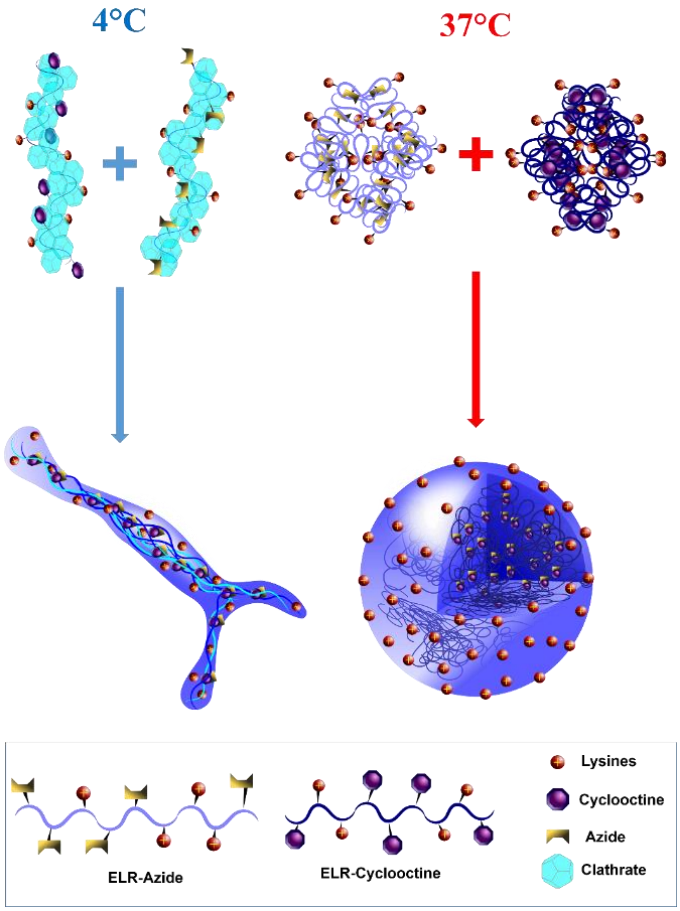

Fig. 8. *Schematic representation of the proposed mechanism governing click nanogel formation and the behavior above and below Tt.*

4. CONCLUSIONS

DLS, zeta potential, and microrheological measurements have been correlated in this work to gain an insight into the influence of temperature, and the concomitant changes in the aggregation state of ELRs around their T_t, on the microscopic structure and shape of nanogel. FTIR measurements were used to verify that the gel formation is based on a covalent crosslinking between azide and cyclooctyne groups.

Briefly, for the thermally sensitive ELRs studied herein, the reaction temperature dramatically affects the dimensionality of gel growth for these cross-linked hydrogels. Below T_t, gels grow in an essentially monodimensional mode and linear (fibrilar) structures with a high aspect ratio are the dominant geometric feature observed. However, above T_t, the crosslinking reaction is dominated by the previous self-organization of the ELR chains and their tendency to adopt globular structures. This circumstance seems to drive the newly formed nanogels to achieve a homogeneous, isotropic and three-dimensional hydrogel that is spherical in shape. As such, the observed nanometric shapes correspond to the fractal image of the arrangement of the ELR chains below and above T_t.

These results show, for the first time, that it is possible to easily obtain nanogels with strikingly different topographies. Such nanogels have potential uses in numerous different biomedical uses. Secondly, these results are also relevant as regards our understanding of the different macroscopic properties observed when preparing cross-linked ELR macrogels. According to the results presented here, the crosslinking temperature markedly affects the microstructure of the final hydrogels, with the ELR T_t being the characteristic temperature that determines one mode of gelation or another.

5. ACKNOWLEDGMENTS

We acknowledge financial support from the EU through the European regional development fund (ERDF) NMP3-LA-2011-263363, HEALTH-F4-2011-278557, PITN-GA-2012-317304), from the MINECO (MAT-2010-15982, MAT2010-15310, PRI-PIBAR-2011-1403 and MAT2012-38043-C02-01), the JCyL (projects VA152A12-2, VA244U13 and VA155A12-2), the CIBER-BBN, and the JCyL and the Instituto de Salud Carlos III under the "Network Center of Regenerative Medicine and Cellular Therapy

6. REFERENCES

(1) Urry, D. W.; Urry, K. D.; Szaflarski, W.; Nowicki, M., Elastic-Contractile Model Proteins: Physical Chemistry, Protein Function and Drug Design and Delivery. *Adv. Drug Delivery Rev.* **2010**, 62, 1404-1455.

(2) Karle, I. L.; Urry, D. W., Crystal Structure of Cyclic (APGVGV)2, an Analog Of Elastin, And A Suggested Mechanism For Elongation/Contraction Of The Molecule. *Biopolymers* **2005**, 77, 198-204.

(3) Rodríguez-Cabello, J. C.; Martín, L.; Alonso, M.; Arias, F. J.; Testera, A. M., "Recombinamers" as Advanced Materials for the Post-Oil Age. *Polymer* **2009**, 50, 5159-5169.

(4) Wright, E. R.; Conticello, V. P., Self-Assembly of Block Copolymers Derived from Elastin-Mimetic Polypeptide Sequences. *Adv. Drug Delivery Rev* **2002**, 54, 1057-1073.

(5) González de Torre, I.; Santos, M.; Quintanilla, L.; Testera, A.; Alonso, M.; Rodríguez Cabello, J. C., Elastin-Like Recombinamer Catalyst-Free Click Gels: Characterization of Poroelastic and Intrinsic Viscoelastic Properties. *Acta Biomater* **2014**, 10, 2495-2505.

(6) Jiang, Y.; Chen, J.; Deng, C.; Suuronen, E.; Zhong, Z., Click Hydrogels, Microgels and Nanogels: Emerging Platforms for Drug Delivery and Tissue Engineering. *Biomaterials* **2014**, 35, 4969-4985.

(7) Steinhilber, D.; Witting, M.; Zhang, X.; Staegemann, M.; Paulus, F.; Friess, W.; Küchler, S.; Haag, R., Surfactant Free Preparation of Biodegradable Dendritic Polyglycerol Nanogels by Inverse Nanoprecipitation for Encapsulation and Release of Pharmaceutical Biomacromolecules. . *J. Controlled Release*. **2013**, 169, 289-295.

(8) Dmitri, O.; Sujit, K.; Zheyi, Y.; Xia, Y.; Jöns, H., Orthogonal Chemoselective Assembly of Hyaluronic Acid Networks and Nanogels for Drug Delivery. *Macromolecules* **2013**, 46.

(9) Mason, T. G.; Weitz, D. A., Optical Measurements of Frequency-Dependent Linear Viscoelastic Moduli of Complex Fluids. *Phys. Rev. Lett.* **1995**, 74, 1250-1253.

(10) Cicuta, P.; Donald, A. M., Microrheology: A Review of the Method and Applications. *Soft Matter* **2007**, 3, 1449-1455.

(11) Breedveld, V.; Pine, D. J., Microrheology as a Tool for High-Throughput Screening. *J. Mater. Sci.* **2003**, 38, 4461-4470.

(12) Squires, T.; Mason, T., Fluid Mechanics of Microrheology. *Annu. Rev. Fluid Mech*. **2009**. 640, 343.

(13) Schnurr, B.; Gittes, F.; MacKintosh, F. C.; Schmidt, C. F., Determining Microscopic Viscoelasticity in Flexible and Semiflexible Polymer Networks from Thermal Fluctuations. Macromolecules **1997**, 30, 7781-7792.

(14) Narita, T.; Knaebel, A.; Munch, J.-P.; Candau, S. J., Microrheology of Poly(vinyl alcohol) Aqueous Solutions and Chemically Cross-Linked Gels. Macromolecules **2001**, 34, 8224-8231.

(15) Nisato, G.; Hébraud, P.; Munch, J. P.; Candau, S. J., Diffusing-wave-spectroscopy Investigation of Latex Particle Motion in Polymer Gels. *J. Physical Review* E **2000**, 61, 2879-2887.

(16) Dasgupta, B.; Weitz, D., Microrheology of Cross-Linked Polyacrylamide Networks. *Phys. Rev. E: Stat., Nonlinear, Soft Matter Phys*.**2005**, 71, 21504.

(17) Narita, T.; Mayumi, K.; Ducouret, G.; Hébraud, P., Viscoelastic Properties of Poly(vinyl alcohol) Hydrogels Having Permanent and Transient Cross-Links Studied by Microrheology, Classical Rheometry, and Dynamic Light Scattering. *Macromolecules* **2013**, 46, 4174-4183.

(18) Yang, Y.; Bai, M.; Klug, W. S.; Levine, A. J.; Valentine, M. T., Microrheology of Highly Crosslinked Microtubule Networks is Dominated by Force-Induced Crosslinker Unbinding. *Soft Matter* **2013**, 9, 383-393.

(19) McGrath, J.; Hartwig, J.; Kuo, S., The Mechanics of F-Actin Microenvironments Depend on the Chemistry of Probing Surfaces. *Biophys. J*. **2000**, 79, 3258-3266.

(20) Lee, H.; Ferrer, J.; Nakamura, F.; Lang, M.; Kamm, R., Passive and Active Microrheology for Cross-Linked F-Actin Networks in vitro. *Acta Biomater*. **2010**, 6, 1207-1218.

(21) Luan, Y.; Lieleg, O.; Wagner, B.; Bausch, A., Micro and Macrorheological Properties of Isotropically Cross-Linked Actin Networks. *Biophys. J*. **2008**. 15, 94, 688-93

(22) Peters, R., Fiber Optic Device for Detecting the Scattered Light or Fluorescent Light from a Suspension. Google Patents **2000**.

(23) John, F. M.; Klaus, S.; Brian, V., The Determination of Very Small Electrophoretic Mobilities in Polar and Nonpolar Colloidal Dispersions Using Phase Analysis Light Scattering. *J. Colloid Interface Sci*. **1991**, 143.

(24) Mason, T. G., Estimating the Viscoelastic Moduli of Complex Fluids Using the Generalized Stokes–Einstein Equation. *Rheol. Acta* **2000**, 39, 371-378.

(25) Amin, S.; Rega, C.; Jankevics, H., Detection of Viscoelasticity in Aggregating Dilute Protein Solutions through Dynamic Light Scattering-Based Optical Microrheology. *Rheol. Acta* **2012**, 51, 329-342.

(26) Freitas, C., Effect of Light and Temperature on Zeta Potential and Physical Stability in Solid Lipid Nanoparticle (SLN™) Dispersions. *Int. J. Pharm. (Amsterdam, Neth.)* **1998**. 168, 221-229

(27) Jiang, J.; Oberdörster, G.; Biswas, P., Characterization of Size, Surface Charge, and Agglomeration State of Nanoparticle Dispersions for Toxicological Studies. J. *Nanopart. Res.* **2009**, 11,77-89.

(28) Griffith, A.; Notley, S., ph Dependent Stability of Aqueous Suspensions of Graphene with Adsorbed Weakly Ionisable Cationic Polyelectrolyte. *J. Colloid Interface Sci.* **2012**, 369, 210-215.

(29) White, B.; Banerjee, S.; O'Brien, S.; Turro, N.; Herman, I., Zeta-Potential Measurements of Surfactant-Wrapped Individual Single-Walled Carbon Nanotubes. *J. Phys. Chem. C* **2007** 111, 13684-13690.

(30) Dasgupta, B. R.; Tee, S.-Y.; Crocker, J. C.; Frisken, B. J.; Weitz, D. A., Microrheology of Polyethylene Oxide Using Diffusing Wave Spectroscopy and Single Scattering. *Phys. Rev. E: Stat. Phys., Plasmas, Fluids, Relat. Interdiscip. Top*. **2002**, 65, 051505.

(31) Urry, D. W., *What Sustains Life? Consilient Mechanisms for Protein-Based Machines and Materials.* Springer-Verlag: New York, 2006.

CHAPTER 6:

SURFACE MODIFICATION BY A CATALYST FREE COVALENT LAYER BY LAYER APPROACH OF CLICKABLE ELASTIN-LIKE RECOMBINAMERS

I. González de Torre[1], L. Quintanilla[1], M. Alonso[1], J. Carlos Rodríguez-Cabello[1].

[1] BIOFORGE, CIBER-BBN, Campus "Miguel Delibes" Centro I+D, Universidad de Valladolid, Paseo Belén 11, 47011, Valladolid, Spain.

González de Torre, I.; Quintanilla, L.;; Alonso, M.; Rodríguez-Cabello, J. C. Surface modification by a catalyst free covalent layer by layer approach of clickable elastin-like recombinamers. Acta Biomaterialia. Under review.

ABSTRACT:

A layer-by-layer (LBL) technique involving clickable elastin-like recombinamers (ELRs) and without the need for any other molecules has been explored in this work as a means of biofunctionalizing different structures, ranging from simple, flat pieces to more complicated metallic grids comprising several different materials. Bioactive sequences, such as RGD or any other peptide domain that can be incorporated into the ELR backbone, can also be used in this approach.

The diffusion ability of the ELRs allows the experimental setup to be designed with both a washing and a non-washing step after the deposition of each component, thus allowing the washing step to be skipped without compromising interlayer integrity and a rapid increase in coating thickness up to the micrometre range. The resulting coatings have been characterized by contact angle measurements, FTIR, fluorescence, optical and scanning electron microscopy, XPS and AFM to evaluate the topographical features of the layers and their mechanical properties.

Several important advantages, such as layer formation in only a short time, mild, catalyst-free conditions, the possibility of incorporating drugs covalently bonded to the ELRs, and complete control over layer thickness, which means control over the resulting mechanical properties, are gained using this catalyst-free covalent LBL technique.

1. INTRODUCTION

Non-biological implants currently form the basis of prosthetic implants to treat numerous defects produced by diseases, ageing or trauma. The processes and interactions that occur between the surface of the implant and the biological system concerned are a key issue to be taken into account and, consequently, the response of the biological system to the artificial implant will determine the fate of that implant, in other words its acceptance or rejection. To improve the success ratio of implant integration, numerous surface-modification techniques have been proposed over the last few years. In particular, the layer-by-layer (LBL) technique introduced by Iler in 1966 [1] is an easy means of performing the consecutive self-assembly of layers of at least two different materials onto substrates [2, 3].

The essential concept of LBL is the sequential deposition of two complementary polymers that exhibit a mutual interaction. Multipoint interactions must exist between the constituents of the coatings to enable their sequential adsorption. In addition to electrostatic contacts, other driving forces for LBL assembly include hydrophobicity, van der Waals forces, hydrogen bonding, and covalent bonding [4-10]. Indeed, use of these conventional LBL approaches has led to the development of various noteworthy applications, the most important of which is possibly the modification of biomedical surfaces in order to improve their interaction with biological tissues or fluids or to improve or prevent cell adherence [11-13]. Other uses include the construction of biosensors that are able to produce a measurable response to variations in their environment (pH, temperature or presence of specific biomolecules) [14-17] or the creation of micro-reactors in

which specific chemical reactions can take place in isolation from the surrounding environment and recreating the optimal conditions needed for those reactions [18].

In general, the type of molecular interactions that are currently used in LBL structures strongly limits the type of macromolecules that can be employed, thereby also limiting the spectrum of potential applications that can be obtained using this technique. As a result, it is surprising that covalent bonding has received relatively little attention as the main interaction between the complementary components, especially given the fact that covalent bond formation is the strongest inter-layer interaction that can be employed and that covalent bonding can also be based on complementary pairs of reactive species. The reason for this lack of covalent bonding-based approaches is likely to be due to some obvious disadvantages exhibited by the resulting LBL constructs in comparison with other, more common LBL options. These include the longer times needed to form each layer, as a result of the longer reaction times required, and the relatively harsh conditions that must be employed. For this reason, the use of a fast, orthogonal and mild reaction for LBL construction would represent an important breakthrough in this field.

One of the most successful reactions between complementary reactive species that fulfils the above-mentioned requirements, especially in the biomedical field, is "click chemistry", which is based on the well-known Huisgen 1,3-dipolar cycloaddition of azides and alkynes [19]. In addition, this reaction is stereospecific, easy to perform in aqueous solution under mild conditions, and provides high reaction yields. The use of azides and cyclooctynes, which can be considered to be activated alkynes, is

supported by their stability within biological systems and the absence of side products. This reaction has been widely employed in cell-surface labelling [20], for surface modifications [10], including modifications with ELRs [21], proteins [22], peptides [9] and DNA [23], and in drug discovery [24], amongst many others. Traditionally, these reactions have been carried out in the presence of a metal ion as catalyst [25]. However, herein we use a catalyst-free click reaction with ELRs that has previously been described in the literature [26]. Based on this previous experience with the use of click chemistry, herein we will explore its suitability for an LBL approach and test this possibility with a relatively new family of polymers, namely elastin-like recombinamers (ELRs). ELRs are the recombinant version of a type of protein polypeptide based on the repetition of certain sequences from natural elastin, specifically the pentamer (VPGXG), where X can be any amino acid except proline. This sequence endows the protein with elastic properties [27] along with many other of the most striking properties of the natural polypeptide, such as high biocompatibility and LCST behaviour [28, 29]. Moreover, as ELRs are produced using recombinant techniques, this allows complete control over the amino-acid sequence, thereby allowing the polypeptide chain to be tailored at the gene level. Numerous relatively complex and multifunctional materials can be obtained using this technique. As an example, ELRs exhibiting functionalities such as specific (REDV) [30] or general (RGD) [31] cell adhesion, protease sensitivity (VGVAPG) [30] or mineralization capacity (DDDEEKFLRRIGRFG) [32] have been described. Specific functionalities can be included in the backbone of ELRs. In this work, primary amines have been incorporated into the two ELRs employed. This amine functionality comes from the inclusion of lysine residues distributed

homogeneously throughout the amino-acid sequence of the recombinamers. These lysine residues can subsequently be modified to bear the reactive groups required to perform a catalyst-free click reaction, as described by Gonzalez de Torre et al. [26].

As such, this work aims to demonstrate the suitability of an LBL approach based on complementary clickable ELRs in order to explore the possibility of developing a more versatile and robust surface-modification technique than that used in current LBL approaches. This approach will be tested using model surfaces of different natures, including polystyrene, titanium and glass. Finally, this technique will also be tested on a model device, namely a 3D metallic mesh.

2. MATERIALS AND METHODS

All solvents and chemicals were of analytical grade. EterneonTM-Azide (480 / 635) and Acetylene Fluor 488 were obtained from Jena Bioscience, whereas cyclooctyne was obtained from SynAffix. B.V. (Heyendaalseweg 1356525 AJ Nijmegen. The Netherlands) and copper(II) sulfate pentahydrate (CuSO4•5H2O) was purchased from Fluka. All other reagents were obtained from Sigma-Aldrich.

2.1.Modified ELRs

The ELRs used (HRGD6 and VKVx24) and their click modifications have been previously described elsewhere [26]. The addition of fluorescence probes to modified ELRs was carried out as follows:

2.1.1 VKVx24-Eterneon

A solution of EterneonTM-Azide (480 / 635) (1 mg, 0.083 equiv.) in DMF (0.5 mL) was added to a solution of VKVx24-Cyclooctyne (100 mg, 1 equiv.) in DMF (5 mL) at room temperature (r.t.) under a nitrogen atmosphere. The resulting orange mixture was stirred at r.t. for three hours, after which time 17.5 mL of acetone was added to the crude reaction mixture to give an orange solid. This solid was centrifuged at 37 °C and washed with additional acetone (10 mL). This process was repeated three times. The excess organic solvent was then removed under reduced pressure to yield an orange solid, which was purified by dialysis with doubly distilled water (3x25 L) to yield 89 mg of an orange solid.

2.1.2 HRGD6-Acet-fluor

A solution of Acetylene Fluor 488 (2.5 mg, 0.083 equiv.) in DMF (0.5 mL) was added to a solution of HRGD6-N3 (100 mg, 1 equiv.) in DMF (4 mL) at r.t. to form a green-yellow solution. A solution of CuSO4 (2.7 mg, 0.011 mmol) and (+)-sodium L-ascorbate (5.70 mg, 0.029 mmol) in doubly distilled water (200 μL) was then added to give an intense pink mixture. The crude reaction mixture was stirred for two days at r.t., after which time 17.5 mL of diethyl ether was added to give a pink solid. This solid was centrifuged at 37 °C and washed with acetone (10 mL), repeating this process three times. The excess organic solvent was then removed under reduced pressure to yield a pink solid, which was purified by dialysis with doubly distilled water (3x25 L) to yield 82 mg of a pink solid.

2.2.Substrates

Polystyrene and titanium sheets were purchased from Aldrich, whereas glass surfaces were obtained from Thermo Scientific and Nitinol 3D metallic meshes (length: 1.5 cm) were kindly provided by Conic cardiovascular.

Substrates were cleaned using an argon plasma for 5 minutes (Harrick plasma cleaner). After this first step, the surfaces were activated using an oxygen plasma (30 minutes) to form a negative charge on the substrate surface. Thus, the negatively charged surfaces are ready to interact electrostatically with the positive residues from the modified ELRs.

2.3.Assembly of ELRs click multilayers

Each click layer is formed by two sub-layers, each of which corresponds to an ELR clickable solution. All the following steps were carried out at r.t. The first ELR sub-layer (VKVx24-eterneon), which bears positively charged lysines, interacts electrostatically with the negatively charged surface of the substrates, whereas the second ELR sub-layer (HRGD6-azide) reacts chemically with the first ELR sub-layer, in a catalyst-free click reaction, to form the first complete ELR click layer. Similarly, the second layer is initiated by the reaction of a new VKVx24-eterneon sub-layer with the HRGD6-azide sub-layer from the previous complete layer. This process can be repeated as often as needed. For this work we have tested one, two and five complete ELR click layers.

Two different approaches were used to construct those multilayers. The first of these consists of alternate successive 15 second immersions in each ELR click solution, with a drying time of 2 minutes between immersions and a five-minute washing step with

ultrapure water before each immersion. This washing step is skipped in the second approach with the expectation that the interphase between complementary layers, and therefore the thickness of each individual layer, will increases upon interpenetration of the sub-layers by diffusion, thereby shortening the whole process.

LBL coating of the 3D metallic mesh was carried out without washing steps by consecutive immersion in each ELR click solution, as previously described for polystyrene, glass and titanium surfaces.

2.4.Characterization techniques

2.1.3 FTIR

FTIR analysis was conducted using a Bruker FTIR spectrophotometer (Bruker, USA). For each spectrum, a 1024 scan interferogram was collected in single beam absorption mode with a 2 cm^{-1} resolution in the region 4000-600 cm^{-1}. Several FTIR absorption spectra were collected for each sample and five measurements were averaged to obtain the final FTIR absorption spectrum. Residual water vapor absorption was subtracted from the sample spectra interactively.

Spectral calculations were performed using the OPUS (version 4.2) software (MATTSON INSTRUMENT, INC.).

2.1.4 XPS

X-ray photoelectron spectroscopy surface analysis was used to monitor the modifications produced in the outermost (1–10 nm) layers of the surfaces. XPS experiments were carried out using a Physical Electronics (PHI) 5500 spectrometer equipped with a

monochromatic X-ray source (Al Ka line with an energy of 1486.6 eV and 350 W). The pressure inside the analysis chamber was 10-7 Pa. All measurements were performed at an angle of 45° with respect to both the X-ray source and analyzer. Survey scans were taken in the range 0–1100 eV and high resolution scans were obtained for the C1s, N1s, and O1s peaks. The elemental surface composition was estimated from the area of the different photoemission peaks taken from the survey scans modified by their corresponding sensitivity factors.

2.1.5 AFM

AFM measurements were performed using a Dimension 3100 microscope controlled by a Nanoscope IV controller system (Digital Instruments) in tapping mode using V-shaped Si3N4 tips (OMCL TR400PSA, Olympus, Japan). AFM images were taken from PBS immersed samples, with a nominal spring constant of 0.32 N/m. The scan area was 10 μm x 10 μm and the root-mean-square (RMS) roughness of the surfaces was evaluated for regions of 6 μm x 6 μm.

Surface roughness quantifies the vertical variations of a real surface from its ideal form. One of the most common parameters used to describe the degree of roughness of a surface is the root mean square (RMS) roughness, which is defined as (Equation 1):

$$Rq = \sqrt{\frac{1}{n}\left(\sum_{i=1}^{n} y_i^2\right)} \qquad \text{Equation 1}$$

where "n" corresponds to the total number of pixels in the image and "I" corresponds to the number of individual pixels. This parameter is especially useful when these variations in Z height are positive and negative from the ideal mean line. Five randomized

sections from three different surfaces were created for each image to determine the surface roughness of the polymeric surfaces.

2.1.6 Contact angle

Contact angle measurements were determined using a sessile drop method and a Data Physics OCA20 system instrument. The drop profile images during micro-syringe dispensation were recorded using an adapted CCD video camera. Contact angles were measured on both sides of the drop and the average values are reported. The stainless-steel needle tip was always kept at the top of the sessile drop and immersion of the needle into the drop was avoided during the measurements to prevent distortion of the drop shape by the needle. Nine measurements from three different locations on each sample were measured to ensure a representative value of the contact angle.

2.1.7 Optic and fluorescence microscopy

Optical and fluorescence microscopy were used to gain an initial insight into surface coverage by the ELR click layers. Images were acquired using a Nikon ECLIPSE 80i and a Nikon ECLIPSE Ti microscope as the merged image from the grey, green and red channels.

2.1.8 SEM

Scanning electron microscopy (SEM) was used to investigate the sample morphology. Micrographs were obtained by SEM (FEI Quanta 200 FEG) in low vacuum mode with no prior coating procedures or sample preparation. Morphological details (such as thickness of the LBL assembly obtained under different processing

conditions) were evaluated quantitatively using the ZEN (Blue Edition, 2012) software package (Carl Zeiss Microscopy).

2.1.9 Statistical analysis

Data are reported as mean ± SD (n = 3). Statistical analysis involved a one-way analysis of variance using the Holm-Sidak method. A p value lower than 0.05 was considered to be statistically significant. (**) $p < 0.001$, (*) $p < 0.05$, and $p > 0.05$ indicates no significant differences (n.s.d.).

3. RESULTS

The LBL coating was characterized by several techniques.

3.1.FTIR

The infrared spectra of bare polystyrene, glass and titanium surfaces (A-series, B-series and C-series, respectively), and their respective coatings with one, two or five non-washed and washed ELR click layers can be found in Figure 1. Each series shows the evolution of the spectral profile as the surface is covered by successive ELR click layers using the two coating approaches applied in this work.

It is easy to follow the coating process for each substrate from the FTIR spectra by the changes in its characteristic spectral bands when a new ELR click layer is added.

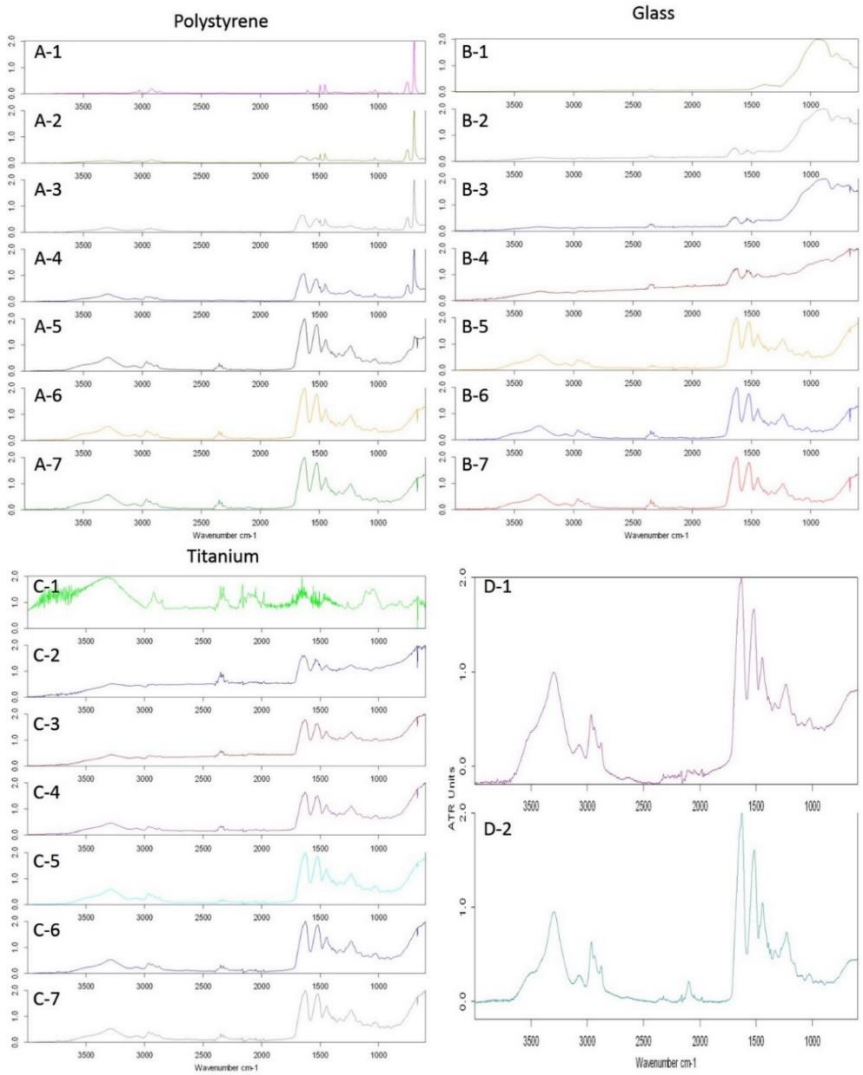

***Figure 1**. Infra-red spectra series for the three considered substrates: polystyrene, glass and titanium (A, B and C series, respectively). First spectra of each series corresponds to bare substrate. The second, third and fourth spectra of each series correspond to a single, double and five layers after the corresponding washing steps. Fifth, sixth and seventh spectra of each series represent one, two and five layer without any washing step. D-series shows the I.R. spectra of VKVx24-Eterneon and HRGD6-Acet-fluor (1 and 2, respectively) as control samples.*

As can be seen, after the first washed layer the spectral characteristics of each substrate are clearly recognizable together with the bands for each layer. As the thickness of the coating increases, these substrate signals are masked by the signals corresponding to every new ELR click layer, and after deposition of

the fifth layer they can barely be seen under the ELR coating spectrum. In the case of non-washed layers, the substrate bands disappear after deposition of the first layer, irrespective of the substrate, with the spectra for one, two and five non-washed layers being practically identical.

3.2.XPS characterization

The XPS diagrams show the evolution of the atomic percentage of the atoms in the outer layers of the surface as a function of each new ELR click layer (Figure 2). The orbitals used to calculate the concentrations were C1s, O1s, N1s, Si2p, S2p, Na1s, Al2p, Zn2p3/2, Cl2p, Ti2p, Ca2p, Fe2p, P2p and K2s.

As can be seen from the left row of Figure 2, a marked variation in the percentage of the more representative atoms in each substrate is found even for the first washed layer. For instance, for glass surfaces, the silicon percentage decreases drastically from 15% to 2%, whereas the proportion of carbon and nitrogen atoms, which are typical of ELRs, increases. A similar behaviour is observed for titanium substrates, in which the percentage of titanium decreases from uncoated surfaces to coated ones even after deposition of the first layer. High levels of carbon on glass and titanium samples is mainly due to extrinsic hydrocarbon deposition onto the sample surfaces since these samples were exposed to air prior to the XPS analysis[33]. For polystyrene substrates, the percentage of nitrogen increases from a value of around 2% for uncoated polystyrene to a value close to 20% after deposition of the first washed layer. Non-washed surfaces (right row in Figure 2) exhibited a similar behaviour. All these findings confirm the FTIR results as regards the change in

chemical composition of the surface of the substrates after each layer is deposited.

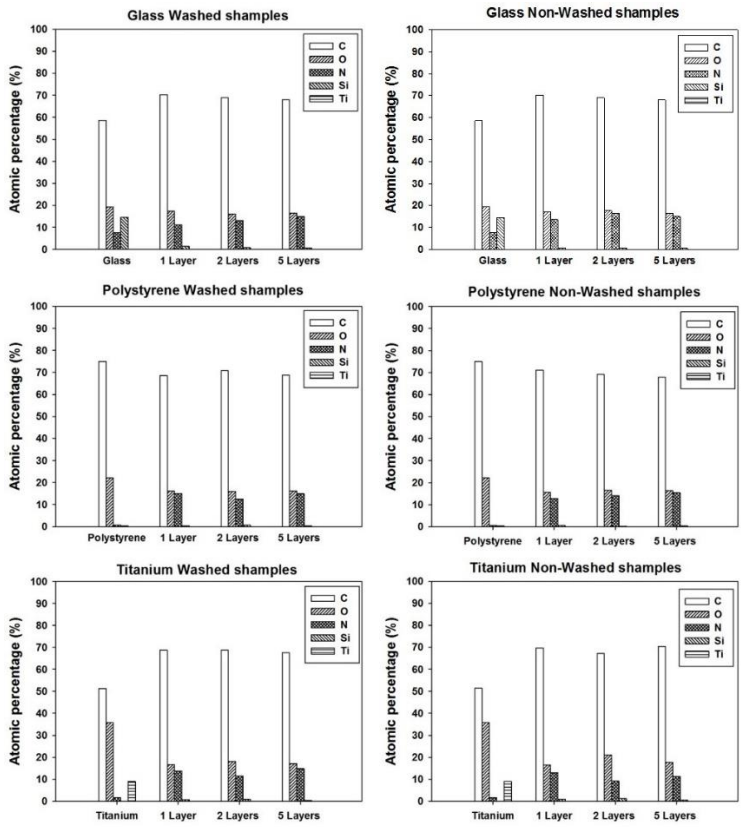

Figure 2. *Evolution of the atomic percentage on the outer surface as function of the number of layers for washed samples (left row) and non-washed samples (right row).*

3.3.Contact angle

The contact angle technique provides an estimation of the hydrophobicity of the surfaces and the changes as a consequence of the LBL process.

The dependence of contact angle on the number of layers has been plotted in Figure 3 for polystyrene, glass and titanium. The contact angle for coated samples can be seen to increase significantly with respect to the bare substrate, thus meaning that a higher hydrophobicity is found for each coated sample.

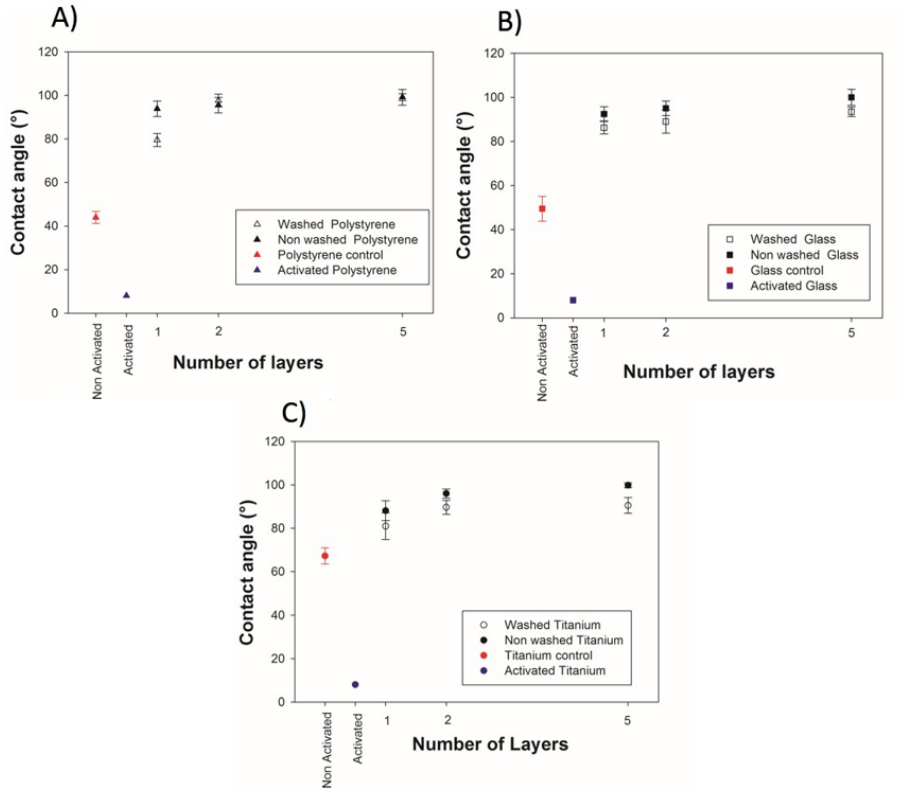

***Figure 3**. Dependence of the contact angle as function of the number of deposited layers for polystyrene (A), glass (B) and titanium (C). The contact angle for the control samples was measured in a non-activated sample since contact angles of activated control samples are small enough to be measured under our experimental conditions (contact angle < 8°).*

Non-activated polystyrene, glass and titanium substrates exhibited contact angles of 43°, 50° and 67° respectively. After the plasma cleaning process and surface activation, the contact angles for all materials were lower than 8° and could not be measured under our experimental conditions. The low values exhibited by the bare surfaces indicate their effective activation, which means they are very hydrophilic. After the LBL assembly process, these values increased to around 85°, 90° and 95° for one, two and five ELR click layers, respectively, after the washing steps, irrespective of the substrate.

The contact angle values obtained for those samples that did not undergo a washing step were 90°, 95° and 100° for one, two and five layers, respectively, irrespective of the substrate. These values are slightly higher than for the corresponding washed samples. No noticeable differences could be found between substrates for a fixed number of immersions for both methods.

3.4.Optic and fluorescence and scanning electron microscopy

Fluorescent microscopy images for coated titanium are shown in Figure 4. Both "washed" and "non-washed" samples have been included. Images for the other substrates (polystyrene and glass) can be found in the supporting information (Figures 1 and 2, respectively).

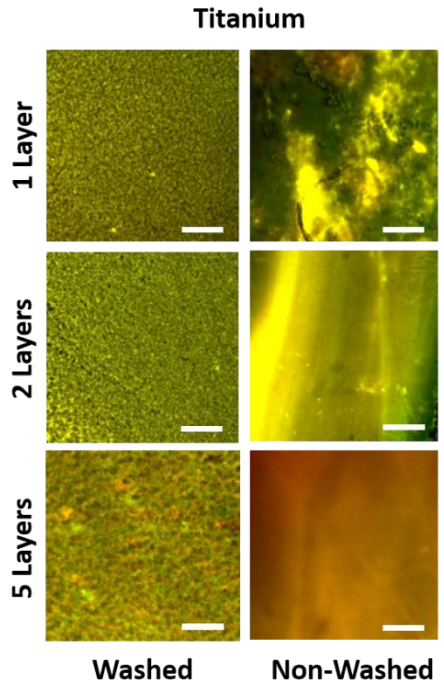

***Figure 4**. Fluorescence pictures of the evolution of the overall aspect of the titanium surface structure with each new layer.*

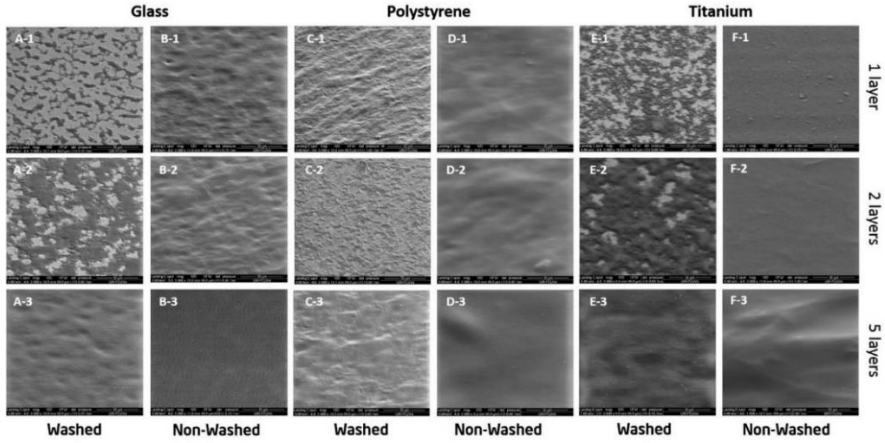

***Figure 5**. SEM pictures of glass, polystyrene and titanium substrates covered by 1, 2 and 5 layers using the washing method (A, C, and E rows) or without the washing step (B, D and, F rows).*

Although the surface of each sample was coated by LBL assembly of recombinamers, the assembly uniformity and thickness depend on both the number of layers and the method used for deposition ("washed" or "non-washed" samples). The fluorescent images indicate the homogeneous distribution of the fluorescent label.

A comparison of the two approaches used in this work shows that a more uniform coating is obtained for one, two or five layers when no washing steps are included in the coating procedure. As can be seen from the SEM images (Figure 5), after the first washing step the surfaces are covered by a thin layer through which the topographical details of the surfaces are barely visible beneath ELR click layer. As the washing step eliminates unreacted solution, in the case of a single layer the coating on the substrate will be quite thin and the coverage less extensive, as can be clearly seen from the fluorescence images. These results are in agreement with the FTIR results.

This approach has also been applied to samples with more complex structures, such as metallic meshes. The corresponding images are shown in Figure 6. Optical and fluorescence microscopy offers an initial view of the coating on such surfaces. Even after deposition of the first ELR click layer, a complete and smooth coating of the 3D metallic mesh can be observed (see Figure 6-A). Further SEM images for these complex structures show how the succession of ELR click layers completely cover the structure, adapting their shape and topography perfectly. A closer look at the SEM micrographs shows that some small cracks are present on the coating around the metallic edges of the mesh. However, as these were not observed by optical or fluorescence microscopy, they are likely artefacts from the drying process prior to SEM.

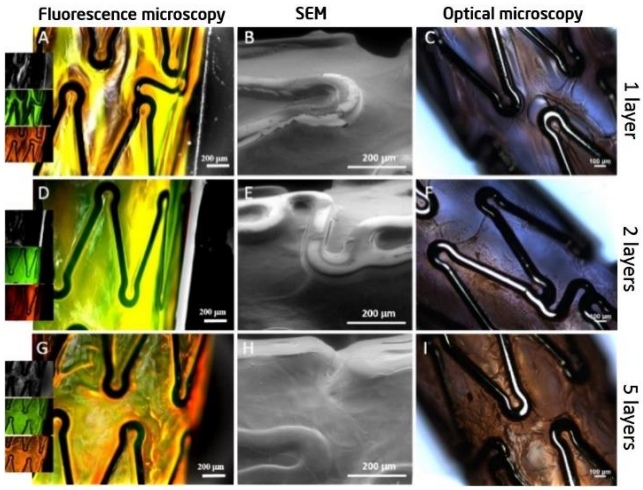

***Figure 6**. Fluorescence (images A, D and G), SEM (images B, E and H) and optical (images C, F and I) micrographs 3D metallic mesh after the LBL process. Inserts in fluorescence pictures show the grey, green and red channels that compose the merged images.*

An SEM investigation of the evolution of the surface covering as a function of the number of layers gave an initial quantitative estimation of the layer thickness. Thus, quantitative SEM measurements corroborate the qualitative results obtained from optical and fluorescence microscopy.

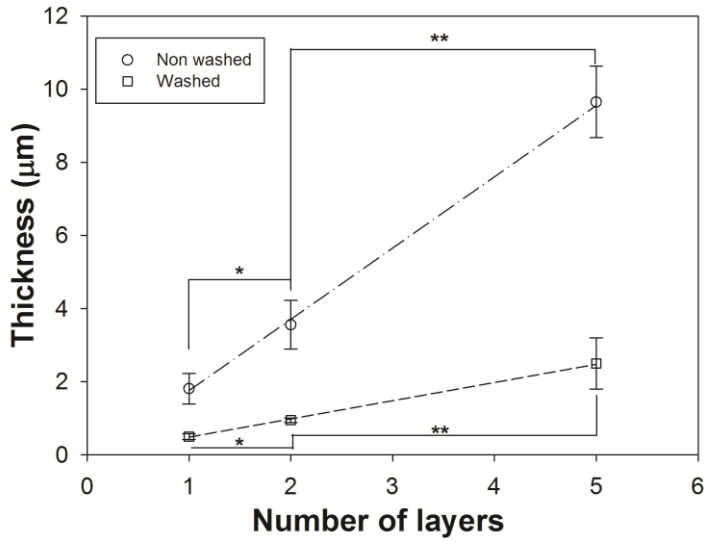

***Figure 7**. Evolution of the thickness of both non-washed and washed ELR-film as function of the number of layers. Thickness was obtained by SEM evaluation.*

The surface coating for non-washed samples is uniform even from the first layer and a smooth coating of the samples is obtained, with the topographical details of the substrate being completely hidden beneath the ELR click layers. An average thickness of 1.8 μm was found for a single ELR click layer, whereas the thickness increased to 3.5 and 9.5 μm for two and five layers, respectively, in an almost linear manner irrespective of the substrate. A similar behaviour was found for washed samples, although, obviously, the thickness obtained was lower than that for the non-washed samples for the same number of layers. In this case, and as can be seen from Figure 7, the thickness grew from around 500 nm to 2.5 μm.

3.5.AFM results

The nano-topography and surface mechanical properties were measured by atomic force microscopy. Changes to the surface topography are evident after each new layer, and Figure 8 shows the differences between uncoated and coated titanium substrates

with or without the washing step (Figure 8, left and right columns, respectively). Equivalent figures for the other substrates can be found in the supporting information (Figures 3 and 4, respectively). The topography evolves from a flaky metallic surface to a rougher surface for the washed layers, with the roughness decreasing as the number of layers increases. Non-washed layers produce a smoother and more homogeneous nano-topography than washed samples, although complete surface coverage is obtained with both methods.

As far as the mechanical properties of the coated samples are concerned (see Figure 9), a decrease in the Young's modulus can be observed with each new layer. This trend is identical for both washed and non-washed samples and for all substrates analysed. The contribution of the substrates to the Young's modulus decreases as the thickness of the coating increases.

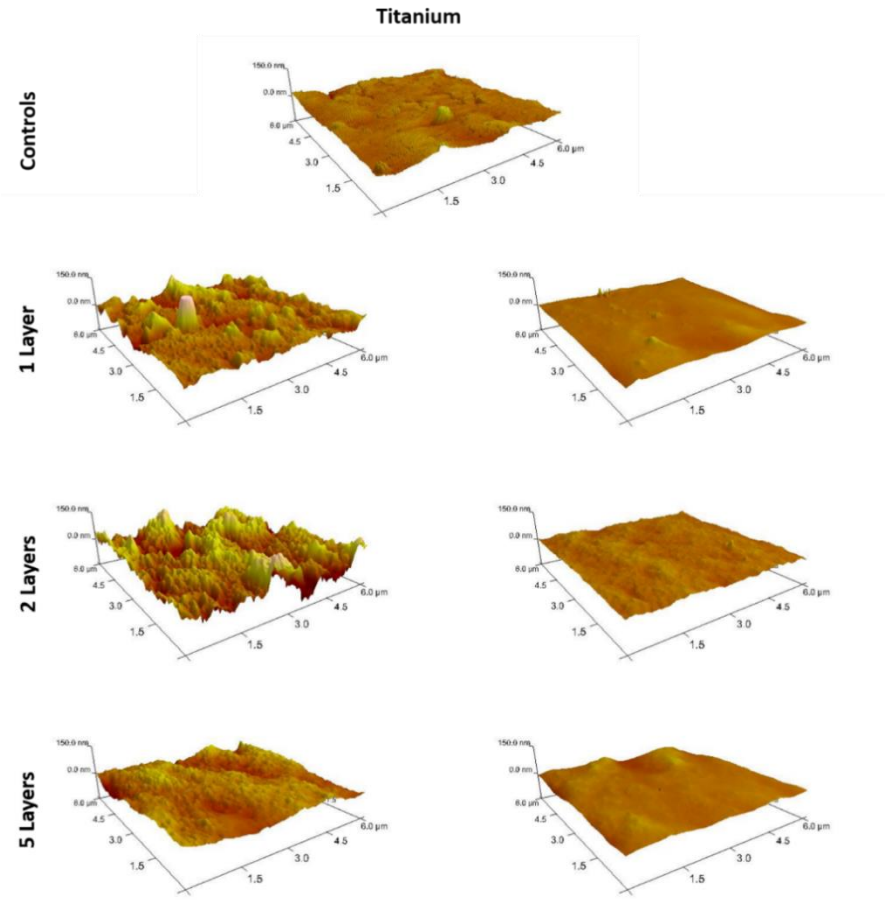

***Figure 8**. Nano-topography of uncoated titanium and its evolution after one, two and five washed layers (left row) and non-washed layers (right row).*

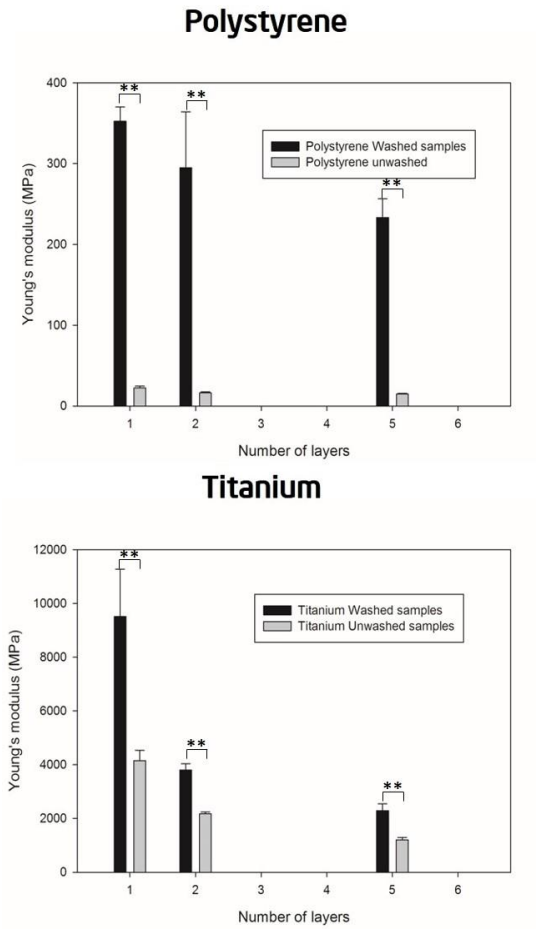

***Figure 9**. Young's modulus evolution as function of the number of layers obtained by AFM technique.*

4. DISCUSSION

As can be seen from the ever-increasing number of publications on this topic, LBL technology has grown in importance over the past few years due to its versatility for creating thin polymeric layers in an easy manner. However, despite the wide-ranging applicability of this technique, some drawbacks, especially a reduction in deposition time, which increases markedly with the number of layers to be deposited, still need to be addressed. In addition, a greater variety and versatility of the materials used, and

increased stability of the resulting multilayer structures, are also desirable. The need for controlled conditions (pH, temperature, and ionic strength) may affect the LBL process and, if living systems are involved in the LBL process, their survival may be compromised. An LBL process based on strong covalent crosslinking interactions may provide an excellent way of avoiding all these drawbacks. In this paper we describe an alternative LBL method based on the application of catalyst-free click chemistry to ELRs. This leads to a completely cytocompatible technique [26, 34] for biofunctionalizing surfaces made from different materials and with complex structures. The reduction in the time required for the LBL process (down to 20 seconds) allows a high control over the diffusion of the two ELR click solutions, thereby resulting in a reproducible and controlled thickness that increases in a linear manner as a function of the number of layers, as can be seen from the SEM evaluation of non-washed samples. These short reaction times and mild reaction conditions are suitable for cell-encapsulation applications that combine cells and materials in the same LBL approach. Such applications are currently being evaluated in our laboratory. Moreover, catalyst-free click technology allows us to introduce a large number of substances such as drugs, growth factors, and other bioactive compounds that may need to be covalently attached to the ELRs without affecting layer formation. As a first approach in this paper, a fluorescence probe has been covalently bonded to our modified ELRs.

Microscopy (optical, florescence, and SEM) offers us a first insight into the coating efficiency, showing a good covering from the first washed layer, where the surface topography is covered but still present under the ELR click layer, to the fifth non-washed layer,

where a thicker, soft and continuous ELR click layer completely covers the surface irregularities.

The FTIR and XPS results show the variation in the surface layers at an atomic level. A clear evolution from the typical spectra for each substrate to the specific spectra for the ELRs can be observed in the results from both techniques.

The contact angles values highlight the variation in surface hydrophobicity before and after plasma cleaning and after deposition of the ELR click layers, with contact angle values increasing to around 100°, which represents a substantial increase in surface hydrophobicity for washed and non-washed samples.

The AFM results indicate a good and complete covering of the substrates by layers that provide a completely different nano-topography than that observed for the bare substrates. Moreover, the mechanical properties also change, resulting in a lower Young's modulus with each additional layer. Significant differences were also found between the two methods tested (with or without washing step), thus meaning that the surface mechanical properties of the system can be controlled by varying the number of layers or the method used to form them.

5. CONCLUSIONS

In this work, structures as simple as flat pieces or as complicated as metallic grids, made of several materials, have been biofunctionalized using LBL techniques involving clickable ELRs and without the need for any other molecules. The use of an ELR containing a bioactive sequence such as RGD will improve cell

adhesion to these functionalized surfaces. Moreover, any other peptide domains that can be incorporated into the ELR backbone can also be used in this approach.

The diffusion abilities of the ELRs allow the experimental setup to be designed with both a washing and a non-washing step after deposition of each component. This allows the washing step to be skipped without losing interlayer integrity as well as a rapid increase in coating thickness up to a few micrometres. The resulting coatings have been characterized by contact angle measurements, FTIR, fluorescence, optical and scanning electron microscopy, XPS and AFM to evaluate the topographical features of the layers and their mechanical properties.

Finally, this work has made use of relatively simple ELRs as model candidates and as a proof of concept. However, in principle, the same approach can be applied to much more functional and complex materials, including many other macromolecular materials not pertaining to the ELR family.

6. ACKNOWLEDGEMENTS

We acknowledge financial support from the EU through the European regional development fund (ERDF) NMP3-LA-2011-263363, HEALTH-F4-2011-278557, PITN-GA-2012-317304), from the MINECO (MAT-2010-15982, MAT2010-15310, PRI-PIBAR-2011-1403 and MAT2012-38043-C02-01), the JCyL (projects VA152A12-2, VA244U13 and VA155A12-2), the CIBER-BBN, and the JCyL and the Instituto de Salud Carlos III under the "Network Center of Regenerative Medicine and Cellular Therapy

7. REFERENCES

[1] Iler RK. Multilayers of colloidal particles. Journal of Colloid and Interface Science 1966.

[2] Costa RR, Mano JF. Polyelectrolyte multilayered assemblies in biomedical technologies. Chemical Society Reviews 2014;43:3453-79.

[3] Boudou T, Crouzier T, Ren K, Blin G, Picart C. Multiple Functionalities of Polyelectrolyte Multilayer Films: New Biomedical Applications. Advanced Materials 2010;22:441-67.

[4] Bertrand P, Jonas A, Laschewsky A, Legras R. Ultrathin polymer coatings by complexation of polyelectrolytes at interfaces: suitable materials, structure and properties. Macromolecular Rapid Communications 2000;21:319-48.

[5] Costa RR, Custodio CA, Arias FJ, Rodriguez-Cabello JC, Mano JF. Layer-by-Layer Assembly of Chitosan and Recombinant Biopolymers into Biomimetic Coatings with Multiple Stimuli-Responsive Properties. Small 2011;7:2640-9.

[6] Decher G. Fuzzy Nanoassemblies: Toward Layered Polymeric Multicomposites. Science 1997;277:1232-7.

[7] Hammond PT. Engineering materials layer-by-layer: Challenges and opportunities in multilayer assembly. AIChE Journal 2011;57:2928-40.

[8] Tang Z, Wang Y, Podsiadlo P, Kotov NA. Biomedical Applications of Layer-by-Layer Assembly: From Biomimetics to Tissue Engineering. Advanced Materials 2006;18:3203-24.

[9] Cameron RK, Kim W, Georgina KS, Angus PRJ, Frank C. Peptide-Functionalized, Low-Biofouling Click Multilayers for Promoting Cell Adhesion and Growth. Small 2009;5.

[10] Yang W, Pranantyo D, Neoh K-G, Kang E-T, Teo S, Rittschof D. Layer-by-layer click deposition of functional polymer coatings for combating marine biofouling. Biomacromolecules 2012;13:2769-80.

[11] Costa RR, Custódio CA, Testera AM, Arias FJ, Rodríguez-Cabello JC, Alves NM, et al. Stimuli-Responsive Thin Coatings Using Elastin-Like Polymers for Biomedical Applications. Advanced Functional Materials 2009.

[12] Zhiyong T, Wang Y, Podsiadlo P, Kotov NA. Biomedical Applications of Layer-by-Layer Assembly: From Biomimetics to Tissue Engineering. Advanced Materials 2006;18:3203-24.

[13] Schneider A, Bolcato-Bellemin A-LL, Francius G, Jedrzejwska J, Schaaf P, Voegel J-CC, et al. Glycated polyelectrolyte multilayer films: differential adhesion of primary versus tumor cells. Biomacromolecules 2006;7:2882-9.

[14] Pan Y, Zhang Y, Li Y. Layer by layer self assembled multilayer films of single walled carbon nanotubes and tin disulfide nanoparticles with chitosan for the fabrication of biosensors. Journal of Applied Polymer Science 2013;128:647-52.

[15] Kreft O, Javier AM, Sukhorukov GB, Parak WJ. Polymer microcapsules as mobile local pH-sensors. Journal of Materials Chemistry 2007;17:4471-6.

[16] Yu Y, Yin M, Mullen K, Knoll W. LBL-assembled multilayer films of dendritic star polymers: surface morphology and DNA hybridization detection. Journal of Materials Chemistry 2012;22:7880-6.

[17] Garcia J, Zhang Y, Taylor H, Cespedes O, Webb ME, Zhou D. Multilayer enzyme-coupled magnetic nanoparticles as efficient, reusable biocatalysts and biosensors. Nanoscale 2011;3:3721-30.

[18] Radtchenko IL, Giersig M, Sukhorukov GB. Inorganic particle synthesis in confined micron-sized polyelectrolyte capsules. Langmuir 2002.

[19] Huisgen R. 1,3-Dipolar Cycloadditions. Past and Future. Angewandte Chemie International Edition in English 1963;2:565-98.

[20] Laughlin ST, Baskin JM, Amacher SL, Bertozzi CR. In vivo imaging of membrane-associated glycans in developing zebrafish. Science 2008;320:664-7.

[21] Pierna M, Santos M, Arias F, Alonso M, Rodriguez-Cabello J. Efficient cell and cell-sheet harvesting based on smart surfaces coated with a multifunctional and self-organizing Elastin-Like Recombinamer. Biomacromolecules 2013.

[22] Baskin J, Prescher J, Laughlin S, Agard N, Chang P, Miller I, et al. Copper-free click chemistry for dynamic in vivo imaging. Proceedings of the National Academy of Sciences of the United States of America 2007;104:16793-7.

[23] Wenge U, Ehrenschwender T, Wagenknecht H-A. Synthesis of 2'-O-propargyl nucleoside triphosphates for enzymatic oligonucleotide preparation and "click" modification of DNA with nile red as fluorescent probe. Bioconjugate Chemistry 2013;24:301-4.

[24] Matthew W, John M, Ying-Chuan L, Steven MS, William L, Arthur JO, et al. Inhibitors of HIV-1 Protease by Using In Situ Click Chemistry. Angewandte Chemie 2006;118.

[25] Kennedy D, McKay C, Legault M, Danielson D, Blake J, Pegoraro A, et al. Cellular consequences of copper complexes used to catalyze bioorthogonal click reactions. Journal of the American Chemical Society 2011;133:17993-8001.

[26] González de Torre I, Santos M, Quintanilla L, Testera A, Alonso M, Rodríguez Cabello JC. Elastin-like recombinamer catalyst-free click gels: Characterization of poroelastic and intrinsic viscoelastic properties. Acta Biomaterialia 2014;10:2495-505.

[27] Rodriguez-Cabello JC, Martin L, Girotti A, Garcia-Arevalo C, Arias FJ, Alonso M. Emerging applications of multifunctional elastin-like recombinamers. Nanomedicine (London, U K) 2011;6:111-22.

[28] Rodríguez-Cabello JC, Martín L, Alonso M, Arias FJ, Testera AM. "Recombinamers" as advanced materials for the post-oil age. Polymer 2009;50:5159-69.

[29] Wright ER, Conticello VP. Self-assembly of block copolymers derived from elastin-mimetic polypeptide sequences. Advanced Drug Delivery Reviews 2002;54:1057-73.

[30] Girotti A, Reguera J, Rodriguez-Cabello JC, Arias FJ, Alonso M, Matestera A. Design and bioproduction of a recombinant multi(bio)functional elastin-like protein polymer containing cell adhesion sequences for tissue engineering purposes. J Mater Sci Mater Med 2004;15:479-84.

[31] Liu J, Heilshorn S, Tirrell D. Comparative cell response to artificial extracellular matrix proteins containing the RGD and CS5 cell-binding domains. Biomacromolecules 2004;5:497-504.

[32] Barbosa JS, Costa RR, Testera AM, Alonso M, Rodriguez-Cabello JC, Mano JF. Multi-Layered Films Containing a Biomimetic Stimuli-Responsive Recombinant Protein. Nanoscale Res Lett 2009;4:1247-53.

[33] Michiardi A, Hélary G, Nguyen PC, Gamble LJ, Anagnostou F, Castner DG, et al. Bioactive polymer grafting onto titanium alloy surfaces. Acta biomaterialia 2010;6:667-75.

[34] González de Torre I, Wolf F, Santos M, Rongen L, Alonso M, Jockenhoevel S, et al. Elastin-like recombinamer-covered stents: Towards a fully biocompatible and non-thrombogenic device for cardiovascular diseases. Acta Biomaterialia 2014.

8. SUPPORTING INFORMATION

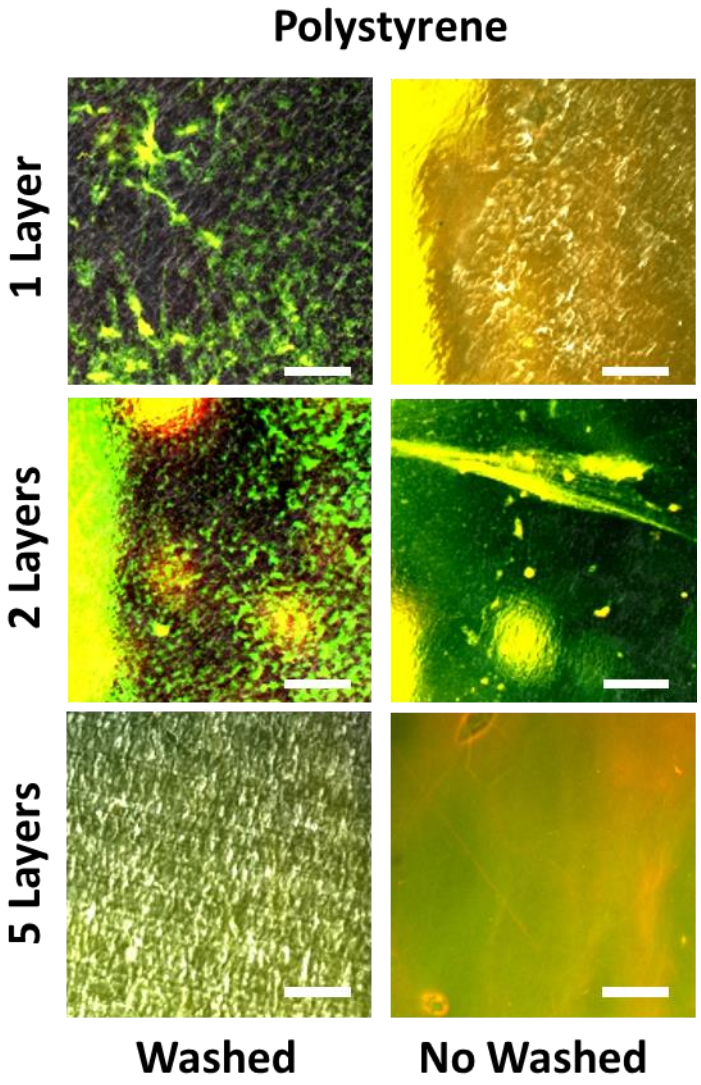

Figure 1. Fluorescence images showing the evolution of the overall aspect of the polystyrene surface structure with each new layer.

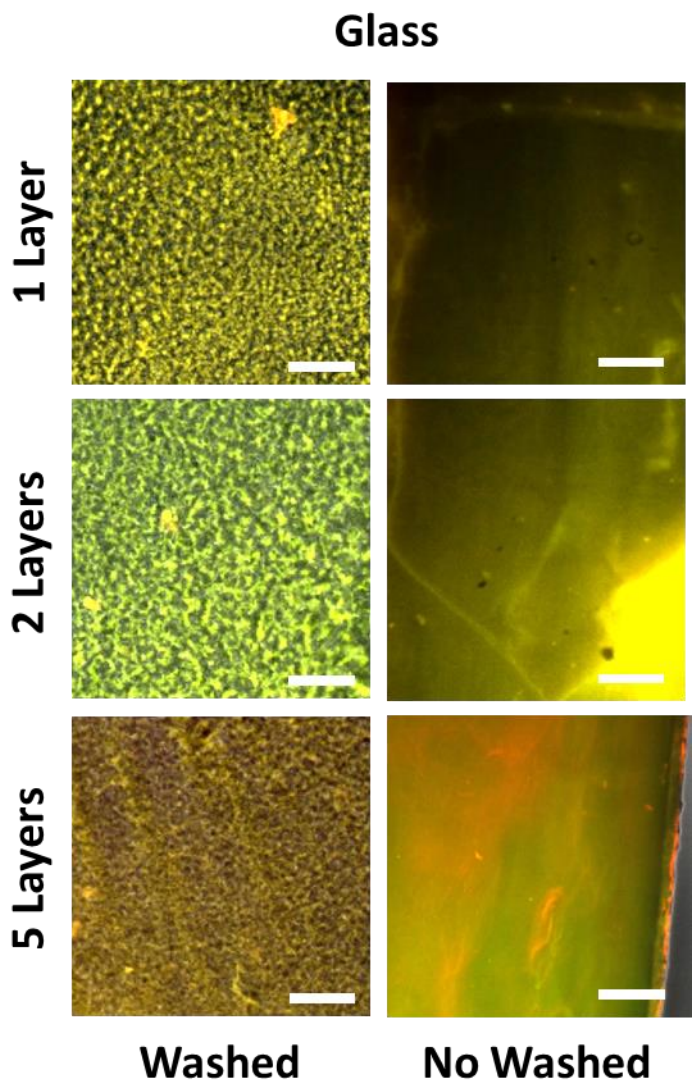

Figure 2. Fluorescence images showing the evolution of the overall aspect of the glass surface structure with each new layer.

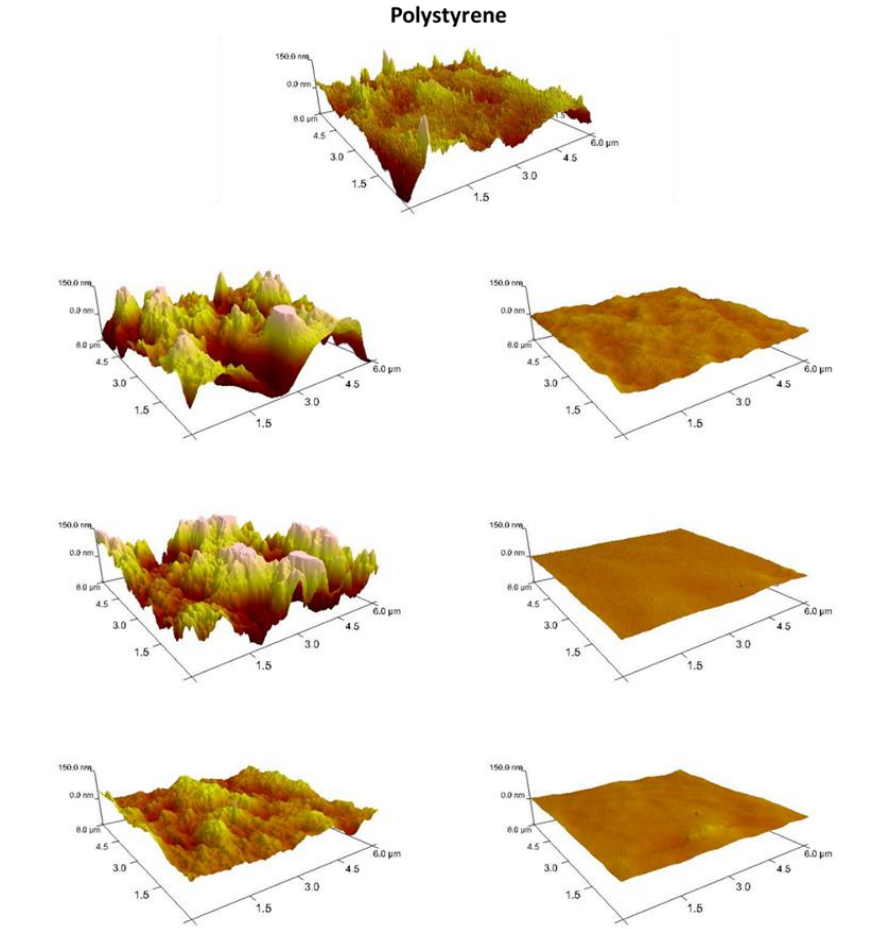

Figure 3. Nano-topography of uncoated polystyrene and its evolution after one, two and five washed (left column) and non-washed layers (right column).

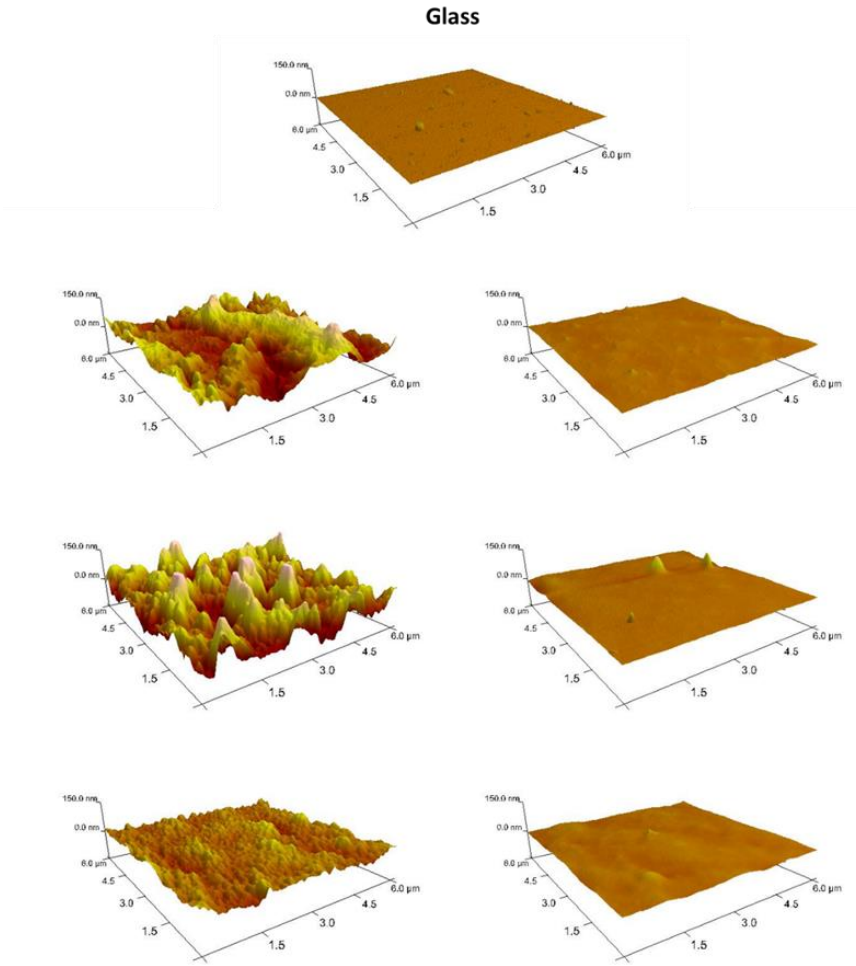

Figure 4. Nano-topography of uncoated glass and its evolution after one, two and five washed (left column) and non-washed layers (right column).

CHAPTER 7:

ELASTIN-LIKE RECOMBINAMER-COVERED STENTS: TOWARDS A FULLY BIOCOMPATIBLE AND NON-THROMBOGENIC DEVICE FOR CARDIOVASCULAR DISEASES

Israel González de Torre[1],*, Frederic Wolf[2], Mercedes Santos[1], Lisanne Rongen[2], Matilde Alonso[1], Stefan Jockenhoevel[2,3], José C. Rodríguez-Cabello[1], Petra Mela[2]

[1] BIOFORGE, CIBER-BBN, Campus "Miguel Delibes" Centro I+D, Universidad de Valladolid, Paseo Belén 11, 47011, Valladolid, Spain
[2] Tissue Engineering and Textile Implants, AME, Helmholtz Institute, RWTH Aachen, Germany
[3] Institut für Textiltechnik, RWTH Aachen University, Aachen, Germany

González de Torre, I.; Wolf, F.; Santos, M.; Rongen, L.; Alonso, M.; Jockenhoevel, S.; Rodríguez-Cabello, J. C.; Mela, P. Elastin-like recombinamer-covered stents: Towards a fully biocompatible and non-thrombogenic device for cardiovascular diseases. Acta Biomaterialia 2015, 12 (0), 146-155.
DOI:10.1016/j.actbio.2014.10.029

Abstract:

We explored the use of recently developed gels obtained by catalyst free click reaction of elastin-like recombinamers (ELR) to fabricate a new class of covered stents. The approach consists in embedding bare metal stents in the ELR-gels by injection molding, followed by endothelialization under dynamic pressure and flow conditions in a bioreactor. The mechanical properties of the gels could be easily tuned by choosing the adequate concentration of the ELR components and their biofunctionality could be tailored by inserting specific sequences (RGD and REDV). The elastin-like recombinamer-covered stents (ELR-covered stents) exhibited mechanical stability under high flow conditions and could undergo crimping and deployment without damage. The presence of RGD in the ELR used to cover the stent supported full endothelialization in less than two weeks in vitro. Minimal platelet adhesion and fibrin adsorption were detected after exposure to blood as shown by immunostaining and scanning electron microscopy. These results prove the potential of this approach towards a new and more effective generation of covered stents which exclude the atherosclerotic plaque from the blood stream and have high biocompatibility, physiological hemocompatibility and reduced response of the immune system.

1. INTRODUCTION

Vascular stenting is a widely adopted intervention to treat narrowed or weakened (e.g. presenting non obstructive lesions, aneurysms, dissections) coronary and peripheral vessels by stabilizing them and maintaining them patent. Despite the simplicity of the concept and the knowledge gained in the last decades on the interactions between stent, vascular tissue and blood, the re-occlusion of the vessels after stenting with bare metal stents remains a major problem [1] [2, 3]. To avoid this complication, drug eluting stents (DES) have been developed with the aim of suppressing the proliferation of smooth muscle cells. This concept proved to be successful preventing cellular ingrowth, however late stent thrombosis has been reported [4, 5], likely occurring because the same drugs hinder the healing of the endothelial layer and the presence of the polymeric coating results in wall inflammation. Recently published clinical studies reported the improved performance of the new generations of drug eluting coronary stents with respect to the occurrence of late thrombosis [6, 7].

Recognizing the importance of a rapid and complete endothelial regeneration, stents with the capability of attracting endothelial progenitor cells (EPCs) have been proposed [8]. The mimicry of EPC homing holds great promise for in vivo self-endothelialization of medical devices, however it depends heavily on the use of not yet identified, highly selective capture molecules able to bind exclusively EPCs [9, 10]. Furthermore, the role of EPCs in re-endothelialization following vascular injury and the effect on intimal hyperplasia is still controversial [11,12].

Covered stents represent an alternative family of devices consisting of BMS in combination with a layer made of synthetic polymers [13, 14] or based on naturally occurring materials [15-18]. Autologous native [19] and engineered [20, 21] tissue was also used for covering or embedding BMS. The layer functions as a barrier to exclude the atherosclerotic plaque from the blood flow in the lumen of the vessel, potentially preventing neointima hyperplasia and therefore re-occlusion of the vessel [22]. Ideally, the membrane should also support endothelialization to achieve a physiological hemocompatibility. Furthermore, covered stents are indicated to seal degenerated vein grafts, to cover vascular perforations and exclude symptomatic aneurysms [23, 24]

Despite the possible advantages that covered stents might have with respect to bare and coated ones, especially in the peripheral vascular system, their full potential has not been fully explored. The main challenge is to identify the optimal material able to cover the stent in a mechanically stable way under physiological pressure and flow conditions, possessing elasticity to undergo crimping and deployment without damage, biocompatible, hemocompatible and supporting endothelial cell adhesion/ proliferation to full coverage.

Here we propose the use of elastin-like recombinamers (ELRs) to fabricate endothelialized covered stents. ELRs are bioengineered polymers based on the natural elastin, produced by recombinant techniques. They possess an extremely low polydispersity, thermosensitive behavior and the possibility to include different bioactive sequences for cell adhesion and proliferation or sequences sensitive to enzymes [25]. These polymers exhibit high biocompatibility [26] and hemocompatibility

[27, 28]. Notably, because ELRs are formed by the repetition of aminoacid sequences present in the natural elastin, they are ignored by the host immune system as well as their degradation products [29, 30]. ELRs have been exploited for applications as nanovaccines [31], protein [32] and drug delivery [33, 34] and tissue engineering [35]. ELRs gels have demonstrated to be an optimal artificial extracellular matrix for different cell lines, such as fibroblasts and neuroblasts [36], chondrocytes [37, 38], epithelial cells from the ocular surface [39] and endothelial cells (HUVECs) [40]. In general terms, ELRs are positioned midway between natural products and synthetic polymers. Interestingly, they show the advantages of an engineered material because of the exhaustive control over their composition, functionality and mechanical properties, while still keeping the biological origin and nature. That is why ELRs could be an ideal candidate for creating bioactive and more efficient stents similarly to other biomedical applications where ELRs have the potential to outperform more conventional materials [31-35].

Recently, we showed the successful modification of ELRs by the Huisgen 1,3-dipolar cycloadition of azides and alkynes [41] according to the concept of click chemistry [42, 43]. In this way, we could produce gels under physiological conditions, in a completely cell-friendly process without the need of any catalyst. The biocompatibility of the click reactions has been tested in the presence of cells [44-46] and inside living organisms [47]. Click reactions have been largely employed in drug discovery [48], bioconjugation with proteins [46] and DNA [49], cell surface labeling [50], and surface modifications with ELRs [51] among other molecules.

Here we used the newly developed ELR-Catalyst Free Click Gels (ELR-CFCGs) [41] to cover self-expandable stents by embedding in the gels by injection molding technique. The ELR-covered stents were endothelializated dynamically in a bioreactor with the goal of obtaining an endovascular device with 1) a physical barrier for the atherosclerotic plaque; 2) physiological hemocompatibility; 3) mechanical stability; 4) no inflammatory reaction.

The quality of the embedding process was evaluated by scanning electron microscopy (SEM), the mechanical stability of the ELR-layer was tested under high shear stress conditions. The ability of ELR-CFCGs with different biofunctional sequences to support adhesion and proliferation of human umbilical endothelial cells (HUVECs) was tested by immunocytology. The catheter-based delivery of the ELR-stents was simulated by crimping the devices and keeping them in the crimped position for 20 minutes, representing the maximum estimated delivery time. After deployment the stents were exposed to blood contact in a Chandler loop [52, 53] for 1 hour and the surface performance was evaluated in terms of platelet adhesion by immunochemistry and fibrin deposition by SEM.

2. MATERIALS AND METHODS

2.1.ELRs biosynthesis, modification and characterization:

The ELRs used in this work were obtained by using standard genetic engineering techniques. Their purification was performed with several cycles of temperature-dependent reversible precipitations, by centrifugation below and above their transition temperature (Tt), making use of the intrinsic thermal behavior of

these compounds [54]. The ELRs were subsequently dialyzed against purified water and freeze-dried. Three different ELRs were obtained: VKVx24, a structural recombinamer without any bioactive sequence; HRGD6, a recombinamer with the universal cell-adhesion epitope (RGD) and REDVx10, bearing a cell-adhesion domain (REDV) which is more specific for endothelial cells than RGD. The amino-acid sequences of these polymers are: MESLLP VG VPGVG [VPGKG(VPGVG)5]23 VPGKG VPGVG VPGVG VPGVG VPGV for VKVx24; MGSSHHHHHHSSGLVPRGSHMESLLP [(VPGIG)2(VPGKG)(VPGIG)2]2AVTGRGDSPASS[(VPGIG)2(VPGKG)(VPGIG)2]2 for HRGD6 and MESLLP[(VPGIG)2(VPGKG)(VPGIG)2EEIQIGHIPREDVDYHLYP(VPGIG)2(VPGKG)(VPGIG)2(VGVAPG)3]10V for REDVx10. The purity and chemical characterization of ELRs were verified by sodium dodecyl sulfate polyacrylamide gel electrophoresis (SDS-PAGE) and matrix-assisted laser desorption/ionization time-of-flight (MALDI-TOF) amino-acid composition analysis, differential scanning calorimetry (DSC) and nuclear magnetic resonance (NMR) [54, 55]. ELRs were chemically modified by transformation of the ε-amine group in the lateral lysine chain to bear cyclooctine and azide groups as we recently reported [46]. In addition to VKVx24-cyclooctine and HRGD6-N3, novel VKVx24-N3, REDV-N3, REDVx10-cyclooctine, HRGD6-cyclooctine were prepared and characterized by NMR, Fourier transform infrared spectroscopy (FTIR), and DSC. (See Figs. 1 to 6 in supporting information).

2.2.Gel formation (ELRs-CFCGs):

Gels were formed by catalyst free click reactions between an azide group and an activated cyclooctine group. Solutions of ELRs-cyclooctine and ELRs-azide were prepared in purified water at the

desired concentration and kept at 4°C for at least 24 h. ELRs-CFCGs were obtained by mixing the solutions (ELR-cyclooctine, ELR-azide) at 4 °C inside the appropriate mold (e.g. well-plates, cylindrical and tubular molds). After 15 minutes at 4 °C, the gels were completely formed. Specifically VKVx24-VKVx24 (VKV-CFCG), HRGD6-HRGD6 (RGD-CFCG) and REDVx10-REDVx10 (REDV-CFCG) were obtained and characterized by DSC and FTIR (see Figs. 7 and 8 in supporting information).

2.3.Rheological measurements:

Rheological experiments were performed on a strain-controlled AR-2000ex rheometer (TA Instruments USA). Cylinder-shaped gels, cast in a custom-made mold, were placed between the nonporous parallel stainless steel plates (12 mm diameter) of the rheometer. The gap between the plates was adjusted using a normal force around 0.2 N in order to prevent slippage. A gap higher than 1000 μm was always reached after the sample relaxed until equilibrium. Measurements were carried out at two temperatures: 4 °C (formation temperature), and 37 °C. Sample temperature was controlled and maintained by using a Peltier device. Mechanical properties of nine gels of each kind of ELRs-CFCG were evaluated. Two different measurements in a shear deformation mode were performed after determining the strain amplitude range in which the gels exhibited linear viscoelasticity. Specifically: i) a dynamic strain sweep (with amplitudes ranging between 0.1 % and 20 %) was carried out at the frequency of 1 Hz to measure the dynamic shear modulus ($|G^*|$) as a function of the strain. ii) a dynamic frequency sweep was accomplished between 0.05 Hz and 50 Hz at a fixed strain (corresponding to the hydrogel

linear region) to determine the dependence of the |G*| and the loss phase angle (δ) on the frequency.

2.4.Cell isolation and culture:

Endothelial cells were isolated from veins of human umbilical cords, length depended on the donor. Usually they were approximately 25 cm length. The human umbilical cords were kindly provided by the department of gynecology at the University Hospital Aachen in accordance with the human subjects approval of the ethics committee (votum of the local ethics committee: #EK 2067). The veins were washed with phosphate-buffered saline (PBS; Gibco, Karlsruhe, Germany) before removing the endothelial cells by using 1 mg/mL collagenase (Sigma, Seelze, Germany). The human umbilical vein endothelial cells (HUVECs) were seeded on 2% gelatin pre-coated cell culture flasks and incubated with Endothelial Cell Basal Medium (EBM-2; Lonza, Walkersville, USA). This was supplemented with ECM-2 kit (0.1% insulin, 0.1% gentamicin, 0.1% ascorbic acid, 0.4% human fibroblast growth factor, 0.1% endothelial growth factor, 0.04% hydrocortisone, 0.1% epidermal growth factor, 0.1% heparin (Lonza)), 10% fetal bovine serum (FBS; Gibco) and 1% antibiotic/antimycotic solution (Gibco). Cells were cultured in 5% CO2 and 95% humidity at 37 °C and serially passaged 3 times using 0.25% trypsin/0.02% EDTA solution (Gibco). The medium was changed every 3-4 days. Prior to stent endothelialization, the endothelial cells phenotype was verified by positive immunofluorescence staining for von Willebrand factor (vWf).

2.5.Cell proliferation on ELRs-CFCGs:

HUVECs proliferation was evaluated on three different ELR-CFCGs types at day 1, 5 and 9 after cell seeding. For each time

point a 96 well-plate was used where 3 gels were moulded for each gel type. Each gel was composed mixing 15µl ELR-cyclooctine plus 15µl ELR-azide both solution at 75mg/mL. VKVx24-CFCGs, REDVx10-CFCGs and HRGD6-CFCGs were molded, sterilized by UV-light for 3h and washed with medium for at least 2h. On each gel, 2500 HUVECs were seeded and 100 µL endothelial medium (supplemented EBM-2, Lonza) were added. Gelatin gels seeded with HUVECs in the same way served as positive control, while VKVx24-CFCGs without cells served as negative controls. Live/Dead staining was performed according to the manufacturer's instruction (Molecular Probes™) and fluorescence intensity was measured at 530 nm and 645 nm (Tecan Infinite 200 micro plate reader). The fluorescence intensity at 530 nm was converted into cell number by using calibration curves obtained with known-numbers of HUVECS seeded on 96 well-gelatin-precoated plate 24 hours before the measurement (1.000 to 10.000 cells/well in 100 µL in the medium used for HUVECs culture).

2.6.ELR-covered stents molding:

Self-expanding laser-cut (Biotronik Aston Pulser) and warp-knitted nitinol stents were used. The warp-knitted stents were produced at the Institute of Textile Engineering (Institut für Textiltechnik) of the RWTH Aachen University (Aachen, Germany) processing a nitinol wire with a diameter of 76 µm (NiTi Nr.1SE; FortWayneMetals, Indiana, USA) with a double raschel warp knitting machine (Karl Mayer, Obertshausen, Germany) with two bar tricot interloop and a loop density of 12 loops/inch. The stents were placed on a metal mandrel and heat fixated at 500°C for 15min in a high-temperature kiln (Heraeus). The stents (2.5 cm long) were embedded in ELR-CFCGs by injection molding. The mold

consisted of a gas-permeable outer silicone cylinder (inner diameter=8 mm; Ismatec), and an inner coaxial casting cylinder (outer diameter=5.5 mm), machined from polytetrafluorethylene (PTFE; Kuempel-Kunststoff-Verarbeitungswerk). For the moulding process, the stent was positioned in the annular space between the inner and outer cylinders. The mold has a small notch where the stent fits, placing it in the correct position. That space between cylinders was then filled with the ELR components at 4 °C to obtain the desired ELR-CFCG (Fig. 1). Specifically ELR-CFCGs with cell adhesion sequences (8 RGD-covered stents and 6 REDV-covered stents were evaluated) were employed at a concentration of 75 mg/mL. After 15 minutes at 4 °C, the system was brought to room temperature for 5 minutes before demolding. The stents were sterilized under UV light (4 x 1 h) and incubated in sterile PBS for 1 hour, at 37°C. PBS was changed and the stent was kept in PBS for two more hours and, finally, PBS was changed again and the pieces were hydrated in PBS for 24 hours.

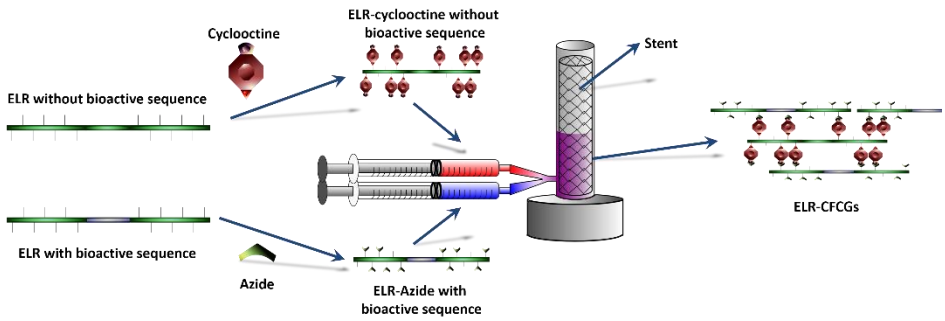

Fig. 1 *Schematic representation of the ELR-covered stents molding procedure.*

2.7.Mechanical stability of ELR-covered stents

The ELR-covered stents were exposed for 24 hours to high water flow in a closed-loop flow system to evaluate the robustness of the polymer coating. The system consisted of a centrifugal pump (Eheim, universal 1250) connected to a PMMA reservoir through

silicone tubes (inner diameter 6.4 mm; Ismatec). The flow rate was set to 2.5 l/min resulting in a shear stress of 2 Pa according to the equation [56].

$$P=4\,\eta\,Q/\pi r3 \qquad \text{Eq. 1}$$

where P is the shear stress, η the viscosity, r is the inner radius of the covered stent and Q the flow rate.

The attachment of the ELR-layer was evaluated by measuring the difference of the dry weight of the ELR-covered stents before and after exposure to the flow. The dry weight was determined after storing the ELR-stent in a 70 % ethanol solution overnight and subsequently placing it in an oven (Binder GmbH, Germany) at 60 °C for 90 min.

2.8.ELR-covered stents endothelialization and conditioning:

The stents were placed in sterile silicon tubes (inner diameter 8mm; Ismatec) which were filled with endothelial medium containing 10x106/mL HUVECs and clamped at both ends. The tubes were mounted onto a metallic bar connected to a programmable roller pump (MCP-Process; Ismatec), which was used to rotate the ELR-covered stent about their longitudinal axis in the horizontal position for 20 s, followed by a 3-min stationary phase to allow endothelial cell attachment. The cycle was repeated for 6 h at 37 °C and 5% CO2. After cell seeding, the ELR-covered stents (plus outer cylinders) were connected to a flow-loop bioreactor system under sterile conditions. The system consisted of a peristaltic pump to generate the flow (MCP-Process; Ismatec), a clamp distal to the stent to regulate the pressure, a pressure sensor (Codan Medical GmbH), a medium reservoir and platinum-cured silicone tubings (Ismatec), with high gas transfer coefficients for

both oxygen and carbon dioxide to provide stable culture conditions. The complete bioreactor system was maintained in a standard incubator at 37 C and 5% CO2. The culture medium used in the bioreactor system was endothelial medium and was exchanged weekly under sterile conditions. The pressure was regulated at physiological values (80/120 mmHg), monitored and recorded on a PC with LabVIEW software (National Instruments Corporation, Austin, USA) via an analog/digital converter (USB6009; National Instruments Germany GmbH). A flow of 60 mL/min was generated and maintained during the first 24 hours and then gradually increased up to 110 mL/min in steps of 10 mL/min every 24 hours. The flow was maintained until day 15 of cultivation until the stents were carefully removed from the bioreactor system. During the whole conditioning period, the pH, pCO2, pO2, glucose and lactose levels in the medium were monitored every 48 hours with a blood-gas analyzer (Radiometer EML100; Radiometer). 4 RGD-covered stents and 3 REDV-covered stents were subjected to dynamic endothelialization.

2.9.Thrombogenicity assay after simulated catheter-based delivery:

The catheter-based delivery procedure of ELR-covered stents (with and without endothelial cell layer) was simulated by crimping them from a diameter of 6 mm to 2 mm (HV200 Machine Solutions) and keeping them in the crimped configuration for 20 minutes, evaluated as maximum delivery time. After deployment by self-expansion upon removal of the mechanical constraint, the stents were exposed to in vitro circulation of human blood for 1 hour to evaluate their thrombogenicity. BMSs and Gore Tex® small caliber vascular grafts (inner diameter=6 mm) were used as

controls. The stents were placed into Chandler-loop systems [52, 57] realized with closed silicone tubing circuits with a length of 30 cm and internal diameter of 6.4 mm, filled with 7 mL of human blood. The blood was drawn from a healthy donor and was treated with Tri Natriumcitrate (0.106 mol/L) to prevent coagulation. The rotational speed of the Chandler loops resulted in a shear rate of 479 s-1 and a shear stress of ~ 1.7 Pa (considering a blood dynamic viscosity of 3.5 x10-3 kg/ms) [58].

After 1 hour of circulation, the stents were washed with PBS and cut into pieces for SEM visualization and immunohistochemistry analysis by CD41/CD61 staining (Acris Antibodies GmbH, Herford, Germany) of adherent and activated platelets. Samples were viewed using an epifluorescence microscope (AxioObserver; Carl Zeiss). Images were acquired using a monochromatic digital camera (AxioCam MRc; Carl Zeiss).

2.10. Scanning electron microscopy:

Samples for SEM investigation were fixed in 2% glutaraldehyde in 0.1 M Sorenson's buffer (pH 7.4) at room temperature for 1h. They were rinsed with sodium phosphate buffer (0.2 M, pH 7.39, Merk) and dehydrated consecutively in 30%, 50%, 70% and 90% acetone and then three times in 100% acetone for 10 minutes. After critical-point-drying in CO2, they were sputter-coated (Leica EM SC D500) with a 20 nm gold-palladium layer. Images were obtained with an ESEM XL 30 FEG microscope (FEI, Philips, Eindhoven, the Netherlands) with accelerating voltage of 10 kV. Some of the SEM images were colored with Jasc Paint Shop Pro 9 software (Corel).

2.11. Statistical analysis:

Values are expressed as mean ± standard deviation (SD). A parametric two-way analysis of variance (ANOVA) was used to evaluate the data with post-hoc differences between groups using Holm-Sidak method with Sigma Plot version 11.0. A p-value lower than 0.05 was considered statistically significant.

3. RESULTS AND DISCUSSION

Three different ELRs (VKVx24, HRGD6 and REDV) have been chemically modified through their lysine residues to incorporate two different reacting groups (azides and cyclooctines). These modified ELRs maintain the characteristic thermosensitive behavior of the ELRs (see thermograms in supporting info) defined by their transition temperature (Tt). Below Tt, water forms clathrates structures surrounding the apolar moieties of the ELRs chains, which keep them hydrated and solubilized in a random conformation. On the contrary, above the Tt, ELRs chains adopt a more ordered structure excluding the surrounding water and precipitating.

3.1.Mechanical properties

The mechanical properties of the gels obtained from different recombinamer concentrations solutions (50, 100 and 150 mg/mL) were tested. There were no differences on rheological results of hydrogels with different composition of ELRs at the same concentration. The rheological results for RGD-CFCGs are shown as representative of the whole set.

According to the principle of small deformation rheology, hydrogels must be tested within their linear viscoelastic range to

ensure their stability [59-61]. In our gels, |G*| did not show any dependence on the strain amplitude up to about 10 % at a frequency of 1 Hz indicating linear viscoelastic behavior. Therefore, all subsequent rheological tests were performed for 1% strain.

The dependence of |G*| and δ on the recombinamer concentration was measured at a fixed frequency of 1 Hz. (Fig. 2). As expected, the stiffness of the gels increased linearly with increasing concentration at both tested temperatures (Fig. 2 A). The phase angles were low for all concentrations (Fig. 2 B), characteristic of high elastic, energy storing gels [62]. Thus, the elastic behavior dominates over the loss behavior in these hydrogels. No significant dependence was found in the loss phase angle with gel concentration at a given temperature. The loss angle is higher at 37 °C than at 4 °C as expected considering the phase transition of ELRs [40].

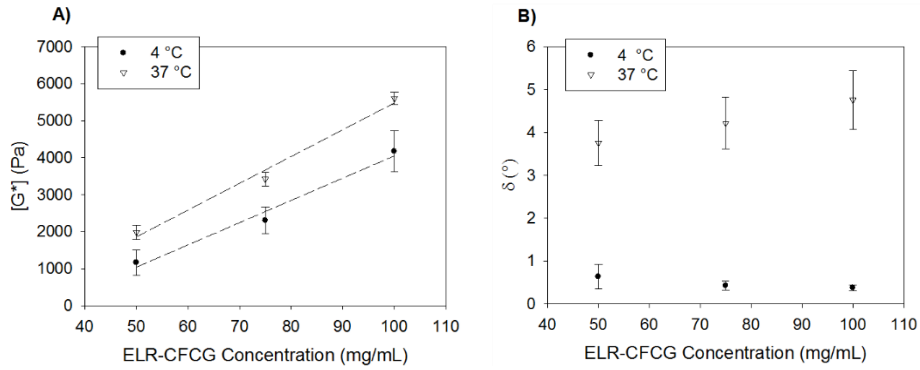

Fig. 2. *Rheological measurements at 1Hz and 1% strain. A) Effect of the ELR-CFCG concentration on the complex modulus, r2=0.986 and r2=0.981 at 37 and 4 °C respectively. B) Loss angle of the ELR-CFCGs at formation temperature (4°C, solid symbols) and at physiological temperature (37 °C, open symbols). No statistical differences were found for the loss phase angle values between different gel concentrations at a given temperature.*

After preliminary tests with high shear stress and physiological pressure conditions, we choose the intermediate concentration of 75mg/mL to fabricate the ELR-covered stents. Gels

obtained with this concentration exhibit a storage modulus of around 2700 Pa (see Fig. 10. of supporting info), which corresponds to a stiffness supporting the formation of confluent endothelial monolayers, in contrast to softer gels supporting the assembly of endothelial cells into networks [63].

3.2.Proliferation test

REDV and RGD sequences have been selected as bioactive sequences to be included into the amino-acid sequence of ELRs for this work. The first one corresponds to a specific adhesion sequence for endothelial cells [64, 65] and the second one a well-known integrin-mediated adhesion epitope for many types of cells [66-68]. In order to determinate the best combination of ELRs to improve the adhesion and proliferation of the HUVECs on the surface of the gels, proliferations assays were performed on RGD-CFCGs, REDV-CFCGs and VKV-CFCGs. VKV-CFCGs do not bear any bioactive sequence.

The chosen gel concentration (75 mg/mL) combines a good elasticity and a suitable environment for a good cell-colonization of the material. In general terms, these tests demonstrated that the presence of bioactive sequences improved the adhesion and proliferation on ELRs-CFCGs especially in the case of the RGD-CFCGs, which showed the best results (Fig.3). Nevertheless, REDV-CFCGs showed better cell adhesion and proliferation than the non-bioactive VKV-CFCGs, although their proliferation values were clearly lower than those of the RGD-based gels.

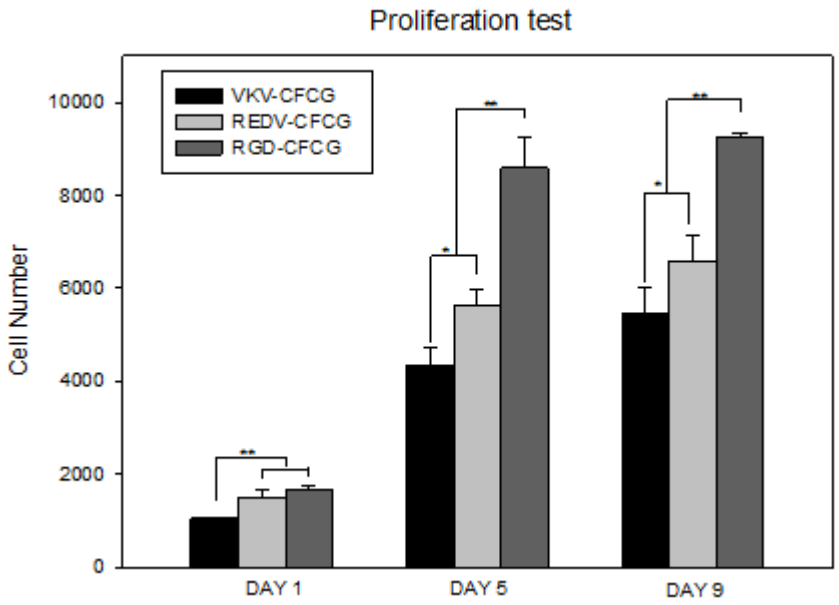

***Fig. 3**. Proliferation test of HUVECs at day 1, 5 and 9. Results come from three different experiments for every day and as average of at least three wells for every kind of gel and day. (* = p<0.05, ** = p<0.001).*

3.3.Stent coating

Laser-cut and warp-knitted nitinol stents were coated with RDG-CFCGs and REDV-CFCGs (Fig. 4 A, B and C). A uniform layer with no voids was formed covering completely the stent struts as verified by light microscopy and SEM. SEM analysis revealed a thickness of the gel layer coating the stents of about 100μm, (Fig. 4 D, E).

The simplicity of the fabrication method confirmed the processability of the ELRs as previously demonstrated for aggregates [69], nanoparticles [70], fibers [71], microstructured layers [72].

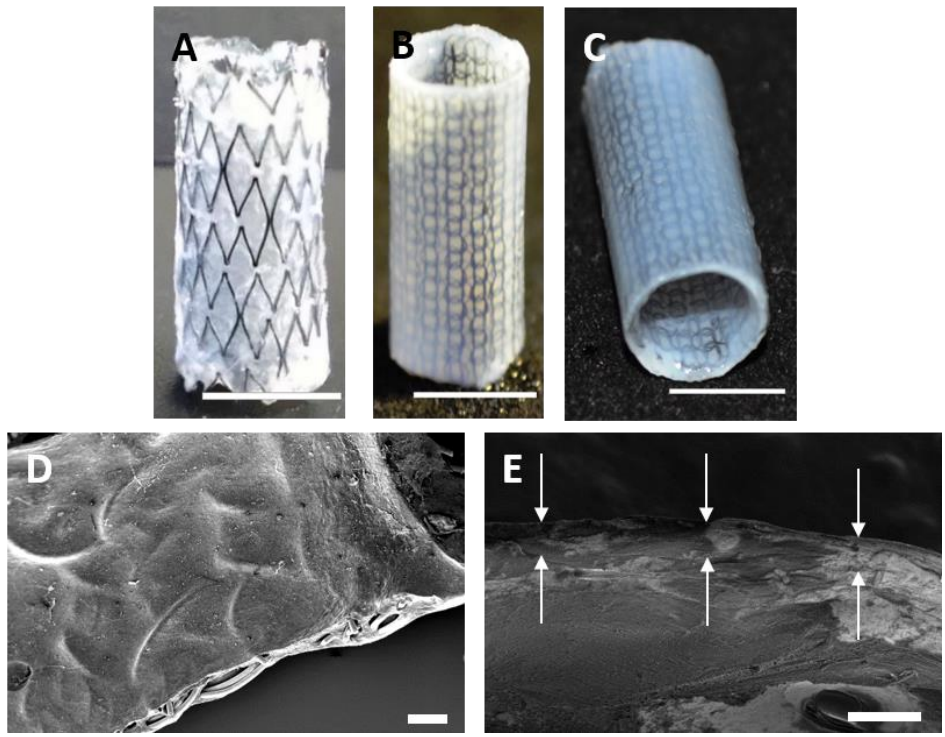

***Fig. 4**. Laser-cut stent (A) and warp-knitted nitinol stent (B, C) covered by ELR-CFCG. SEM image of an ELR-stent (D). Transversal view and SEM detail of the thickness of the gel coating the stent (G). Scale bars: 5 mm for pictures A, B and C, 200 µm for pictures D and E.*

3.4.Crimping and flow test

Exposure of the ELR-stents to a shear stress resulted in a difference in dry weight before and after the test of less than 0.1%. This means that the gels did not detach from the nitinol stent. Inspection under light microscopy did not reveal any damage. To verify the suitability of delivering the RGD- and REDV-devices through a catheter, they were crimped and deployed to the original diameter. Light microscopy and SEM investigation did not show any fracture or tear in the gel layers (Fig. 5A-B). Figure 5C shows a stent cut open to allow internal inspection. The lack of appreciable damage was evident on the inner surface of the stent.

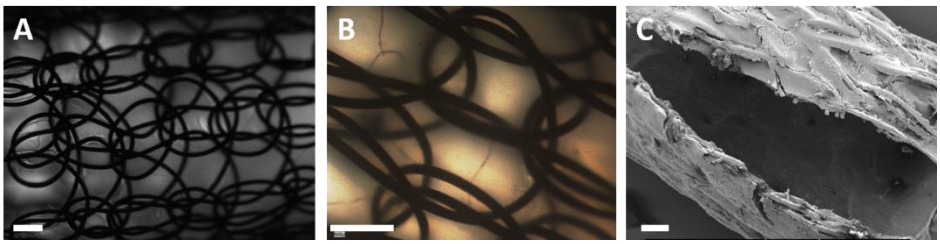

***Fig. 5**. A-B) light microscopy and C) SEM pictures of ELR-covered stents after crimping and flow test. Scale bars: 500 µm.*

3.5.Endothelialization

RGD-covered stents and REDV-covered stents were subjected to dynamic endothelialization for either 7 or 15 days. The levels of glucose decreased (from 5.5 to 5.0 mmol/L) and the levels of lactose raised from 0.6 mmol/L to 1.8 mmol/L. The pH values were around 7.2, and the levels of CO2 and O2 were maintained around 37mmHg and 160 mmHg, respectively. All these factors indicated cell growth and absence of contaminations.

LIVE/DEAD staining showed a high number of HUVECs colonizing the RGD-covered stents after 7 days. (Fig. 6 A). Cell proliferation onto REDV-covered stents after seven days (Fig. 6 C) was lower in agreement with the results from the proliferation test showed in Fig. 3. A confluent layer of HUVECs was achieved after fifteen days on RGD-covered stents (Fig. 6 B) but not for REDV-covered stents (Fig. 6 D). The presence of the RGD domain induces a better cell adhesion and proliferation than REDV sequence, also under dynamic conditions.

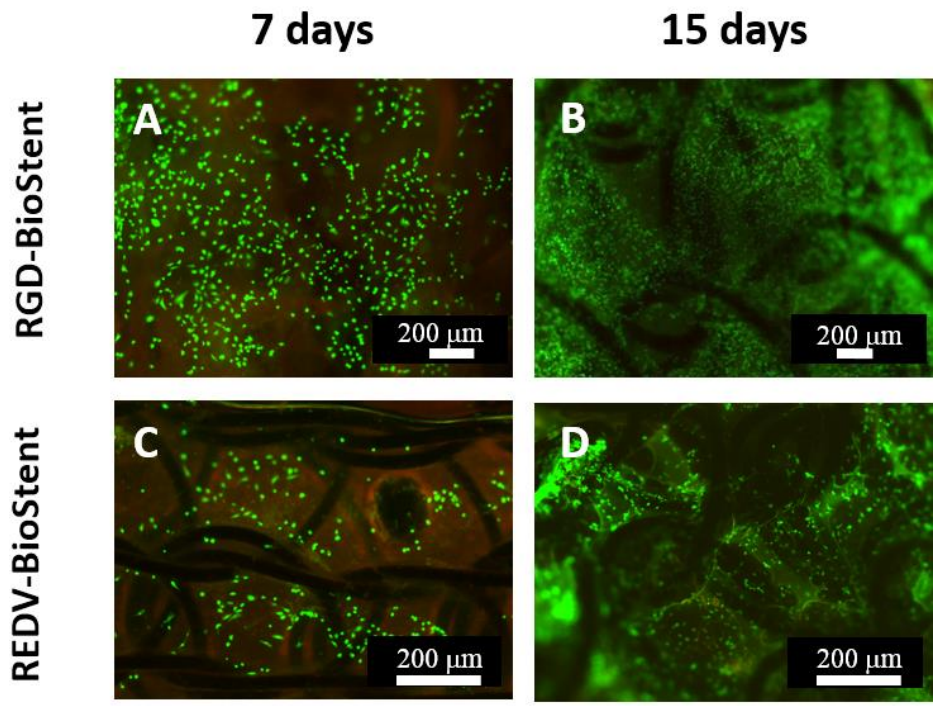

Fig. 6. *Micrographs of ELR-covered stents after Live/Dead staining of the HUVECs. RGD-covered stents after seven days (A) and fifteen days (B). REDV-covered stents after seven days (C) and fifteen days (D). Cells reached confluence after 15 days on RGD-covered stents. (B), but not on REDV-covered stents (D).*

3.6.Thrombogenicity assay

The reaction of blood components to the presence of the stent was evaluated by a thrombogenicity test. CD41/CD61 immunostaining for activated and adherent platelets was performed over Gore-Tex® control, RGD-covered stents and REDV-covered stents with and without endothelial cells. As can be seen in Figure 7, a high number of activated and adherent platelets were present on the Gore-Tex® control after 1 hour of blood contact. While in our devices, only few platelets were attached or activated on the gels surface (white arrows) with and without cell coverage. The endothelial cells were retained on the surface after exposure to physiological shear stress in the Chandler loop, however, ultimately

the strength of the attachment of the cells to the ELR layer has to be evaluated in vivo.

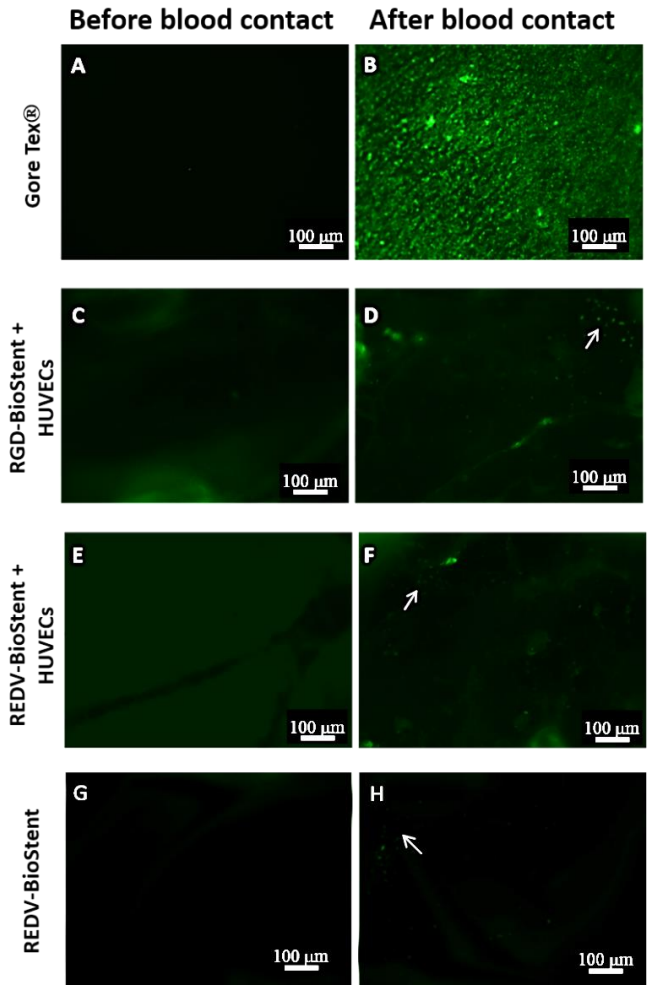

Fig. 7. *CD41/CD61 immunostaining for activated and adherent platelets in Gore Tex® control (A, B), RGD-covered stents (C, D),REDV-covered stents (E, F) after endothelialization and RGD-covered stents before endothelialization (G,H).*

The results offered by cd41/cd61 immunostaining test were corroborated by SEM investigation. A clear formation of a fibrin network (green-colored network) could be seen on BMS after the thrombogenicity assay (Fig. 8. B). Some thrombocytes can be seen helping the formation of the fibrin clot. Other blood components such as erythrocytes (red-colored cells) can be found on top the

fibrin. The presence of a fibrin network is evident on the Gore Tex® control as well (Fig. 8 D)

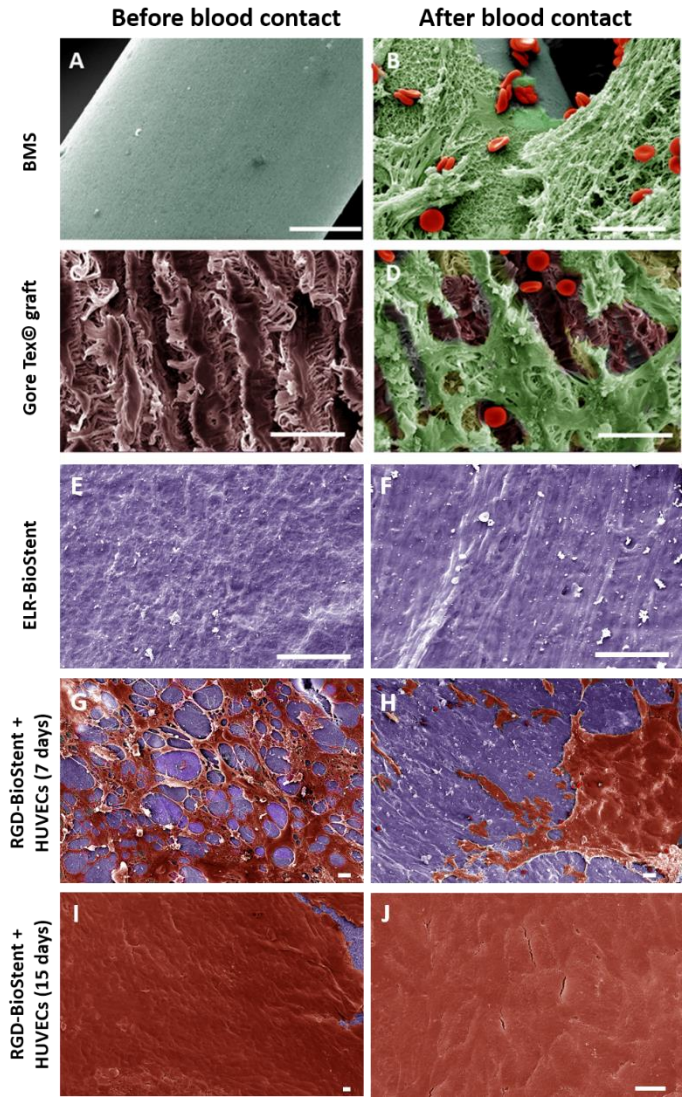

Fig. 8. *SEM pictures before and after thrombogenicity assays of warp-knitted BMS (A, B), Gore Tex® vascular graft (C, D), ELR-covered stents with no endothelialization (E, F) and ELR-covered stents during (G, H) and after (I, J) endothelialization. Scale bars 20 μm.*

The results on the BMS and Gore Tex® graft confirm the well-known insufficient hemocompatibility of these implants that contributes to (sub)acute thrombosis of BMS [73] and results in

high occlusion rates of synthetic small caliber grafts [74]. In clear contrast, minimal platelets adhesion and fibrinogen adsorption were detected on the surface of ELR-covered stents even without an endothelial cell layer (Fig. 8 F). These first results indicate that the new devices exhibit a high hemocompatibility, although blood clotting test should be performed to confirm this. It has been shown that elastin present in the vascular wall elicits minimal platelet adhesion and aggregation [75] and that intimal hyperplasia might be inhibited at the anastomoses of Dacron vascular grafts coated with tissue-derived elastin [76]. Minimal thrombogenicity of recombinant elastin polymers has also been reported in grafts coated with the polymers and exposed to the blood flow in a primate ex vivo shunt model [27]. Here we showed for the first time the suitability of newly developed ELRs to create covered stents. Considering that endothelial denudation at the site of endovascular intervention has been associated with thrombosis and intimal hyperplasia [77] and that, despite the advances in biomaterials development, the native endothelium remains the ideal surface for blood contact, we opted for an in vitro endothelialization of the stent to be performed prior to implantation. In this way, physiological hemocompatibility is achieved. The fact that also incomplete endothelial layers resulted in reduced thrombogeneicity (Fig. 8 H), suggests the possibility of an endovascular device to be seeded shortly before implantation, without in vitro culture, to guarantee the presence of ECs which will proliferate on the stent in vivo after implantation. This concept can be pushed further to a cell-free device capable of in vivo endothelialization by capturing EPCs. While the concept of mimicking the homing of EPCs can potentially revolutionize the field of implants in contact with blood, whether intra or extracorporeal, it completely relies on the use of

biomolecules that bind selectively and exclusively to EPCs. Although such molecules have not been identified yet, we do not have concerns about the possibility of including them by recombinant techniques or by chemical modification in ELRs, which would then form the inherently non-thrombogenic surface of the device. Furthermore, ELR-CFCGs fit well in the strategies for the next generations of stents like the drug-eluting stents, as they could, for example, embed drugs to be released over time to support the healing process.

4. CONCLUSIONS

Restenosis and thrombosis after stent implantation remain important clinical complications, which drive continuous development in the field of interventional cardiology and radiology. We have shown the applicability of recently developed ELR-CFCGs as coating for vascular stents with the ultimate goal of producing a new endovascular device featuring 1) a physical barrier for the atherosclerotic plaque; 2) physiological hemocompatibility; 3) mechanical stability. The new ELR-covered stents presented here open the door to a more effective generation of covered stents for the treatment of peripheral vascular disease and conditions such as aneurysms, fistulae, ruptures and perforations also in coronary and cerebral vessels. However, the potentially non-inflammatory nature of the ELRs covered stents still needs to be tested in-vivo.

Furthermore, the ELR-CFCG coating fits well in the currently developing strategies for the next generations of stents such as drug-eluting and EPCs capturing stents. Indeed, the ELR-CFCG could incorporate bioactive compounds to be released over time to support the healing process and their inherent hemocompatibility

together with the possibility of inserting the desired bioactive sequences are crucial properties towards the realization of stents capable of in-vivo self-endothelialization. These options will be explored in future investigations in our groups as well as in vivo assays to test the benefits of this novel generation of biocompatible stents.

5. ACKNOWLEDGEMENTS

We acknowledge financial support from the EU through the European regional development fund (ERDF), from the MINECO (MAT-2010-15982, MAT2010-15310, PRI-PIBAR-2011-1403 and MAT2012-38043), the JCyL (projects VA049A11, VA152A12 and VA155A12), the CIBER-BBN, and the JCyL and the Instituto de Salud Carlos III under the "Network Center of Regenerative Medicine and Cellular Therapy of Castilla and Leon". Funding was also provided by IZKF Aachen (Interdisciplinary Centre for Clinical Research) of the Medical Faculty of the RWTH Aachen University and by the German Research Foundation (DFG, MTBo07) a within the excellence initiative.

6. REFERENCES

1. Curcio A, Torella D, Indolfi C. Mechanisms of smooth muscle cell proliferation and endothelial regeneration after vascular injury and stenting: approach to therapy. Circ J. 2011;75(6):1287-96.

2. Sigwart U, Puel J, Mirkovitch V, Joffre F, Kappenberger L. Intravascular Stents to Prevent Occlusion and Re-Stenosis after Transluminal Angioplasty. N. Engl. J. Med.. 1987;316(12):701-6.

3. Kornowski R, Hong MK, Tio FO, Bramwell O, Wu H, Leon MB. In-Stent Restenosis: Contributions of Inflammatory Responses and Arterial Injury to Neointimal Hyperplasia. J. Am. Coll. Cardiol. 1998;31(1):224-30.

4. Farb A, Sangiorgi G, Carter AJ, Walley VM, Edwards WD, Schwartz RS, et al. Pathology of Acute and Chronic Coronary Stenting in Humans. Circulation. 1999;99(1):44-52.

5. Pfisterer M, Brunner-La Rocca H, Buser P, Rickenbacher P, Hunziker P, Mueller C, et al. Late clinical events after clopidogrel discontinuation may limit the benefit of drug-eluting stents: an observational study of drug-eluting versus bare-metal stents. J. Am. Coll. Cardiol. 2006;48(12):2584-91.

6. Urfman, G. D.; Morrissey, S.; Jarcho, J. A.; Drazen, J. M., Drug-Eluting Coronary Stents — Promise and Uncertainty. New England Journal of Medicine 2007, 356, (10), 1059-1060.

7. Stefanini, G. G.; Holmes, D. R., Drug-Eluting Coronary-Artery Stents. New England Journal of Medicine 2013, 368, (3), 254-265

8. Kutryk MJB, Kuliszewski MA. In vivo endothelial progenitor cell seeding for the accelerated endothelialization of endovascular devices. Am J Cardiol. 2003;92(6A):94l-5l.

9. Avci-Adali M, Stoll H, Wilhelm N, Perle N, Schlensak C, Wendel HP. In vivo tissue engineering: mimicry of homing factors for self-endothelialization of blood-contacting materials. Pathobiology. 2013;80(4):176-81.

10. Wendel HP, Avci-Adali M, Ziemer G. Endothelial progenitor cell capture stents--hype or hope? Int. J. Cardiol.. 2010;145(1):115-7; author reply 7-8.

11. Hagensen MK, Raarup MK, Mortensen MB, Thim T, Nyengaard JR, Falk E, et al. Circulating endothelial progenitor cells do not contribute to regeneration of endothelium after murine arterial injury. Cardiovascular res. 2012;93(2):223-31.

12. Heleen, M. M. v. B.; Gökhan, E.; Oana, S.; Patrick, W. S.; Willem, J. v. d. G., The Genous™ endothelial progenitor cell capture stent accelerates stent re-endothelialization but does not affect intimal

hyperplasia in porcine coronary arteries. Catheter Cardiovasc Interv2012; 79: 231-42.

13. Briguori C, Sarais C, Sivieri G, Takagi T, Di Mario C, Colombo A. Polytetrafluoroethylene-covered stent and coronary artery aneurysms. Catheter Cardiovasc Interv. 2002;55(3):326-30.

14. Nakayama Y, Nishi S, Ueda-Ishibashi H, Matsuda T. Fabrication of micropored elastomeric film-covered stents and acute-phase performances. J. Biomed. Mater. Res., Part A. 2003;64(1):52-61.

15. Nagai N, Nakayama Y, Nishi S, Munekata M. Development of novel covered stents using salmon collagen. J. Artif. Organs. 2009;12(1):61-6.

16. McKenna C, Camrud A, Sangiorgi G, Kwon H, Edwards W, Holmes D, et al. Fibrin-film stenting in a porcine coronary injury model: efficacy and safety compared with uncoated stents. J. Am. Coll. Cardiol.. 1998;31(6):1434-8.

17. Bueno RR, Tanguay JF, Brito FS, Jr., Guerios EE, Tarastchuk JE, Sanches PA, et al. Evaluation of the efficacy and safety of a stent covered with biosynthetic cellulose in a rabbit iliac artery model. J Invasive Cardiol. 2009;21(8):392-6.

18. Thierry B, Merhi Y, Silver J, Tabrizian M. Biodegradable membrane-covered stent from chitosan-based polymers. J Biomed Mater Res A. 2005;75(3):556-66.

19. Stefanadis C, Toutouzas K, Tsiamis E, Vlachopoulos C, Vaina S, Tsekoura D, et al. Stents covered by an autologous arterial graft in porcine coronary arteries: feasibility, vascular injury and effect on neointimal hyperplasia. Cardiovascular res. 1999;41(2):433-42.

20. Weinandy S, Rongen L, Schreiber F, Cornelissen C, Flanagan TC, Mahnken A, et al. The BioStent: novel concept for a viable stent structure. Tissue Eng., Part A. 2012;18(17-18):1818-26.

21. Nakayama Y, Zhou YM, Ishibashi-Ueda H. Development of in vivo tissue-engineered autologous tissue-covered stents (biocovered stents). J. Artif. Organs. 2007;10(3):171-6.

22. Elsner M, Auch SchwelkW,BrittenM, et al.Coronary stent grafts covered

by a polytetrafluoroethylene membrane. Am J Cardiol 1999;84:335–8.

23. Jamshidi P, Mahmoody K, Erne P. Covered stents: a review. International journal of cardiology 2008;130:310-8.

24. Antonello M, Frigatti P, Battocchio P, Lepidi S, Cognolato D, Dall'Antonia A, et al. Open repair versus endovascular treatment for asymptomatic popliteal artery aneurysm: results of a prospective randomized study. Journal of vascular surgery 2005;42:185-93

25. Rodríguez-Cabello JC, Martín L, Alonso M, Arias FJ, Testera AM. "Recombinamers" as advanced materials for the post-oil age. Polymer. 2009;50(22):5159-69.

26. Urry DW. Molecular Machines - How Motion and Other Functions of Living Organisms Can Result from Reversible Chemical-Changes. Angew. Chem., Int. Ed. Engl.. 1993;32(6):819-41.

27. Jordan SW, Haller CA, Sallach RE, Apkarian RP, Hanson SR, Chaikof EL. The effect of a recombinant elastin-mimetic coating of an ePTFE prosthesis on acute thrombogenicity in a baboon arteriovenous shunt. Biomaterials. 2007;28(6):1191-7.

28. Woodhouse KA, Klement P, Chen V, Gorbet MB, Keeley FW, Stahl R, et al. Investigation of recombinant human elastin polypeptides as non-thrombogenic coatings. Biomaterials. 2004;25(19):4543-53.

29. Rodriguez-Cabello JC, Martin L, Girotti A, Garcia-Arevalo C, Arias FJ, Alonso M. Emerging applications of multifunctional elastin-like recombinamers. Nanomedicine (London, U K). 2011;6(1):111-22.

30. Shokouhi B, Coban C, Hasirci V, Aydin E, Dhanasingh A, Shi N, et al. The role of multiple toll-like receptor signalling cascades on interactions between biomedical polymers and dendritic cells. Biomaterials. 2010;31(22):5759-71.

31. García-Arévalo C, Bermejo-Martín JF, Rico L, Iglesias V, Martín L, Rodríguez-Cabello JC, et al. Immunomodulatory Nanoparticles from Elastin-Like Recombinamers: Single-Molecules for Tuberculosis Vaccine Development. Mol. Pharmaceutics. 2013;10(2):586-97.

32. Bessa PC, Machado R, Nurnberger S, Dopler D, Banerjee A, Cunha AM, et al. Thermoresponsive self-assembled elastin-based nanoparticles for delivery of BMPs. J Controlled Release. 2009.

33. Dreher MR, Raucher D, Balu N, Colvin OM, Ludeman SM, Chilkoti A. Evaluation of an elastin-like polypeptide-doxorubicin conjugate for cancer therapy. J Controlled Release. 2003;91(1-2):31-43.

34. Wu Y, MacKay JA, McDaniel JR, Chilkoti A, Clark RL. Fabrication of elastin-like polypeptide nanoparticles for drug delivery by electrospraying. Biomacromolecules. 2009;10(1):19-24.

35. Singh AK, Srivastava GK, Martín L, Alonso M, Pastor JC. Bioactive substrates for human retinal pigment epithelial cell growth from elastin-like recombinamers. J. Biomed. Mater. Res., Part A. 2013:n/a-n/a.

36. Jeon W, Park B, Wei J, Park R-W. Stimulation of fibroblasts and neuroblasts on a biomimetic extracellular matrix consisting of tandem repeats of the elastic VGVPG domain and RGD motif. J. Biomed. Mater. Res., Part A. 2011;97(2):152-7.

37. McKegney FP, Schwartz BJ, O'Dowd MA. Reducing unnecessary psychiatric consultations for informed consent by liaison with administration. Gen Hosp Psychiat. 1992;14(1):15-9.

38. Betre H, Setton LA, Meyer DE, Chilkoti A. Characterization of a genetically engineered elastin-like polypeptide for cartilaginous tissue repair. Biomacromolecules. 2002;3(5):910-6.

39. Martínez-Osorio H, Juárez-Campo M, Diebold Y, Girotti A, Alonso M, Arias F, et al. Genetically engineered elastin-like polymer as a substratum to culture cells from the ocular surface. Curr. Eye Res. 2009;34(1):48-56.

40. Liu J, Tirrell D. Cell response to RGD density in cross-linked artificial extracellular matrix protein films. Biomacromolecules. 2008;9(11):2984-8.

41. González de Torre I, Santos M, Quintanilla L, Testera A, Alonso M, Rodríguez Cabello JC. Elastin-Like Recombinamers Catalyst-Free Click Gels: Characterization of poroelastic and intrinsic viscoelastic properties. Acta Biomater. 2014.

42. Huisgen R. 1,3-Dipolar Cycloadditions. Past and Future. Angew. Chem., Int. Ed. Engl. 1963;2(10):565-98.

43. Kolb HC, Finn MG, Sharpless KB. Click Chemistry: Diverse Chemical Function from a Few Good Reactions. Angew. Chem., Int. Ed. 2001;40(11):2004-21.

44. Zou Y, Yin J. Cu-free cycloaddition for identifying catalytic active adenylation domains of nonribosomal peptide synthetases by phage display. Bioorg. Med. Chem. Lett. 2008;18(20):5664-7.

45. Link AJ, Vink MK, Agard NJ, Prescher JA, Bertozzi CR, Tirrell DA. Discovery of aminoacyl-tRNA synthetase activity through cell-surface display of noncanonical amino acids. Proc. Natl. Acad. Sci. U. S. A. 2006;103(27):10180-5.

46. Baskin JM, Bertozzi CR. Bioorthogonal Click Chemistry: Covalent Labeling in Living Systems. QSAR Comb. Sci. 2007;26(11-12):1211-9.

47. Dehnert K, Baskin J, Laughlin S, Beahm B, Naidu N, Amacher S, et al. Imaging the sialome during zebrafish development with copper-free click chemistry. Chembiochem. 2012;13(3):353-7.

48. Matthew W, John M, Ying-Chuan L, Steven MS, William L, Arthur JO, et al. Inhibitors of HIV-1 Protease by Using In Situ Click Chemistry. Angew. Chem.. 2006;118.

49. Wenge U, Ehrenschwender T, Wagenknecht H-A. Synthesis of 2'-O-propargyl nucleoside triphosphates for enzymatic oligonucleotide preparation and "click" modification of DNA with nile red as fluorescent probe. Bioconjugate Chem. 2013;24(3):301-4.

50. Laughlin ST, Baskin JM, Amacher SL, Bertozzi CR. In vivo imaging of membrane-associated glycans in developing zebrafish. Science. 2008;320(5876):664-7.

51. Pierna M, Santos M, Arias F, Alonso M, Rodriguez-Cabello J. Efficient cell and cell-sheet harvesting based on smart surfaces coated with a multifunctional and self-organizing Elastin-Like Recombinamer. Biomacromolecules. 2013.

52. Chandler A. In vitro thrombotic coagulation of the blood; a method for producing a thrombus. Lab. Invest. 1958;7(2):110-4.

53. Christensen K, Larsson R, Emanuelsson H, Elgue G, Larsson A. Coagulation and complement activation. Biomaterials. 2001;22(4):349-55.

54. Girotti A, Reguera J, Rodriguez-Cabello JC, Arias FJ, Alonso M, Matestera A. Design and bioproduction of a recombinant multi(bio)functional elastin-like protein polymer containing cell adhesion sequences for tissue engineering purposes. J Mater Sci Mater Med. 2004;15(4):479-84.

55. Costa R, Custódio C, Arias F, Rodríguez-Cabello J, Mano J. Layer-by-layer assembly of chitosan and recombinant biopolymers into biomimetic coatings with multiple stimuli-responsive properties. Small. 2011;7(18):2640-9.

56. Darby R. Chemical engineering fluids mechanics. In: Press C, editor.2001. p. 559

57. Gong J, Larsson R, Ekdahl K, Mollnes T, Nilsson U, Nilsson B. Tubing loops as a model for cardiopulmonary bypass circuits: both the biomaterial and the blood-gas phase interfaces induce complement activation in an in vitro model. J. Clin. Immunol. 1996;16(4):222-9.

58. Gaamangwe, T.; Peterson, S.; Gorbet, M., Investigating the Effect of Blood Sample Volume in the Chandler Loop Model: Theoretical and Experimental Analysis. Cardiovasc Eng Tech 2014, 5 (2), 133-144.

59. Meyvis T, Stubbe B, Van Steenbergen M, Hennink W, De Smedt S, Demeester J. A comparison between the use of dynamic mechanical analysis and oscillatory shear rheometry for the characterisation of hydrogels. Int. J. Pharm. 2002;244(1-2):163-8.

60. Kavanagh GM, Ross-Murphy SB. Rheological characterization of polymer gels. Prog. Polym. Sci. 1998; 23(3):533 - 62.

61. Tschoegl NW. The phenomenological theory of linear viscoelastic behavior : an introduction. Springer-Verlag: Berlin ; New York. 1989.

62. Trabbic-Carlson K, Setton LA, Chilkoti A. Swelling and mechanical behaviors of chemically cross-linked hydrogels of elastin-like polypeptides. Biomacromolecules. 2003;4(3):572-80.

63 Saunders R, Hammer D. Assembly of Human Umbilical Vein Endothelial Cells on Compliant Hydrogels. Cell Mol Bioeng. 2010;3(1):60-7.

64. Wei Y, Ji Y, Xiao L-L, Lin Q-k, Xu J-p, Ren K-f, et al. Surface engineering of cardiovascular stent with endothelial cell selectivity for in vivo re-endothelialisation. Biomaterials. 2013;34(11):2588-99.

65. Ceylan H, Tekinay A, Guler M. Selective adhesion and growth of vascular endothelial cells on bioactive peptide nanofiber functionalized stainless steel surface. Biomaterials. 2011;32(34):8797-805.

66. Kakegawa T, Mochizuki N, Sadr N, Suzuki H, Fukuda J. Cell-adhesive and cell-repulsive zwitterionic oligopeptides for micropatterning and rapid electrochemical detachment of cells. Tissue Eng., Part A Part A. 2013;19(1-2):290-8.

67. Wohlrab S, Müller S, Schmidt A, Neubauer S, Kessler H, Leal-Egaña A, et al. Cell adhesion and proliferation on RGD-modified recombinant spider silk proteins. Biomaterials. 2012;33(28):6650-9.

68. Conconi M, Ghezzo F, Dettin M, Urbani L, Grandi C, Guidolin D, et al. Effects on in vitro and in vivo angiogenesis induced by small peptides carrying adhesion sequences. J. Pept. Sci. 2010;16(7):349-57.

69. Nardecchia S, Gutierrez MC, Ferrer ML, Alonso M, Lopez IM, Rodriguez-Cabello JC, et al. Phase behavior of elastin-like synthetic recombinamers in deep eutectic solvents. Biomacromolecules. 2012;13(7):2029-36.

70. Martin L, Castro E, Ribeiro A, Alonso M, Rodriguez-Cabello JC. Temperature-triggered self-assembly of elastin-like block co-recombinamers:the controlled formation of micelles and vesicles in an aqueous medium. Biomacromolecules. 2012;13(2):293-8.

71. Huang L, McMillan RA, Apkarian RP, Pourdeyhimi B, Conticello VP, Chaikof EL. Generation of Synthetic Elastin-Mimetic Small Diameter Fibers and Fiber Networks. Macromolecules. 2000;33(8):2989-97.

72. Martin L, Alonso M, Moeller M, Rodriguez-Cabello JC, Mela P. 3D microstructuring of smart bioactive hydrogels based on recombinant elastin-like polymers. Soft Matter. 2009;5(8):1591-3.

73. Uribe González J, Peña Duque M, Larraga M. Early stenosis in a Gore-Tex graft connected to the left main: an emergency transradial angioplasty for a complication in a Cabrol procedure. J Invasive Cardiol. 2012;24(10):539-42.

74. Zilla P, Bezuidenhout D, Human P. Prosthetic vascular grafts: wrong models, wrong questions and no healing. Biomaterials. 2007;28(34):5009-27.

75. Barnes MJ, MacIntyre DE. Platelet-reactivity of isolated constituents of the blood vessel wall. Haemostasis. 1979;8(3-5):158-70.

76. Ito S, Ishimaru S, Wilson SE. Application of coacervated alpha-elastin to arterial prostheses for inhibition of anastomotic intimal hyperplasia. ASAIO J. 1998;44(5):M501-5.

77 Kipshidze N, Dangas G, Tsapenko M, Moses J, Leon MB, Kutryk M, et al. Role of the endothelium in modulating neointimal formation: vasculoprotective approaches to attenuate restenosis after percutaneous coronary interventions. J. Am. Coll. Cardiol. 2004;44:733-9.

7. SUPPORTING INFORMATION

7.1.Materials

7.1.1. ELR bioproduction

ELR production was carried out using genetic-engineered protein biosynthesis in Escherichia Coli, while its purification was performed with several cycles of temperature-depending reversible precipitations as described elsewhere[1].

[1] Girotti, A.; Reguera, J.; Arias, J.; Alonso, M.; Testera, A.M. and Rodríguez-Cabello, J.C. "Influence of the Molecular Weight on the Inverse Temperature Transition of a Model Genetically Engineered Elastin-like pH-Responsive Polymer". Macromolecules (2004), 37, 3396-3400

7.2.Instrumental methods

7.2.1. Proton nuclear magnetic resonance 1H- and 13C-NMR Spectroscopy

NMR analysis was carried out using a 400 MHz Agilent Technologies equipment with an Agilent MR console 400 and a One NMR probe. The measurements were carried out at 298 K with samples of 20–30 mg of the modified elastin like recombinamers, purified, and dissolved in DMSO-d6. Chemical shifts (δ) are given in ppm.

The nondeuterated dimethyl sulfoxide peaks at d = 2.5 ppm, and d = 39.51 ppm were used as internal reference for 1H and 13C NMR spectra, respectively.

7.2.2. Fourier Transform Infrared Spectroscopy (FTIR).

FTIR analysis was conducted with a Bruker FTIR spectrophotometer (Bruker, USA). For each spectrum, a 512-scan interferogram was collected at single beam absorption mode with a 2 cm^{-1} resolution within the 4000- 600 cm^{-1} region. For each sample several FTIR absorption spectra were collected. Five measurements were averaged to obtain the final FTIR absorption spectrum of the sample. Residual water vapour absorption was interactively subtracted from the sample spectra.

Spectral calculations were performed by the OPUS (version 4.2) software (MATTSON INSTRUMENT, INC.).

7.2.3. . Differential Scanning Calorimetry (DSC) measurements

DSC experiments were performed on a Mettler Toledo 822^e DSC with a liquid nitrogen cooler accessory.

Both temperature and enthalpy were calibrated with an indium standard at the same experimental conditions used for the studied materials. Water solutions of ELRs at 50 mg mL^{-1} were prepared at different values of pH. In a typical DSC run, 20 µL of the solution was placed inside a standard 40 µL aluminium pan hermetically sealed. The same volume of water was placed in the

reference pan. As for ELR-hydrogel analysis, 20 mg of the hydrated hydrogel was placed in the sample pan. To account for the exact amount of polymer in the assayed hydrogel, the sample was lyophilized and weighted after DSC run.

All samples were equilibrated for 10 min at 0ºC inside the sample chamber just before the beginning of each experiment, and then, heated from 0 to 60 ºC at a heating rate of 5ºC/min. The scans were run under a nitrogen atmosphere.

7.3.Characterization of modified-ELRs

7.3.1. VKVx24 modifications

7.3.1.1. Azide modifications

A)

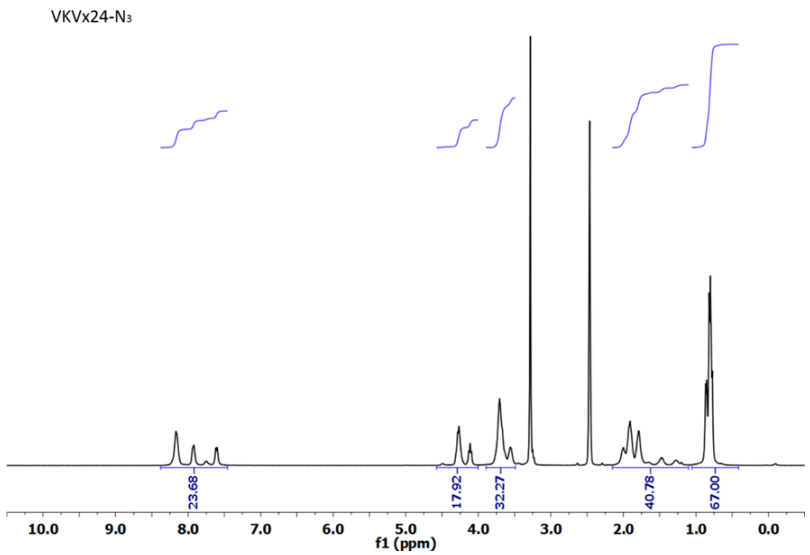

B)

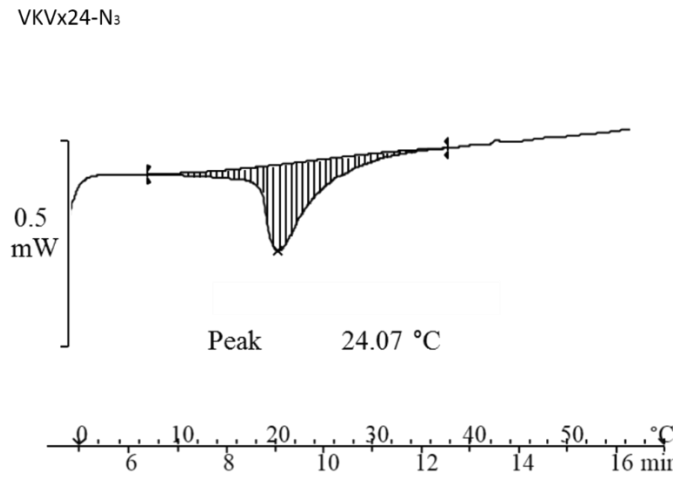

C)

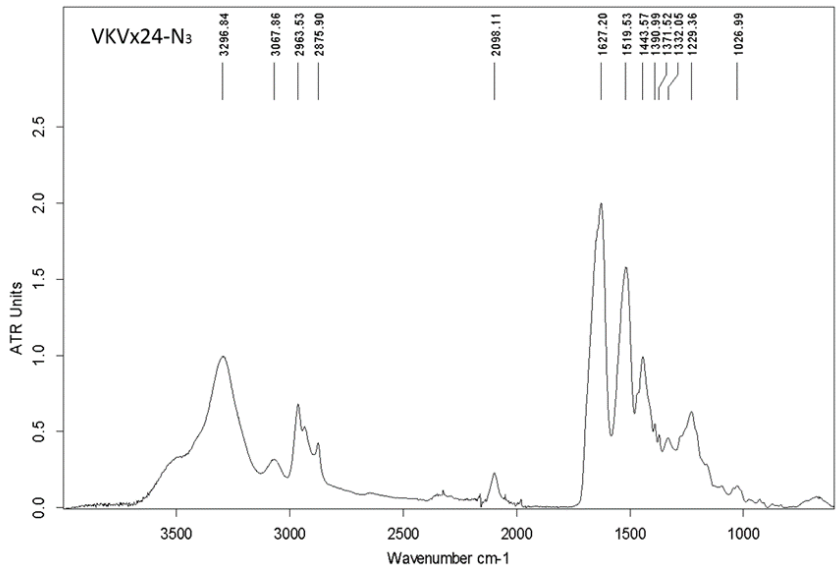

Fig. 1 ^{1}H-NMR (DMSO-d_6) spectrum (A), DSC thermogram (B) and FTIR spectrum (C) for VKVx24-N_3

7.3.1.2. Cyclooctine modifications

A)

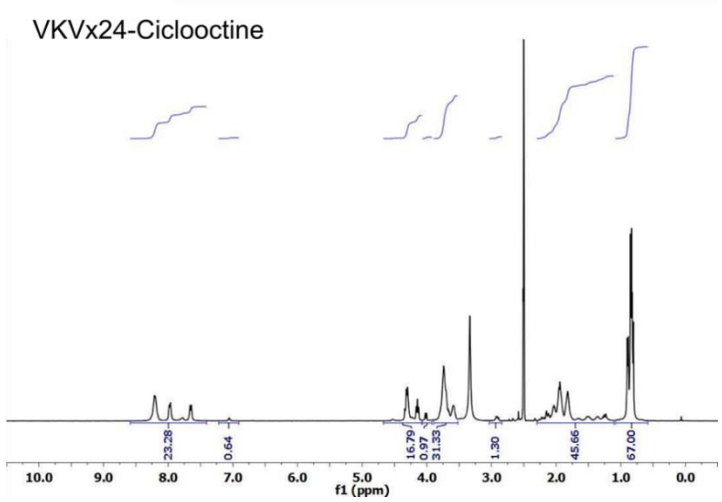

B)

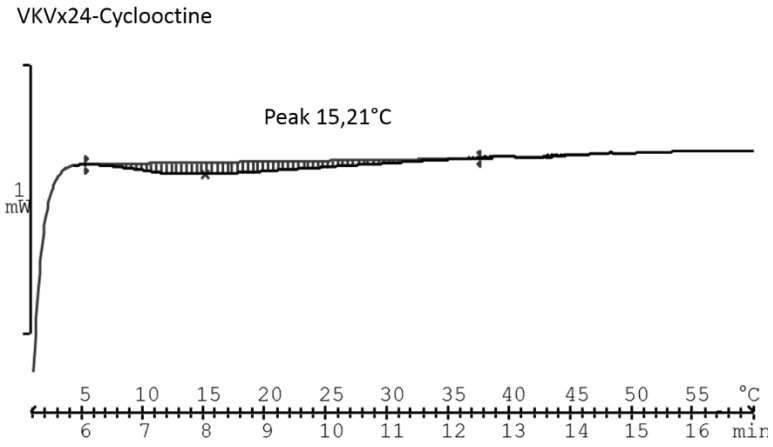

C)

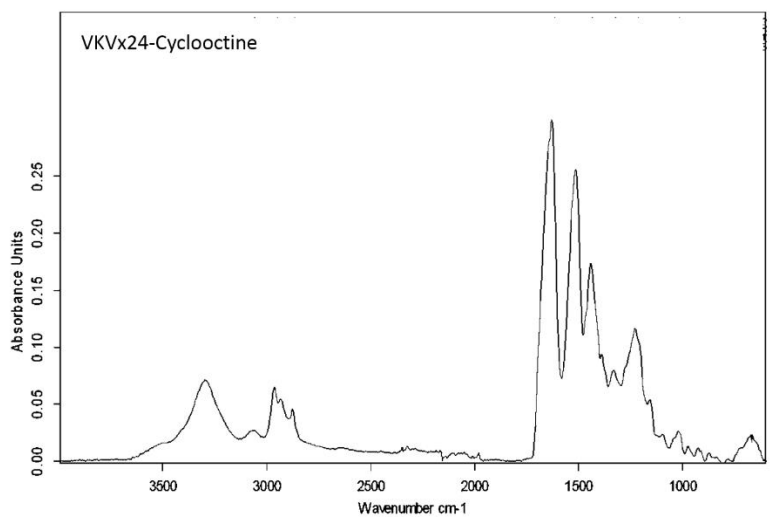

Fig. 2 ^{1}H-NMR (DMSO-d6) spectrum (A), DSC thermogram (B) and FTIR spectrum (C) for VKVx24-cyclooctine.

7.3.2. HRGD modifications

7.3.2.1. Azide modifications

A)

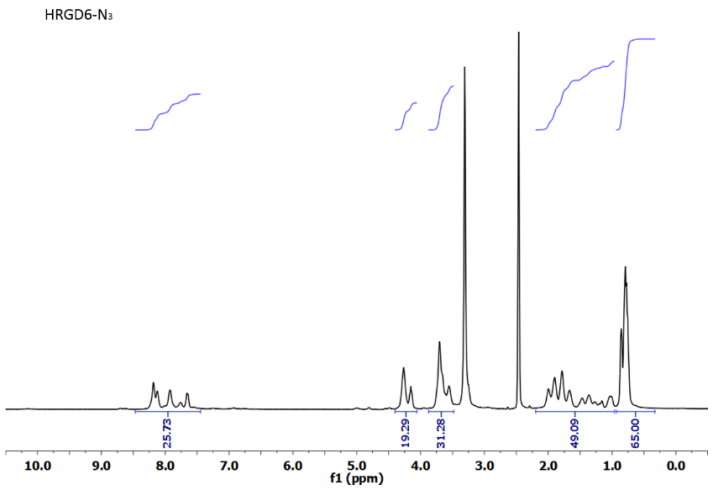

B)

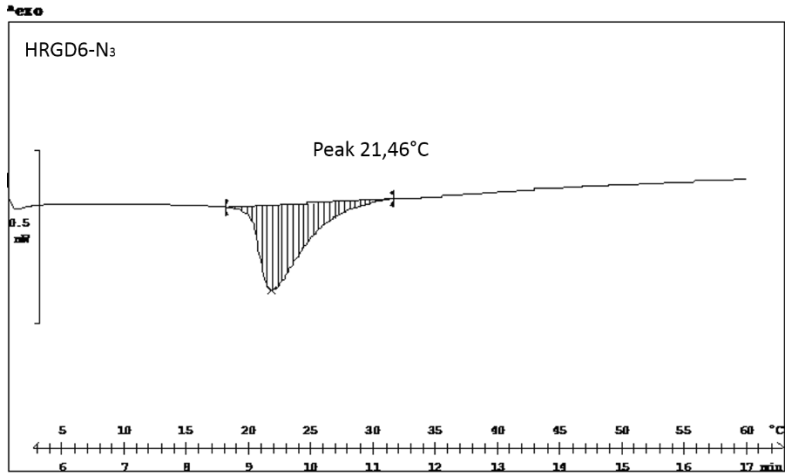

C)

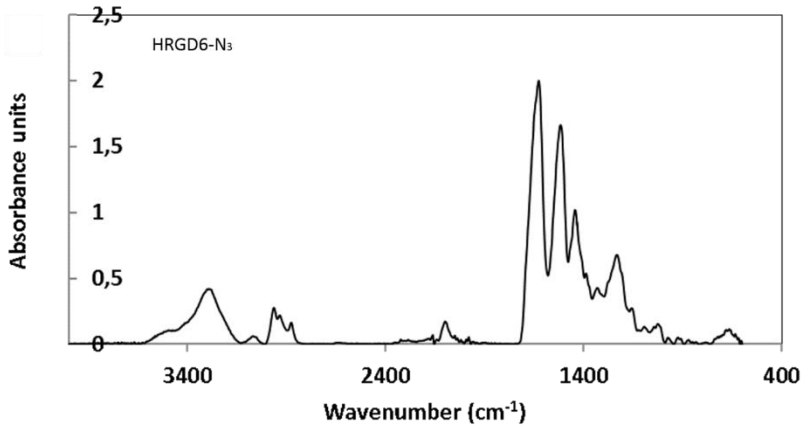

Fig. 3 ^{1}H-NMR (DMSO-d_6) spectrum (A), DSC thermogram (B) and FTIR spectrum (C) for HRGD6-N_3

7.3.2.2. Cyclooctine modifications

A)

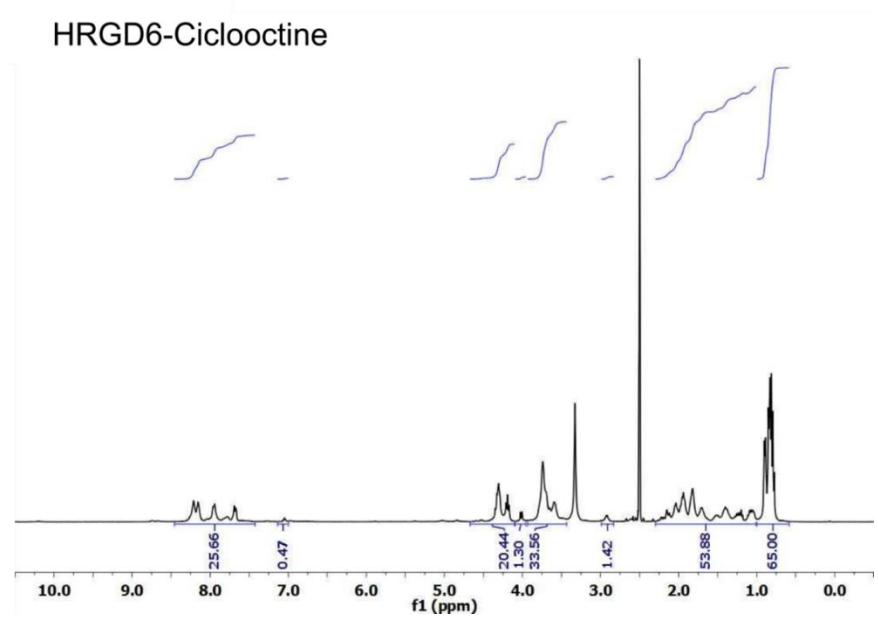

B)

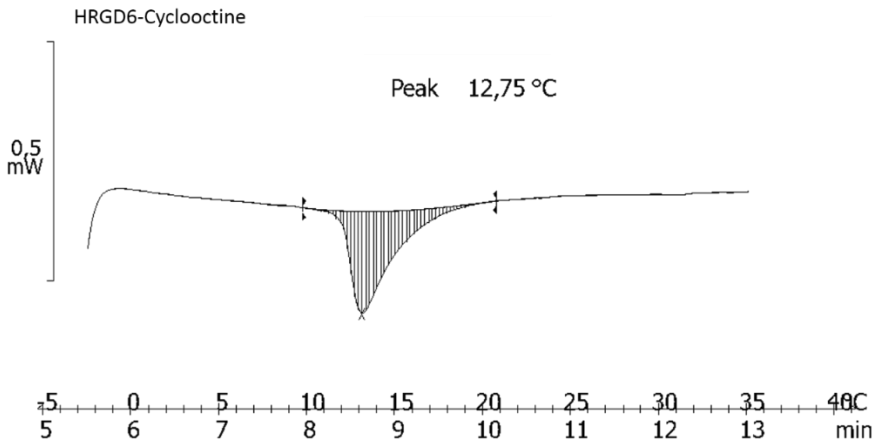

C)

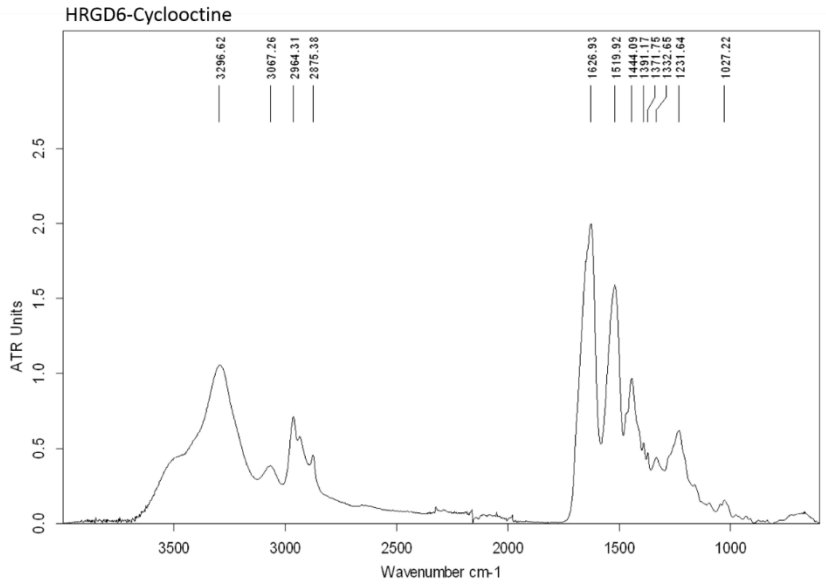

Fig. 4 ^{1}H-NMR (DMSO-d_6) spectrum (A), DSC thermogram (B) and FTIR spectrum (C) for HRGD6-cyclooctine**.**

7.3.3. REDVx10 modifications

7.3.3.1. Azide modifications

A)

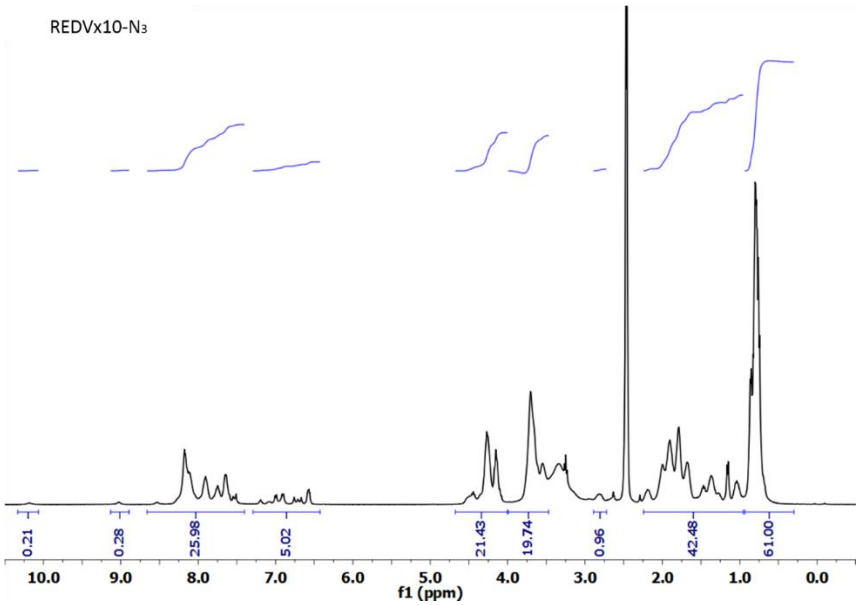

B)

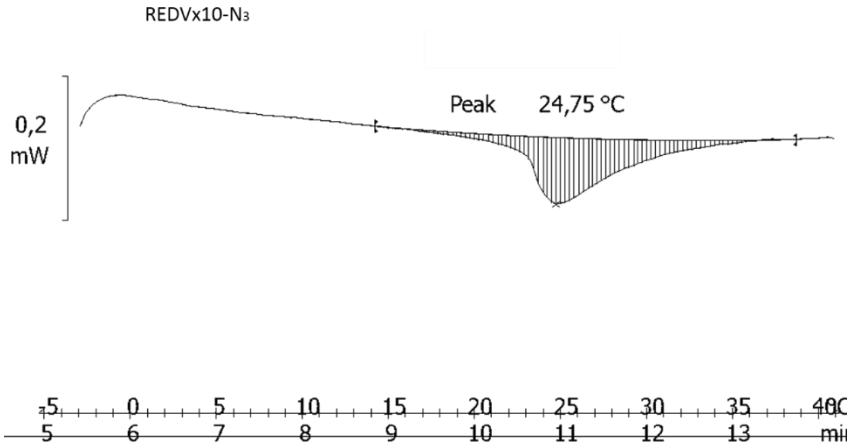

C)

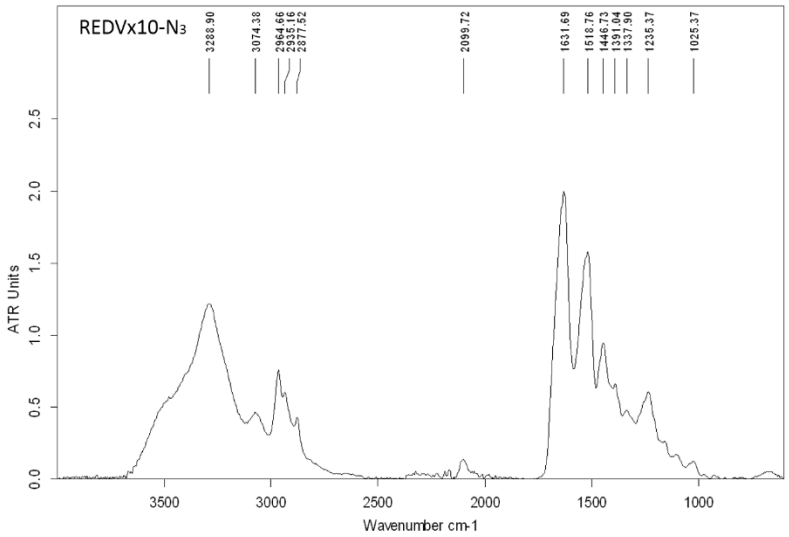

Fig. 5 ^{1}H-NMR (DMSO-d_6) spectrum (A), DSC thermogram (B) and FTIR spectrum (C) for REDVx10-N_3

7.3.3.2. Cyclooctine modifications

A)

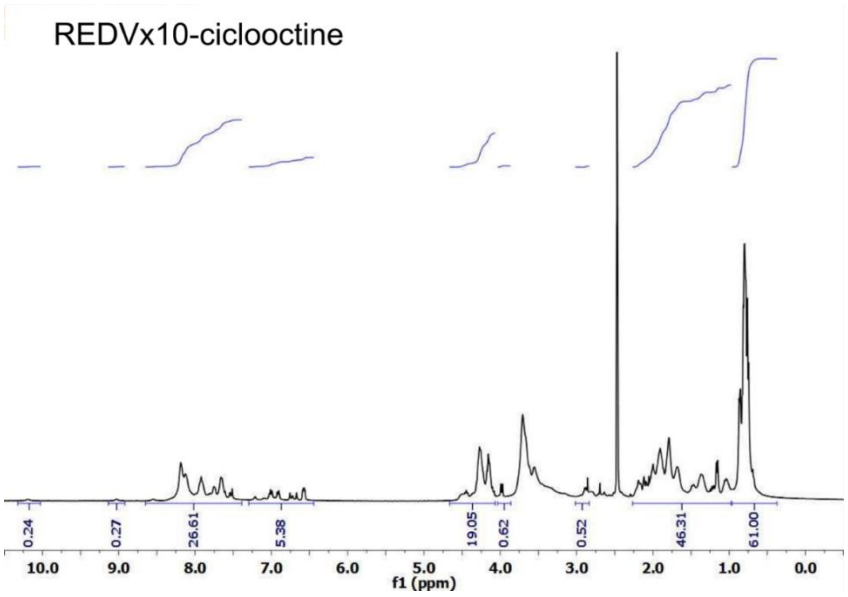

B)

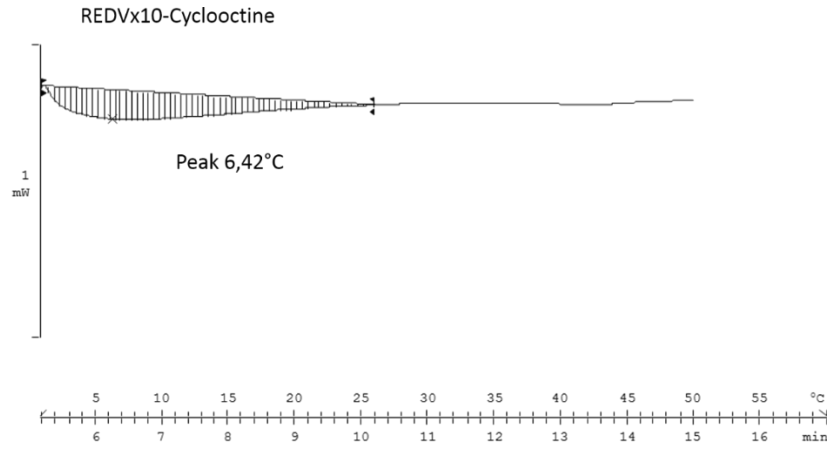

C)

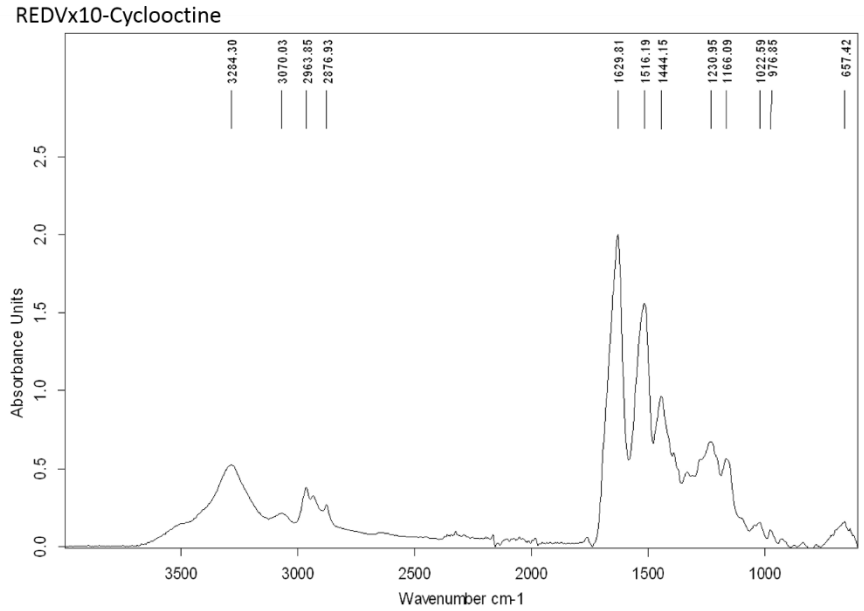

Fig. 6 ^{1}H-NMR (DMSO-d_6) spectrum (A), DSC thermogram (B) and FTIR spectrum (C) for REDVx10-cyclooctine.

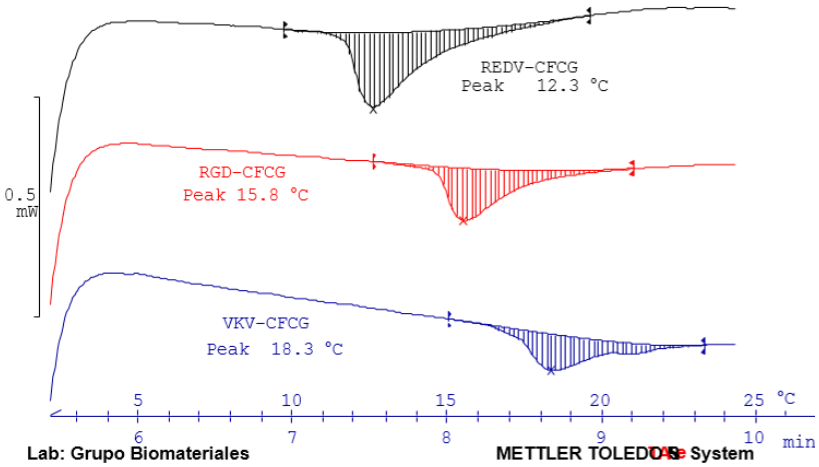

Fig. 7 DSC thermograms for VKV-CFCGs, RGD-CFCGs and REDV-CFCG.

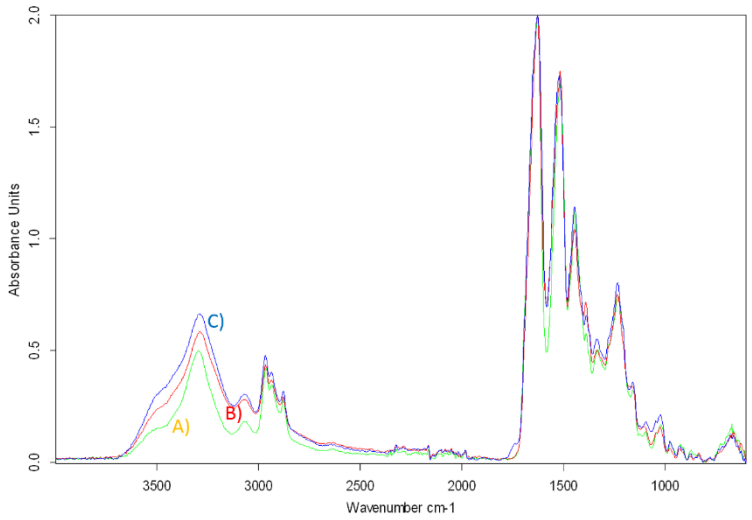

Fig. 8 FTIR spectrum for VKV-CFCGs (A), RGD-CFCGs (B) and REDV-CFCG (C).

7.4.Rheological results

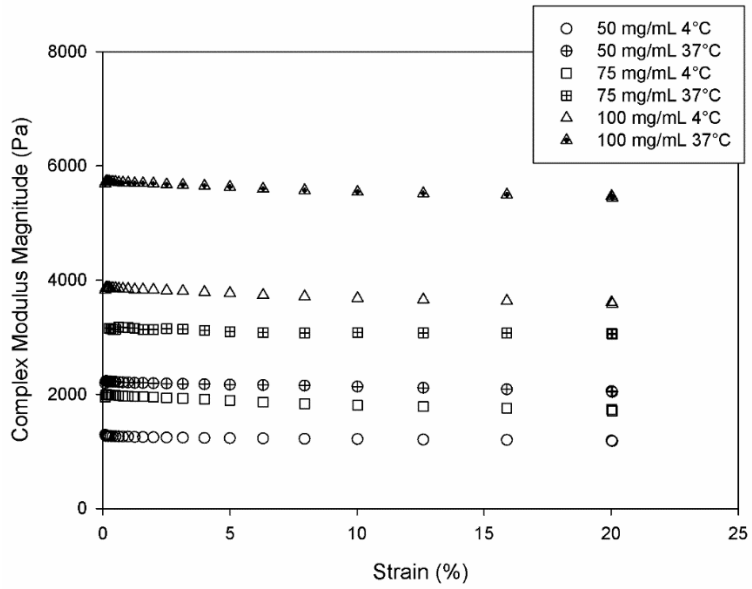

Fig. 9 Complex module magnitude at a frequency of 1 Hz as a function of the strain amplitude at 4°C and 37°C for ELR-CFCGs with recombinamer concentrations of 50 mg/mL, 75 mg/mL and 100 mg/mL.

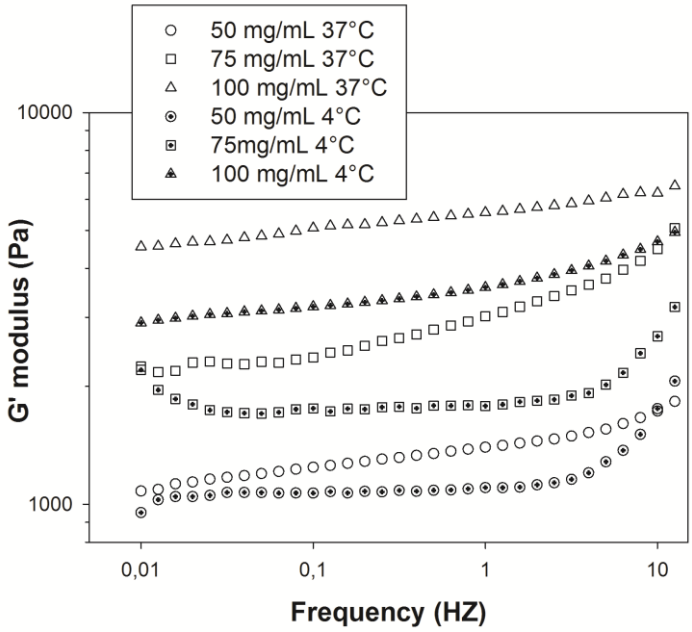

Fig. 10 Storage modulus (Pa) as a function of the frequency (Hz) at 4°C and 37°C for ELR-CFCGs with recombinamer concentrations of 50 mg/mL, 75 mg/mL and 100 mg/mL.

CHAPTER 8:

EA-VALVE DEVELOPMENT OF A TISSUE-ENGINEERED ELASTIN-BASED HEART VALVE PROSTHESIS

I. González de Torre[1], R. Moreira[2], M. Alonso[1], S. Jockenhoevel[2,3], J. Carlos Rodríguez-Cabello[1], P.Mela[2].

[1] BIOFORGE, CIBER-BBN, Campus "Miguel Delibes" Centro I+D, Universidad de Valladolid, Paseo Belén 11, 47011, Valladolid
[2] Department of Tissue Engineering and Textile Implants, AME-Institute of Applied Medical Engineering, Helmholtz Institute, RWTH Aachen University, Aachen, Germany
[3] Institut für Textiltechnik, RWTH Aachen University, Aachen, Germany

Gonzalez de Torre, I.; Moreira, R.; Alonso, M.; Jockenhoevel, S.; Rodríguez-Cabello, J. C.; Mela, P. Ea-valve development of a tissue-engineered elastin-based heart valve prosthesis. Acta Biomaterialia. Under review

ABSTRACT

Aortic stenosis and regurgitation are the most common aortic valve failure in Europe and North America. Several prostheses for aortic valve replacement have been developed in the last decades but still significant limitations such as the need of a long-term anticoagulation therapy and failure by calcifications have to be overcome. Moreover, these prostheses cannot evolve with the patient, neither self-repair nor adapt to the changing hemodynamic conditions. In this work we present an Elastin–like recombinamer based aortic tissue engineered heart valve (EA-valve) colonized by human umbilical vein smooth muscle cells (HUVSMCs). These EA-valves provides the needed mechanical properties allowing the normal cell growing and colonization of the scaffold and with an excellent functionality after 21 days of in vitro conditioning in a specially designed bioreactor. Histological and immunohistological stainings showed remarkable tissue development with abundant aligned collagen fibers. An excellent coaptation, corroborated by ultrasound echography, was obtained after the conditioning period. This study presents the proof-of-principle for the realization of an Elastin-recombinamer tissue-engineered aortic valve with a simple injection molding process readily adaptable to the patient's anatomy and pathological situation by producing a patient-specific rapid prototyped mold.

1. INTRODUCTION

Valvular heart disease (VHD) is one of the main problems that people suffers related with a heart failure and often requires intervention[1]. The principal strategies to substitute these inefficient valves, are based on the use of bioprosthetic acellular matrix valves[2-4], bioresorbable scaffolds[5, 6] and constructs containing entrapped cells[7, 8]. All these approaches have led to longer life expectancy of patients, but, all of them still present some key limitations. Acellular matrixes can bear toxic residues from the decellulation process and these residues can detrimentally affect to the mechanical and citocompatible properties of these prostheses[9]. Moreover even during months after implantation, these acellular matrixes are not able to repopulate their structures with healthy cells from the patient[10] and some tissue overgrowth and infiltration with inflammatory cells can be observed. Even with these drawbacks these kind of valves can last up to 20 years before malfunction, but after that period the valve have to be substituted by a new one. Bioreasorbable scaffolds have several problems like fibrosis, retraction and malfunction[9]. Perhaps the most promising approach is the fabrication of scaffolds that contain entrapped cells that can grow and develop their own extracellular matrix. The material to prepare these scaffolds play a crucial role for the future of the construct. For instance, scaffolds based on collagen showed that cells entrapped inside enter in apoptosis and produce matrix metalloproteinases[11]. Fibrin is an alternative to collagen as substrate[12] to form valves[8, 13, 14] with entrapped cells but still some disadvantages, shrinking of the gels and initial low mechanical stiffness[15] have to be overcome.

Recently, elastin-like recombinamers catalyst free click gels (ELR-CFCGs)[16] have come to the fore. They can bear bioactive domains that improve their cytocompatibility, they exhibit adequate mechanical properties and low thrombogenicity[17]. All these characteristics postulate the ELR-CFCGs as plausible candidates to be applied in the formation of aortic valves.

2. MATERIALS AND METHODS

2.1.ELRs biosynthesis, modification and characterization

The ELRs used in this work were obtained by using standard genetic engineering techniques. Their purification was based on the intrinsic thermal behavior of these compounds[18]. The ELRs were subsequently dialyzed against purified water and freeze-dried. VKVx24, a structural recombinamer without any bioactive sequence and HRGD6, a recombinamer with the universal cell-adhesion epitope (RGD) were obtained. The amino-acid sequences of these polymers and purity were described elsewhere[17]. ELRs were chemically modified by transformation of the ε-amine group in the lateral lysine chain to bear cyclooctine and azide groups as we recently reported[16]

2.2.Cell isolation, expansion and immunocytochemistry

Autologous cells (a mixed population of smooth muscle cells (SMCs)/fibroblasts) were isolated from veins of human umbilical cords kindly provided by the department of gynecology at the University Hospital Aachen in accordance with the human subjects approval of the ethics committee (votum of the local ethics committee: #EK 2067). The vein was washed with phosphate-

buffered saline (PBS; Gibco, Karlsruhe, Germany) following removal of endothelial cells by using 1 mg/ml collagenase (Sigma, Seelze, Germany). The digested vein was minced into 1-mm rings and then bathed in primary cell culture media Dulbecco´s Modified Eagle Medium (DMEM; Gibco) supplemented with 10% FBS (Gibco) and 1% antibiotic/antimycotic solution (Gibco) for primary explant culture. To obtain a sufficient number, the cells were serially passaged 5-6 times using 0.25% trypsin/0.02% EDTA solution (Gibco) and cultured in 5% CO2 and 95% humidity at 37 °C. Prior to valve moulding, the SMCs/fibroblasts phenotype was verified by the presence of alpha-smooth muscle actin (alpha-SMA) positive cells and total absence of expression of von Willebrand factor (vWf). The cells were fixed with ice-cold methanol (-20 ºC) and rehydrated in PBS. Unspecific epitopes were blocked, permeabilized with normal goat serum (NGS; Dako) and incubated for 1 h at 37 ºC with the following primary antibodies: 1:400 mouse anti-alpha-SMA (A 2547; Sigma) and 1:200 rabbit anti-vWf (A0082; Dako). The samples were incubated with either rhodamine or fluorescein-conjugated secondary antibodies: 1:400 mouse (A11005, Molecular Probes) for alpha-SMA and 1:400 rabbit (A11012, Molecular Probes) for vWf. The cells were counterstained with 4', 6-diamino-2-phenylindole (DAPI) nuclei acid stain (Molecular Probes) and observed in a microscope equipped for epi-illumination (AxioObserver Z1; Carl Zeiss GmbH). Images were acquired using a digital camera (AxioCam MRm; Carl Zeiss GmbH).

2.3.Valve concept

The E-valve consists of a tissue-engineered valve featuring the native shape of semilunar heart valves i.e., semilunar-triangular shaped leaflets attached to the wall. As a scaffold material, we use ELRs as a cell carrier. In order to facilitate the

suturing for implantation, the wall was reinforced with a warp-knitted textile mesh.

Valves were formed by catalyst free click reactions between an azide group and an activated cyclooctine group. Solutions of ELRs-cyclooctine and ELRs-azide (90 mg/mL) were prepared in DPBSx1 at the desired concentration and kept at 4°C for at least 24. 30 millions of HUVMCs were suspended in 500 µL of PBSx1 and mixed with the HRGD6-N3 solution previously prepared. Both solutions (VKVx24-cyclo and HRGD6-N3 plus cells final concentration 75 mg/mL) were co-injected inside a 15 mm diameter aortic shape mould and kept 35 minutes at r.t.

2.4.Bioreactor system and operation

The valves (n=3) were carefully removed from the mould ancultivated under static conditions for 7 days following dynamic conditioning for 14 days at 37 °C, 5% CO2 and 21% O2 in a custom-made bioreactor. The dynamic bioreactor consists of two polymethyl methacrylate (PMMA) chambers and a linear magnetic actuator (Typ810; Mönninghoff GmbH), as described previously (ref to Weber 2014). Briefly, the lower chamber function as a ventricle pump connected to an upper chamber where the valve is placed. The magnetic actuator displaces stroke volumes trough the valve. The frequency ranged from 20 to 40 bpm, increased in steps of 5 bpm every 3-4 days. The gas exchange was guaranteed by an external peristaltic pump (MCP Process, Ismatec), recirculating the medium through gas-permeable silicone tubes (ISMAPRENE, IDEX Health and Care GmbH) and by a gas filter placed on the top of the bioreactor. The valves were cultured in low-glucose medium DMEM (Gibco) supplemented with 10% FCS, antibiotic/antimycotic solution, 1.0 mM L-ascorbic acid 2-phosphate (Sigma). The culture

medium was replaced every 4 days. The culture conditions were monitored every 2 days by measuring glucose and lactate concentrations, pO2, pCO2 and pH by means of an automatic blood gas analyser (Radiometer ABL 800 Flex, Radiometer Medical A/S). All PMMA components were sterilized by low-temperature (58 °C) hydrogen peroxide gas plasma (STERRAD 100S Sterilisation System, Ethicon GmbH) at least 4 days before use. Other components were sterilized by autoclaving.

2.5.Tissue analysis

Tissue samples were rinsed in PBS, fixed in Carnoy´s fixative and embedded in paraffin for subsequent histological analysis.

2.6.Bright field microscopy

Carnoy´s fixed, paraffin-embedded native ovine pulmonary and tissue-engineered valves were sectioned at 3 µm thickness longitudinally and stained by standard Haematoxylin and Eosin (H&E) protocol for analysis of general tissue morphology. Sections were analysed by routine bright field microscopy (AxioImager D1; Carl Zeiss GmbH) and images were acquired using a digital colour camera (AxioCam MRc; Carl Zeiss GmbH).

2.7.Immunohistochemistry

Non-specific sites on Carnoy´s-fixed tissue, paraffin-embedded sections from native ovine and tissue-engineered valves were blocked and the cells were permeabilized with 5% NGS (Sigma) in 0.1% Triton-PBS. Sections were incubated for 1 h at 37 ºC with the following primary antibodies: 1:1000 mouse anti-α-SMA (A 2547; Sigma); 1:200 rabbit anti-type collagen I (R 1038; Acris);

1:25 rabbit anti-type collagen III (R 1040; Acris) and 1:200 rabbit anti-elastin (20R-ER003; Fitzgerald). The sections were incubated for 1 h at 37º C with either rhodamine or fluorescein-conjugated goat-anti-mouse or goat-anti-rabbit secondary antibodies: 1:400 mouse (A 11005; Molecular Probes) for alpha-SMA; 1:400 rabbit (A11008; Molecular Probes) for collagen type I and elastin, and 1:300 rabbit immunoglobulins/biotinylated (E 0432; Dako) for collagen type III. Collagen type III signal was amplified by an additional incubation with 1:1000 streptavidin/TRITC (RA 021; Acris). Native ovine pulmonary valve served as a positive control. As negative controls, samples were incubated in diluent and the second antibody only. Tissue sections were counterstained with DAPI nuclei acid stain (Molecular Probes). Samples were observed in a microscope equipped for epi-illumination (AxioObserver Z1; Carl Zeiss GmbH). Images were acquired using a digital camera (AxioCam MRm; Carl Zeiss GmbH).

3. RESULTS

3.1.Macroscopic evaluation

After the moulding process the valve was removed and Fig. 1 shows how the ELR-CFCG perfectly adopt de shape of the aortic valve mould, both the vascular side as well as the ventricular side. (Fig. 1 A and B respectively)

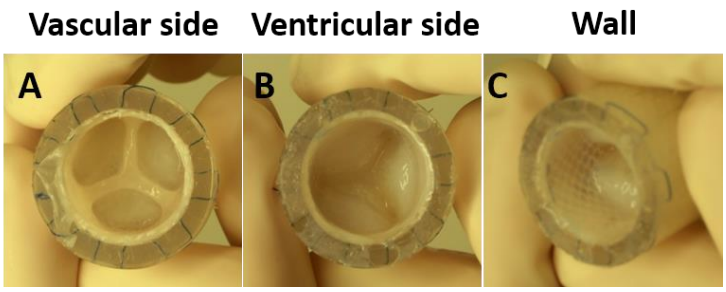

***Figure 1**. Macroscopic aspect of an EA-valve few moments after the molding process.*

The valve functionality was evaluated after 7 days of static cultivation and 15 days of dynamic cultivation by recording the opening and closure of the leaflets with a high speed camera. Ultrasound echography helped to corroborate the valve's functionality. Fig. 2 shows the opening and close position (Fig. 2 A and B pics, and Fig. 2 C and D pics, respectively) of the valve during the bioreactor conditioning. A complete opening without flow restriction is achieved during the ventricular ejection step included in the systole stage, while a total closure with an efficient coaptation of the leaflets avoiding regurgitation is observed during the diastole stage. After all mechanical test the valve remained perfectly attached to the warp-knitted textile mesh of the walls (Fig. 2 E). Even after remove the textile mesh from the silicon tube, the ELR-CFCG remained attached to the textile mesh retaining the aortic valve shape (Fig. 2 F).

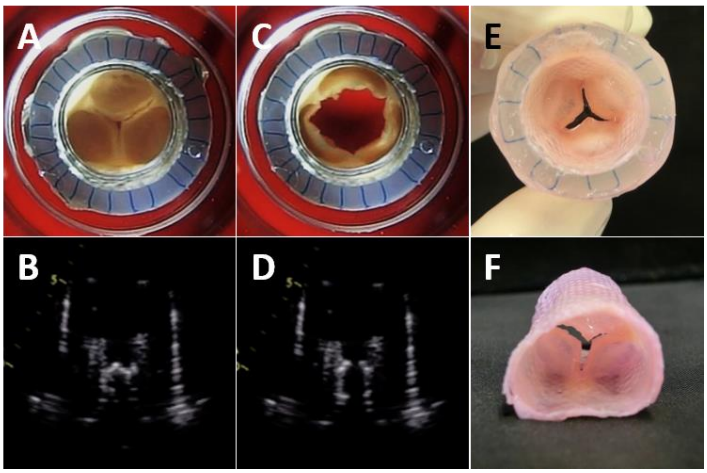

***Figure 2**. Ultra slow motion (A and C) and ultrasound echography (B and D) pictures of the EA-valves in the open and close position. Macroscopic aspect of the EA-valves with and without silicon tube (E and F respectively) after 21 days of in vitro culture.*

3.2.Tissue analysis

Paying attention to immunochemistry pictures in Fig. 3, the presence of α-SMA (A, B), collagen I (C, D) and III (E, F) is clearly evident. Moreover certain alignment of α-SMA and collagen I can be found in the leaflets (pics B and D respectively), where the movement of the valve is stronger than in the wall where no alignment of α-SMA, collagen I and III (pics A, C and E respectively) can be observed. In fact, even in the ELR-CFCG matrix certain orientation in the longitudinal direction is found in the leaflets (pic H).

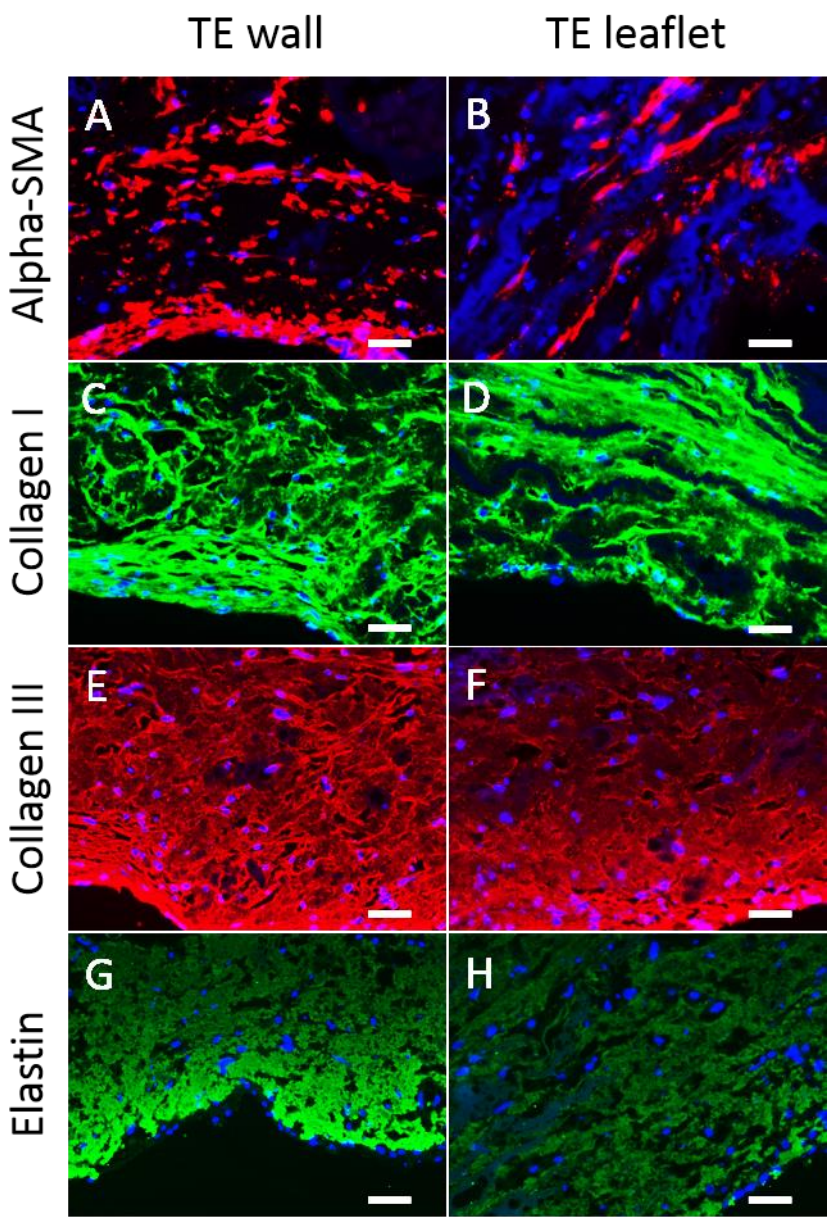

***Figure 3**. Tissue analysis of the EA-valves after 21 days of in vitro culture. immunohistochemical staining against alpha-smooth muscle actin (A, B), collagen I (C, D), collagen III (E, F) and elastin (G, H). Dapi was used for nuclei staining in all samples. Scale bars 50 μm.*

3.3.Burst strength

A simple method to characterize the mechanical properties of a tissue is the burst strength test. It consists on apply certain pressure to find the point of structural failure. As can be seen in Fig. 4, the textile reinforcement in the wall drives to higher values of pressure in the burst strength test that in the leaflets in samples without cells. But that difference disappears after the 21 days of valve conditioning, increasing from 152.7±65.0 mmHg to 642.8±135.5 mmHg (more than four times the initial value). This increase is not so high in the wall, from 414.5±80.1 mmHg to 579.5±145.8 mmHg. And even when these values are still far from values for native aortic valve[19] (around 5500 mmHg) it is easy to suppose that high values will be achieved after longer culture times.

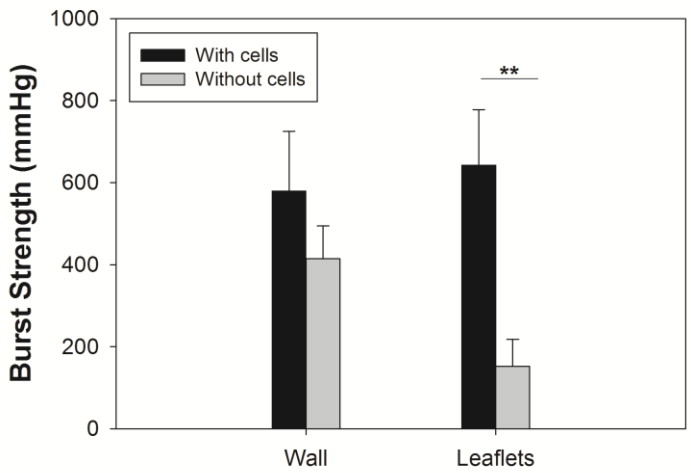

Figure 4. *Failure pressure on burst strength test of the two different areas (wall and leaflets) of the EA-valves without and with embedded cells after 21 days of in vitro culture (grey and black bars, respectively).*

4. DISCUSSION

In this work a tissue engineered elastin like recombinamer based aortic valve (EA-valve) is present. This EA-valves exhibit the characteristic 3D geometry of the native aortic valve. EA-valves are designed as a homogeneous scaffold composed by ELR-CFCGs, the walls of the EA-valves contains a tube of warp-knitted textile mesh to permit a correct fixation of the valves to the bioreactor. These EA-valves are obtained by injection moulding[20], which means that specific moulds, based on magnetic resonance tomography of the native valve, can be designed for the unique anatomy of each patient. In this way tailor made valves can be produced to satisfy the needs of each pathology. In fact, and thanks to the new 3D printing technology, each specific mould could be obtained in very short time. This study shows the proof of principle of the feasibility of tissue engineered EA-valves with HUVSMCs and conditioned in a specially designed bioreactor. Moreover this EA-valves exhibit good mechanical properties after the conditioning process and an excellent functionality as can be observed from the slow motion recorded images as well as from the ultrasound echography analysis of the valve movement. The specific conditions of the static and dynamic cultivation periods allow and induce the production of a-SMA, collagen I and III, the main proteins together with elastin in the native valves. In fact, certain alignment in the longitudinal direction is observed in the immunopictures for collagen I and a-SMA in the leaflets (Fig. 3 B, D), induced by mechanical stress[21, 22]as well as in the artificial ECM of ELR-CFCG (Fig. 3 H). This longitudinal orientation is not found in the wall due it withstands less mechanical stress than the leaflets. The production of all these components of the ECM during the cultivation period produces a

significant increase in the values of the burst strength test. This increase in the mechanical properties of the EA-valve, that even exceeds the values of the burst strength for the wall that includes the textile reinforcement, is attributed exclusively to the ECM produced by the cells during the 21 days of culture, and it is reasonable to believe that longer culture times will drive to a higher mechanical properties and to a stronger tissue. The presence of enough elastin is a key factor that scaffolds have to comply for vascular tissue applications[23]. But the elastogenesis is a process that hardly occurs in vitro[23, 24], and the absence of an appropriate elastin network is possibly the underlying factor that determines the failure of the tissue engineered valves and vascular grafts[24-27]. The ELR-CFCGs provides this needed elasticity and mechanical properties[16] and, based on the results showed by the immunostaining pictures, the ERL-CFCGs offer an artificial ECM that permit a normal growing of the cells producing the needed structures that will provide the enough strength and mechanical properties to this EA-valves. Moreover, the proved low thrombogenicity of the ELR-CFCGs on other devices designed for cardiovascular applications[17] make us suppose that this low thrombogenicity can be extrapolated to our EA-valves.

5. CONCLUSION

Elastin like recombinamer based aortic valves (EA-valves) have been designed and produced, exhibiting an excellent functionality after 21 days of in vitro culture, with a total opening of the leaflets during the ventricular ejection in the systole, and an effective closure with and excellent coaptation during the diastole period simulated in a specially designed bioreactor. The tissue

analysis of the EA-valves shows an oriented production, in the leaflets, of collagen I and α-SMA, as well as certain alignment of the ELR-CFCG that form the construct. This production of collagen I and III α-SMA among other ECM components drives to an increase of the strength of the EA-valves. All this features, together with the low thrombogenicity are a very promising starting point for the first in vivo tests that will be carried out in our laboratories.

6. ACKNOWLEDGMENTS

We acknowledge financial support from the EU through the European regional development fund (ERDF), from the MINECO (MAT-2010-15982, MAT2010-15310, PRI-PIBAR-2011-1403 and MAT2012-38043), the JCyL (projects VA049A11, VA152A12 and VA155A12), the CIBER-BBN, and the JCyL and the Instituto de Salud Carlos III under the "Network Center of Regenerative Medicine and Cellular Therapy of Castilla and Leon". Funding was also provided by IZKF Aachen (Interdisciplinary Centre for Clinical Research) of the Medical Faculty of the RWTH Aachen University and by the German Research Foundation (DFG, MTBo07) a within the excellence initiative.

7. REFERENCES

[1] Iung B, Baron G, Butchart EG, Delahayed F, Gohlke-Bärwolf C, Levang OW, et al. A prospective survey of patients with valvular heart disease in Europe: The Euro Heart Survey on Valvular Heart Disease. European Heart Journal 2003;24:12311243.

[2] Brendel K, Duhamel RC. Body implants of extracellular matrix and means and methods of making and using such implants. Google Patents; 1989.

[3] Klement P, Wilson GJ, Yeger H. Process for preparing biological mammalian implants. Google Patents; 1988.

[4] Konertz W, Dohmen PM, Liu J, Beholz S. Hemodynamic characteristics of the Matrix P decellularized xenograft for pulmonary valve replacement during the Ross operation. J Heart Valve … 2005.

[5] Shinoka T, Breuer C, Tanel R, Zund G, Miura T, Ma P, et al. Tissue engineering heart valves: Valve leaflet replacement study in a lamb model. The Annals of Thoracic Surgery 1995;60.

[6] Sodian R, Sperling JS, Martin DP, Egozy A, Stock U, Mayer JE, et al. Fabrication of a trileaflet heart valve scaffold from a polyhydroxyalkanoate biopolyester for use in tissue engineering. Tissue engineering 2000;6:183-8.

[7] Tranquillo RT, Girton TS, Neidert M. Tissue equivalent approach to a tissue-engineered cardiovascular valve. Google Patents; 2003.

[8] Moreira R, Gesche VN, Hurtado-Aguilar LG, Schmitz-Rode T, Frese J, Jockenhoevel S, et al. TexMi: development of tissue-engineered textile-reinforced mitral valve prosthesis. Tissue engineering Part C, Methods 2014;20:741-8.

[9] Vesely I. Heart valve tissue engineering. Circulation research 2005;97:743-55.

[10] Mitchell RN, Jonas RA, Schoen FJ. Pathology Of Explanted Cryopreserved Allograft Heart Valves: Comparison With Aortic Valves From Orthotopic Heart Transplants. The Journal of Thoracic and Cardiovascular Surgery;115:118-27.

[11] Grinnell F. Fibroblast biology in three-dimensional collagen matrices. Trends in cell biology 2003;13:264-9.

[12] Williams C, Johnson S, Robinson R, Tranquillo RT. Cell Sourcing and Culture Conditions for Fibrin-Based Valve Constructs. Tissue Engineering 2006;0:1005968361.

[13] Weber M, Heta E, Moreira R, Gesche VN, Schermer T, Frese J, et al. Tissue-engineered fibrin-based heart valve with a tubular leaflet design. Tissue engineering Part C, Methods 2014;20:265-75.

[14] Robinson P, Johnson S, Evans M, Barocas V, Tranquillo RT. Functional tissue-engineered valves from cell-remodeled fibrin with commissural alignment of cell-produced collagen. Tissue engineering Part A 2008;14:83-95.

[15] Jockenhoevel S, Zund G, Hoerstrup S, Chalabi K, Sachweh J, Demircan L, et al. Fibrin gel -- advantages of a new scaffold in cardiovascular tissue engineering. European journal of cardio-thoracic surgery : official journal of the European Association for Cardio-thoracic Surgery 2001;19:424-30.

[16] González de Torre I, Santos M, Quintanilla L, Testera A, Alonso M, Rodríguez Cabello JC. Elastin-like recombinamer catalyst-free click gels: Characterization of poroelastic and intrinsic viscoelastic properties. Acta Biomaterialia 2014;10:2495-505.

[17] Gonzálezde Torre, I.; Wolf, F.; Santos, M.; Rongen, L.; Alonso, M.; Jockenhoevel, S.; Rodríguez-Cabello, J. C.; Mela, P. Elastin-like recombinamer-covered stents: Towards a fully biocompatible and non-thrombogenic device for cardiovascular diseases. Acta Biomaterialia 2015, 12 (0), 146-155

[18] Girotti A, Reguera J, Rodriguez-Cabello JC, Arias FJ, Alonso M, Matestera A. Design and bioproduction of a recombinant multi(bio)functional elastin-like protein polymer containing cell adhesion sequences for tissue engineering purposes. J Mater Sci Mater Med 2004;15:479-84.

[1] Iung B, Baron G, Butchart EG, Delahayed F, Gohlke-Bärwolf C, Levang OW, et al. A prospective survey of patients with valvular heart disease in Europe: The Euro Heart Survey on Valvular Heart Disease. European Heart Journal 2003;24:12311243.

[2] Brendel K, Duhamel RC. Body implants of extracellular matrix and means and methods of making and using such implants. Google Patents; 1989.

[3] Klement P, Wilson GJ, Yeger H. Process for preparing biological mammalian implants. Google Patents; 1988.

[4] Konertz W, Dohmen PM, Liu J, Beholz S. Hemodynamic characteristics of the Matrix P decellularized xenograft for pulmonary valve replacement during the Ross operation. J Heart Valve … 2005.

[5] Shinoka T, Breuer C, Tanel R, Zund G, Miura T, Ma P, et al. Tissue engineering heart valves: Valve leaflet replacement study in a lamb model. The Annals of Thoracic Surgery 1995;60.

[6] Sodian R, Sperling JS, Martin DP, Egozy A, Stock U, Mayer JE, et al. Fabrication of a trileaflet heart valve scaffold from a polyhydroxyalkanoate biopolyester for use in tissue engineering. Tissue engineering 2000;6:183-8.

[7] Tranquillo RT, Girton TS, Neidert M. Tissue equivalent approach to a tissue-engineered cardiovascular valve. Google Patents; 2003.

[8] Moreira R, Gesche VN, Hurtado-Aguilar LG, Schmitz-Rode T, Frese J, Jockenhoevel S, et al. TexMi: development of tissue-engineered textile-reinforced mitral valve prosthesis. Tissue engineering Part C, Methods 2014;20:741-8.

[9] Vesely I. Heart valve tissue engineering. Circulation research 2005;97:743-55.

[10] Mitchell RN, Jonas RA, Schoen FJ. Pathology Of Explanted Cryopreserved Allograft Heart Valves: Comparison With Aortic Valves From Orthotopic Heart Transplants. The Journal of Thoracic and Cardiovascular Surgery;115:118-27.

[11] Grinnell F. Fibroblast biology in three-dimensional collagen matrices. Trends in cell biology 2003;13:264-9.

[12] Williams C, Johnson S, Robinson R, Tranquillo RT. Cell Sourcing and Culture Conditions for Fibrin-Based Valve Constructs. Tissue Engineering 2006;0:1005968361.

[13] Weber M, Heta E, Moreira R, Gesche VN, Schermer T, Frese J, et al. Tissue-engineered fibrin-based heart valve with a tubular leaflet design. Tissue engineering Part C, Methods 2014;20:265-75.

[14] Robinson P, Johnson S, Evans M, Barocas V, Tranquillo RT. Functional tissue-engineered valves from cell-remodeled fibrin with commissural alignment of cell-produced collagen. Tissue engineering Part A 2008;14:83-95.

[15] Jockenhoevel S, Zund G, Hoerstrup S, Chalabi K, Sachweh J, Demircan L, et al. Fibrin gel -- advantages of a new scaffold in cardiovascular tissue engineering. European journal of cardio-thoracic surgery : official journal of the European Association for Cardio-thoracic Surgery 2001;19:424-30.

[16] González de Torre I, Santos M, Quintanilla L, Testera A, Alonso M, Rodríguez Cabello JC. Elastin-like recombinamer catalyst-free click gels: Characterization of poroelastic and intrinsic viscoelastic properties. Acta Biomaterialia 2014;10:2495-505.

[17] González de Torre I, Wolf F, Santos M, Rongen L, Alonso M, Jockenhoevel S, et al. Elastin-like recombinamer-covered stents: Towards a fully biocompatible and non-thrombogenic device for cardiovascular diseases. Acta Biomaterialia 2014.

[18] Girotti A, Reguera J, Rodriguez-Cabello JC, Arias FJ, Alonso M, Matestera A. Design and bioproduction of a recombinant multi(bio)functional elastin-like protein polymer containing cell adhesion sequences for tissue engineering purposes. J Mater Sci Mater Med 2004;15:479-84.

[19] Yamanami M, Yahata Y, Uechi M, Fujiwara M, Ishibashi-Ueda H, Kanda K, et al. Development of a Completely Autologous Valved Conduit With the Sinus of Valsalva Using In-Body Tissue Architecture Technology A Pilot Study in Pulmonary Valve Replacement in a Beagle Model. Circulation 2010;122.

[20] Jockenhoevel S, Chalabi K, Sachweh J, Groesdonk H, Demircan L, Grossmann M, et al. Tissue Engineering: Complete Autologous Valve Conduit-A New Moulding Technique< SUP>∗</SUP>. The Thoracic and cardiovascular surgeon 2001;49:287-90.

[21] Kanda K, Matsuda T. Mechanical stress-induced orientation and ultrastructural change of smooth muscle cells cultured in three-dimensional collagen lattices. Cell transplantation 1994;3:481-92.

[22] Akhouayri O, Lafage-Proust MH, Rattner A, Laroche N, Caillot-Augusseau A, Alexandre C, et al. Effects of static or dynamic mechanical stresses on osteoblast phenotype expression in three-dimensional contractile collagen gels. Journal of Cellular Biochemistry 2000;76:217-30.

[23] Patel A, Fine B, Sandig M, Mequanint K. Elastin biosynthesis: The missing link in tissue-engineered blood vessels. Cardiovascular research 2006;71:40-9.

[24] Mol A, Smits AIPM, Bouten CVC, Baaijens FPT. Tissue engineering of heart valves: advances and current challenges. Expert Review of Medical Devices 2009;6:259-75.

[25] Lee TC, Midura RJ, Hascall VC, Vesely I. The effect of elastin damage on the mechanics of the aortic valve. Journal of biomechanics 2001.

[26] Anidjar S, Salzmann JL, Gentric D, Lagneau P, Camilleri JP, Michel JB. Elastase-induced experimental aneurysms in rats. Circulation 1990;82:973-81.

[27] Schoof PH, Takkenberg JJM, van Suylen R-J, Zondervan PE, Hazekamp MG, Dion RAE, et al. Degeneration of the pulmonary autograft: An explant study. The Journal of Thoracic and Cardiovascular Surgery 2006;132:1426-32.

FINAL CONCLUSIONS:

FINAL CONCLUSIONS

Hybrid Elastin-like recombinamers-Fibrin gels (ELR-FGs) have been prepared in a concentration range of 2.5 to 15 mg/mL by a simple method. These ELR-FGs improve the mechanical properties of the well-known fibrin gels. These mechanical properties can be easily tuned from a storage modulus of 100 Pa to 1200 Pa by simple variations in the recombinamer concentrations. The ELRs introduce specific biofuctionalities that can improve the bioactivity of these ELR-FGs, promoting a complete and fast cell colonization of these new hybrid gels. All these improvements facilitates the use of this combination in more complex systems as exemplified by the formation of artificial heart valves made by a combination of fibrin gels in the walls and ERL-FGs in the leaflets.

These heart valves can be easily produced, with or without cells, by simple casting of the mixture of the macromolecular solutions in an appropriate mould. Even when the functionality of these hybrid valves were not ideal, they represent a clear improvement with respect to the current valves made exclusively of fibrin.

The ELRs used (VKVx24, HRGD6 and REDV) can be easily modified to bear different reactive groups (azides, alquines and cyclooctynes) by simple chemical reactions. These modified ELRs react through a click reaction to obtain totally citocompatible hydrogels (ELR-CGs and ELR-CFCGs, with and without catalyst respectively). These hydrogels have tuneable mechanical properties in the range of 1 to 12 kPa by variations on the concentration of each component. These mechanical properties matches whith those found in natural tissues. A poroviscoelastic

model as a plausible model to explain the physical behaviour of these hydrogels.

Several cell lines (HFF-1, HUVECs, MCs and HUVSMCs) have been seeded in these ELR-based hydrogels. The normal growing of these cells proves the cytocompatibility of the ELR click gels regardless the biofunctionalization of the ELRs, although ELR with cell adhesion sequences improve the adhesion and proliferation of those cells. Moreover, the best results in adhesion and proliferation were obtained for the ELR bearing the RGD sequence, but the specificity of the REDV sequence was not evaluated.

When these hydrogels are obtained at very low concentrations (less than 1 mg/mL), they form nanogels with different structures, sizes, surface charge and microrheological properties as function of the formation temperature (above or below of the transition temperature). For instance, the nanoparticles formed below the transition temperature exhibit a non-regular structure and a size of around 100 nm and a zeta potential about +10 mV, while the nanogels formed above the transition temperature show a spherical structure with a diameter of around 500 nm and a zeta potential of +26 mV. These values of size and zeta potential are adequate for many drug encapsulation applications. A fractal model of nanogel formation has been demonstrated.

A reactive layer by layer technology has been developed with these modified ELRs. Different materials and devices (glass, polystyrene, titanium and coronary stents) have been functionalized with several reactive layers of modified ELRs. Layers of 500 nm or 2 μm can be obtained depending on the employed procedure (with or without a washing step, respectively). This

simple technique allows a total control over the thickness of the coating of the surfaces. In this way, we can obtain a nanometer scale coating capable of covering complex structures, such as coronary stents, with a nanometer coat. Moreover fluorescent probes can be attached to the backbone of the ELRs. That also suggest that different drugs of biomedical interest could be also incorporated to the structure of the ELRs by identical means, contributing to further increase the biofunctionalization possibilities of different materials of biomedical use.

It has been shown that the ELR-CFCGs hydrogels obtained using catalyst free technology exhibit a high potentiality as "scaffolds" in the treatment of cardiovascular disease through tissue engineering.

These ELR-CFCGs can be used to develop a new kind of bio-Stents. These bio-Stents are made of a metallic stent covered by an ELR-CFCG of 100 μm thickness. These devices were tested under flowrates close to physiological conditions in the aorta and they exhibit excellent mechanical properties. Moreover these new ELR covered stents enhance the endothelization inside the construct due to the bioactive sequences (RGD or REDV) that are included in the backbone of the polymers. This endothelization was complete after 15 days of in vitro dynamic culture. Thrombogenicity test proved a low platelet adhesion, which along with the biocompatibility of the ELRs, makes to this new bio-stents practically undetectable by the immune system of the host.

Based on the proved good properties of the ELRs-CFCGs, more complex structures such as ELR-based aortic valves (EA-valves) have been produced using these ELR-CFCGs. Human umbilical vein smooth muscle cells (HUVSMCs) have been included

inside the hydrogel during the moulding process that will produce the aortic valves. After this moulding process, the valves were cultured using a specially designed bioreactor during 21 days. During that time, cells grew inside the artificial valve developing their own ECM and improving the mechanical properties of the EA-valves. These mechanical properties were evaluated though a burst strength test, and the result showed a significate increase of the pressure at break from 150 mmHg to 650 mmHg, without or with cells respectively, after 21 days of dynamic in vitro culture. These EA-valves exhibit excellent functionality after the culture time, with a very good opening and a complete leaflets coaptation, corroborated by slow motion pictures and ultrasound echography. The tissue analysis of these EA-valves after the culture period revealed the alignment of collagen I and a-SMA as well as the ELR-CFCG in the leaflets which emulated the structure of the native valves.

As final conclusion ELR based hydrogels obtained by the technologies explained in this thesis have proven to be adequate candidates to be applied in the field of tissue engineering, and especially in cardiovascular diseases, being able to generate, among other devices, heart valves with complex high functionality and outstanding mechanical properties. And their biofunctionality and cytocompatibility has been clearly proven due to such hydrogels showed similar behaviour and properties than the natural extracellular matrix.

All the exposed results in this work makes us to think in a clear potential applicability of these materials in the biomedical field.